NUREG/CR-4138
SAND85-0135
R3

Data Analyses for Nevada Test Site (NTS) Premixed Combustion Tests

A. C. Ratzel

May 1985

Sandia National Laboratories
Albuquerque, NM 87185
Operated by
Sandia Corporation
for the
U.S. Department of Energy

Prepared for
Division of Accident Evaluation
and
Division of Engineering Technology
Office of Nuclear Regulatory Research
U.S. Nuclear Regulatory Commission
Washington, D.C. 20555
NRC FIN Nos. A1246, A1270

Abstract

This report provides results from an in-depth analysis of twenty-one of the twenty-four premixed large-scale combustion experiments sponsored by the U. S. Nuclear Regulatory Commission (NRC) and the Electric Power Research Institute (EPRI) and conducted by EG&G at the Nevada Test Site (NTS). These experiments were performed in a 2048 cubic meter spherical vessel (hydrogen dewar) with mixtures of hydrogen, steam, and air ignited by glow plugs or heated resistance coils. Hydrogen concentrations ranged from 5 to 13% (by volume) and steam concentrations from 4 to 40%. Several tests also incorporated spray systems and/or fans which enhanced the combustion rate and significantly altered the postcombustion gas cooling.

In this work, data provided by EPRI from instrumentation designed to characterize the thermal environment in the dewar during and following combustion have been evaluated. The data reduction package SMOKE has been used to process data from thin-film gauges, Gardon and Schmidt-Boelter heat flux gauges, capacitance calorimeters, gas and wall thermocouples, and pressure sensors. Local measurements of the heat transfer are provided from the calorimetry, and global averages are inferred from the pressure. Instrumentation "goodness" for each test is assessed based on the raw data and on comparisons of local and global results. Graphical and tabular results are provided for each test, and trends observed from the results are reported. This information should be useful for benchmarking existing computer codes used in modeling nuclear containment and associated safety-related equipment response to degraded-core accidents and for improving combustion and heat transfer models currently used in these computer simulations.

Contents

List of Figures

Figures in Appendix B

Figures in Appendix C

List of Tables

Tables in Appendix A

Acknowledgements

This work was performed in support of the Hydrogen Burn Survival and Hydrogen Behavior Programs at Sandia National Laboratories, Albuquerque, NM. J. Haugh of EPRI and J. E. Shepherd of Sandia provided technical and background data on the testing procedures and on the instrumentation used in the NTS experiments. J. E. Shepherd, S. N. Kempka, and A. W. Reed were involved in the development of the SMOKE data analysis package.

I would also like to express my appreciation to the following persons who reviewed the original draft of this document and who provided constructive changes and suggestions which have been incorporated in this work.

J. C. Cummings – SNLA
J. T. Hitchcock – SNLA
D. W. Larson – SNLA
B. W. Marshall Jr. – SNLA
J. E. Shepherd – SNLA
C. C. Wong – SNLA
W. S. Farmer – NRC
K. I. Parczewski –NRC
C. G. Tinkler – NRC
P. Worthington – NRC
J. Haugh – EPRI

Nomenclature

Symbols		
A	Dewar surface area	[m^2]
C_v	Gas specific heat at constant volume	[J/kg-K]
F_c	Correction factor for sapphire (Eq.(3))	
P	Gas pressure	[kPa]
q	Heat flux	[W/cm^2]
Q	Energy deposition	[J/cm^2]
R	Gas constant	[kPa-m^3/kg-K]
t	Time	[s]
Δt	Time interval	[s]
T	Temperature	[K]
$T_{1/2}$	Temperature threshold = $(T_m + T_0)/2$	[K]
V	Dewar volume	[m^3]
x	Depth into dewar wall	[m]

Greek		
α_g	Gas absorptance	
α_w	Dewar wall thermal diffusivity	[m^2/s]
ϵ	Emittance	
ρ	Gas density	[kg/m^3]
σ	Stefan-Boltzmann constant	[W/m^2-K^4]
τ	Transmittance	

Subscripts	
all	Pertaining to the entire test
AIC	Pertaining to adiabatic isochoric combustion
c	Sapphire cover
C	Convective component
g	Gas
m	Maximum condition
mp	Pertaining to time interval between time of peak pressure and time of the measured maximum
off	Baseline value
P	Pertaining to peak pressure
ref	Reference condition
R	Radiative component
RU	Uncorrected radiative component
q_T	Pertaining to time of pressure-inferred peak total flux
T	Total
$T_{1/2}$	Pertaining to the temperature threshold
w	Dewar wall
0	Initial precombustion condition

Executive Summary

This report provides results from an in-depth analysis of twenty-one of the twenty-four premixed combustion experiments sponsored by the U. S. Nuclear Regulatory Commission (NRC) and the Electric Power Research Institute (EPRI) and conducted by EG&G at the Nevada Test Site (NTS). These tests were performed to study combustion processes in a large-scale vessel and to evaluate associated safety-related equipment response to the resulting thermal environments. The experiments were performed in a 2048 cubic meter spherical vessel (hydrogen dewar) with mixtures of hydrogen, steam, and air ignited by glow plugs or heated resistance coils. Hydrogen concentrations ranged from 5 to 13% (by volume) and steam concentrations from 4 to 40%. Several tests also incorporated spray systems and/or fans which enhanced the combustion rate and significantly altered the postcombustion gas cooling. Additional tests (to be reported elsewhere) addressed the effects of localized combustion from diffusion flames which were generated by ignition of streams of steam–hydrogen mixtures injected into the dewar.

In this work, data provided by EPRI from instrumentation associated with estimating the thermal environment in the dewar during and following combustion have been evaluated. Data from the representative safety-related equipment installed in the dewar to assess equipment survival issues have not been reviewed. Further, this work has been restricted to the analysis of only those data records which were provided to Sandia on computer tapes. The data reduction package SMOKE has been used to process data from thin-film gauges and capacitance calorimeters (Sandia supplied), Gardon and Schmidt-Boelter heat flux gauges (EPRI supplied), gas and wall thermocouples (EPRI supplied), and pressure sensors (Sandia and EPRI supplied). Local estimates of the heat transfer are obtained from the calorimetry, and global averages are inferred from the pressure. Instrumentation "goodness" for each test has been assessed based on reviews of the raw data and on comparisons of local and global results.

Graphical and tabular results are provided for each test, and trends observed from the results are reported. Overall conclusions about the the instrumentation and associated performance are as follows:

- Pressure signals from the different sensors are reasonably consistent and can be used to provide global estimates of postcombustion total and radiative heat transfer.

- Global estimates of the gas temperature inferred from the gas pressure compare well with measured temperatures from the 3-mil thermocouples. Results from the 32-mil thermocouples do not follow the early transients associated with combustion but they do agree well with the 3-mil data and pressure-inferred temperatures for the late-time cool-down period.

- Early-time total heat flux results from Sandia-supplied thin-film gauges and capacitance calorimeters are generally comparable with the EPRI-supplied total calorimetry for the lean (< 8%) hydrogen concentrations. The total calorimetry results deviate significantly for those experiments (at higher concentrations) conducted near the end of testing. The global estimates of total heat transfer rate from the pressure are typically less than the local measurements for lean combustion and higher for precombustion concentrations above 10% hydrogen (by volume). Results obtained from most of the calorimetry for the severe combustion tests are suspect, due to deterioration of the gauges (resulting from the cumulative testing) and/or insufficient cooling.

- Total energy deposition results from the EPRI-supplied calorimetry are generally consistent with the global results inferred from the pressure data. The thin-film energy deposition results are typically 30–50% lower than either the global pressure-inferred or local results obtained from EPRI calorimetry.

- Sandia-supplied calorimetry for estimation of the local radiative heat transfer were inoperable for most of the testing, and data from EPRI-supplied radiative calorimetry could not be reduced given uncertainties in the calibration and the correction terms to account for the sapphire cover plates. For postcombustion times, global estimates of radiative heat transfer inferred from the pressure appear to be $\sim$ 30–50% of the total heat transfer inferred from the pressure for the lean combustion tests. For initial hydrogen concentrations > 8%, the radiative transfer dominates the early postcombustion cooling mechanism in the absence of sprays, especially for tests with large initial steam concentrations.

The information provided in this report should be useful for benchmarking existing computer codes used in modeling nuclear containment response to degraded–core accidents and also for resolving issues pertaining to functionability of safety-related equipment in containment during such accidents. The results obtained from this study, coupled with results obtained from intermediate-scale combustion testing (*e.g.*, such as from the FITS and VGES facilities at Sandia Laboratories, Albuquerque), should also be useful in future modeling activities to upgrade the combustion and heat transfer models currently used in reactor safety computer simulations.

1 Introduction

Over the time period of July 1983 through January 1984, two series of premixed combustion experiments were conducted by EG&G at the Nevada Test Site (NTS). This work, sponsored by the U. S. Nuclear Regulatory Commission (NRC) and the Electric Power Research Institute (EPRI), was performed to study combustion processes in a large-scale vessel (Hydrogen Behavior Test Series 1) and to evaluate associated safety-related equipment response to the resulting thermal environments (Equipment Survival Test Series 2). Personnel from Sandia National Laboratories, Albuquerque, N.M. (SNLA), in support of the Hydrogen Behavior and Hydrogen Burn Survival Programs, were also directly involved in this venture, providing technical guidance and fielding instrumentation for testing. Twenty-four combustion experiments were performed in a 2048 cubic meter spherical vessel (hydrogen dewar 15.85 m in diameter) with mixtures of hydrogen, steam, and air ignited by glow plugs and heated resistance coils. Hydrogen concentrations for these tests ranged from 5 to 13% (by volume) and steam concentrations from 4 to 40%. Several tests also incorporated spray systems and/or fans which enhanced the combustion rate and significantly altered the post-combustion gas cooling. Additional tests (to be reported elsewhere) addressed the effects of localized combustion from diffusion flames which were generated by ignition of streams of steam–hydrogen mixtures injected into the dewar.

An enormous quantity of data was obtained from this formidable testing program which could be used to better quantify combustion environments. Available data included, for example, gas pressure data, gas and wall thermocouple data, calorimetry data, and data from instrumentation mounted on/within safety-related equipment exposed to the combustion environments in the dewar. Unfortunately, given the financial and manpower constraints imposed on the undertaking, much of the data have received only limited attention from EPRI. The exception being that, for equipment which became inoperative or performed in an unsatisfactory manner during testing, EPRI personnel have attempted to determine sources of possible failure modes. Similarly, significant attention has been given to evaluating the electrical cables that charred during the more severe premixed combustion tests.

In response to NRC requests for assistance in interpreting and assessing the results obtained from the NTS testing program, we have conducted an in-depth analysis of the data. In this work, data provided by EPRI from instrumentation designed to characterize the thermal environment in the dewar during and following combustion have been evaluated. Data from the representative safety-related equipment installed in the dewar to assess equipment survival issues have not been reviewed. Further, this work has been restricted to the analysis of those data records which were provided to Sandia on computer tapes. These data represent but a fraction of the available data recorded at NTS; nonetheless, the data provide a reasonable base from which estimates for the thermal environment (*i.e.*, gas state and associated heat transfer) in the dewar can be obtained.

The data reduction package SMOKE, developed at SNLA to analyze data from premixed combustion experiments in confined vessels, has been used in this work. This suite of computer codes had been previously used to analyze data obtained from intermediate-scale combustion experiments conducted at the Fully Instrumented Test Site (FITS) at SNLA. Additional computer codes have been added to SMOKE during this study to preprocess (and manipulate) the NTS data to desired formats and to model instrumentation not previously analyzed by SMOKE. The instrumentation evaluated in this work includes thin-film gauges and capacitance calorimeters (SNLA supplied), Gardon and Schmidt-Boelter heat flux gauges (EPRI supplied), gas and wall thermocouples (EPRI supplied), and pressure sensors (SNLA and EPRI supplied). Local estimates of the heat transfer are provided for the calorimetry, and global averages are inferred from the pressure. Instrumentation "goodness" for each test has been assessed based on reviews of the raw data and on comparisons of local and global results.

A description of the NTS test facility and the instrumentation evaluated in this study are presented, and a description of the data analysis tool SMOKE is presented. Graphical and tabular results are provided for each of the twenty-one premixed combustion tests for which data were provided, and overall trends observed from the results are reported. Overall conclusions about the "goodness" of the instrumentation and the associated performance are also given. The information provided in this report should be useful for benchmarking existing computer codes used in modeling nuclear reactor containment response to degraded–core accidents and also for resolving issues pertaining to functionability of safety-related equipment in containments during such accidents. The results obtained from this study, coupled with results obtained from intermediate-scale combustion testing (*e.g.*, such as from the FITS and VGES facilities at Sandia Laboratories, Albuquerque), should also be useful in future modeling activities to upgrade the combustion and heat transfer models currently used in reactor safety computer simulations.

2 Experimental Facility and Instrumentation

2.1 NTS Dewar

The premixed and continuous–injection combustion experiments were performed in an existing facility located at test cell C, Nevada Test Site (NTS). This spherical test vessel, shown in Figure 1, has a diameter of 15.85 m (2048 m^3 volume) and a design pressure of $\sim$ 700 kPa. The dewar is comprised of two concentric stainless steel spheres, each 19 mm thick with an intermediate layer of perlite insulation $\sim$ 1.0 m thick. The facility had previously been used as a hydrogen dewar and required renovation prior to commencement of the testing (details on these modifications are included in the EPRI final report on the NTS work [1][1]). In addition, the facility was modified to include the following:

- a heated-water spray system in the vessel, consisting of 16 or 17 Sprayco model 1713A hollow cone nozzles (each rated at 15 gpm) with the necessary control system and manifolding
- a boiler to generate 2.1 kg/s steam at 1000 kPa for vessel and gas preheating
- a hydrogen–steam manifold system and mixing chamber (outside the dewar) to deliver specified mixtures of combustible gas for premixed and continuous–injection combustion testing
- two mixing fans in the vessel, each rated at 2.4 m^3/s (5000 cfm), to be used for pretest equilibration and during some tests
- an air compressor (rating of 0.28 m^3/s (600 cfm)) to supply air to the mixing fans and primary spray pump air motors as well as for post-test purge and refill operations.
- a gas sampling system for pre- and post-test evaluations of the gas uniformity and combustion completeness.

In addition, hydrogen was supplied from gas cylinders in a tube trailer; after mixing with steam, it was injected into the dewar through a nozzle $\sim$ 2.0 m in diameter above the bottom either as a diffuse stream or as a jet depending upon the test configuration. A schematic of the facility, taken from [2], is provided in Figure 2. Additional details on the facility and on the features of the important systems incorporated for testing (in particular, the water spray system and gas sampling system) are given in [1] and [2].

[1] Numbers in brackets are the references cited in this work and are given in the References Section.

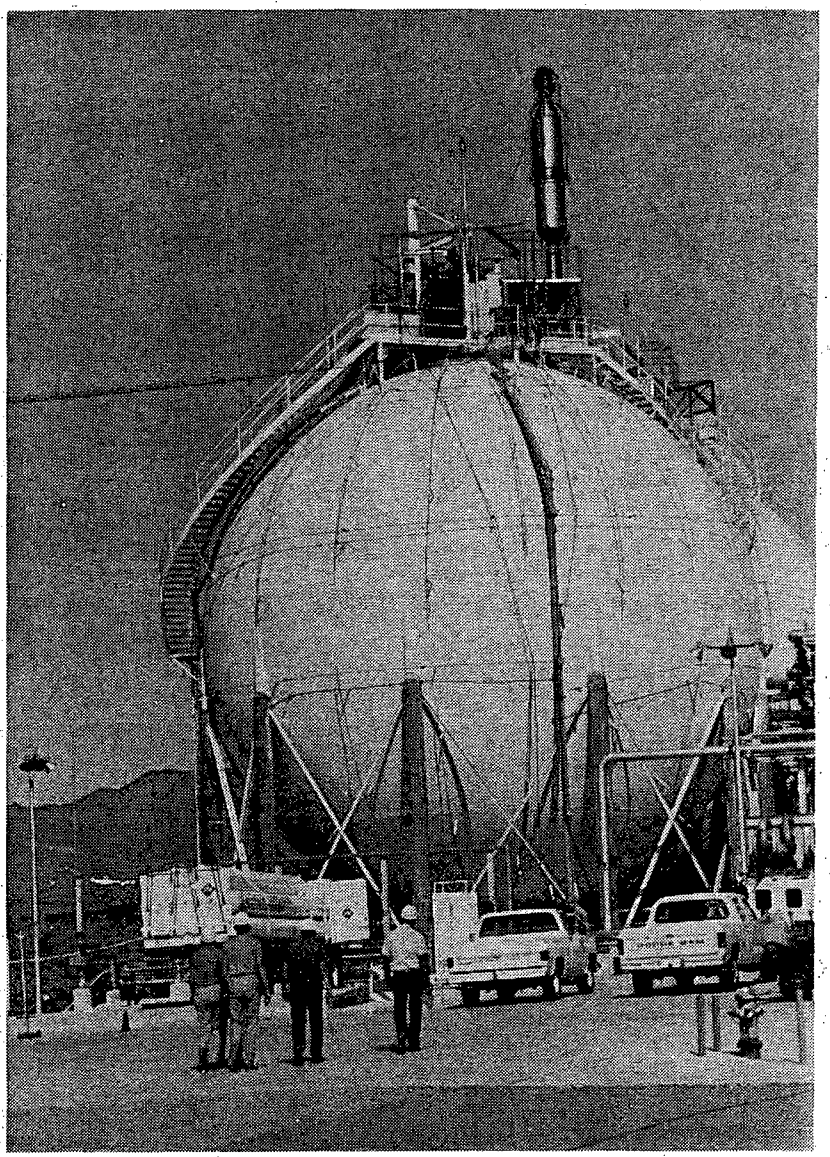

Figure 1: Hydrogen dewar located at test cell C, Nevada Test Site

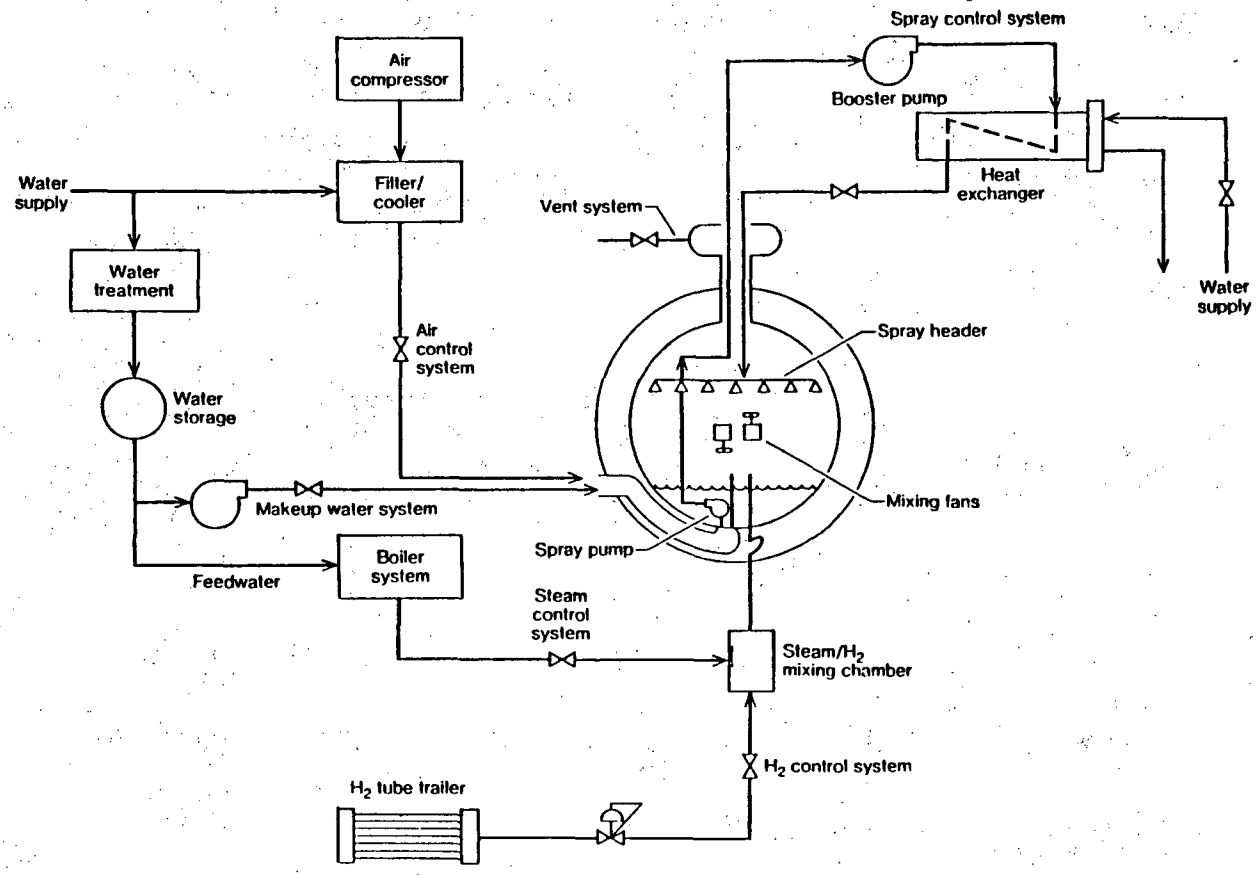

Figure 2: Mechanical schematic of the EPRI/EG&G Nevada Test Facility

The premixed combustion tests were initiated using ignition sources typical of those currently being installed in nuclear reactor containments for deliberate ignition safety systems. Six General Motors (GM) glow plugs and six Tayco coil igniters were mounted in the vessel as shown in Figure 3. The ignition sources were positioned to allow for combustion initiation on the central vertical axis of the sphere at the top, bottom, or center of the dewar and also along the vessel walls. Each ignition device was a hot surface (temperatures $\sim$ 1000–1400 K, depending on the input voltage) and each could be independently operated. For most of the premixed combustion testing, bottom ignition was utilized, although there are redundant tests in which the ignition site was changed to assess the effects of initiation location on combustion completeness and severity. Note that in this work, the general location of ignition (*i.e.*, bottom, top, etc.) will be provided for each test as opposed to the particular igniter. For the latter specifications, the reader will need to consult [1].

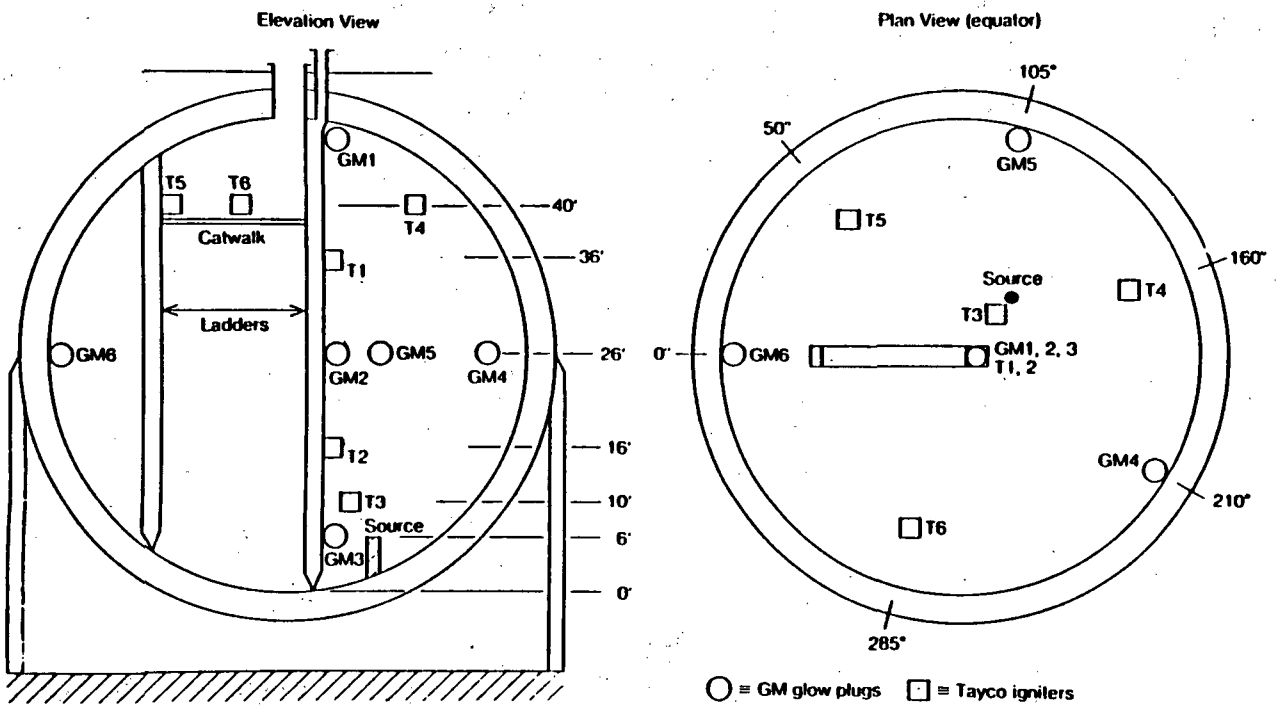

Figure 3: Igniter types and locations in the NTS dewar

A NEFF Instrument Corporation "System 720" data acquisition system was used to record and process data from each test. Figure 4 shows the data acquisition and control functions used in the test program. Included in this schematic is the remote unit, located at the top of the dewar, which was connected to the NEFF computer located in the manned trailer near the site. All data processing was performed on-site by EG&G and EPRI personnel. The data provided to Sandia for analysis was transformed from measured signals (*e.g.*, millivolts) to appropriate temperatures, pressures, and heat fluxes. Two sampling rates were used to record signals from several of the instrumentation. SNLA requested and received data traces recorded at the slower sampling rates which were used in this data evaluation. Again, for additional information on the data acquisition system, the reader should consult References [1-3].

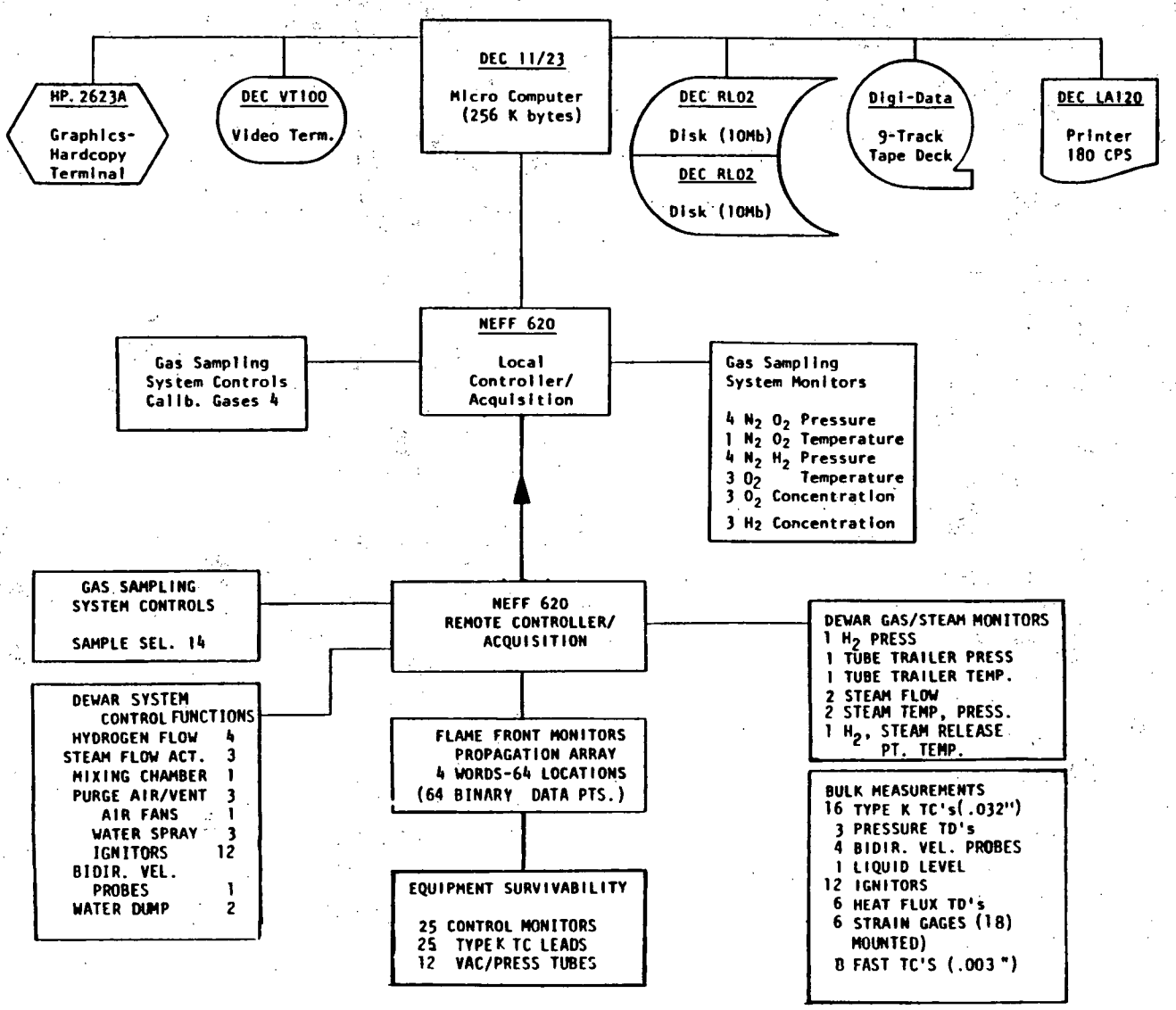

Figure 4: Data acquisition and control at the dewar (taken from Reference [2])

2.2 Analyzed Instrumentation

A significant quantity of instrumentation was installed in the dewar for the purposes of (1) providing data pertinent to quantifying combustion phenomena and (2) providing equipment-specific response data in combustion environments. Since the intent of this work has been to quantify the thermal environment in the dewar during and following combustion, only instrumentation included in the dewar for characterizing the environment has been evaluated (results pertinent to equipment functionability/survivability have been previously addressed in References [4-6] and will be included in the EPRI final report [7]). In Table 1, the instrumentation for this characterization is given along with a breakdown of what data were actually made available to Sandia for analysis. Note that testing was divided into two parts (referred to in this work as the Hydrogen Behavior and Equipment Survival Test Series) and that some of the instrumentation was available only for the latter test series.

Table 1: Instrumentation for Quantifying the Thermal Environment

Type of Instrumentation	Source‡	Number of Channels†		Test Series*
		Total	Sandia	
Pressure Sensors				
Capacitance	S	2	2	1 & 2
Strain Gauge	E	3	0–3	1 & 2
Dewar Temperature				
Gas Temperature (3-mil)	E	8	0–3	1 & 2
Gas Temperature (32-mil)	E	3	0–2	1 & 2
Wall Temperature (32-mil)	E	7	0–2	1 & 2
Total Heat Flux				
Gardon Gauge	E	1	1	1
Schmidt-Boelter Thermopile Gauge	E	5	5	2
Thin-film Gauge	S	1	1	1 & 2
Copper Slug Calorimeter	S	1	1	1 & 2
Brass Flat-Plate Gauge	S	3	3	2
Aluminum Cube	S	3	3	2
Radiative Heat Flux				
Gardon Gauge	E	1–2	1–2	1 & 2
Schmidt-Boelter Thermopile Gauge	E	2	2	2
Thin-film Gauge	S	1	1	1 & 2
Copper Slug Calorimeter	E	1	1	1 & 2

‡ Instrumentation provided by SNLA (S) or EPRI/EG&G (E)

† Total available from testing and quantity provided to Sandia

* Hydrogen Behavior (1) and/or Equipment Survival (2) Test Series

A listing of the pressure, temperature, and heat flux instrumentation for which data were provided for SNLA evaluation is given in Table 2 along with their respective locations in the Cartesian coordinate frame established by EPRI/EG&G.[2] The coordinate system origin is assumed to be centered in the dewar as shown in Figure 5. Figures 6, 7, and 8 provide schematic representations of the different instrumentation locations (defined in Table 2) as seen in elevation and plan views. A complete listing and appropriate discussion of the instrumentation is also included in Reference [1].

Brief descriptions of each type of instrumentation which was evaluated are provided in the following subsections. Further discussion of this instrumentation, pertinent to the modeling used in the data analysis, is provided in Section 3.

Pressure Sensors

Three sensors manufactured by Setra (models 270 and 204) were selected by EG&G and EPRI for pressure measurement. Two of these gauges were rated for 0–100 psi (gauges P101 and P102) and one for 0–50 psi (P103) pressure measurement, with frequency response quoted to range between 20 and 330 Hz, respectively. Initially, one of these gauges (P101) was installed in the dewar and two of the gauges were installed outside of the dewar at the ends of 6.35 mm O.D. thin–wall tubing which extended into the containment. The latter installation technique was used to thermally protect the sensing elements. Following failure of the internally mounted sensor (early in the Hydrogen Behavior Series), all three Setra sensors were mounted outside the dewar for the Equipment Survival tests in communication with the gas through tubing which ranged in length between $\sim$ 6.0 and 12.0 m [1].

In addition, Sandia supplied two strain-gage type pressure transducers manufactured by Precise Sensors, both of which were mounted inside the dewar. The transducers were of the same design (model 141-3) and both had response characteristics on the order of 1.0 kHz, but with two different sensitivities (0-100 psi (P104) and 0-200 psi (P105) full–scale ranges). These gauges were designed to operate without active water or air cooling. Felt-metal thermal protection was installed in front of each gauge sensing element to minimize thermal effects on gauge performance. Errors were estimated to be $\sim$ 1.4 kPa (0.2 psi) in reading the pressure and 0.001 mV (out of a full–scale output of 25 mV) in controlling and reading the voltage.

[2]For the Hydrogen Behavior Tests, J. E. Shepherd initially requested a limited quantity of data records which could be used to compare with the SNLA-provided instrumentation results. For the latter tests performed in the Hydrogen Behavior Series and for all tests of the Equipment Survival Program, additional instrumentation records were requested and received. In April 1984, upon initiation of this data evaluation work, additional data for gas and wall thermocouples and for the EPRI pressure sensors were requested. These data were not provided, since the data recording system had been previously dismantled.

Table 2: Evaluated Instrumentation from NTS Tests

Instrumentation Designation	Source SNLA/EPRI	Test Series†	Location in Dewar* (x,y,z)	Figure/Symbol
Pressure Sensors				
P101	EPRI	2	0,0,21	6/ 1
P102	EPRI	1 & 2	-5,-5,0	6/ 2
P103	EPRI	2	-5,-5,20	6/ 3
P104	SNLA	1 & 2	-1,-1,26	6/ 4
P105	SNLA	1	16,0,6	6/ 5
		2	16,0,-20	6/ 6
Gas Temperature (3-mil)				
T101	EPRI	1 & 2	1,-2,19	7/ 1
T102	EPRI	2	-1,-1,1	7/ 2
T105	EPRI	1 & 2	-10,-15,19	7/ 3
Gas Temperature (32-mil)				
T114	EPRI	1	9,0,21	7/ 4
T118	EPRI	1 & 2	20,0,0	7/ 5
T151	EPRI	1 & 2	-5,-5,6	7/ 6
Wall Temperature (32-mil)				
T120	EPRI	1 & 2	-2,-3,26	7/ 7
T121	EPRI	1 & 2	-18.4,1,18.4	7/ 8
Gardon Gauge‡				
H105 (R)	EPRI	1 & 2	1,3,25.5	8/ 1
H106 (T/R)§	EPRI	1 & 2	0,3,25.5	8/ 2
Schmidt-Boelter Gauge‡				
H501 (R)	EPRI	2	1,-2.5,2	8/ 3
H502 (T)	EPRI	2	1,-2.5,2	8/ 4
H503 (T)	EPRI	2	1,-2.5,2	8/ 5
H504 (T)	EPRI	2	14.5,-2.5,2	8/ 6
H505 (R)	EPRI	2	-4.5,-2.5,2	8/ 7
H506 (T)	EPRI	2	-4.5,-2.5,2	8/ 8
H507 (T)	EPRI	2	-4.5,-2.5,2	8/ 9
Thin-film Gauge‡				
H231 (R)	SNLA	1 & 2	2,4,25	8/ 10
H232 (T)	SNLA	1 & 2	1,4,25	8/ 11
Copper Slug Calorimeter‡				
H103 (R)	SNLA	1 & 2	14,-3,21	8/ 12
H104 (T)	SNLA	1 & 2	14,-4,21	8/ 13
Brass Flat-Plate Gauge‡				
T501, T502, T503 (T)	SNLA	2	-3,-2.5,2	8/ 14
Aluminum Cube‡				
T504, T505, T506 (T)	SNLA	2	-3.5,-2.5,2	8/ 15

† Hydrogen Behavior (1) and/or Equipment Survival (2) Test Series

* Approximate coordinate locations (Figure 5) are given in units of feet. Instrument positions are shown in Figures 6-8; numbers after the figure numbers locate the instrumentation

‡ Radiative (R) or Total (T) instrumentation

§ Gauge H106 was re-configured from a total to a radiative gauge prior to NTSP08

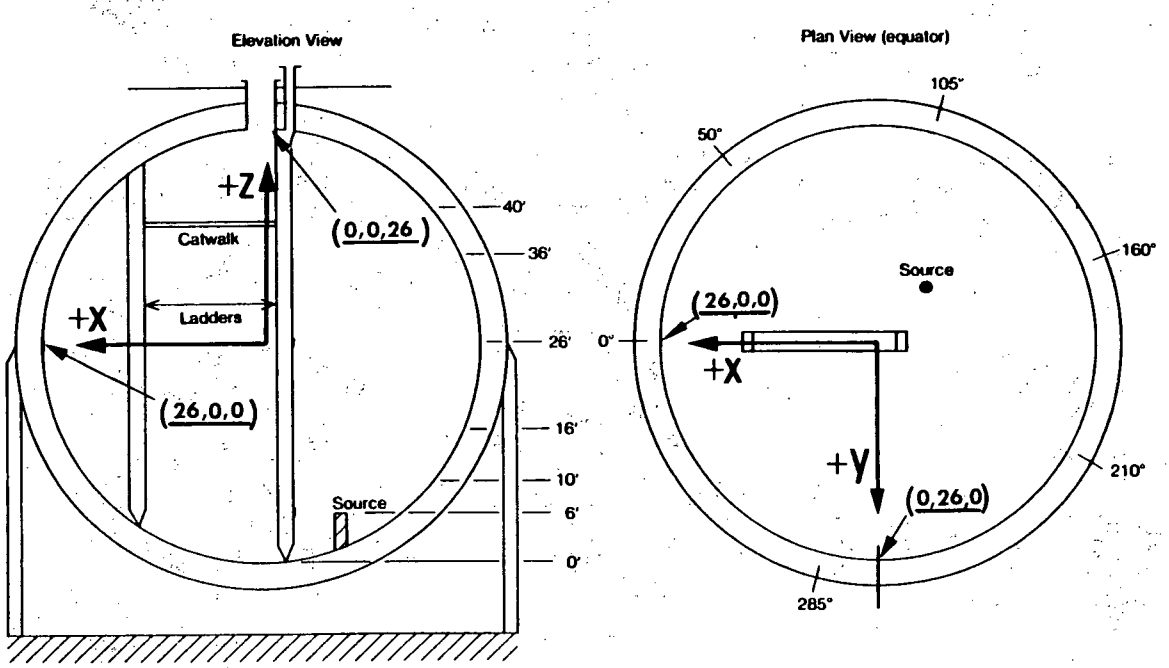

Figure 5: Coordinate system used to define instrumentation locations in the dewar

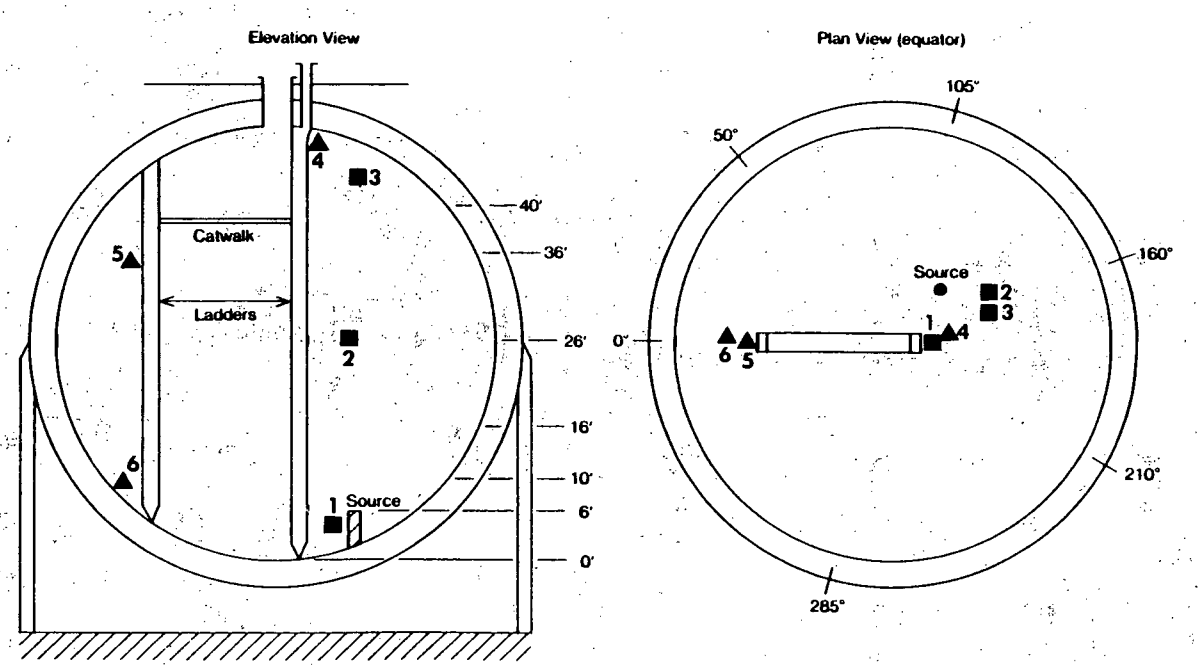

Figure 6: Schematic of pressure instrumentation locations in the dewar; see Table 2 for identification of specific sensors

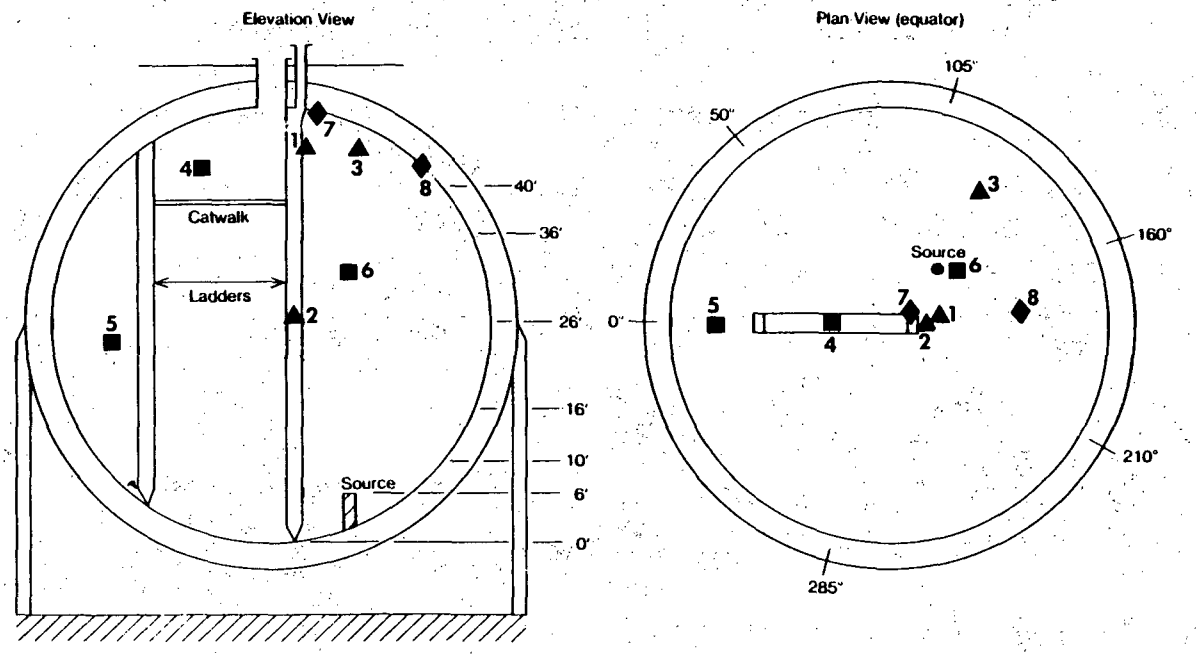

Figure 7: Schematic of thermocouple instrumentation locations in the dewar; see Table 2 for identification of specific sensors

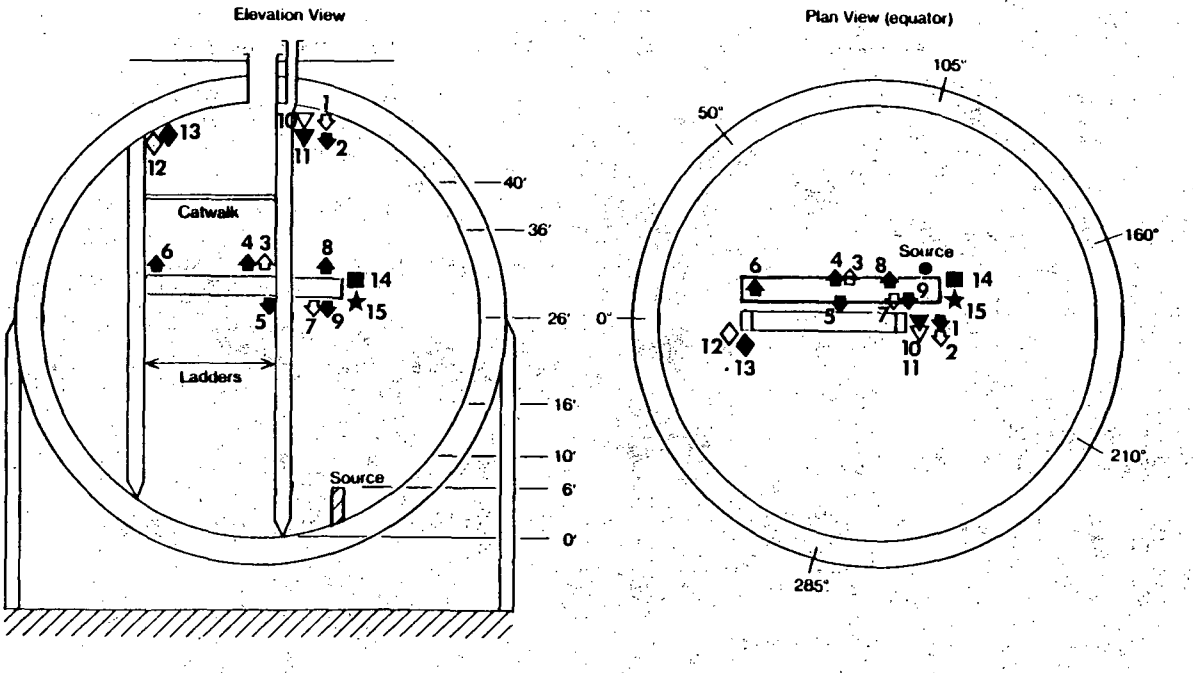

Figure 8: Schematic of heat flux instrumentation locations in the dewar; see Table 2 for identification of specific sensors. Filled symbols are total calorimeters and open figures are radiative calorimeters. The equipment platform was actually directly under the catwalk but has been moved in plan view to facilitate review of instrumentation placements

Temperature Measurement Instrumentation

Chromel-alumel thermocouples obtained from Omega Engineering, Inc., were used to measure gas and wall temperatures in the dewar. Quick-response (quoted at 1 Hz), 3-mil and more durable 32-mil (with much slower response characteristics) grounded sheathed thermocouples were used for measuring the gas temperatures. In addition, 32-mil thermocouples were mounted to the dewar walls.

Gardon and Schmidt-Boelter Thermopile Gauges

Two Gardon gauges, obtained from Medtherm Corporation, were installed near the top of the dewar and used throughout both test series. These gauges operate in the following manner [8]: heat is absorbed in a thin metallic circular foil and is conducted radially to the copper heat sink attached to the periphery of the foil; the difference in temperature is taken between the center and edge of the foil and related to the heat transfer rate. Initially, one of the gauges was configured as a total gauge and one as a radiative gauge by inclusion of a sapphire cover. During the latter part of the first test series, prior to test NTSP08, the total Gardon gauge was reconfigured to be a radiative calorimeter. Apparently, air-purge features to limit condensation on the sapphire cover were not incorporated for the radiative gauges. The two Gardon gauges were not water-cooled for tests in the Hydrogen Behavior Series; water-cooling was made available during the Equipment Survival Test Program [9].[3]

Seven Schmidt-Boelter gauges (five configured as total and two as radiative gauges) were used in the Equipment Survival test series. These gauges operate as capacitance calorimeters, with heat being absorbed at the front surface and being transferred to a plane upon which a thermopile is mounted. The measured temperature difference is then related to the heat flux. The gauges were installed on the equipment platform interspersed between the safety-related equipment tested by EPRI/EG&G as shown in Figure 9. All Schmidt-Boelter gauges were water-cooled, and the radiative gauge sapphire covers were also air-purged to reduce condensation. The specific gauge locations on the platform, as well as their orientation, are given in Table 3.

[3]Several discussions with J. Haugh of EPRI on these matters resulted following initial data processing. His review of the experimental log books and of photographs taken at various stages of testing were used to resolve uncertainties about gauge water-cooling and the other mentioned uncertainties.

Table 3: Location and Orientation of Schmidt-Boelter Gauges

Instrumentation	Configuration	Location†	Orientation‡
H501	Radiative	B	Up
H502	Total	B	Up
H503	Total	B	Down
H504	Total	C	Up
H505	Radiative	A	Down
H506	Total	A	Up
H507	Total	A	Down

† A = A location (above the gas inlet source)
B = B location (near dewar centerline)
C = C location (closest to dewar wall near off-axis rake)
‡ Instrumentation views top (Up) or bottom (Down) of dewar

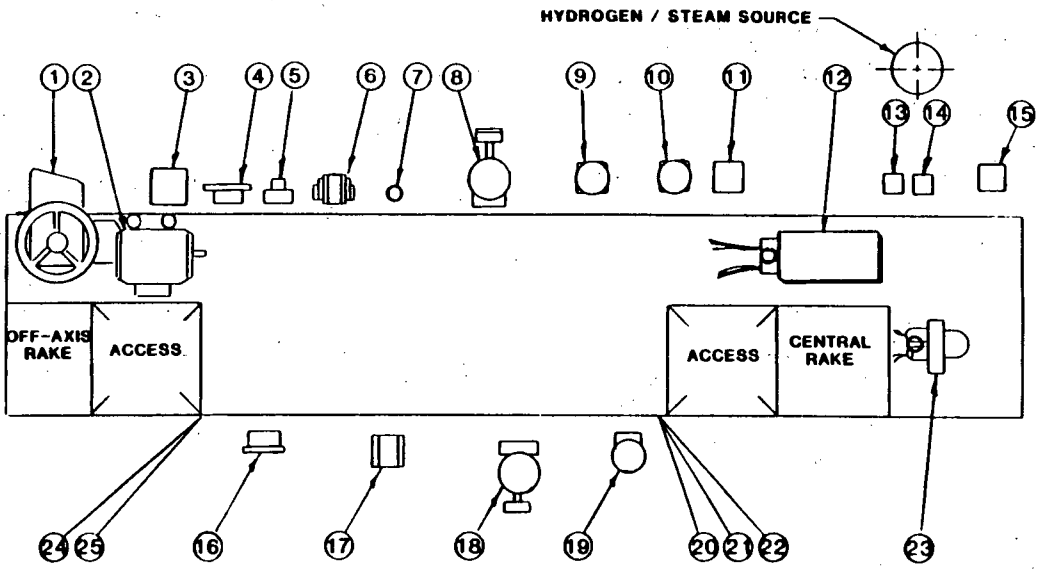

Figure 9: Schematic of instrumentation and equipment placements on the equipment platform

Thin-film Gauges

Sandia provided two thin-film heat flux gauges which were installed near the top of the dewar and which operated during all tests in the dewar. The thin-film gauges were developed by J. E. Shepherd [10] and were fabricated at SNLA. These types of gauges had previously been used in combustion work at the Sandia Fully Instrumented Test Site (FITS) and had been shown to be robust and responsive devices (*i.e.*, fractions of a millisecond response times) for measuring the highly transient heat transfer rates associated with combustion [11]. Each gauge consisted of a 300-Angstrom-thick platinum resistance element vapor-deposited on the polished front surface of a synthetic glass ceramic MACOR substrate ~ 100 mm (4.0 in) in diameter and ~ 50 mm (2.0 in) thick. The front surfaces were covered with a protective coating of Al_2O_3 and then with a layer of highly absorptive, spectrally flat NEXTEL paint. The MACOR substrate was mounted in a protective stainless-steel housing with only the front surface exposed. One of the thin-film gauges was configured as a radiative calorimeter by including a 6.35 mm (0.25 in) thick sapphire window over the sensing element and evacuating the space between the cover and MACOR surface. An electrical heater unit was also provided for the radiative gauge to maintain the sapphire cover at elevated temperatures to limit steam condensation effects. Figure 10 provides post-test photographs of the total and radiative thin-film gauges after removal from the dewar.

The gauges operated in the following manner. A constant current of 10 mA was applied to the resistance element and the voltage drop across the element was monitored. From the voltage drop, the resistance of the sensing element could be determined, and from previously calibrated resistance-temperature characteristics, the gauge front surface temperature could be determined. These calibration data were provided by Sandia and were included in the data processing work performed on-site using the NEFF computer system.

Copper Slug Calorimeters

Two capacitance (slug) calorimeters, developed by J. E. Shepherd and fabricated at Sandia [10,11], were provided for radiative and total heat flux measurements during the two test series. These calorimeters consisted of a 35.5 mm (1.4 in) diameter copper (OFHC) disk mounted on an MACOR insulating substrate. Each front surface was coated with NEXTEL paint, and the sensing element was a chromel-alumel intrinsic thermocouple, constructed by brazing the 10-mil thermocouple wires to the back surface of the disk. The radiative and total calorimeter disks were 0.5 mm and 1.4 mm (0.019 and 0.056 in) thick, respectively. As with the thin-film radiative gauge, one of the slug gauges was configured as a radiative calorimeter by including a 6.35 mm (0.25 in) thick sapphire window over the sensing element and evacuating the space between the cover and copper surface. This calorimeter also included an electrical heater unit to limit condensation on the sapphire. The protective housing for the slug calorimeters was comparable to that of the thin-film gauges, shown in Figure 10.

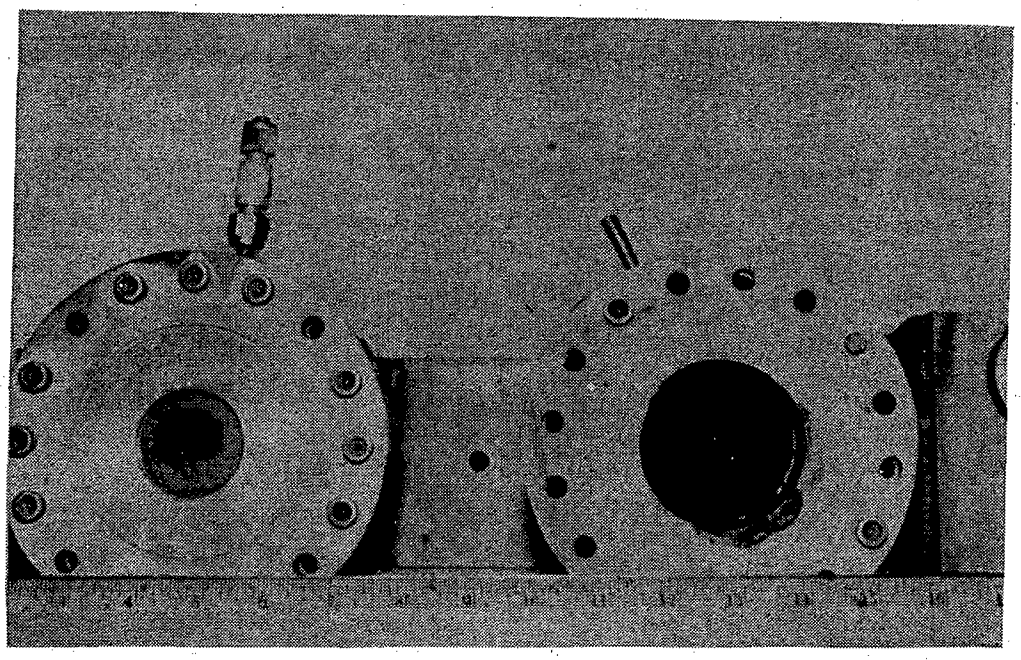

A: Front View of Thin-Film Gauges

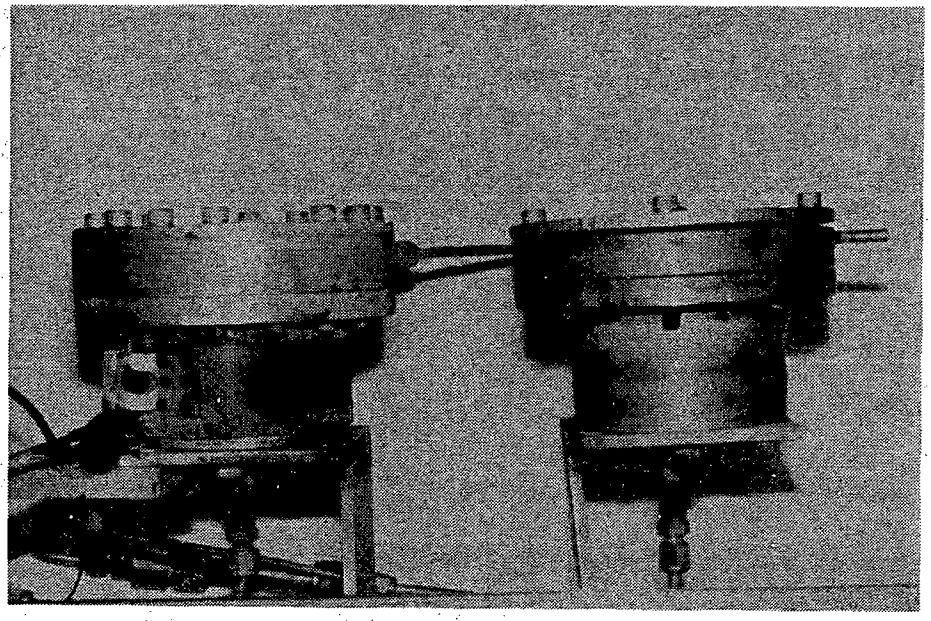

B: Side View of Thin-Film Gauges

Figure 10: Post-test photographs of the thin-film gauges used at NTS

Brass Flat-Plate Gauge

A flat-plate calorimeter, comprised of a 0.5 mm (0.020 in) thick, 0.15 m (6.0 in) square brass plate fastened to a 12.7 mm (0.50 in) thick rigid felt insulation, was provided by the Hydrogen Burn Survival (HBS) Program at Sandia for measurement of the total heat flux. This type of calorimeter had previously been used in equipment survival studies conducted at FITS [12] and at the Central Receiver Test Facility (CRTF) at Sandia [13]. Three 5-mil chromel-alumel thermocouples were mounted to the back surface of the brass using epoxy. The front surface of the calorimeter was coated with NEXTEL black paint. This gauge was installed on the equipment platform (see Figure 9) for use during the Equipment Survival Test series.

Aluminum Cube

The hollow cube calorimeter, provided by the HBS Program at Sandia to measure total fluxes, was a 0.1 m (4.0 in) cube fabricated out of 3.2 mm (0.125 in) thick aluminum. As with the flat-plate calorimeter, this type of capacitance calorimeter had previously been used in equipment survival studies conducted at FITS and at the CRTF at Sandia [12,13]. The exterior surface was black anodized and three chromel-alumel thermocouples were epoxied near the centers of three interior surfaces (orientation of top and two sides when installed in the dewar). The thermocouple wires were fed through a 25 mm (1.0 in) diameter hole on the NTS-configured downward-facing surface, which was then covered with tape. The cube was positioned on the equipment platform near the center rake above the gas injection source (see Figure 9).

2.3 Test Procedures

Typical operating procedures for the premixed combustion tests were as follows:

- The dewar was first preheated (if required) by injection of steam and by spraying heated liquids into the dewar. All tests occurred at saturated conditions, with temperatures ranging from ~ 300 K to 360 K. Spray systems and fans were operated to bring the environment to a quasi-uniform heated state. The environment was monitored using pressure sensors and gas and wall thermocouples. The intent was to increase the dewar wall temperatures prior to testing to minimize condensation effects.

- After the vessel reached the desired preheat conditions, hydrogen and steam mixtures were introduced into the dewar from the mixing chamber. Spray systems and fans remained on to mix the gas. Pretest gas sampling from three (of six total) points in the dewar was used to verify that uniform gas mixing had occurred prior to initiation of combustion. In addition, gas and wall temperatures were monitored.

- Following quasi-equilibration of the gas and walls of the dewar, the spray systems and fans were turned off (unless the test called for the systems to be operative), a delay (~ 10 minutes) allowed for further equilibration, and then the desired ignition source was initiated. Combustion normally began some 20–80 seconds later (time for hot sources to heat-up and ignite the local concentrations of hydrogen).

- Upon completion of the test, gas sampling was performed to estimate combustion completeness and uniformity. The dewar gas was then purged and replaced with ambient air in preparation for subsequent testing.

Note that for some of the lean hydrogen combustion tests, local conditions around the ignition sources were not immediately conducive for combustion or that combustion would be limited only to upward propagation.[4] In these instances, different igniters were triggered or spray systems and/or fans were operated again to facilitate combustion. Further, in one of the continuous–injection tests, the initial mixture of hydrogen and steam could not be ignited. Upon completion of the gas injection, the fans were used to mix the gases, resulting in a premixed combustion environment which was then ignited (test NTSP08 as designated in this work). For additional discussion on operating procedures used in the testing, see Reference [1].

[4] Such situations were expected by the NRC; tests were specified by the NRC during pretest condition selection meetings to better assess these combustion initiation and completeness uncertainties.

3 Data Analysis

The data analysis work performed at SNLA was restricted to operating on those data records which were provided on computer tapes. As indicated in the previous section, the raw data recorded for each piece of instrumentation were processed by EPRI/EG&G into temperature, pressure, and heat flux results some of which were then written onto tapes for SNLA use. These data were processed using pretest series instrumentation calibrations, and do not account for variations which might have occurred as a result of the instrumentation being exposed to the severe environments. In this work, the results provided by EPRI/EG&G are assumed to be correct, and no attempt has been made to modify the signals based on post-test calibrations or based on our interpretations as to how the instrumentation actually functioned (instead of how it was expected to operate).

The data analysis activities consisted of three major parts as described below:

- Data preprocessing – Taking the data files provided on computer tape, reducing the number of time-signal pairs to usable quantities by eliminating redundant and off-scale data and reorganizing the data into forms more compatible for SNLA analysis.

- Data processing – Smoothing or fitting the data, if necessary, and then operating on the data using SMOKE, a suite of computer codes developed at SNLA.

- Data interpretation – Analyzing the data and results obtained from SMOKE processing and comparing results from different tests to determine instrumentation "goodness" and the applicability of the results.

In this section, the preprocessing and processing steps defined above are discussed. The results and our assessment of the data are provided in Section 5. Included in this section is a description of SMOKE and of the modeling theory used in the SMOKE data analyses. These descriptions are intended to be cursory. For additional information, the reader should consult the SMOKE documentation [14].

3.1 SMOKE Description

SMOKE is a suite of computer codes developed at SNLA to expedite the analysis and interpretation of data from confined premixed combustion experiments. This data analysis package includes computer codes for organizing the data, processing the data, and presenting results. It was initially developed for analyses of data from FITS and VGES to provide estimates of the peak heat fluxes (radiative and total) and cumulative energy depositions from different calorimeters as well as those inferred from the pressure signals. Modifications to the computer codes were performed to generalize the algorithm, and to allow for analyses of the Gardon and Schmidt-Boelter gauges, the

HBS instrumentation, and the wall and gas thermocouple data. In addition, preprocessing computer codes were modified and created to organize the data records into SMOKE-compatible formats.

A schematic of the flow sequence of SMOKE, as utilized in the NTS data analyses, is given in Figure 11. Discussion of the preprocessing and processing activities performed in SMOKE are given in the following two sections.

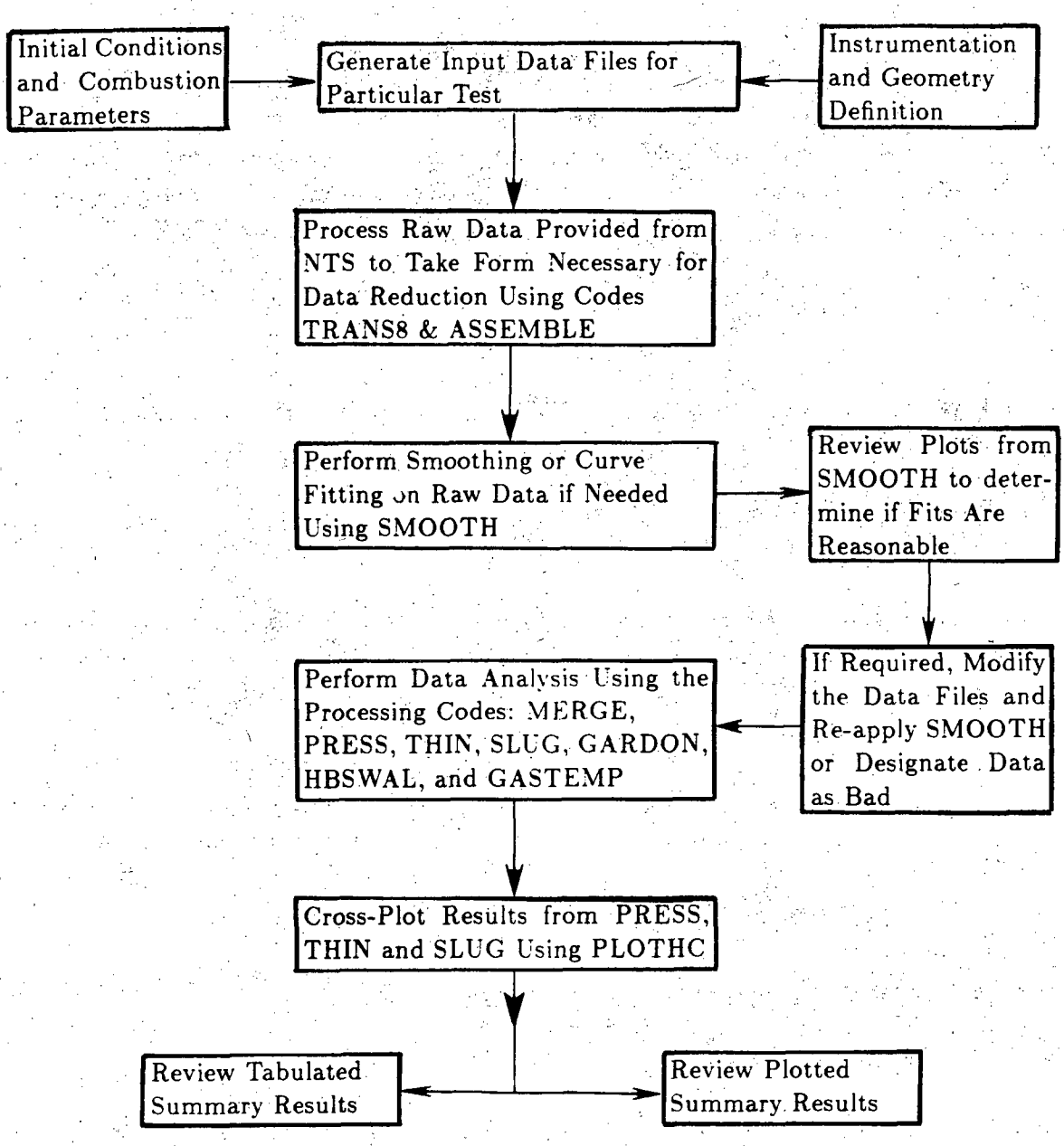

Figure 11: Schematic of SMOKE operation

3.1.1 SMOKE Data Preprocessing

Data preprocessing in SMOKE was accomplished in two steps: (1) selective "culling" of the time-data pairs and subsequent arrangement into formats required for use in SMOKE processing computer codes and (2) smoothing or fitting of calorimetry data to reduce signal noise and curve fitting of the pressure data to provide smooth signals and first derivatives needed for the pressure signal processing. In addition, subsidiary data input files containing the precombustion conditions in the dewar, estimates of combustion completeness, and geometry specifications were generated during preprocessing as shown in Figure 11.

The computer tapes provided by EPRI/EG&G consisted of data records for 6 to 35 pieces of instrumentation depending upon the test. Typically, over 2000 time-data pairs were provided per instrument for test durations ranging between 400 and 1000 seconds following completion of combustion (typical sampling rates of 0.04 seconds and greater). Much of the data were redundant or oscillated about some mean value. Since much of the data was, therefore, unimportant for quantifying the postcombustion environment, a data "culling" computer code, TRANS8, developed by J. Shepherd, was utilized to select 200-500 time-data pairs appropriate for analyses.

The TRANS8 code operates as follows: it reads all the data pairs, locates the minimum and maximum values, and counts and orders the number of different incremental values between adjacent data. TRANS8 then selects a minimum increment for the data, such that less than 500 data pairs are available for analysis and writes these data pairs to files. In addition, TRANS8 provides histograms of the data incremental distributions and plots of the selected data. If the data are found to be too sparse (in this work, less than 20 good time-data pairs), then TRANS8 omits the data file. This latter feature of TRANS8 served as the initial assessment of data "goodness".

Following the "culling" exercise of TRANS8, the plotted data files were reviewed, and obviously "bad" data records were omitted. At this point, data were judged bad only if (1) they were physically incorrect (*i.e.*, negative temperatures, pressures, etc.,) or (2) if the data were so noisy or oscillated so much that future processing would be meaningless. Data considered to be "good" in this exercise were then ordered into SMOKE-compatible formats using the code ASSEMBLE. This operation combined the different data pairs into 12 data files with each file having common time frames (using linear interpolation). For cases where data were bad, null files were generated and "flags" were provided internal to the data sets to prevent further data analysis.

The data files generated by ASSEMBLE which contained gas temperature data or Gardon, thin-film, and Schmidt-Boelter gauge data were then ready for SMOKE processing. For all other data sets, additional data preprocessing using the computer code SMOOTH was available if needed. SMOOTH is an interactive code which operates on the data using smoothing filters or a rational-function fit. The smoothing filter used in this work was a Hanning filter of user-specified width. The rational-function fit allows the user to specify the orders of the numerator and denominator polynomials comprising the curve fit. This latter option is particularly useful for obtaining continuous data

and first derivatives for the data. Details on the "smoothing" options in SMOOTH are given in [14].

In the NTS data analysis work, all pressure signals were preprocessed using the rational-function fit, since smooth, continuous first derivatives were needed to estimate the total heat transfer rates following combustion. Only the pressure data for times after the peak pressure were fit, since pressure signal processing in SMOKE is only for postcombustion times. The usual rational-function fit used was a third order polynomial for the numerator and a second order polynomial for the denominator. A comparison of typical pressure data before and after smoothing with the rational-function fit is given in Figure 12. All other signals which were preprocessed using SMOOTH were treated with a Hanning smoothing filter with half-widths ranging between 2 and 10 data points. A typical 'before and after' data file for a total slug calorimeter data set (using a half-width Hanning filter of three) is shown in Figure 13.

3.1.2 SMOKE Data Processing

SMOKE data processing was initiated upon completion of the smoothing and curve fitting operations. The data processing was performed using the seven computer codes listed in Table 4.

Table 4: SMOKE Data Processing Computer Codes

Computer Code	Instrumentation Processed or Major Purpose
MERGE	Performs AIC calculation† and creates files needed by other processing codes
PRESS	Pressure Sensors
THIN	Radiative and Total Thin-Film Gauges
SLUG	Radiative and Total Slug Calorimeters
GARDON	Gardon and Schmidt-Boelter Gauges
HBSWAL	Brass Flat-Plate, Aluminum Cube, and Wall Thermocouples
GASTEMP	Gas Thermocouples

† Adiabatic Isochoric Combustion calculation

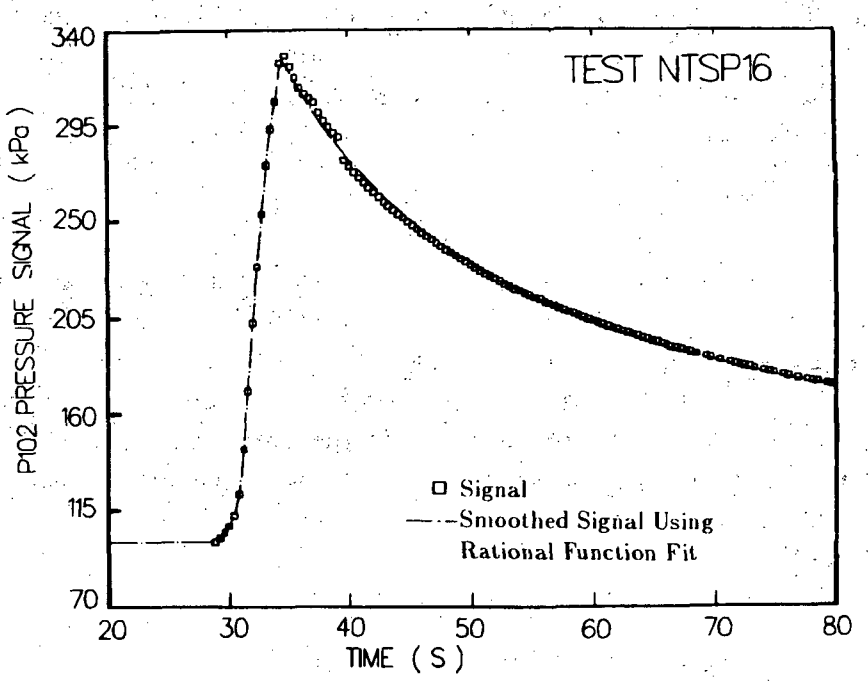

Figure 12: Comparison of data for pressure sensor P102 (test NTSP16) before and after using the rational-function fit

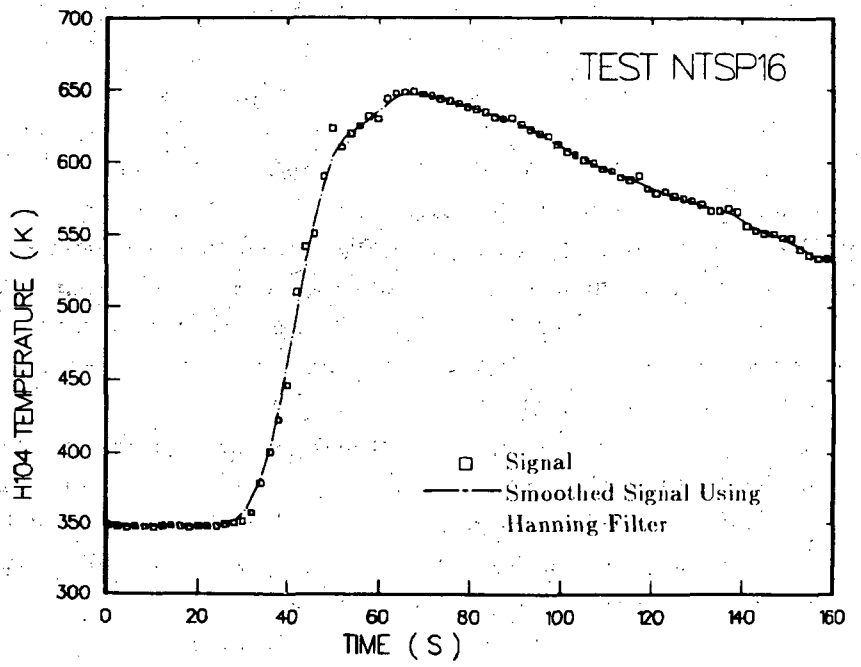

Figure 13: Comparison of data for total slug calorimeter H104 (test NTSP16) before and after smoothing using the Hanning filter option

Brief descriptions of the important computer codes of SMOKE which process the data are given below. In addition, cursory descriptions of the modeling theory and of the associated pertinent assumptions incorporated in these analyses are provided. Reference [14] provides additional details on the modeling procedures of SMOKE.

MERGE

MERGE locates the pertinent precombustion data, test geometry, and instrumentation data for a given test and orders them into files compatible for usage by other SMOKE computer codes. In addition, an adiabatic isochoric combustion (AIC) calculation is performed in MERGE using the precombustion data and combustion completeness estimates. These results are used in the pressure data processing work and provide upperbound gas pressure, gas temperature, and energy deposition estimates for comparison with the measured and processed data.

PRESS

PRESS processes pressure data for up to three sensors. Included in PRESS are subroutines for estimating the gas thermophysical properties, for computing gas absorptances and emittances, and for computing the vessel wall temperatures. "Hot-wall" (*i.e.*, no condensation) and "cold-wall" (*i.e.*, wall condensation is occurring) analysis options are also included to account for steam mass transfer effects after completion of combustion.

PRESS locates the maximum pressure and computes from the pressure signal an average gas temperature. "Global" (*i.e.*, average) estimates of the postcombustion radiative transfer and total energy transfer from the gas to the vessel walls are also obtained from PRESS. The associated average wall heat-up is estimated using the total heat flux as the heat input and solving the one-dimensional transient conduction problem for a slab (assuming an insulated back boundary and a constant slab thermal diffusivity α_w). Estimates of combustion duration are also obtained from the pressure signal processing, based on the time from combustion initiation to the peak pressure and to the time of maximum total heat transfer from the gas.

Data processing in PRESS is based on the following modeling theory. For a closed vessel, information about the global heat transfer rate following combustion can be inferred from the pressure-time records, as first suggested by Means and Ulrich [15]. The global heat transfer rate is proportional to the time derivative of the pressure, and the radiative loss rate is related to the absolute pressure (through the temperature). A schematic of the important steps followed in pressure signal processing is provided in Figure 14 for tests in which steam condensation effects are unimportant. For this case, the gas concentration is assumed constant and is obtained from an AIC calculation. The average gas temperature is then calculated from the pressure using the ideal gas equation of state. The total heat transfer rate (q_T) is the product of the pressure derivative, the vessel volume-to-area ratio (V/A), the gas specific heat (C_v), and the

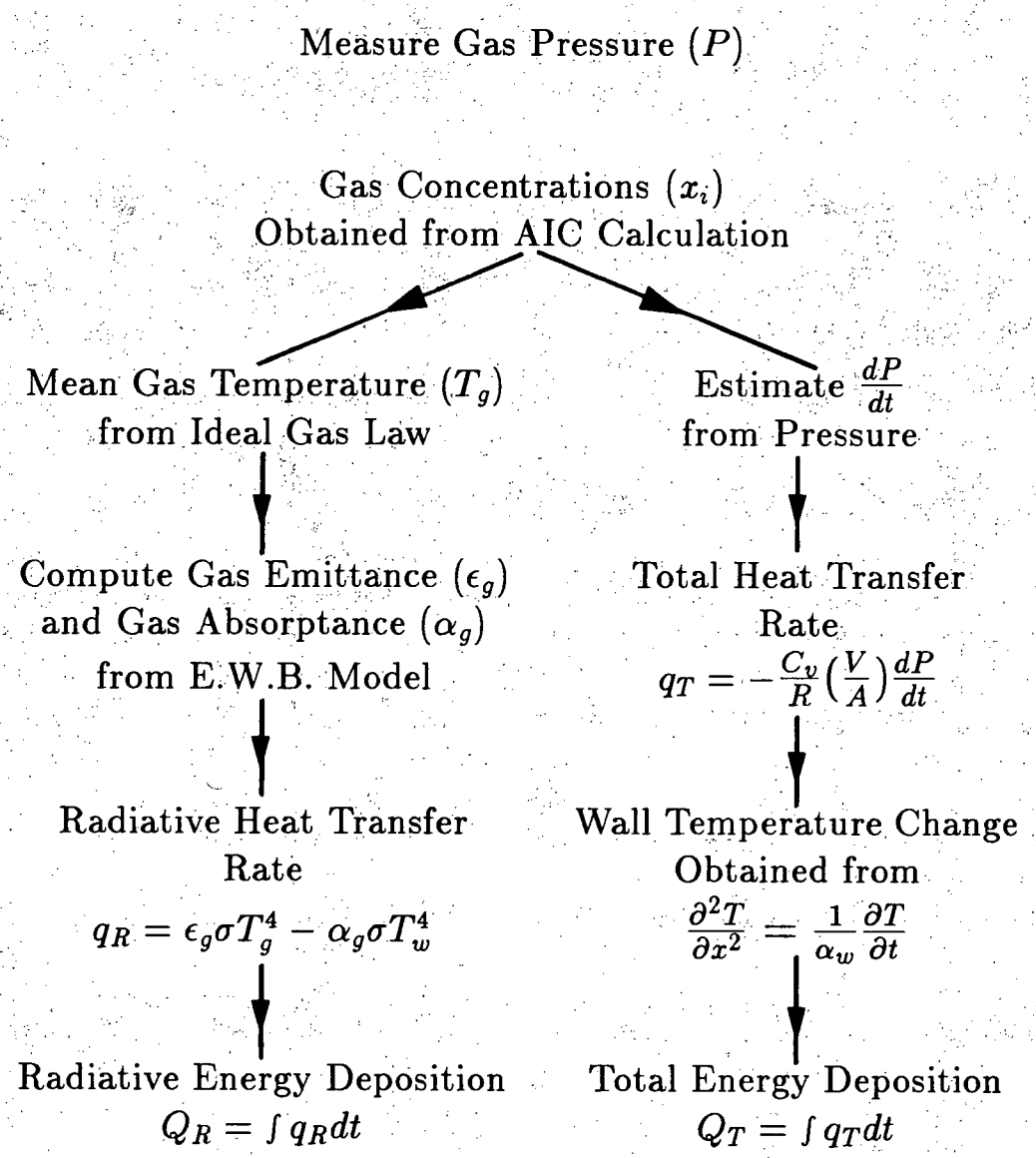

Figure 14: Schematic of pressure data processing when steam condensation is unimportant

gas constant (R):

$$q_T = -\frac{C_v}{R}\left(\frac{V}{A}\right)\frac{dP}{dt}. \quad (1)$$

The radiative heat transfer (q_R) is the difference between the energy emitted from the gas and that reabsorbed by the gas from the walls, as given by Eq.(2).

$$q_R = \epsilon_g \sigma T_g^4 - \alpha_g \sigma T_w^4 \quad (2)$$

The dewar walls are assumed to be radiatively black surfaces. The gas emittance (ϵ_g) and absorptance (α_g) are computed using an exponential wide-band (E.W.B.) model [16] and depend on the gas composition, gas temperature (and wall temperature for the absorptance), gas pressure, and a characteristic radiating beam length. This length is equal to two-thirds the dewar diameter.

When steam condensation effects are negligible, the difference between the total and radiative heat transfer is the convective heat transfer rate. The analysis is more complicated when condensation occurs on the vessel walls during a test. Specifically, the time rate of change of the mass of the steam must be included in the derivative of the state equation and the total heat transfer rate. Since the steam concentration is not measured during testing, the condensation rate must be inferred from the pressure using the extended Chilton-Colburn analogy [17] to relate the mass transfer and convective heat transfer coefficients. This analysis is based on the classic film analysis of diffusion and accounts for the thermal interaction of the mass flux with the diffusive heat flux. Since the state, conservation, and rate equations are coupled, they must be solved simultaneously. Note that the analogy assumes saturation conditions; when the wall is superheated relative to the gas, the previously described "hot-wall" model is utilized. A more detailed description of this procedure is given in [14].

PRESS was not modified for the NTS analyses to account for water spray evaporation, and hence, heat transfer results are not provided for the tests with sprays operative. Similarly, estimates of the gas and wall average temperatures during the postcombustion cool-down are omitted since these results would be obtained from an analysis which couples the heat and mass transfer energy exchanges.

THIN

THIN operates on the data obtained from the total and radiative thin-film gauges. The thin-film gauges are modeled as one-dimensional devices, with temperature variations perpendicular to the gauge front surfaces. The platinum temperature is assumed equal to that of the front surface of the MACOR. This insulating substrate is large enough that it allows the calorimeter to be modeled as a semi-infinite medium for the times associated with combustion and with the early gas cooling (typically 20–100 s). Using the thermal properties of the MACOR and the front-surface temperatures, the surface heat flux is calculated from the numerical solution to the conduction problem in a one-dimensional semi-infinite slab [14]. It is also assumed that the MACOR is "cold" (relative to the combustion gases) during testing so that radiation heat losses

from the blackened gauges are negligible. Therefore, energy deposition results can be obtained for the thin-film gauges by integration of the heat fluxes.

When the thin-film gauge is configured as a radiative calorimeter, additional processing is required to account for the sapphire cover. A significant fraction of the radiation from the steam component of the combustion products occurs in the 6.3 μm vibrational band and the rotational band for gas temperatures less than 1000 K [16]. Since the sapphire is nearly opaque for wavelengths greater than 6.0 μm, the fraction of radiative heat flux attenuated by the cover must be accounted for. This absorbed fraction is computed in PRESS using the E.W.B. model [16] and can vary between 0.30 and 0.90 during gas cool-down. The correction factor F_c is applied according to Eq.(3), where q_R and q_{RU} are the corrected radiative flux and the radiative flux computed without accounting for the cover, respectively, and τ_c is the effective sapphire transmittance for wavelengths less than 6.0 μm ($\tau_c = 0.80$).

$$q_R = \frac{q_{RU}}{\tau_c(1 - F_c)} \tag{3}$$

Note that the sapphire transmittance depends upon the cover cleanliness and probably varied during a test series.

SLUG

The computer code SLUG operates on the data obtained from the total and radiative copper slug calorimeters. The copper slug calorimeters are modeled as one-dimensional devices, with temperature variations perpendicular to the gauge front surfaces. The thermal model consists of the copper slug with an insulating air gap of 25 mm (1.0 in) and a MACOR backing material 51 mm (2.0 in) thick. The back surface of the MACOR is assumed to be adiabatic. Back surface thermocouple data from the copper are used in the finite-difference inverse thermal conduction computer code SODDIT [18], which has been included in SLUG as a subroutine package. From these analyses, front surface temperatures and absorbed fluxes are computed. When the slug calorimeter is configured as a radiative gauge, the sapphire cover effects are accounted for in the same manner as described above for thin-film data processing.

The slug calorimeters operate as one-dimensional devices for only the early part of a test. Further, these gauges tend to heat-up rapidly leading to significant radiative and convective heat losses. Thus, energy deposition results from the slug calorimeters are typically very low and, although computed by SLUG, will not be provided in this work.

HBSWAL

The computer code HBSWAL, developed for the NTS data analysis, processes data from the HBS flat-plate and hollow–cube calorimeters and from the wall thermocouples. HBSWAL models each of these instruments as a one-dimensional slab and uses SODDIT to estimate the surface total heat fluxes from the thermocouple data.

The flat-plate calorimeter is modeled as a composite of 0.5 mm (20 mil) of brass with an insulating felt backing 3.2 mm (0.125 in) thick (actual thickness of felt is 12.7 mm). The back of the 3.2 mm insulating layer is assumed to be perfectly adiabatic. The aluminum cube is configured as a composite of aluminum and an insulating layer of air 38 mm (1.5 in) thick.[5] As indicated in Section 2, thermocouple data are measured at the interior surfaces of the aluminum and brass and are used in solving the inverse conduction problem for each calorimeter. Measurements from each thermocouple are analyzed individually, instead of using a single average temperature. Note that in this work, all thermocouple mounts are assumed to be perfect (*i.e.*, the epoxy used for fastening does not alter the thermocouple response for the calorimeter).

HBSWAL also processes the wall thermocouple data, assuming that the dewar wall acts a calorimeter with heat flow perpendicular to the surface. The stainless-steel back surface is modeled as adiabatic, and the front surface temperature is measured. A numerical direct conduction calculation is performed to obtain the net surface heat flux into the dewar.

As with the slug calorimeters, the instruments modeled in HBSWAL heat-up significantly during postcombustion times, and thus heat losses from the front surfaces become important. The energy deposition results obtained from the integration of the total surface fluxes are low as a result, and do not accurately reflect the actual gas-cooling phenomena. The heat flux data obtained from processing the cube and flat-plate calorimeters and the wall thermocouples are assumed to be accurate only for the very early times of the tests (through and beyond times of combustion).

GASTEMP

Program GASTEMP processes the gas thermocouple data to locate the maximum temperature and to determine the time from combustion initiation to the time of peak temperature. The latter quantity can be regarded as a measure of the local combustion duration. In addition, GASTEMP determines the time ($\Delta t_{T_{1/2}}$) at which the gas temperature is greater than the average of the initial and peak temperatures (referred to as $T_{1/2}$). This time, and the associated temperature $T_{1/2}$, provide a measure of the severity of the thermal environment.

[5] It is assumed that gas flow into the cube through the instrumentation feed-through is negligible and that all surfaces heat-up uniformly, thus avoiding significant internal natural convection effects.

GARDON

Program GARDON was developed specifically for the NTS work to process the EPRI/EG&G-provided Gardon and Schmidt-Boelter gauges to obtain peak heat flux and energy depositions. The peak heat fluxes are taken directly from the data records. The energy deposition results are obtained from Eq.(4), where q is the provided heat flux data and q_{off} is a baseline flux estimated from the late-time gauge response (see Figure 15).

$$Q(t) = \int_{t=0}^{t} (q(t) - q_{off}(t))\, dt \tag{4}$$

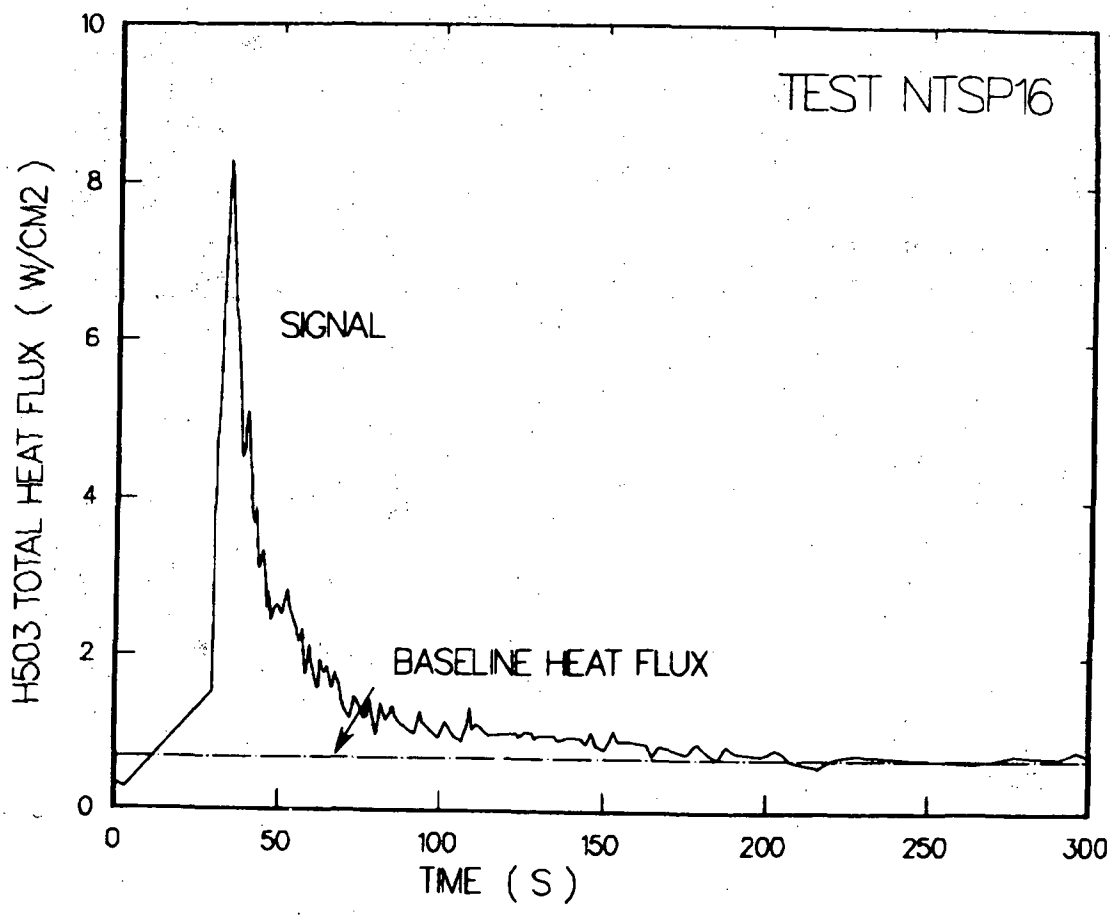

Figure 15: Typical heat flux record for Schmidt-Boelter gauge H503 (test NTSP16)

At times 100–300 seconds after completion of combustion, depending on the particular test, the gas pressure and gas temperature are essentially constant, suggesting that the cooling process is nearly completed. The Gardon and Schmidt-Boelter gauges still typically measure a fixed heat flux associated with the difference between the cooler sensing location and the surface. This baseline flux probably varies during testing; however, since temperature data are not available at the sensing location for this determination, it has been assumed that the baseline value is constant.

It should be noted that the radiative and total gauge signals are processed identically in GARDON. The radiative results provided by EPRI/EG&G supposedly accounted for the sapphire cover through the calibration factors. In reviewing the manner in which Medtherm calibrated the radiative gauges, we believe that the resulting radiative data are in error. The Medtherm calibration procedure [19] uses a blackbody source which is not representative of the steam-radiating spectrum. A significant fraction of the steam radiation is from radiating bands for which the sapphire cover is nearly opaque as was described previously. To correctly quantify the radiative calorimeter response, one would need to use calibration data for the gauge response without the cover, and then correct for the attenuation effects using Eq.(3). Unfortunately, there are no calibration factors for the gauges configured without the sapphire covers. Further, the pre- and post-test calibration data for the radiative gauges varied so significantly (as great as 50% differences) [1], that recalibration of the gauges without the cover would not help significantly. Thus, although the radiative Gardon and Schmidt-Boelter gauges were processed by SMOKE, there will be no presentation of these results.

4 Initial Conditions and Combustion Data

The EPRI/EG&G premixed combustion test program consisted of twenty-four tests using various mixtures of hydrogen (5 to 13% by volume) and steam (4 to 40%). Data were provided to SNLA for twenty-one of these tests. In two of the tests for which no data were received, there was either no combustion or the combustion completeness was so low that the tests were repeated with sprays/fans operative to affect more complete burning. For the third test for which no data were provided, the data acquisition system was inoperative necessitating a 'repeat' experiment.[6]

Nominal precombustion data (*i.e.*, initial conditions) and combustion parameters (*e.g.*, combustion completeness) for the twenty-one tests are provided in Tables 5 and 6, respectively. The tests from the two series have been grouped for presentation in increasing severity (*i.e.*, increasing hydrogen concentration) according to the following:

- Tests with sprays operative are grouped together regardless of other precombustion conditions (designated as 'Tests with Spray System Operative')
- Tests in which the dewar was heated, to allow for gas mixtures with steam concentrations greater than 10% (by volume), are grouped together (designated as 'Steam-Laden Tests')
- Tests in which the dewar was maintained at ambient conditions so that the steam concentration was nominally 5% (by volume), are grouped together (designated as 'Standard Tests')

In these tables, the tests are designated as 'NTS - P - xx', with the 'P' specifying that the test was a premixed combustion experiment and with 'xx' conforming to the EPRI/EG&G numbering system.[7] The dates provided for each test refer to dates given with the data records, and may not be the actual test date.

Initial conditions and combustion parameters were provided by L. Thompson of EPRI [20]. A description of the manner in which the combustion completeness was computed from gas sample results is given in Reference [1]. These data were assumed to be correct and were used as provided unless it was found during SMOKE processing that the measured peak pressure was greater than the peak pressure obtained from an adiabatic isochoric combustion (AIC) calculation. In these situations, the initial hydrogen concentration, the steam concentration, and/or the combustion completeness must be in error, since the AIC values are theoretical maximums obtained by

[6] Nominal precombustion conditions for test NTSP06 were identical to a test in which there was no combustion except that the fans were operative. Nominal precombustion conditions for test NTSP18 were identical to a test in which the combustion completeness was 8% except that sprays were operative. Test NTSP13 was equivalent to a test performed without the data acquisition system operative.

[7] EPRI/EG&G designated duplicate tests (*i.e.*, tests with the same initial conditions) in a given series with a prime. The prime notation is omitted in this work, and the only repeated test, designated as P9′ by EPRI, is referred to as NTSP9P.

neglecting heat losses during combustion. The combustion completeness was modified in these cases as indicated in Table 6 so that the AIC peak pressure would be greater (arbitrarily between 10–15% greater) than the measured values.[8] Figure 16 shows the combustion completeness data for the twenty-one tests plotted against initial hydrogen concentration.[9] Note also that suspended liquid volume percentage data, used in the AIC calculations when the spray system was operative, are provided in Table 6. These values were computed assuming that the spray–droplet fall distance was 10 m, that the droplet residence time in the dewar was known (based on terminal velocity estimates for the spray droplets), and that each Sprayco-1713A nozzle provided 3.4 m^3/hr (15 gpm) water flow. Seventeen nozzles were assumed to be operative for all sprays-operative tests except for test NTSP02, in which sixteen nozzles were used.

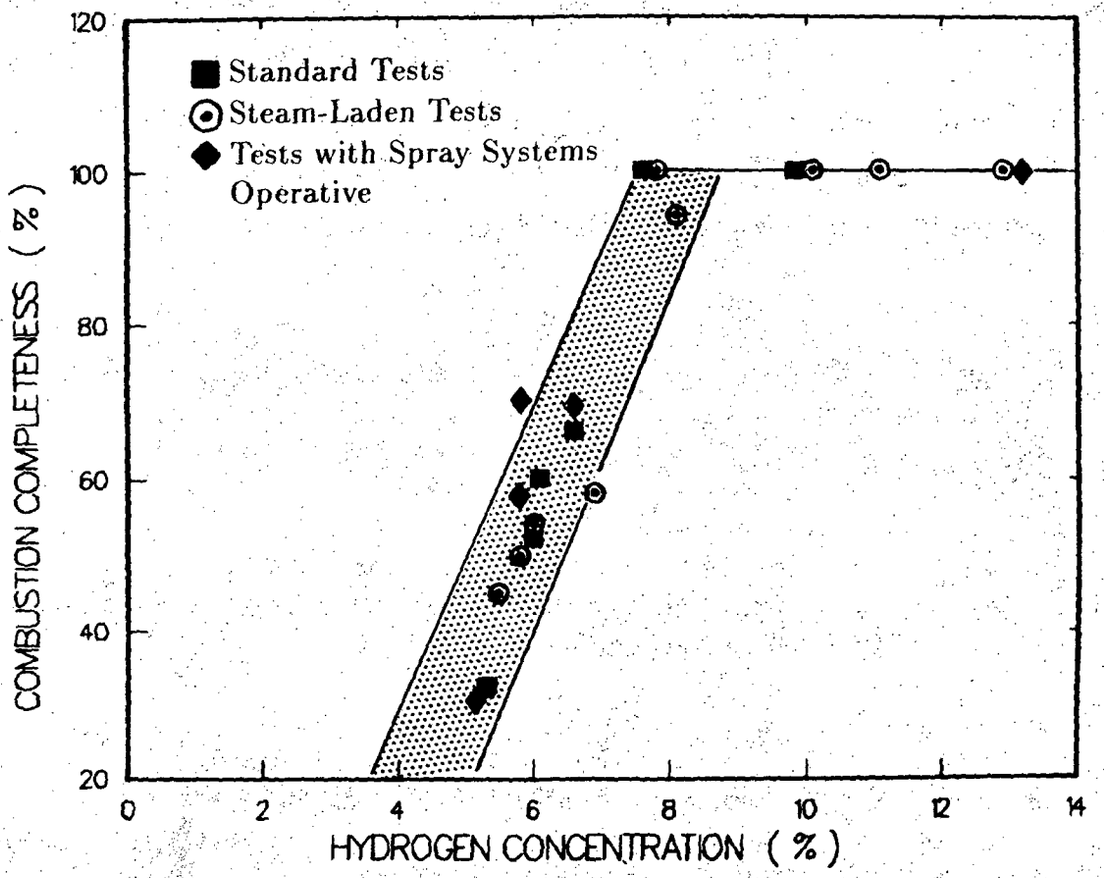

Figure 16: Combustion completeness for NTS premixed combustion tests

[8]Discrepancies between the measures maximum pressures and the AIC pressures were noted for three tests (see Table 6) of the Hydrogen Behavior Series. These lean combustion tests were performed early in the test program during which testing procedures were still being checked out. Measurement of precombustion conditions and gas sampling procedures were improved during later testing, so that even for lean combustion tests, comparisons of the AIC and measured peak pressures were more consistent.

[9]Figure 16 would be quite different if top ignition tests NTSP06 (no fans) and NTSP18 (no sprays) were included. These data have been omitted, since no other data from these tests were evaluated.

Table 5: Initial Conditions for Premixed Combustion Tests

Test Designation	Test Date	Test Series[†]	P_0 kPa	T_0 K	H_2 %	H_2O %	H_2 in Dry Air %
Standard Tests							
NTSP01	04 AUG 83	1	97.4	302.7	5.3	4.2	5.5
NTSP9P	01 DEC 83	2	89.6	302.7	6.0	4.6	6.3
NTSP09	10 NOV 83	2	91.6	301.8	6.1	4.2	6.4
NTSP00	23 JUL 83	1	91.6	303.0	6.6	4.5	6.9
NTSP04	09 AUG 83	1	97.4	305.2	7.7	4.8	8.1
NTSP13	19 DEC 83	2	97.4	303.9	7.8	4.4	8.2
NTSP15	22 DEC 83	2	109.3	303.4	9.9	4.2	10.3
Steam-Laden Tests							
NTSP07	29 AUG 83	1	93.5	325.2	5.5	14.3	6.4
NTSP03	10 AUG 83	1	95.4	325.7	5.8	14.4	7.0
NTSP06	17 AUG 83	1	87.6	323.0	6.0	13.7	7.0
NTSP12	17 NOV 83	2	92.6	339.7	6.9	28.3	9.6
NTSP14	06 DEC 83	2	93.5	347.1	8.1	38.7	13.2
NTSP05	18 AUG 83	1	87.6	340.8	7.8	31.3	11.4
NTSP16	20 DEC 83	2	101.3	342.7	10.1	29.5	14.3
NTSP08	12 SEP 83	1	130.6	348.0	11.1	27.2	15.2
NTSP20	12 JAN 84	2	104.2	342.0	12.9	27.8	17.9
Tests with Spray System Operative							
NTSP22	25 JAN 84	2	93.5	325.5	5.2	14.5	6.1
NTSP11	15 NOV 83	2	93.5	304.6	5.8	4.9	6.1
NTSP02	12 AUG 83	1	88.6	324.1	5.8	16.8	7.0
NTSP18	09 JAN 84	2	105.2	342.2	6.6	27.3	9.1
NTSP21	23 JAN 84	2	102.3	341.3	13.2	27.4	18.2

[†] Tests from series 1 (1) are part of Hydrogen Behavior; Tests from series 2 (2) are part of Equipment Survival

Table 6: Combustion Parameters for Premixed Tests

Test Designation	Test Date	Test Series†	Ignition Location‡	Mixing Fans (On/Off)	Combustion Completeness* %	Suspended Liquid Volume %
Standard Tests						
NTSP01	04 AUG 83	1	B	Off	32./32.	.0000
NTSP9P	01 DEC 83	2	B	Off	53./53.	.0000
NTSP09	10 NOV 83	2	B	Off	60./60.	.0000
NTSP00	23 JUL 83	1	B	Off	66./66.	.0000
NTSP04	09 AUG 83	1	B	Off	100./100.	.0000
NTSP13	19 DEC 83	2	B	Off	100./100.	.0000
NTSP15	22 DEC 83	2	B	Off	100./100.	.0000
Steam-Laden Tests						
NTSP07	29 AUG 83	1	2E	On	45./37.	.0000
NTSP03	10 AUG 83	1	C	On	50./44.	.0000
NTSP06	17 AUG 83	1	T	On	54./54.	.0000
NTSP12	17 NOV 83	2	B	Off	58./58.	.0000
NTSP14	06 DEC 83	2	B	Off	94./94.	.0000
NTSP05	18 AUG 83	1	B	Off	100./100.	.0000
NTSP16	20 DEC 83	2	B	Off	100./100.	.0000
NTSP08	12 SEP 83	1	B	On	100./100.	.0000
NTSP20	12 JAN 84	2	B	Off	100./100.	.0000
Tests with Spray System Operative						
NTSP22	25 JAN 84	2	1E	Off	31./31.	.0011
NTSP11	15 NOV 83	2	T	Off	58./58.	.0011
NTSP02	12 AUG 83	1	C	Off	70./43.	.0010
NTSP18	09 JAN 84	2	T	Off	69./69.	.0011
NTSP21	23 JAN 84	2	B	On	100./100.	.0011

† Tests from series 1 (1) are part of Hydrogen Behavior; Tests from series 2 (2) are part of Equipment Survival

‡ Ignition at Bottom (B), Center (C), Top (T), or by 1 or 2 Igniters on the Wall at the Equator (1E, 2E)

* Combustion completeness (CC) values used in Sandia data analysis/Values provided by EPRI

5 Results

In this section, summary results from the different instrumentation are provided for the twenty-one premixed combustion tests. As a part of this effort, the different instrument performances are assessed, and results from instrumentation which operated effectively are compared. Although representative results are given in this section, the majority of the results are given in three appendices. These appendices are organized as follows:

- Appendix A – Summary Tabular Results
- Appendix B – Comparative Graphical Presentation of Results
- Appendix C – Graphical Results for Individual Tests

Appendices A and B provide comparative tabular and graphical results for the different tests, respectively, while Appendix C provides comparative graphical results for each test from different instruments operating in that test. Appendix C is intended to provide the important temperature, pressure, and heat transfer characteristics needed for studying the different tests individually.

5.1 Assessment of Instrumentation Performance

Evaluation of the instrumentation performance was a two-step process, as indicated previously in Section 3. The data records were initially evaluated during the SMOKE preprocessing work to eliminate data that were overly "noisy" and/or which were physically incorrect (*i.e.*, negative temperatures, pressures, etc.). The second assessment of the instrumentation was performed following SMOKE processing, when the results from different instrumentation were compared (1) for the particular test and (2) with results from other similar tests. This latter assessment was continuously reviewed and updated as information about the instrumentation became available.[10] The following instrumentation assessment represents our best estimates for the quality and usefulness of the results obtained from this work.

Instrumentation performance for tests of the Hydrogen Behavior Series is given in Appendix A in Table A.1 and for tests of the Equipment Survival Series in Tables A.2 and A.3.[11] The tests are arranged in the order in which they were performed, so that trends associated with instrumentation operability can be seen more easily. It should

[10] Important background information needed for the instrumentation assessment was provided by J. Haugh of EPRI, R. Torok of Astron and J. Shepherd of SNLA who were involved with the instrumentation procurement and installation. Frequent discussions with these individuals led to explanations as to how and why instrumentation failed. Additionally, visual and "hands-on" inspection of the SNLA instrumentation following completion of testing provided supporting evidence as to the causes for instrumentation deterioration and/or failure.

[11] Tables and figures start from unity in each of the appendices. A letter prefix is used to specify the appendix where the figure or table is located (*e.g.*, Table A.3 or Figure B.6).

also be noted that test severity generally increased with each test. Instrumentation status for each test is classified as "good", "marginal", or "bad".[12] "Good" instrumentation provides believable signals which are consistent with other sensors and with data from other tests. "Good" implies that (1) the instrument signal quality is believable and (2) that results obtained from signal processing are reasonable. Results for "bad" instrumentation have poor signal quality; signals and inferred results from "bad" records are not provided. "Marginal" suggests that the instrument signal is generally reasonable, although it may deviate from other data. Similarly, an instrument response is termed "marginal" if results obtained from signal processing deviate from expected trends or from results obtained from other sensors. Results from SMOKE processing are given for "marginal" instrumentation to provide a sufficient data base; caution should be exercised when using these results. Examples of marginal pressure signals from sensor P102 are given in Figure 17.[13] Results inferred from these data are used since no other pressure data were available from these tests.

Summary descriptions of the instrumentation operability/usefulness are provided in the following sections.

Pressure Sensors

At least one pressure sensor was available for analysis for each of the twenty-one tests. For the early tests of the Hydrogen Behavior Series, only Sandia-provided pressure sensor data are available. Sensor P104 located at the top of the dewar failed early in testing prior to the third premixed experiment; data from P105 appears to be accurate through test NTSP08. Following completion of this series, the Sandia pressure sensors were replaced and more thermally massive housings (with internal water cooling) were provided to shield these sensors for the Equipment Survival Tests. Nonetheless, both SNLA pressure sensors failed for all tests of the second test series. Failure has been attributed to either failures in the electrical connections and/or to diaphragm overheating.[14]

The Setra pressure sensors appear to have operated effectively for tests in the Equipment Survival Series. Water vaporization in the cooling lines for P102 appears to have been the only major problem encountered in operating these sensors, and once cor-

[12]The instrumentation status for radiative calorimeters H105, H106, H501, and H505 are based only on the data signal trace. Given the calibration problems described in Section 3, SMOKE-processed results will not be provided for these instruments.

[13]It is believed that there was water in the pressure lines for these tests. When combustion occurred, the associated heat-up led to water vaporization which led to erroneous signals near the pressure peaks. This problem was uncovered after test NTSP16 and the water in the lines was purged there after. Note also that the P102 pressure signals were modified prior to smoothing (see Figure 14) to be more consistent with the signals recorded (but not provided) for P101 and P103.

[14]The SNLA pressure transducers were positioned at the top of the dewar (P104) and in the lower part of the dewar (P105) for the Equipment Survival Tests (see Figure 6). P105 had previously been positioned in the upper part of the dewar on the off-axis rake for the Hydrogen Behavior Tests, and had functioned for 7 of the 8 premixed tests of that series.

rected, the three gauge signals were nearly coincident (*e.g.*, see pressure traces of tests NTSP20 and NTSP21 in Appendix C). Data for these gauges, provided in the EPRI data books [21] for tests of the Hydrogen Behavior Series, also appear to be consistent, although the initially unprotected gauge P102 did fail during testing. Afterward, this gauge was positioned outside the dewar and attached to the end of a tube extending into the dewar as described in Section 2.

There is some uncertainty as to which type of gauge functioned better (*i.e.*, with better accuracy). Although the data are sparce, comparisons of the performances of P105 and the Setra transducers are available for test NTSP05, and for comparable tests NTSP04 and NTSP13. As seen in Figure 18, the P105 pressure signals decay more rapidly than do the Setra sensor signals. This suggests (1) that the thermal input is affecting the SNLA sensor, or (2) that the pressure response of the Setra sensors is delayed by the long lengths of tubing between the gauge and dewar gas. Since there are no additional data for comparison to resolve this uncertainty, the results obtained from both types of gauges have been accepted as correct without further modification to the signals. Note that the pressure-inferred total heat fluxes for times following combustion would tend to be higher for P105 than for P101, P102 and P103, since the heat transfer rate is related to the pressure gradient.

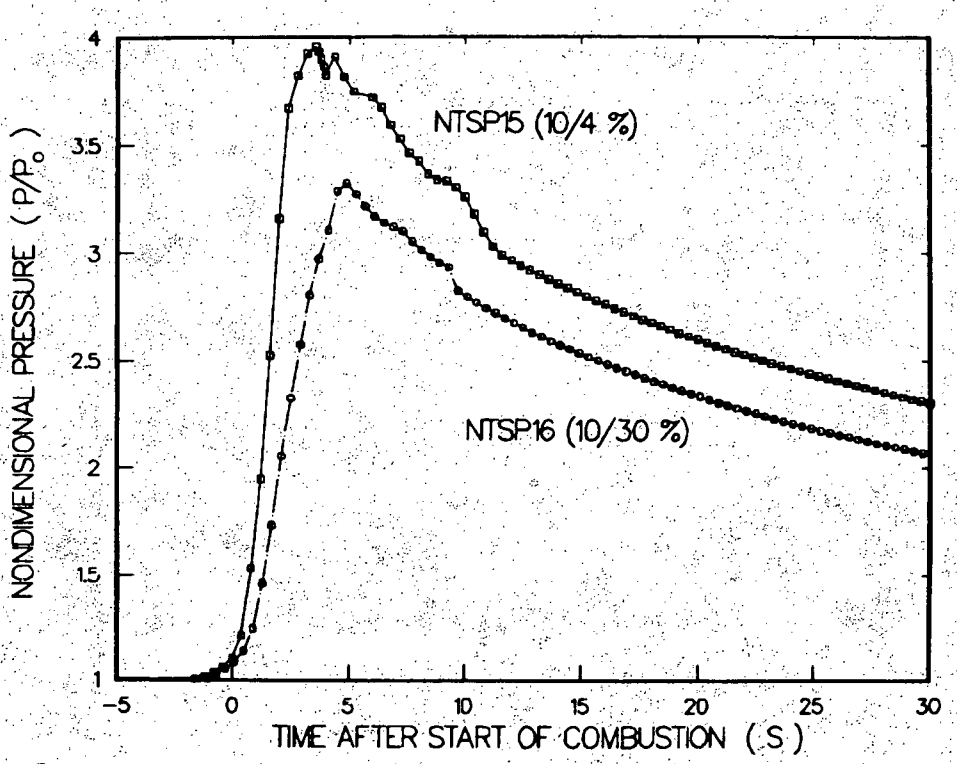

Figure 17: "Marginal" pressure signals for sensor P102. Values in parentheses are the precombustion hydrogen concentration/steam concentration.

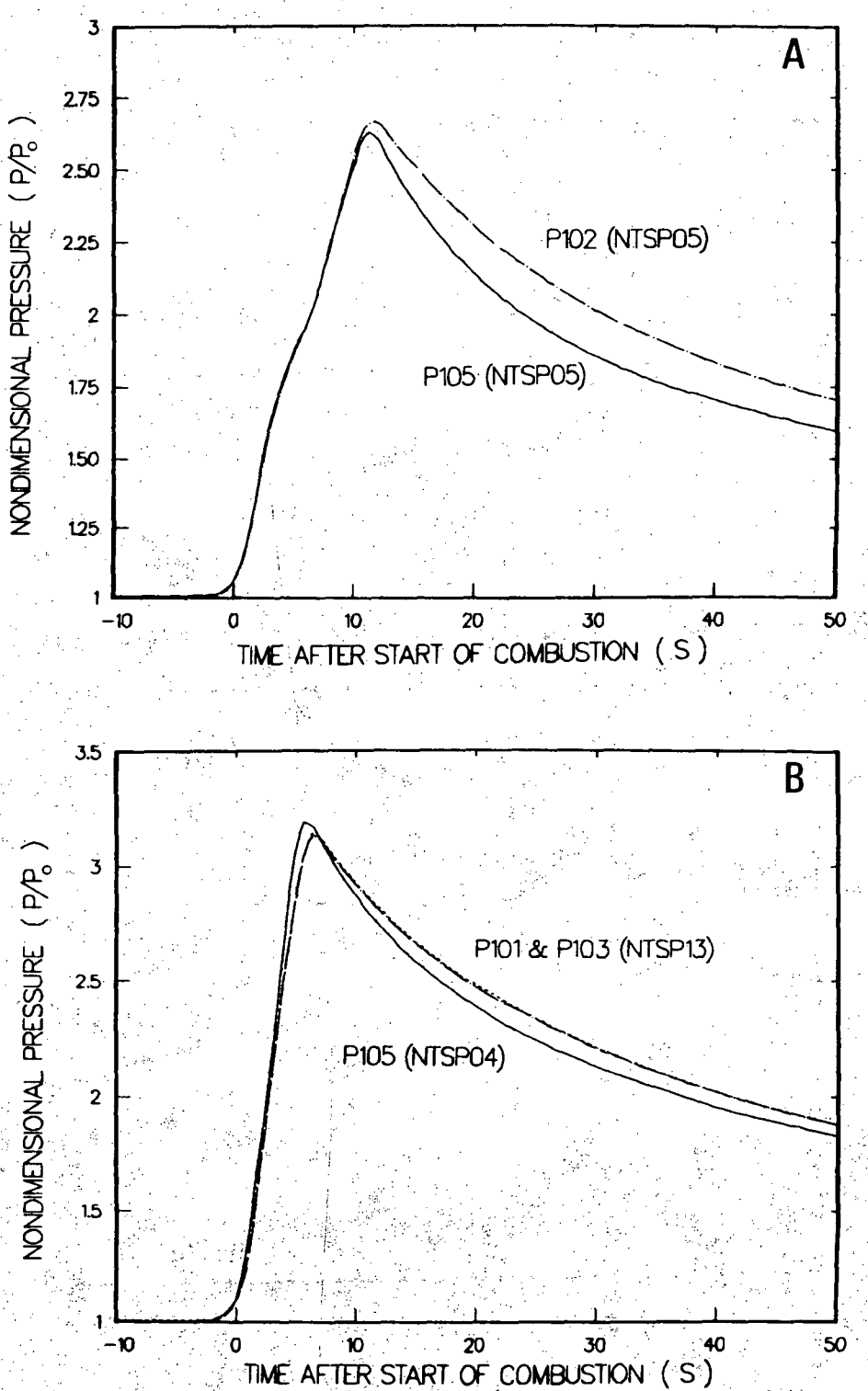

Figure 18: Comparative pressure sensor responses for Sandia (P105) and EPRI (P101, P102, P103) gauges

Gas Thermocouples

The gas thermocouples appear to have operated well for most of the tests in the Equipment Survival Test Series. Gas thermocouple data were provided only for two tests, NTSP05 and NTSP08, of the Hydrogen Behavior Tests; for these tests the thermocouples also appear to have functioned. Most of the thermocouples installed directly above the gas injection source for the Equipment Survival Tests, including T151, failed during the continuous-injection experiments which were performed near the end of testing. In general, the 3-mil gas thermocouples compared well during and after combustion. The 32-mil gas thermocouples also functioned, providing late-time postcombustion gas temperatures which were comparable with 3-mil thermocouple measurements.

Wall Thermocouples

Data for two wall thermocouples were available for 11 tests in the Equipment Survival Test Series and for 2 tests in the Hydrogen Behavior Series. Although the two thermocouples were both installed near the top of the dewar, their responses were usually quite different. Typical responses for these instruments are shown in Figure 19 for test NTSP16. T120 increased in temperature more rapidly during combustion, and also typically measured lower temperatures than T121. The peak heat fluxes inferred from T121 were generally lower than for T120, occurring at times 20–40 s after the times of peak pressure. Causes for these discrepancies are unresolved, and it must be assumed that (1) the thermocouples were mounted to the walls differently or (2) different local heat sinks seriously altered the thermocouple responses. In general, results from T120 are assumed to be more representative of the wall response, based on global estimates of the wall response computed from the pressure signals.

Thin-film Gauges

The total thin-film gauge provided "good" results for 3 of the Hydrogen Behavior Tests and for all 12 of the Equipment Survival Tests. Failures during the first test series are attributed to problems with the electrical connections to the gauge. The radiative thin-film gauge yielded "good" results for only one test, NTSP04. Problems were encountered throughout testing (1) in maintaining the vacuum between the sapphire and the MACOR and (2) in heating the gauge to limit condensation effects. Radiative thin-film signals were recorded for nearly all tests; data processing indicated that the gauge was not operating as intended. Post-test inspection of the gauges indicate that if the electrical connection and heater problems had been resolved during testing, "good" radiative and total heat transfer data would have been obtained for all tests since the gauge sensing elements and the MACOR were undamaged.

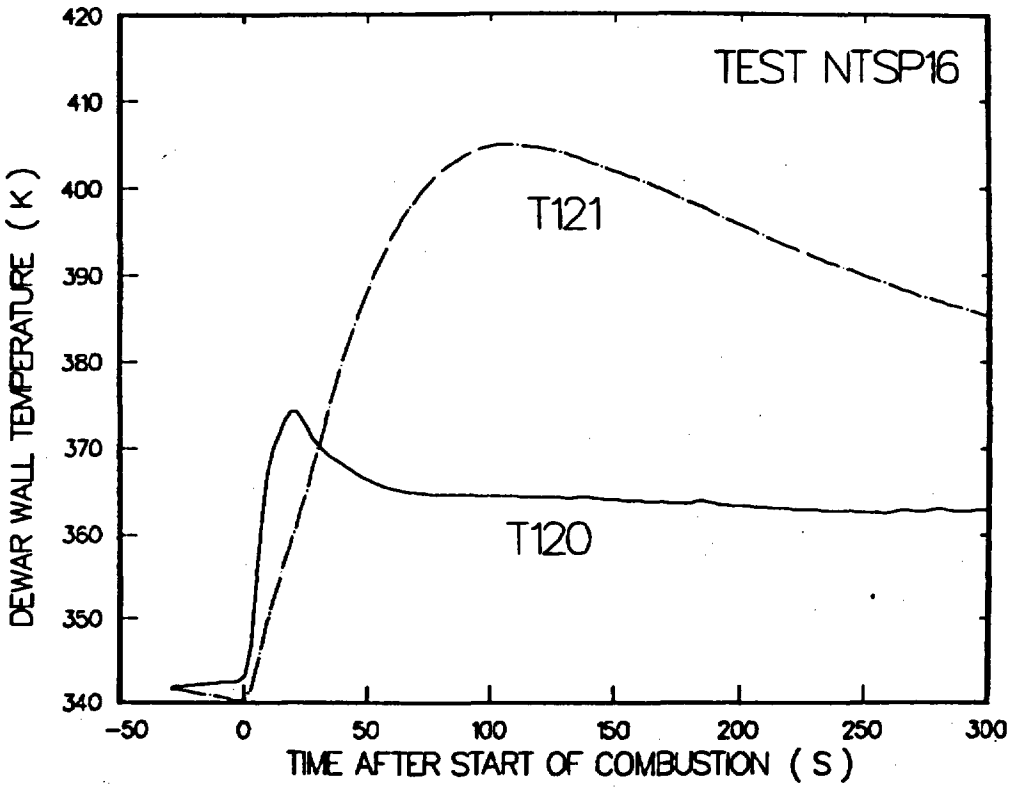

Figure 19: Comparative wall thermocouple response for test NTSP16

In general, the total thin-film gauge functioned as expected for the Equipment Survival tests. It measured peak heat fluxes consistent with the other calorimetry. However, the sampling rates at NTS were probably not sufficient for the thin-film gauge for tests where the initial hydrogen concentration was $\geq 8\%$; peak heat fluxes for these tests probably were not recorded (*i.e.*, heat flux estimates from the thin-film gauge for the most severe premixed combustion tests are low). The true (actual) maximum heat fluxes were not recorded due to undersampling. Note again that these data were probably recorded by the NEFF data acquisition system [1], but that we had requested only those data recorded at the slower sampling rate. In addition, the thin-film gauge underpredicted the total energy deposition. The data processing model (semi-infinite solid, thermal conduction model with constant properties) was not appropriate for late times > 100 seconds after combustion. Further, the surface heat losses were not accounted for in the analyses. This omission was particularly important for the more severe tests since the gauge surface temperature increased significantly (see Figure 20).

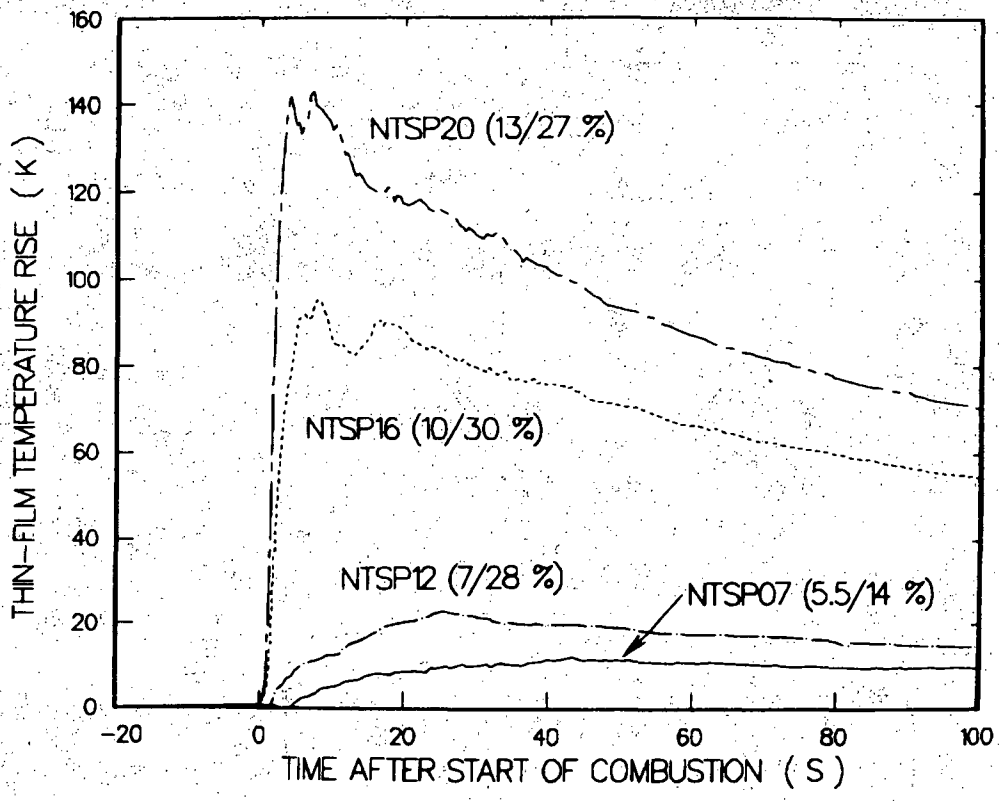

Figure 20: Total thin-film temperature rise histories during different tests. Values in parentheses are the precombustion hydrogen concentration/steam concentration.

Copper Slug Calorimeters

The SNLA total slug calorimeter (H104) was included in the dewar for both test series and provided "good" or "marginal" results for all tests. Results were judged to be "marginal" for cases where the signal was overly noisy or where the measured slug temperatures were not continuous, since such signals were difficult to process and since the results were difficult to assess.[15] As an example, Figure 21 provides typical "marginal" (A) and "good" (B) H104 temperature histories for tests NTSP15 and NTSP16, respectively. When the data for tests with "marginal" traces (e.g. test NTSP16) were processed, anomolous heat flux results following completion of combustion were computed (see Figure 22). Note that the slug temperatures became greater than the surrounding gas after combustion, and consequently, the direction of heat flow reversed. Because of these correspondingly negative fluxes, seen in Figure 22, the slug gauge configuration could not be used to calculate energy deposition.

[15] We believe that the total slug gauge functioned for all tests, and that the strange variations in the signals may well have been the result of local local fluctuations in the environment around the sensor. Unfortunately, there were no other sensors in the vicinity of the slug calorimeter (see Figure 8) to verify/dispute this conjecture. In addition, signals such as are shown in Figure 15-A had not been recorded in prior FITS testing [10].

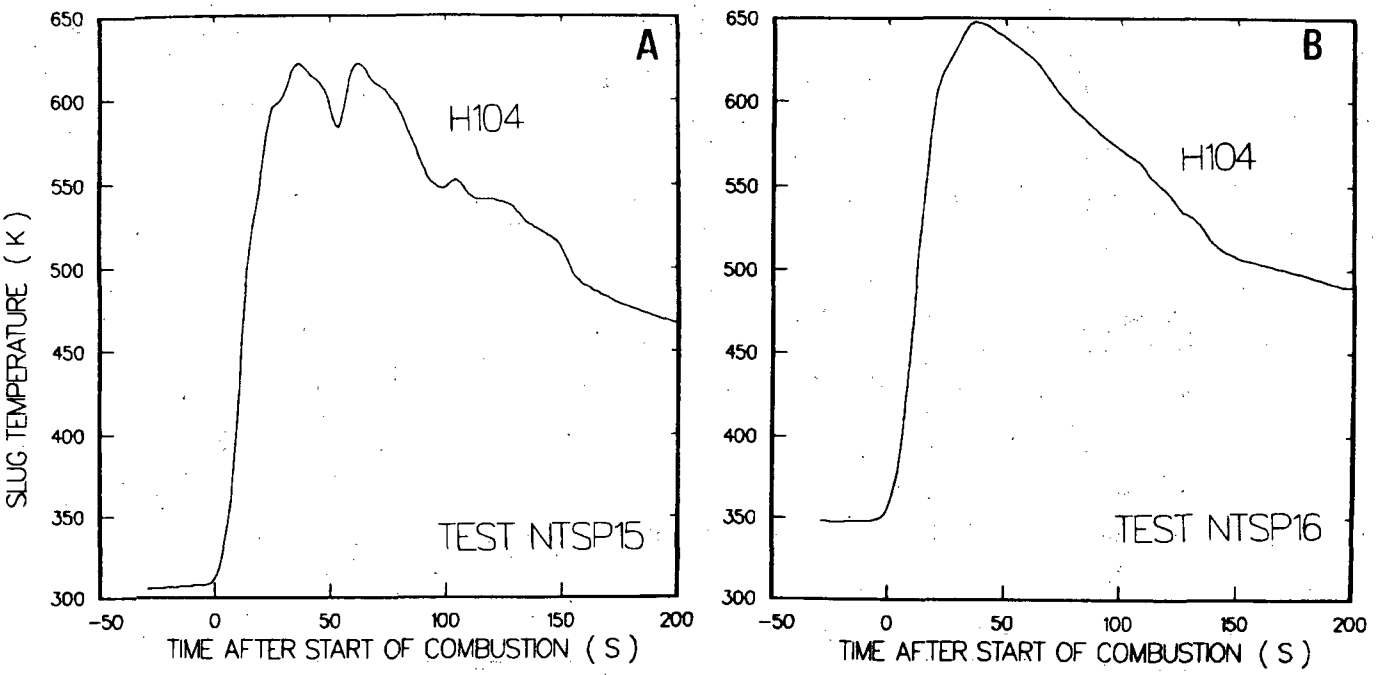

Figure 21: Measured temperatures for slug calorimeter H104 for tests NTSP15 (A) and NTSP16 (B)

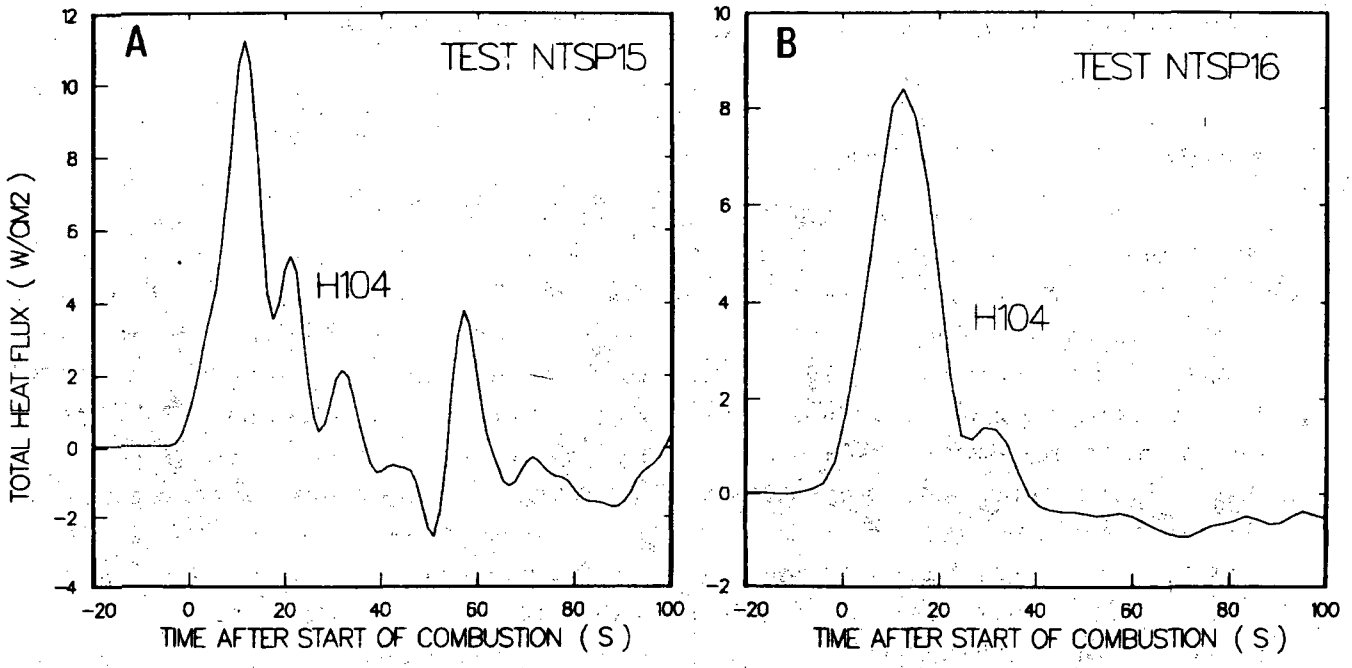

Figure 22: Computed surface heat fluxes for slug calorimeter H104 for tests NTSP15 (A) and NTSP16 (B)

The radiative slug calorimeter (H103) signals appeared to be "good" prior to processing; after SMOKE processing, most H103 signals were judged to be "bad". This is believed to be due to the following problems. As with the radiative thin-film gauge, the heater unit for the slug calorimeter was inoperative for nearly all tests. In addition, the vacuum was not maintained between the sapphire and MACOR, and further, the sapphire surface was heavily coated with contaminants by the conclusion of testing. In general, the variation in cover optical properties, as well as the problems associated with condensation, precluded obtaining radiative results for all but one (NTSP04) of the tests.

Brass Flat-Plate Calorimeter

The flat-plate calorimeter data were inconsistent; all results inferred from this calorimeter were judged to be "bad". Post-test inspection of this gauge revealed that the brass plate had separated from the insulation. The thermocouples were visible from the side and therefore were also in direct communication with the hot combustion gas. This confirmed suspicions about the gauge operability which arose during the interpretation of SMOKE-processed results. Figure 23 provides a view of the damage incurred by the flat-plate gauge; this photograph was taken after completion of testing.

Aluminum Cube Calorimeter

The aluminum cube functioned for most of the tests of the Equipment Survival Series. Thermocouples were mounted to the top (T505) and two of the side (T504, T506) interior surfaces. The top and the side thermocouples T504 and T505 yielded consistent temperature profiles, although the thermocouple attached to the top surface tended to lag and be slightly cooler than the side thermocouple. Much lower temperatures were measured from thermocouple T506 for all tests. The post-test inspection showed that this thermocouple had become unfastened from the cube interior surface and was measuring the internal gas temperature near the wall. Typical temperature profiles for the three cube thermocouples are shown in Figure 24 for test NTSP16.

Results from processing the good thermocouple data were generally consistent with other calorimetry for the lean combustion tests. However, peak heat flux results from T505 were typically less than results from T504. It is thought that a water layer was deposited on the cube top surface prior to combustion (from the sprays used in preconditioning the gas), and that the water served as an insulating layer during the early times of a test. Post-test inspection of the cube also showed that the black anodized surface had deteriorated (in fact, it was almost completely removed). It is postulated that the computed peak heat fluxes for the later tests are low, since the surface deterioration probably occurred as the thermal environment severity increased and as a result of the wetting of the surfaces before testing. This type of surface deterioration had not been encountered in either the VGES or FITS combustion test programs [12,13].

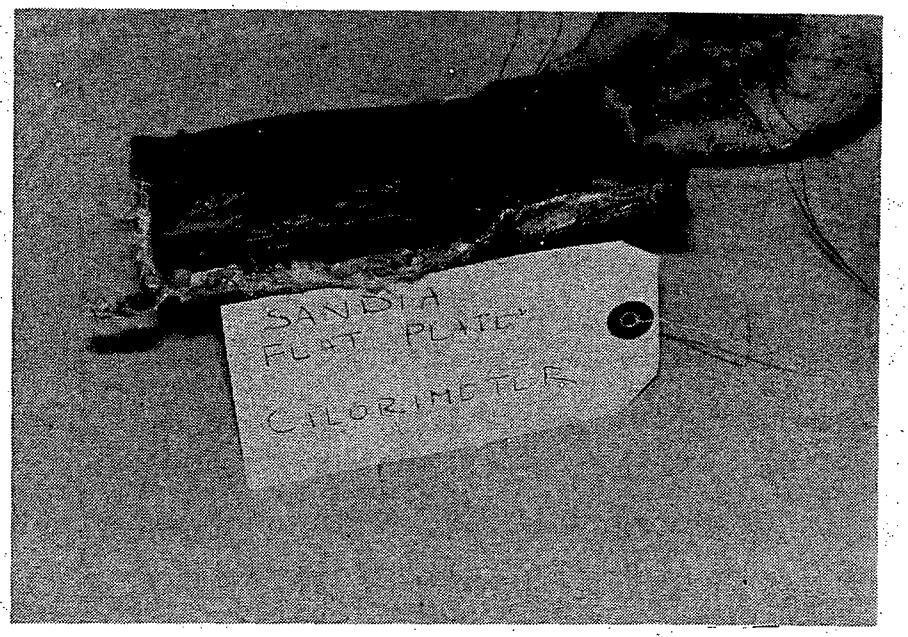

Figure 23: Photograph of brass flat-plate calorimeter, taken after testing

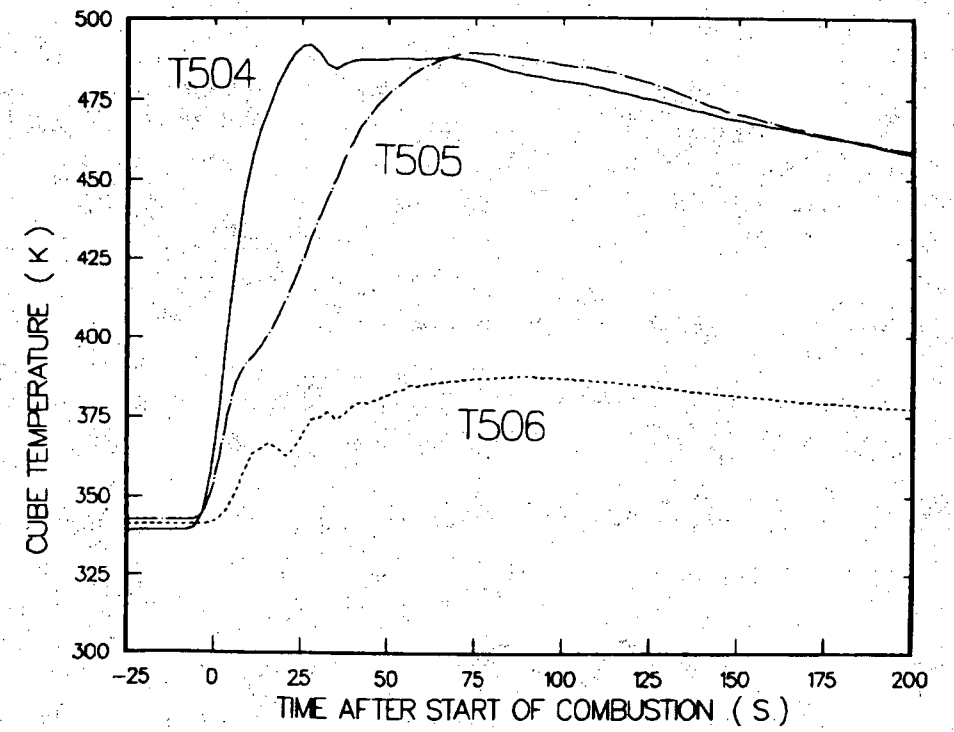

Figure 24: Temperature profiles for the three thermocouples inside the aluminum cube, measured from test NTSP16

Schmidt-Boelter and Gardon Gauges

Two Gardon gauges were provided for both test series and seven Schmidt-Boelter thermopile gauges were included for the Equipment Survival Test Series. As has been indicated previously, results from the radiative gauges (1 or 2 Gardon gauges and 2 Schmidt-Boelter gauges) are omitted given that the calibration data did not correctly account for the steam environment and also given the calibration shifts during testing [1].

Gardon gauge H106 was a total calorimeter for Hydrogen Behavior test NTSP00 through test NTSP08 and then afterward was replaced with a radiative gauge. H106 functioned well for the first 7 tests (data were not provided for the first test), and overall, it provided consistent, believable signals. H106, although uncooled, required no baseline heat flux adjustment for the 6 lean combustion tests in which it operated. The energy depositions computed for H106 are also consistent, except for test NTSP06, when for late times (> 80 s) the heat flux fell below zero (see results in Appendix C). This probably occurred because the gauge overheated during this test, the most severe test for which H106 was configured as a total gauge.

Five Schmidt-Boelter thermopile gauges were configured as total calorimeters. Water cooling was provided for each of these gauges, although the flow rates were probably not sufficient for the most severe tests. In particular, H504 operated ineffectively for most tests due to insufficient cooling.[16] Figure 25 shows a comparison of upward-oriented gauges H502 and H504 for test NTSP16. The gauge heating in H504 is reflected in the lower peak heat flux level and in the negative heat fluxes shortly after completion of combustion. Although heat fluxes and energy depositions are provided for H504 for some of the tests, these data are questionable for all but the very lean combustion tests.

Total gauges H502 and H503 operated for nearly all of the Equipment Survival Tests, while gauges H506 and H507 provided erratic and/or bad results for the latter half of the tests. Typically, the downward-oriented gauges (H503, H507) recorded higher heat fluxes than did the upward-facing calorimeters (H502, H506). It was also noted that the baseline fluxes for H506 and H507 were typically greater than for H502 and H503. Baseline fluxes for H507, in particular, were large, ranging from 1.0–1.2 W/cm^2 for the most severe tests.

[16] In a working meeting held at SNLA June 19, 1984, the EPRI calorimetry status was reviewed by personnel from EPRI, Westinghouse, and Sandia. The cooling problem was discussed, and it was hypothesized that H504, located at position C on the Equipment Platform (see Figure 9), was not cooled sufficiently or possibly not cooled at all. Water cooling to the different gauges on the Equipment Platform came from a location near the dewar center rake. The insulated tubing length to position A on the Equipment Platform was $\sim$ 8-10 m, while the length to H504 and to position B was $\sim$ 14 m. In addition, it was suggested that while the flow rates might have been sufficient, there could have been a blockage in the lines at the H504 gauge connection that would have limited cooling. Additional comments on this problem are included in Reference [1].

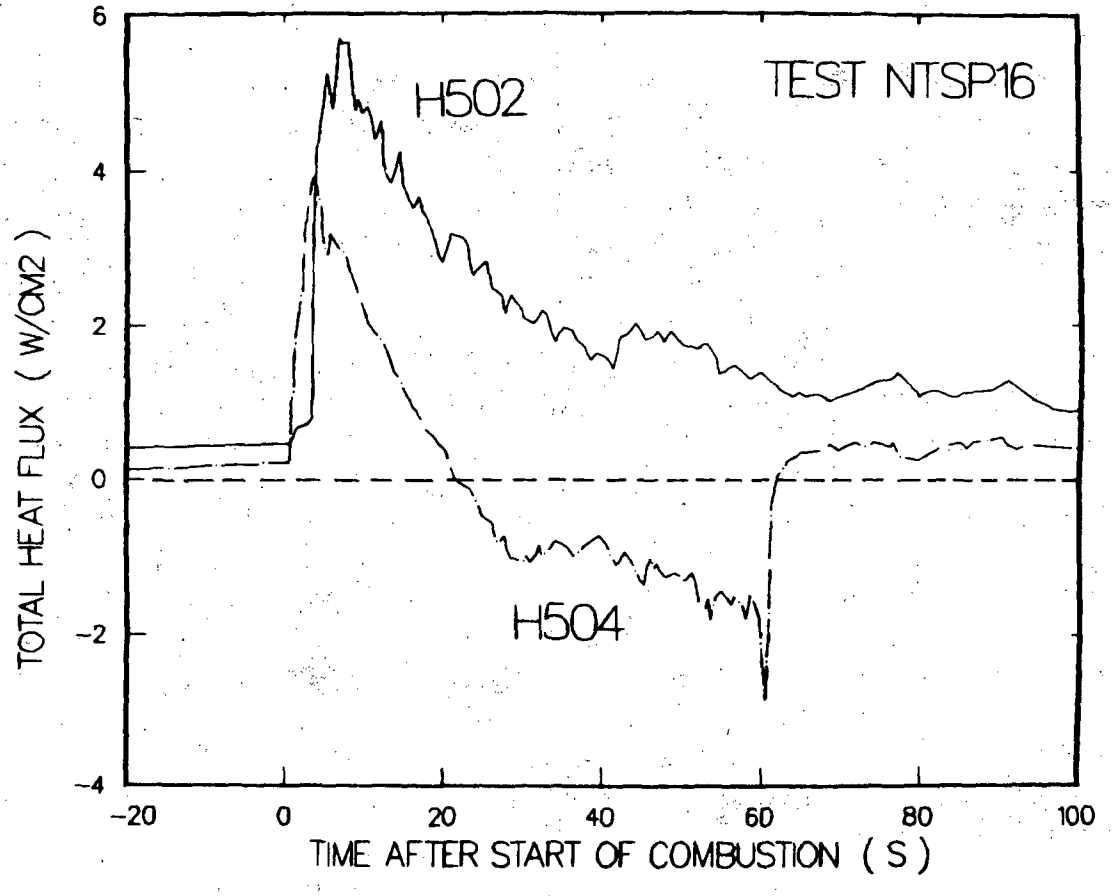

Figure 25: Comparison of Schmidt-Boelter gauges H502 and H504 for test NTSP16

5.2 Gas Pressure Results

Gas pressure profiles, peak pressure results, and combustion duration obtained from the pressure are presented in this section. Gas and wall temperature data and heat transfer results inferred from the pressure are discussed in the following sections in conjunction with the measured quantities. Pressure results for each of the tests are given in Appendix C: (1) for times associated with combustion and (2) for the duration of the experiment. Additional pressure results are given in Appendices A and B, and specific references to these data are cited below.

5.2.1 Comparative Pressure Profiles

Representative comparative pressure profiles for the three classes of tests (*i.e.*, standard, steam-laden, and sprays-on) are given in Figures B.1, B.12, and B.23 of Appendix B, respectively. Trends from these figures are typical of what has been seen in small-scale combustion tests conducted by Sandia at VGES [22] and FITS [23], and by personnel from Whiteshell, EPRI and Acurex [24,25]. That is, lean combustion tests tend to be incomplete, with slow burning and associated small pressure increases. Termination of the combustion is difficult to assess for such tests, and the pressure traces typically exhibit a "roll-over" with a slow initial decay associated with continued local burning. However, the transition between combustion gas heating and post-combustion gas cooling is less distinct for the NTS tests than for tests conducted in smaller test vessels such as the FITS facility. Comparative results for nominal 10% hydrogen–air deflagrations for these two test vessels, in particular, demonstrate the importance of scale for post-combustion times [26].

As the hydrogen concentrations increase, the peak pressures increase and the times to peak pressure decrease. As noted previously in Figure 16, nearly all of the hydrogen was burned for NTS tests in which the initial volume concentration was greater than 7–8%. For higher initial hydrogen concentrations, the pressure rise is nearly linear, followed by an exponential-like decay. The "roll-over" phenomenon is absent, suggesting that combustion is completed almost coincident with the time of peak pressure.

In the following paragraphs, important observations from comparisons of tests from the three different test types are presented along with illustrative figures. Included in these presentations are: (1) comparisons of pressure profiles for redundant tests; (2) effects of ignition site; (3) effects of added steam; and (4) effects of sprays and fans.

Pressure Profiles for Redundant Tests

The premixed combustion tests included only two sets of tests which were redundant, tests NTSP09 and NTSP9P and tests NTSP04 and NTSP13.[17] Comparison of pressure profiles for the latter tests have been provided previously in Figure 18. The

[17] Tests are referred to as redundant if the initial nominal hydrogen and steam concentrations, the location of ignition, and the status of the fans and sprays during testing are identical. Combustion completeness need not be comparable, just the precombustion conditions.

pressure responses are similar, and the reported differences for these 8% hydrogen combustion experiments can probably be attributed to the different instrumentation. The 6% hydrogen combustion tests NTSP09 and NTSP9P, on the other hand, are quite different, as seen in the pressure profiles recorded for P103, given in Figure 26. The combustion process is obviously quite different, although the combustion completeness values used in this work were similar (53% for NTSP9P and 60% for NTSP09).[18]

Good agreement should be expected for redundant tests as the hydrogen concentration and combustion completeness increase. Use of the lean-combustion data to infer phenomena is more difficult, since the combustion is not well-characterized. The data base from the NTS premixed combustion tests is probably not sufficient, by itself, for developing burn correlations for hydrogen concentrations less than 8%.

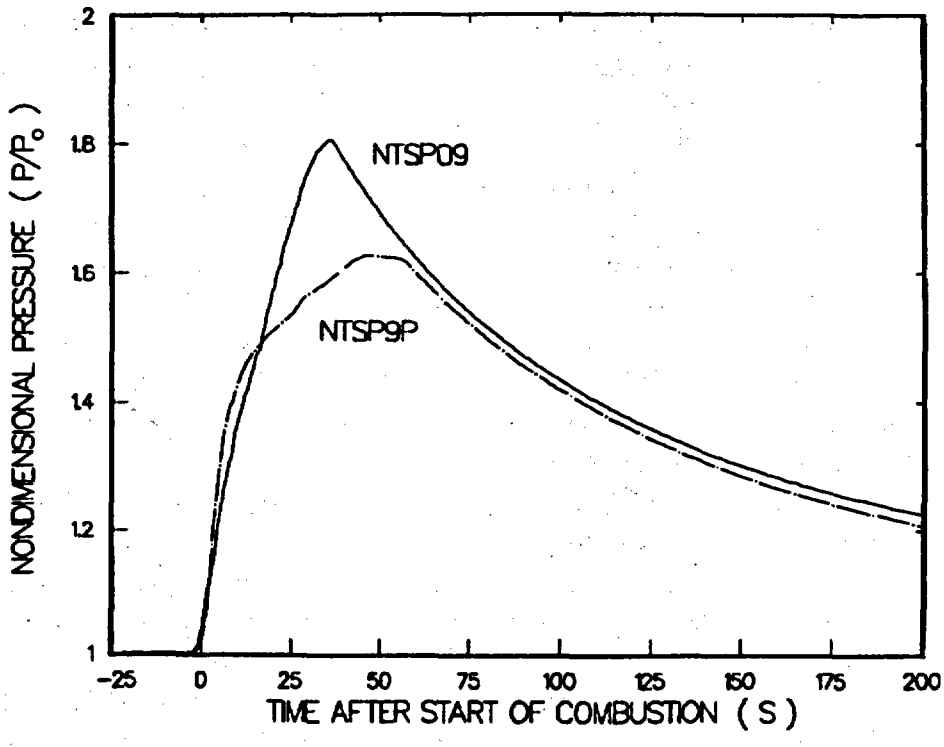

Figure 26: Comparison of pressure profiles for tests NTSP09 and NTSP9P

Effects of Ignition Site on Combustion

Fourteen of the twenty-one premixed combustion experiments were performed with combustion initiated at the bottom of the dewar. Of the remaining seven tests, five were performed in the Hydrogen Behavior Series, and all seven had precombustion hydrogen concentrations less than 7% by volume. For these cases, the ignition location

[18] Also note that combustion in test NTSP09 was initiated by an inadvertant spark (from bare wires) while a glow plug was used to initiate combustion in NTSP9P [1].

is important since downward combustion is limited for lean hydrogen concentrations. Combustion completeness and pressure rise can vary substantially for tests of comparable initial gas states but with different ignition locations.

Comparisons of the pressure profiles are provided in Figures 27 and 28 for six 6% (nominal) hydrogen combustion tests. Fans were operative for the tests compared in Figure 27 and sprays were operative for the tests of Figure 28.[19] Differences between comparable fans-on tests NTSP06 (top ignition) and NTSP03 (center ignition) are slight. Center ignition for the case of sprays-on (test NTSP02), however, tends to produce more complete combustion and associated higher pressures than does top ignition (NTSP11). For both sprays- and fans-on cases, ignition at the wall appears to produce less complete combustion and smaller pressure increases; this may have occurred more because the combustion was incomplete than because of where combustion was initiated. The initial concentrations differed for these tests; at the lean concentrations, this would also affect the combustion completeness. As indicated in the redundant test section, there were not enough tests performed to fully assess the importance of ignition site on lean combustion phenomena. For quiescent tests in which the hydrogen precombustion concentrations are above 8–9%, combustion initiation location should be less important, since upward and downward flame propagation are expected.

Effects of Added Steam

The addition of steam to the precombustion gas reduces the severity of the combustion, since steam serves as a heat sink and inert diluent during combustion. The resulting peak pressures and temperatures are correspondingly lower for tests in which the same quantities of hydrogen are burned. This was seen previously in Figure 17, which compares pressure signals for two 10% hydrogen combustion tests having precombustion steam concentrations of 4 and 30%, respectively. Similar trends are shown in Figure 29, which compares the pressures from three 8% hydrogen combustion tests. Four of the five tests shown in these two figures were reported as complete combustion tests, while test NTSP14 was determined to be 94% complete. The addition of steam reduces the degree of combustion and, for the 39% steam test, also modifies the pressure profile during combustion.

The addition of steam would also be expected to affect the postcombustion cooling, since steam is the radiating source. Similarly, steam condensation during cooldown would tend to be more significant for mixtures having larger initial steam concentrations. The cool wall and equipment surfaces would tend to be more 'wetted', *i.e.*, thermally shielded, during the steam-laden combustion tests.

---

[19] Note that for these lean combustion tests, the combustion occurs in the presence of turbulence generated through either fans or sprays. As indicated previously (footnote 6), a test comparable to test NTSP06 without fans-on was performed and there was no appreciable combustion; that is, downward combustion was not possible without enhanced turbulence. A test comparable to test NTSP18 also was less than 10% complete, requiring a repeat test with sprays-on. The use of fans and/or sprays affects more robust and correspondingly more complete combustion.

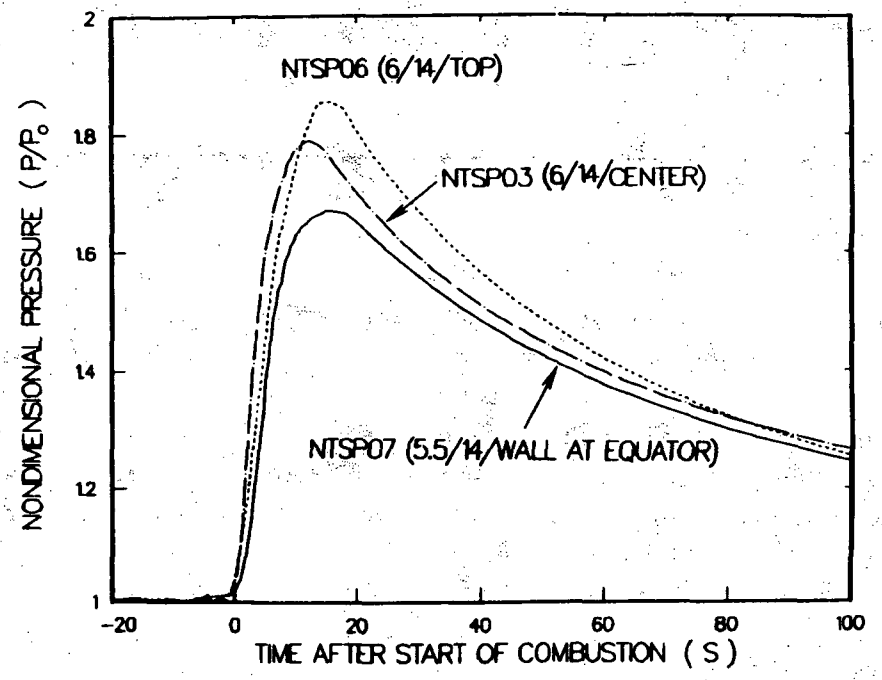

Figure 27: Comparative pressure profiles for three 6% (nominal) hydrogen combustion tests having different ignition sites and with fans operative. Values in parentheses are hydrogen concentration/steam concentration/ignition site.

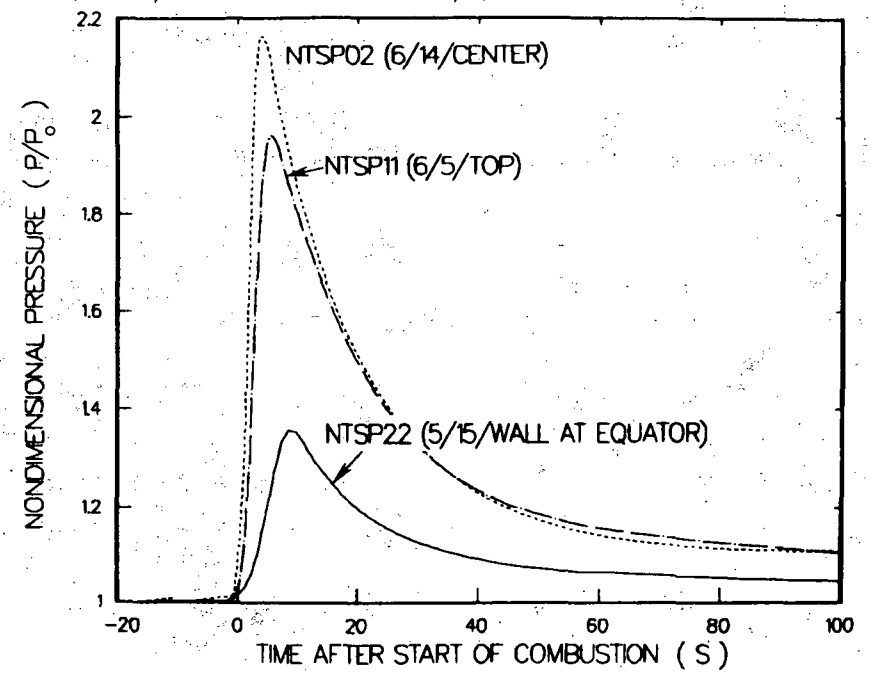

Figure 28: Comparative pressure profiles for three 6% (nominal) hydrogen combustion tests having different ignition sites and with spray systems operative. Values in parentheses are hydrogen concentration/steam concentration/ignition site.

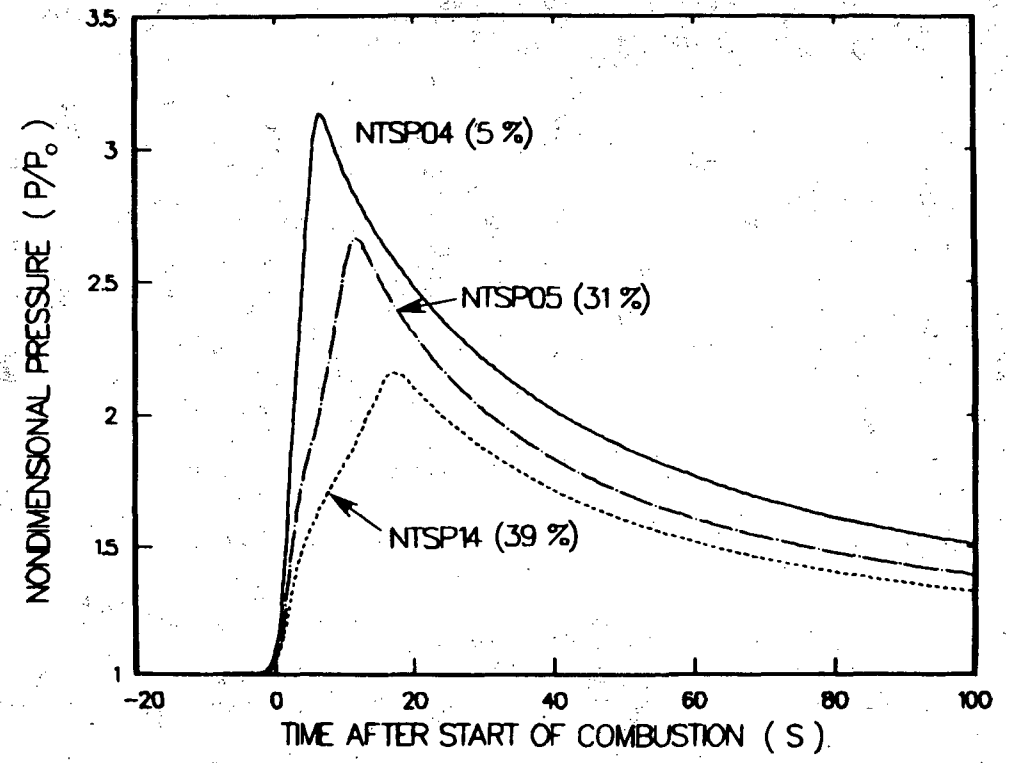

Figure 29: Comparative pressure profiles for three 8% (nominal) hydrogen combustion tests having different precombustion steam concentrations. Numbers in parentheses are the steam concentrations.

Effects of Sprays and Fans

Sprays and fans enhance the rate of combustion for lean mixtures of hydrogen. This is shown in Figure 30, which compares pressure profiles from three 6% hydrogen combustion tests. For the NTS configuration of fans and sprays, sprays are found to promote more turbulence and correspondingly more rapid combustion than do fans. Such trends are less apparent for more severe combustion tests such as are shown in Figure 31. In this comparison of two 13% hydrogen combustion tests, the burn durations are nearly identical as are the pressure maxima. The major differences between these tests occur following completion of combustion, when evaporation of the sprays leads to more rapid cooling. This trend is also seen in the pressure decays of tests NTSP11 and NTSP06, shown in Figure 30.

Overall, these examples show that sprays do not reduce the severity of the actual combustion, and, in fact, probably enhance the burning due to increased turbulence. Benefits from sprays result from the additional cooling mechanism of spray droplet evaporation. From the comparisons of tests with and without fans, it is not apparent that the fans in the NTS dewar modified the postcombustion cooling processes. They did, however, enhance the combustion of lean hydrogen–air–steam mixtures.

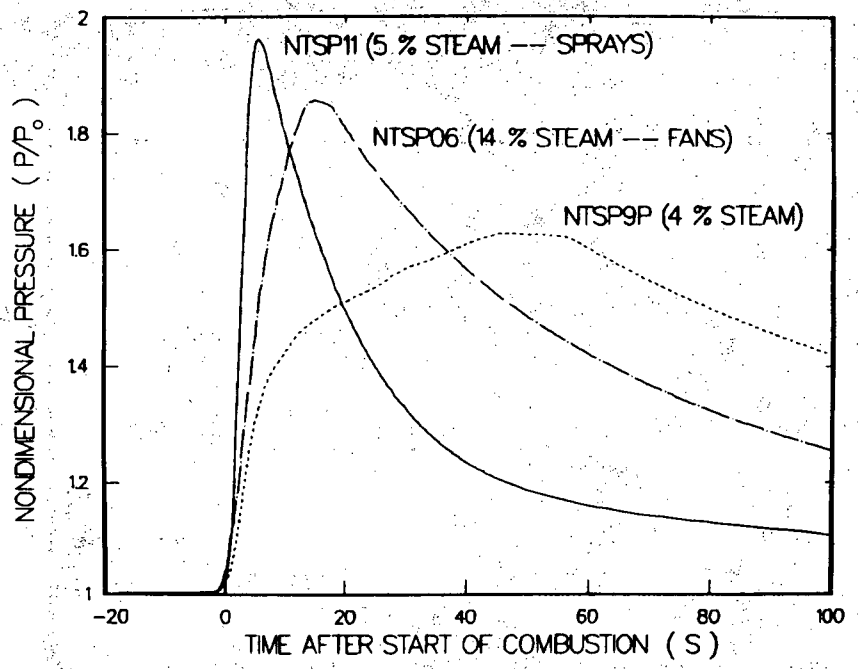

Figure 30: Comparative pressure profiles for three 6% (nominal) hydrogen combustion tests showing the effects of sprays and fans. NTSP11 and NTSP06 are top ignition tests and NTSP9P is a bottom ignition test.

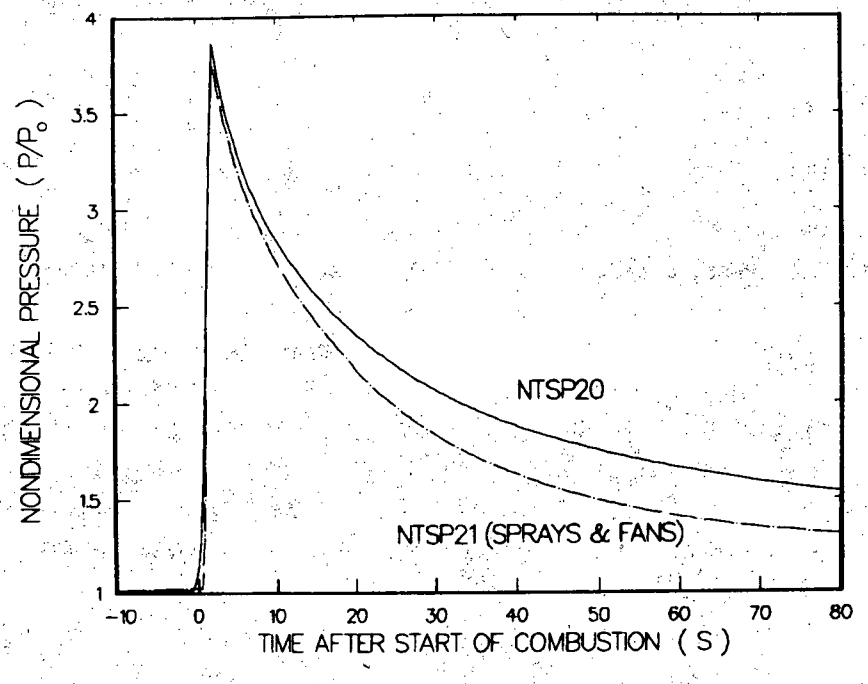

Figure 31: Comparative pressure profiles for two 13% (nominal) hydrogen combustion tests with and without sprays and fans

5.2.2 Peak Gas Pressure Results

Measured peak pressure data for the tests are included in Table A.5 of Appendix A along with computed AIC (theoretical maximum) values. Figure 32 shows peak pressure ratios (measured and AIC calculations) for the tests as a function of hydrogen consumed.[20] These results are also shown in Appendix B in Figures B.2, B.13, and B.24 for standard, steam-laden, and sprays-on tests, respectively. All tabulated and plotted values were taken from the data provided by EPRI, except for tests NTSP08, NTSP20, and NTSP21. For these large hydrogen concentration combustion tests, the data were not sampled sufficiently often (sampling times > 0.04 s) to record the peak. The peak results reported here are SNLA estimates based on extrapolation of the recorded results; typical corrections varied between 5–15 kPa.

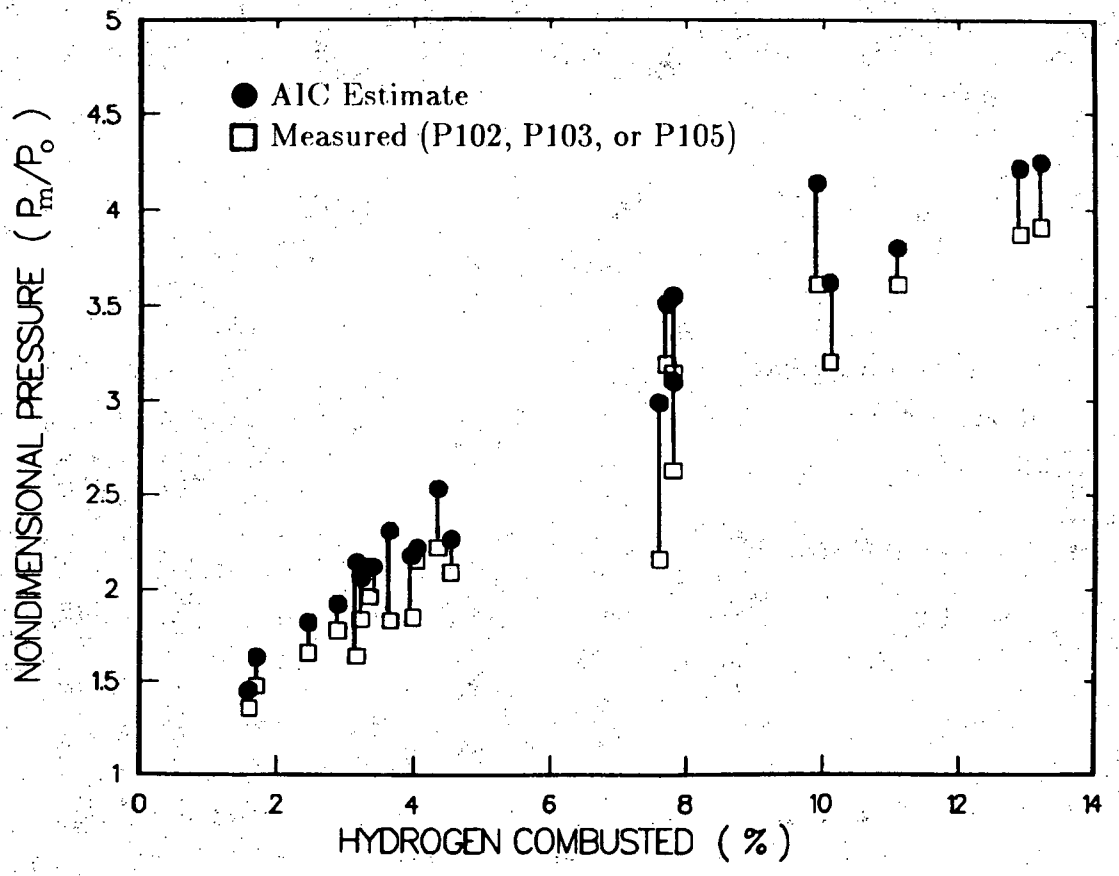

Figure 32: Peak pressure ratios for the NTS premixed combustion tests

[20]Hydrogen consumed is defined as the product of the initial hydrogen concentration and the SNLA assumed combustion completeness. This value is also used in Appendix B in the graphical presentation of combustion duration and peak pressure for the three types of tests.

5.2.3 Combustion Duration

Combustion duration results inferred from the pressure signals are included in Table A.5 of Appendix A and are also plotted in Figures B.3, B.14, and B.25 of Appendix B for the three different test types. Combustion duration is defined in this work as the time interval from combustion initiation to either (1) the time of peak pressure (duration referred to as Δt_P) or (2) the time of peak total heat flux inferred from the pressure (duration referred to as Δt_{q_T}). The combustion initiation time (t_0) is that time at which the gas pressure surpasses 5% of the total pressure increase measured for a test.[21] These values are also given in Table A.5 for each test.

Combustion duration is usually defined in terms of the time to peak pressure, especially for complete combustion tests. For lean hydrogen combustion, this time can be quite long, especially if fans and sprays are not operating. The pressure roll-over for lean combustion is indicative that combustion is still in progress, and that the effects of continued energy release associated with combustion are being offset somewhat by heat transfer from the combustion gases to the dewar. Once combustion is completed, the pressure time rate of change would be expected to decrease continuously. Location of the time of peak pressure is difficult for lean combustion and probably is not a correct time scale for combustion. Instead, it is suggested that the time of the peak heat flux inferred from the pressure is a more representative measure of combustion termination. Note that Δt_P and Δt_{q_T} differ significantly for the lean tests performed at NTS, but for initial hydrogen concentrations above 7%, the two combustion duration values are nearly coincident. This would be expected, since for non-lean hydrogen combustion, the pressure increase and subsequent decrease is steep and the peak pressure defines the transition.

5.3 Gas Temperature Results

Gas temperature results from thermocouple data are provided in Table A.6 of Appendix A, and temperature profiles are compared in Figures B.4, B.15, and B.26 of Appendix B for standard, steam-laden, and sprays-on tests, respectively. Additionally, "global" peak gas temperature ratios (T_m/T_0) obtained from the pressure signal processing are given in Table A.4, and comparisons of the global and measured temperature profiles for standard and steam-laden tests are provided in Appendix C. These comparisons are not provided for sprays-on tests, given the limitations of SMOKE for modeling spray evaporation, as indicated in Section 3.

The peak temperature ratios (T_m/T_0) obtained for the 3-mil thermocouples (Table A.6) compare well with the maximums inferred from the pressure data and with the upperbound AIC values as shown in Figure 33. The times associated with the measured peaks are also consistent with the times of the measured peak pressure, although

[21] Note that combustion duration defined in this manner omits the early-time combustion which occurs essentially at constant pressure (isobaric portion of combustion). More accurate estimations of the combustion duration could be obtained from the video tapes recorded for each test.

the thermocouple peaks generally occurred slightly earlier. Differences between the thermocouple time of peak and the time of peak pressure (Δt_{mp}) are given in Table A.6. The 32-mil thermocouples were not sufficiently sensitive to follow the transients associated with gas heating during combustion and early postcombustion cooling. This is noted from review of the temperature profiles (Appendix C), the measured peaks, and the times of these peaks relative to the time of peak pressure (Appendix A). The late-time temperatures from the 32-mil thermocouples are consistent with data from the 3-mil thermocouples, nonetheless, as shown in the comparative gas temperature figures in Appendix C.

The severity of the environment resulting from combustion can be measured not only by the peak gas temperature, but also by some characteristic time period during which the gas temperature is greater than some specified threshold. In this work, the temperature threshold (specified as $T_{1/2}$) is defined as the average of the initial and maximum gas temperatures. Table A.6 provides the threshold temperatures and the duration ($\Delta t_{T_{1/2}}$) for which the gas temperature is greater than $T_{1/2}$ for the different tests. This time includes both the combustion and postcombustion periods of the experiment. These times are useful for comparing tests which have similar precombustion conditions and different ignition sources and also to assess the effects of fans/sprays on the gas cooling. It is important that comparisons of $\Delta t_{T_{1/2}}$ be made for tests with similar $T_{1/2}$ values to provide consistency. Figure 34 shows such a comparison for gas temperature results from tests NTSP20 and NTSP21. The shorter time $\Delta t_{T_{1/2}}$ for test NTSP21 points out the advantages associated with spray-cooling.

Overall, comparisons of the average gas temperature inferred from the pressure and the measured temperatures for the standard and steam-laden tests are quite good (see figures of Appendix C). The average gas temperature results for the postcombustion times are typically bracketed by the 3-mil and 32-mil data. The average gas temperature profiles tend to follow the 3-mil data very closely at early times; measured gas temperatures are not appreciably greater nor are the temperature decay rates different. This indicates that, at least for the NTS premixed combustion tests, global estimates of the gas temperature and pressure should be sufficient for characterizing the environment.

5.4 Wall Temperature Results

Comparative wall temperature results are provided in Figures B.5, B.16, and B.27 of Appendix B for representative standard, steam-laden, and sprays-on tests, respectively. In addition, results from thermocouples T120 and T121 are compared with average wall temperature estimates obtained during pressure signal processing in Appendix C. Average wall temperature estimates are omitted for sprays-on tests, given limitations in SMOKE pressure processing for these cases.

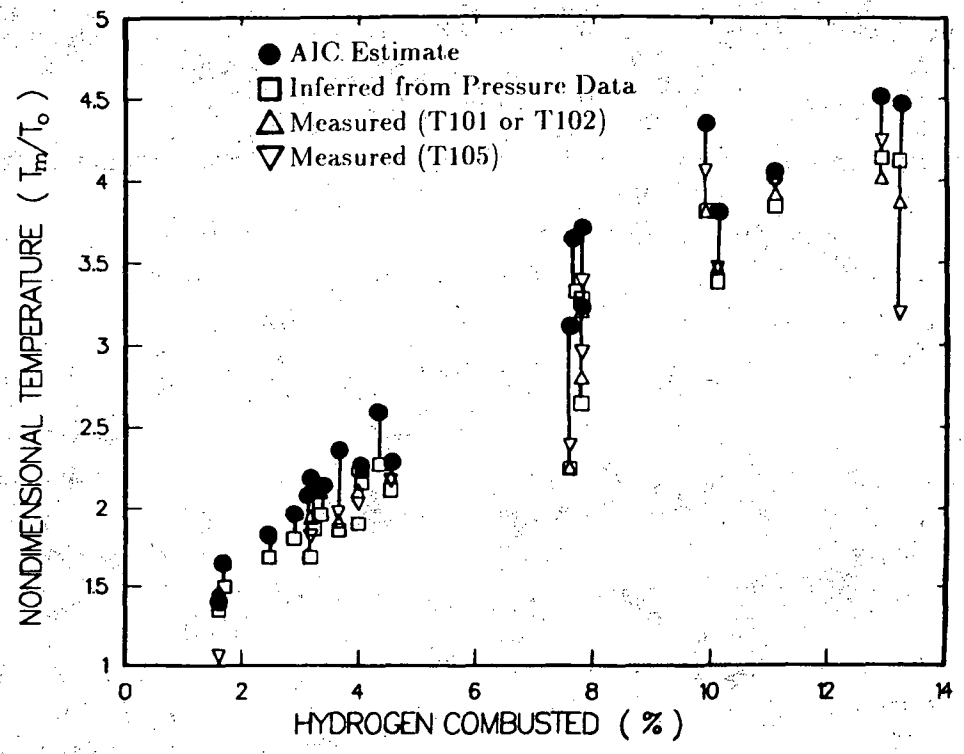

Figure 33: Peak gas temperature ratios for the NTS premixed combustion tests

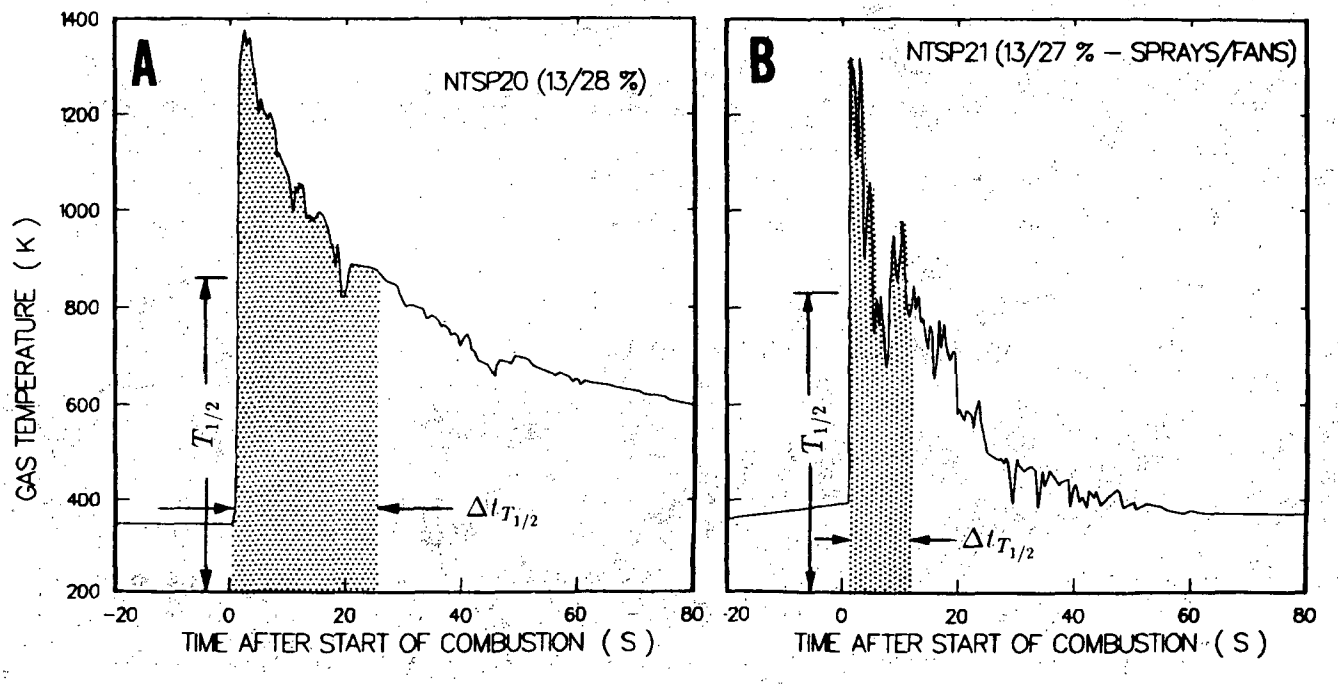

Figure 34: Comparisons of 3-mil thermocouple responses for tests NTSP20 (A) and NTSP21 (B)

It is apparent from the figures in the appendices that thermocouples T120 and T121 respond differently. Thermocouple T120 appears to follow the combustion better; the initial temperature profiles are steeper and the time to peak temperature is earlier than for T121. These effects are reflected in the heat flux results inferred from the wall thermocouples and are discussed in the next section. The temperature profiles for T120 are also more consistent with the average wall temperature estimates, although the magnitudes are often quite different.[22] The early peak and subsequent cooling seen in the average wall and T120 profiles for the more severe tests occur because the stainless steel dewar thermal diffusivity is low. At the early times of the experiment, the heat absorbed at the surface remains near the surface. At late times, the heat into the wall is reduced and the heat is also diffused into the wall. The temperature response of T121 is so different that it is suspected that it must have been mounted (1) on the wall differently, or perhaps (2) to some object on the wall which was not stainless steel. It was believed initially that differences in the local thermal environment at various elevations in the dewar could be determined by review of the thermocouple traces from the seven wall thermocouples. Before significant time and effort is directed towards this end, the specific thermocouple mounts should be reviewed, and the data should be cross-plotted given the above-discussed discrepancies in T120 and T121 signals.

5.5 Heat Transfer Results

5.5.1 Results from Calorimetry

Comparative peak heat flux results and computed energy depositions obtained from the calorimetry are given in Tables A.8 and A.9 and Table A.11 of Appendix A, respectively. These results are also plotted for each of the three classes of tests in Figures B.10, B.21, and B.30 of Appendix B. Representative heat flux and energy deposition profiles for total thin-film gauge H232 (Figures B.6, B.17, and B.28) and for Schmidt-Boelter gauge H503 (Figures B.7, B.18, and B.29) are also provided in Appendix B. These figures compare gauge responses for tests of the same class (*e.g.*, 3 tests from the steam-laden series), but of different severity. Additional heat transfer profiles (fluxes and depositions) for selected Gardon and Schmidt-Boelter gauges and for the thin-film gauge are provided for all tests in Appendix C.

[22] Wall heat-up during combustion is modeled in SMOKE assuming a uniform heating rate. The energy deposition during this time is taken as the product of the AIC energy deposition and the fraction obtained from subtracting the ratio of the measured peak pressure and the AIC peak pressure from unity. This assumed heat input can be thought of as a correcting procedure necessary for reduction of the AIC pressure to the measured pressure level. Once combustion is terminated, the total heat input to the wall is equivalent to the heat losses from the gas. Note that for the lean tests where the pressure 'rolls-over', the total heat flux following combustion is initially low. The wall temperature for these cases tends to decrease for a short time and then increase (*e.g.*, see Figure C.15-C of Appendix C). This discontinuity in the wall temperature profile does not occur if the combustion actually terminates at the time of peak pressure, as is expected for the non-lean tests.

Heat Flux Results from Calorimetry

In general, the peak heat fluxes from the different calorimeters increased with increasing initial hydrogen concentration as would be expected. This results from enhanced convective heat transfer induced by combustion and from increased radiative heat transfer from the steam (that was initially in the vessel and that was produced during combustion). The combustion of gas mixtures with larger initial hydrogen concentrations yields elevated gas temperatures during and following combustion. This in turn leads to larger radiative heat transfer from the gas. The dramatic increase in the radiative flux, q_{Ri}, can be estimated from the peak gas temperatures, T_{mi}, for two tests using Eq.(5):

$$\frac{q_{R1}}{q_{R2}} \propto \left(\frac{T_{m1}}{T_{m2}}\right)^4 \tag{5}$$

It is assumed in Eq.(5) that the steam emittances would be comparable for tests having approximately the same precombustion steam concentration. Table 7 provides estimated increases in the peak radiative heat flux using Eq.(5) for representative tests from the three test classifications. In addition, measured total peak heat flux ratios are provided for Schmidt-Boelter gauge H503, thin-film gauge H232, slug calorimeter H104, and from the aluminum cube thermocouple T504 or T505. Reference fluxes are taken for the tests from each class with the lowest initial hydrogen concentration.

Table 7: Local Peak Radiative and Total Heat Flux Ratios

Test Name	H_2^* (%)	H_2O^* (%)	Radiative Flux Ratio $q_R/q_{R_{ref}}$ †	Total Flux Ratios $q_T/q_{T_{ref}}$ ‡ H232	H503	H104	T504/T505§
Standard Tests							
NTSP9P	6.0	4.6	1.0	1.0	1.0	1.0	1.0
NTSP13	7.8	4.4	7.4	5.64	4.76	5.64	4.33
NTSP15	9.9	4.2	14.9	7.49	9.12	7.49	11.2
Steam-Laden Tests							
NTSP12	6.9	28.3	1.0	1.0	1.0	1.0	1.0
NTSP16	10.1	29.5	7.31	9.54	3.18	3.85	4.21
NTSP20	12.9	27.8	13.3	19.9	5.99	3.38	10.1
Tests with Sprays							
NTSP11	5.8	4.9	1.0	1.0	1.0	1.0	1.0
NTSP18	6.6	27.3	1.18	1.83	1.92	0.88	1.42
NTSP21	13.2	27.4	11.5	12.0	10.6	3.36	13.1

* Precombustion hydrogen and steam concentrations

† From Eq.(5); peak gas temperatures (T101 or T102) taken from Table A.6 of Appendix A

‡ Peak total heat fluxes taken from Tables A.8 and A.9 of Appendix A

§Results from T505 used only for sprays-on tests

The increases in the heat flux ratios are dramatic for each of the classes of comparative tests. Radiative fluxes are shown to increase by factors of 10 and more as the initial hydrogen concentration increases from 6% to 13%. Similar increases are also shown for the different total calorimeters. The "marginal" performances of H503 and H104 for the 13% hydrogen combustion tests are also evident from the lower than expected total flux ratios provided.

Additional trends from the calorimetry are provided by a review of the results in the appendices. The comparative total heat flux profiles shown in Appendix B for H503 and H232 are quite similar. The measured total Gardon and Schmidt-Boelter peak fluxes also compare reasonably well with the computed thin-film fluxes for most of the lean hydrogen combustion tests (see Tables A.8 and A.9 of Appendix A). Data from these instruments differ more for tests conducted after test NTSP15, performed on December 22, 1983.[23] For the latter tests conducted at NTS, there is some concern that the total Schmidt-Boelter gauges were not functioning as expected, since the peak heat fluxes were low (compared to average estimates inferred from the pressure). This may have occurred because the gauges were not water-cooled sufficiently. In addition, as indicated in the thin-film gauge assessment section, the data recording rates may have been too slow for the most severe (13%) hydrogen combustion tests, and the peaks may not have been recorded. Post-test calibrations for the total Schmidt-Boelter gauges performed by Medtherm [19] and for the thin-film gauge performed at SNLA revealed that calibration shifts were less than 10% and such deviations would not account for the reduced peak fluxes.

Generally, the downward-oriented Schmidt-Boelter gauges (H503 and H507) measured larger fluxes than did the upward-oriented gauges (H502 and H506). Given that these gauges were located on the equipment platform near the vertical center of the dewar, this result was somewhat surprising. The upward-oriented gauge responses may have been affected by the equipment on the platform. The radiant exchange with the equipment would have been less than with the gas. Similarly, the forced convective heat transfer induced by combustion might also have been limited by the obstructing equipment. Heat fluxes measured by H507 (downward-oriented) located above the injection source were greater typically than the fluxes measured by downward-oriented gauge H503, located near the dewar vertical centerline (see Figures 8 and 9). These flux profiles and the total peak fluxes were probably in better agreement than is indicated, for example, in Table A.9 of Appendix A, since the tabulated peak fluxes do not account for the baseline flux correction. Typically, this correction was greater for H507 (see Table A.9 of Appendix A). Heat flux results from the upward-oriented gauges H502 and H506 were generally comparable and did not indicate location dependence. Re-

[23] Four–continuous injection combustion tests were performed prior to the last four premixed combustion tests (NTSP18, NTSP20, NTSP21, and NTSP22). The more severe thermal loading on the instrumentation from the continuous–injection tests led to failures of gauges H506 and H507 and has been postulated to have affected the performance of the other Schmidt-Boelter and Gardon instrumentation. Thermocouple T151, above the injection source, failed during the continuous–injection combustion tests, and the total slug calorimeter (H104) results were marginal for two of the last four tests.

sults from the downward-oriented gauge H504 should not be compared with the other Schmidt-Boelter gauge results, except for the lean hydrogen combustion experiments, given the gauge cooling problems described previously.

It is difficult to assess the performance of Gardon gauge H106 used in the Hydrogen Behavior tests, since there are so little other calorimetry data available for comparison. Overall, the data appear consistent for six of the seven tests for which data were provided. The peak heat fluxes were typically higher than were the pressure-inferred fluxes as would be expected given the location of the gauge at the top of the dewar (Figure 8) and that the tests were lean combustion experiments. The measured peaks compared well with heat fluxes computed from the total slug calorimeter H104, which operated for most of the tests in which H106 was a total gauge.

Peak heat flux results from the slug calorimeter H104 and from thermocouple H504 inside the aluminum cube were consistent, generally, with the thin-film and EPRI-provided calorimetry results. Peak heat fluxes from T505 (thermocouple mounted to the top surface of the aluminum cube) were typically lower than T504 results for the more severe tests and were comparable to T504 results for lean combustion experiments (see Table A.8 of Appendix A). The differences may be attributed to (1) differences in the thermocouple mounts, (2) differences in the aluminum exterior surfaces during testing, and/or (3) different exterior surface water layers prior to testing. In the latter case, the top surface of the cube was probably more thoroughly wetted by the sprays used in pretest gas conditioning than were the side walls. This layer would serve as an additional insulating layer during testing.

Peak heat flux results computed from wall thermocouple T120 were generally consistent with other calorimetry results. The peak flux results from T121, on the other hand, were generally lower than those computed for T120 or measured by other calorimetry in the dewar. In addition, the times of peak heat flux for T121 were typically 20–40 seconds after the time of peak pressure. For all other instrumentation, the times of peak heat flux generally occurred prior to the time of peak pressure or at worst, within 1–3 seconds after the peak. The times of peak heat flux are given in Tables A.8 and A.9 of Appendix A in terms of the difference (denoted by $\Delta t_{mp} = t_m - t_p$) between the time corresponding to the instrumentation peak heat flux and the time of peak pressure. For T121, Δt_{mp} was always positive and was also usually large, indicating that the time of peak heat flux occurred late in the test. It was also typically positive for T120 for the more severe combustion tests, when the peak heat flux estimates were lower than measured by the other instrumentation.

As a final comment, it should be noted that Δt_{mp} approached zero for most of the calorimetry for tests where the initial hydrogen concentration was $> 8\%$, indicating that the combustion was over at the time of peak pressure. For the lean combustion experiments when sprays and fans were not operated, Δt_{mp} was large and negative, indicating that the instruments were measuring local combustion-induced heat fluxes. The peaks associated with these measurements were also typically greater than those computed from the pressure data after combustion was terminated.

Energy Deposition Results from Calorimetry

Energy deposition results were computed for the calorimeters by integrating the heat flux measurements. Comparative total results are included for the Gardon and Schmidt-Boelter instrumentation and for the thin-film gauges in Appendices A and B. The heat flux measurements from the other instrumentation were not corrected to account for gauge heatup (and associated increased heat losses), and thus the integrated fluxes were not true measures of the energy deposition from the gas. Note that for the thin-film and EPRI-provided gauges, late-time baseline fluxes were used in Eq.(4). This correction was necessary since the gas was in quasi-equilibrium with the dewar, but not with the cooler thin-film gauge and water-cooled EPRI calorimetry.

Energy depositions for H503 and H232 are provided in Table A.11 of Appendix A. Tabulations of the energy deposition are given for the duration of the experiment ($Q_{T_{all}}$) and for times after the time of peak pressure (Q_{T_P}). The difference between the two depositions provides an estimate of the energy lost from the gas during combustion. Further, Q_{T_P} tabulations for the calorimetry can be compared with the global estimates inferred from the postcombustion pressure decays. Upperbound estimates for energy deposition are also provided for each test. These depositions were obtained using AIC results (denoted by subscript 'AIC') for the final gas state and the precombustion conditions (subscript '0') for the initial state, as shown in Eq.(6):

$$Q_{AIC} = \frac{V}{A}\left[(\rho C_v T)_{AIC} - (\rho C_v T)_0\right]. \tag{6}$$

It is assumed in this upperbound estimate of the average energy deposition that all of the energy released as a result of combustion can be absorbed by the dewar and that the gas can be cooled to its initial state. In fact, the pressure and temperature profiles indicate that the gas state remains elevated for long times after combustion. Energy depositions computed from the calorimeters would be expected to be lower than Q_{AIC}. This is generally found to be the case (see Table A.11 of Appendix A and Figures B.10, B.21, and B.30 of Appendix B).[24]

The comparative plots of Appendix B show that nearly all of the heat removal from the gas (to the dewar) occurred in the first 50-100 seconds after initiation of combustion. The energy deposition profiles approach some asymptote at late times, after which the gas and dewar walls are in equilibrium. Additional cooling for these late times occurs because the vessel is losing heat to the surroundings. In addition, the energy depositions increase significantly with increasing hydrogen concentration; this energy removal from the gas is seen in the initial slopes of the energy deposition curves. This should be expected given the dramatic increases in the heat fluxes with increasing hydrogen concentration and in the subsequent accelelerated heat flux decays following combustion.

[24] Energy deposition results for Gardon gauge H106 and Schmidt-Boelter gauge H507 exceed the upperbound value Q_{AIC} for a number of the tests. H106 was not water-cooled, and the late-time heat fluxes may have been high as a result. H507 measured the largest heat fluxes of the five total Schmidt-Boelter gauges and also required the largest baseline flux correction.

Finally, it is should be noted that the computed thin-film energy depositions are 30–50% less than results from the Gardon and Schmidt-Boelter gauges. It is believed that the thin-film depositions are low because the assumptions used in processing the data (see THIN in Section 3.1.2) become invalid for times $\geq$ 100 seconds after initiation of combustion. The computed heat fluxes would thus be low for late times, and the energy depositions would be correspondingly reduced. The semi-infinite solid assumption is, however, appropriate for early times, and thus the peak fluxes reported for gauge H232 would be expected to be accurate.

5.5.2 Results Inferred from Pressure Measurements

In addition to measuring gas pressure, pressure sensors can be used as global heat flux measuring devices, when the data analysis procedures outlined in Section 3 are applied. In this section, representative heat transfer results obtained from pressure signal processing are provided. Comparative peak total and radiative heat flux results and computed postcombustion energy depositions inferred from the pressure signals are given in Tables A.7 and A.10 of Appendix A, respectively. These results are also plotted for the standard and steam-laden tests in Figures B.11 and B.22 of Appendix B and with the calorimetry results in Figures B.10 and B.21. Representative postcombustion total heat flux and energy deposition profiles (Figures B.8 and B.19) and radiative fluxes and depositions (Figures B.9 and B.20) are also provided in Appendix B for the standard and steam-laden tests. Additional heat transfer profiles inferred from the pressure are provided in Appendix C. These results are usually plotted with "good" calorimetry results to provide comparisons between local measurements and average estimates of heat transfer for each test. Note that pressure-inferred total heat transfer results are not computed for tests with sprays-on, given the limitations of SMOKE (see Section 3.1.2). Radiative depositions from sprays-on tests are included in Table A.10; these values were computed assuming that the gas composition did not change following combustion. Radiative results for these tests are provided only for comparison with standard and steam-laden test results; they should not be used except for this comparison.

Heat Flux Results Inferred from the Pressure

In general, the pressure-inferred heat flux results are consistent, as indicated in the comparative plots and in the tabulations. Results inferred from lean-combustion tests would be expected to be lower than calorimeter results, since average estimates would not account for the nonuniformities associated with localized combustion.[25] Pressure-inferred results for complete combustion tests would be expected to be consistent with

[25] The calorimetry were located in the upper part of the dewar, generally near the centerline. Videos of the lean–combustion tests in the dewar indicate that local combustion occurred in the vicinity of the instrumentation; calorimeter measurements thus would be expected to be greater than the global estimates.

heat flux measurements; previous work using experimental data from intermediate-scale facilities [11] has demonstrated good agreement between pressure-inferred results and calorimetry measurements.

The pressure-inferred peak heat flux results and the postcombustion heat flux profiles for the standard and steam-laden tests are representative of the phenomena measured by the different calorimeters. Increasing the hydrogen concentration (*i.e.*, combustion severity) results in increased peak fluxes. The peak fluxes become quite large (> 25 W/cm^2), unlike the calorimeter measurements, for the most severe tests. The dramatic increases in the peak fluxes are demonstrated in Table 8 for representative standard and steam-laden tests. Fluxes from tests NTSP9P and NTSP12 are used as reference conditions in the standard and steam-laden test comparisons, respectively.

Table 8: Peak Radiative and Total Heat Flux Ratios Inferred from the Pressure

Test Name	H_2/H_2O^* (%)	q_R W/cm^2	q_T W/cm^2	Total Ratio $q_T/q_{T_{ref}}$ †	Radiative Ratios $q_R/q_{R_{ref}}$ †	q_R/q_T	q_R/q_C ‡
Standard							
NTSP9P	6.0/4.6	0.14	0.41	1.0	1.0	0.34	0.52
NTSP00	6.6/4.5	0.62	2.03	4.95	4.43	0.31	0.45
NTSP13	7.8/4.4	3.06	5.79	14.1	21.9	0.53	1.13
NTSP15	9.9/4.2	5.94	10.6	25.8	42.4	0.56	1.27
Steam-Laden							
NTSP12	6.9/28.3	0.55	1.35	1.0	1.0	0.41	0.69
NTSP05	7.8/31.3	2.61	6.31	4.67	4.75	0.41	0.69
NTSP16§	10.1/29.5	6.75	9.65	7.15	12.3	0.70	2.33
NTSP08	11.1/27.2	12.3	21.2	15.7	22.4	0.58	1.38
NTSP20	12.9/27.8	15.3	25.4	18.8	29.9	0.60	1.50

* Precombustion hydrogen and steam concentrations

† NTSP9P and NTSP12 fluxes used as reference conditions

‡ $q_C = q_T - q_R$ in this work

§ Results taken from marginal signal P102 (see Figure 17)

The flux ratios $q_T/q_{T_{ref}}$ and $q_R/q_{R_{ref}}$ vary by factors of $\sim$ 4–40 for the tests considered. The increases in peak flux are not linear as can be seen in the peak heat flux plots of Figures B.11 and B.22. The curves shown on these figures are "eye-ball" estimates of the trends. The peak heat flux increase would be expected to be more substantial (than a linear increase, for example), given that the heat transfer is by coupled convective and radiative exchange; the latter mechanism has been shown previously to be proportional to the gas temperature raised to the fourth power.

It is also apparent from Table 8 that the relative importance of radiative heat transfer increases with test hydrogen concentration, and further, that the radiative mechanism dominates for the most severe tests at early times after combustion. For the lean combustion tests, the average gas temperatures computed from the pressure

are low and convection dominates as the transfer mechanism. For hydrogen concentrations > 8% and steam concentrations ≤ 5%, radiative transfer becomes the more important energy exchange mechanism. For the steam-laden tests, the additional steam (~ 30%) serves as a diluent (*i.e.*, heat sink) and reduces the peak temperatures. It is seen for these tests that the radiative mechanism does not become dominant until hydrogen concentrations in excess of 9–10% are reached. Although the radiative transfer mechanism becomes dominant for the most severe tests, the convective/condensation mechanisms still are important, providing 30–45% of the heat removal from the gas near the maximum conditions.

Energy Deposition Results Inferred from the Pressure

Trends from the pressure-inferred postcombustion energy deposition results are similar to those reported for the total calorimetry. The initial energy deposition following combustion is large, increasing significantly with increasing combustion severity. The energy deposition profiles shown in Appendices B and C typically reach asymptotes 100–150 seconds after completion of combustion. These times are somewhat larger than the 'leveling-off' times reported for H503 and H232. The radiative energy deposition profiles are similar to the total energy depositions, only lower, as would be expected.

Table 9: Radiative and Total Energy Deposition Ratios Inferred from the Pressure

Test	Q_R	Q_T	Total Ratios		Radiative Ratios		
Name*	(W/cm^2)	(W/cm^2)	Q_T/Q_{AIC}†	$Q_T/Q_{T_{ref}}$‡	$Q_R/Q_{R_{ref}}$‡	Q_R/Q_T	Q_R/Q_C§
Standard							
NTSP9P	15.7	48.5	0.47	1.0	1.0	0.33	0.49
NTSP00	23.6	71.8	0.67	2.03	2.02	0.33	0.49
NTSP13	71.3	144.2	0.70	4.09	6.09	0.49	0.96
NTSP15	92.8	197.9	0.67	5.60	7.93	0.47	0.89
Steam-Laden							
NTSP12	26.9	52.6	0.58	1.0	1.0	0.51	1.04
NTSP05	53.6	108.6	0.61	2.06	1.99	0.49	0.96
NTSP16	114.1	155.0	0.60	2.95	4.24	0.70	2.85
NTSP08	190.5	234.3	0.65	4.45	7.08	0.81	4.26
NTSP20	163.6	218.9	0.64	4.16	6.08	0.75	3.00

* Precombustion hydrogen and steam concentrations given in Table 8

† Q_{AIC} was computed from Eq.(6) and is tabulated in Table A.10 of Appendix A

‡ NTSP9P and NTSP12 fluxes used as reference conditions

§ $Q_C = Q_T - Q_R$ in this work

Table 9, shown above, provides comparative radiative and total energy deposition results from representative standard and steam-laden combustion tests. Trends from the energy deposition comparisons of $Q_i/Q_{i_{ref}}$ are similar to those reported for the peak heat fluxes in Tables 7 and 8. As the combustion severity increases, the radiative and

total depositions increase by factors of 2–8 over the reference test energy depositions. Such increases are particularly important when assessing equipment survival issues since the energy deposition is a direct measure of the thermal loading.

The addition of steam to the precombustion gas mixture affects the mechanisms of postcombustion gas cooling. The radiative transfer mechanism is shown to be much more important than the convective mechanism for the more severe steam-laden tests (hydrogen concentrations > 10%), while the two mechanisms have nearly equal importance for the most severe standard test performed at NTS. These generalizations are demonstrated in the Q_R/Q_T and Q_R/Q_C ratios. The increased dominance of the radiative mechanism is attributed to: (1) the increased gas emittance due to the larger precombustion steam concentrations; and (2) smaller total energy depositions for the steam-laden tests. These points are demonstrated in comparing the pressure-inferred energy depositions for tests NTSP15 and NTSP16, two 10% hydrogen combustion tests. The total energy depositions for these tests were $\sim$ 200 J/cm^2 and $\sim$ 150 J/cm^2, respectively, while the radiative depositions were nearly the same ($\sim$ 90 J/cm^2 and $\sim$ 110 J/cm^2, respectively). It is believed that steam condensation is more important for tests with higher initial steam concentrations, and that this mechanism leads to more rapid gas cooling after combustion. The radiative component would be expected to be correspondingly reduced; however, the increased gas emittance somewhat offsets this reduction.

Finally, the ratio of the pressure-inferred total postcombustion energy deposition to the upperbound AIC energy is approximately 0.6–0.7 for most tests. Exceptions would be for the lean-combustion experiments (*e.g.*, test NTSP9P) when the combustion duration is so long that significant energy transfer occurs prior to the time of peak pressure. The energy deposition during combustion is not computed from the pressure; however, from the P_m/P_{AIC} ratios (refer to footnote 22), we would estimate that $\sim$ 15% of the AIC energy is lost to the vessel walls during combustion for non-lean tests, and greater percentages are possible for tests in which the initial hydrogen concentration is < 6-7%. Note also that the energy deposition ratios computed from the pressure signals are comparable to the ratios which would be obtained from the calorimetry for times after the time of peak pressure. The calorimetry factors Q_{T_P}/Q_{AIC} and $Q_{T_{all}}/Q_{AIC}$ can be computed from results in Table A.11 of Appendix A.

5.5.3 Comparison of Local and Global Heat Transfer

Total peak heat fluxes from the calorimetry (*i.e.*, local) and inferred from the pressure (*i.e.*, global) are compared in Figure 35 for the 21 premixed combustion experiments. The curve is a "best estimate" of the pressure-inferred results. The shaded region is provided to bound the representative "good" and "marginal" calorimetry results which are also plotted.

The calorimetry results and global estimates are typical of what would be expected for the lean combustion tests (< 6% hydrogen combusted). The pressure-inferred peak fluxes are generally less than the calorimetry peaks. The scatter in the calorimetry

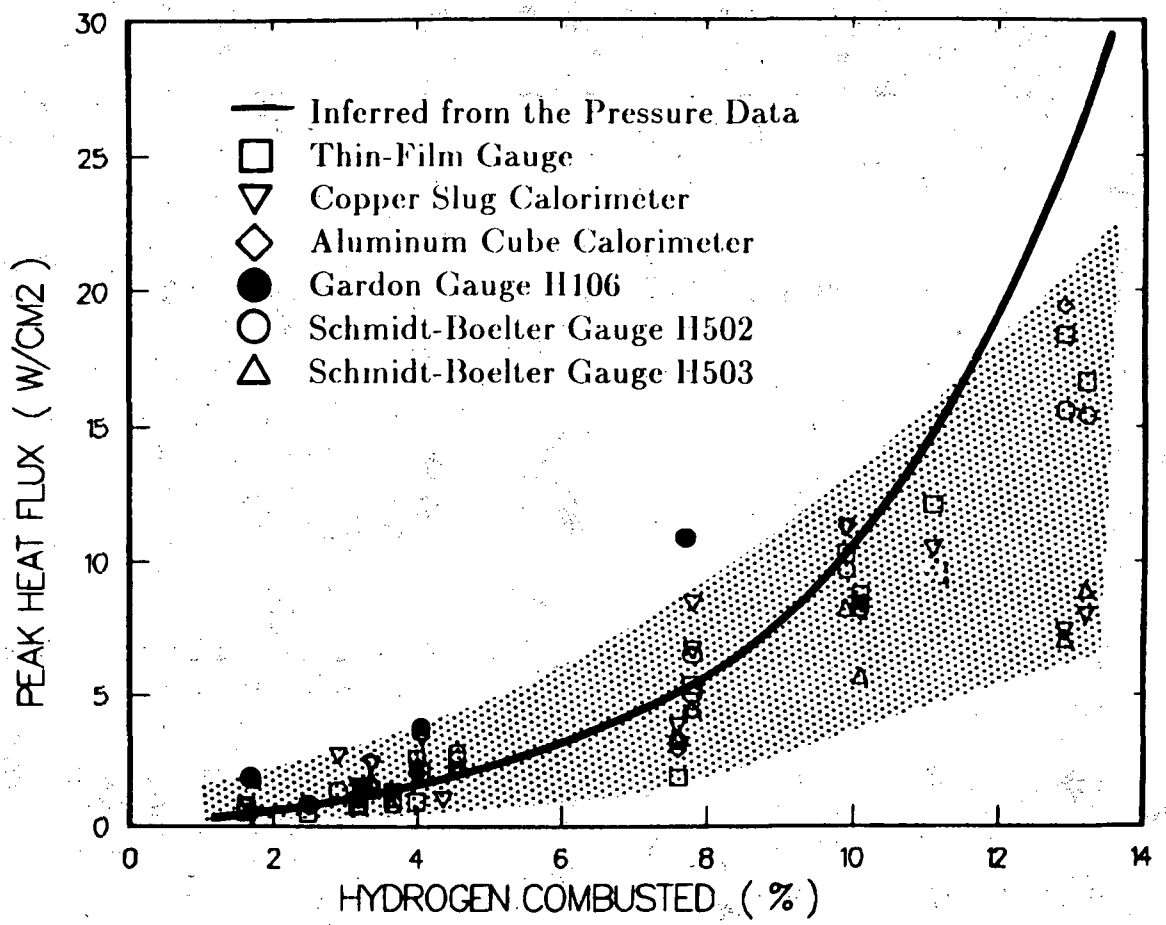

Figure 35: Local and global total peak heat flux comparisons from the NTS premixed combustion tests

results might also be expected since localized (and incomplete) combustion in the dewar would lead to location-dependent flux measurements.

It would be expected that the local effects would diminish as the combustion severity increases, since the combustion should be more uniform. Unfortunately, this is not seen from the results plotted in Figure 35. The large variance in the calorimetry peak fluxes for the latter tests should probably be attributed to the deterioration of the instrumentation as a result of the cumulative testing. Problems such as surface deterioration of the aluminum cube, insufficient water-cooling for the Schmidt-Boelter gauges, insufficient data recording rates, etc., have been discussed throughout the preceding sections. It is believed that the calorimetry peak heat fluxes are too low for the most severe tests, and that the pressure-inferred estimates are probably more representative of the phenomena. This is based on the argument that the radiative flux, which should dominate for the most severe combustion tests, is predicted to be > 15 W/cm^2, and that the early-time convection should be large given the combustion-induced tur-

bulence. Therefore the average peak total fluxes would be expected to be at least 20–25 W/cm^2, and local fluxes perhaps as great as 30–40 W/cm^2.

Similar trends can be noted from the total energy deposition results shown for standard and steam-laden tests in Figure 36. The shaded region becomes progressively larger with increased hydrogen consumption. The energy depositions shown for the calorimetry are for the duration of the experiments, while the pressure-inferred results are for postcombustion times only. It would have been expected, therefore, that the calorimetry depositions would have been greater for all conditions considered, although this is obviously not the case. The deterioration of the calorimetry performance in the most severe (13%) combustion test can be seen again from this figure, since the energy depositions shown for this test are actually less than for the 10% and 11% hydrogen combustion experiments.

Energy depositions measured by the calorimetry for the sprays-on tests are shown in Figure 37. Comparisons of global depositions are not provided, owing to the limitations of the SMOKE pressure signal processing. For this case, the shaded region provides an estimate (which is only a best guess and which has not been verified) of what might be expected when sprays are operative. The different calorimeters measured essentially the same total heat fluxes for the most severe test (NTSP21). Given the rapid decay of the gas pressures and temperatures (measured by thermocouples), the Schmidt-Boelter instrumentation probably did not overheat (leading to erroneous measurements). Similarly, given the short time interval of interest (when sprays are operative), the semi-infinite solid approximation for the thin-film was valid so that these results also are probably reasonable. Note that the upperbound of the shaded region is less than would be expected for the standard and steam-laden tests, given the significant gas cooling obtained from the evaporation of the sprays.

One of the goals in the assessment of the NTS premixed combustion data was to determine if local phenomena were considerably different from global estimates for the phenomena in such a large-scale test vessel. Unfortunately, this issue cannot be resolved based on the data which have been reported in this work. Instrumentation operability has been shown to be questionable for most of the total heat flux instrumentation for at least a few of the tests. In addition, most operable total instrumentation were located in the same vicinity, so that the measurements would have been expected to have been comparable if the instrumentation had functioned as intended. Radiative data, which could be used to characterize local phenomena, also were not obtained. It remains to be seen whether local effects can be characterized, using the remaining wall and gas thermocouple data which were not provided to SNLA. At this time, based on the comparisons presented in this and previous sections, it must be recommended that the global results be used for bounding the experiments and for benchmarking computer simulations.

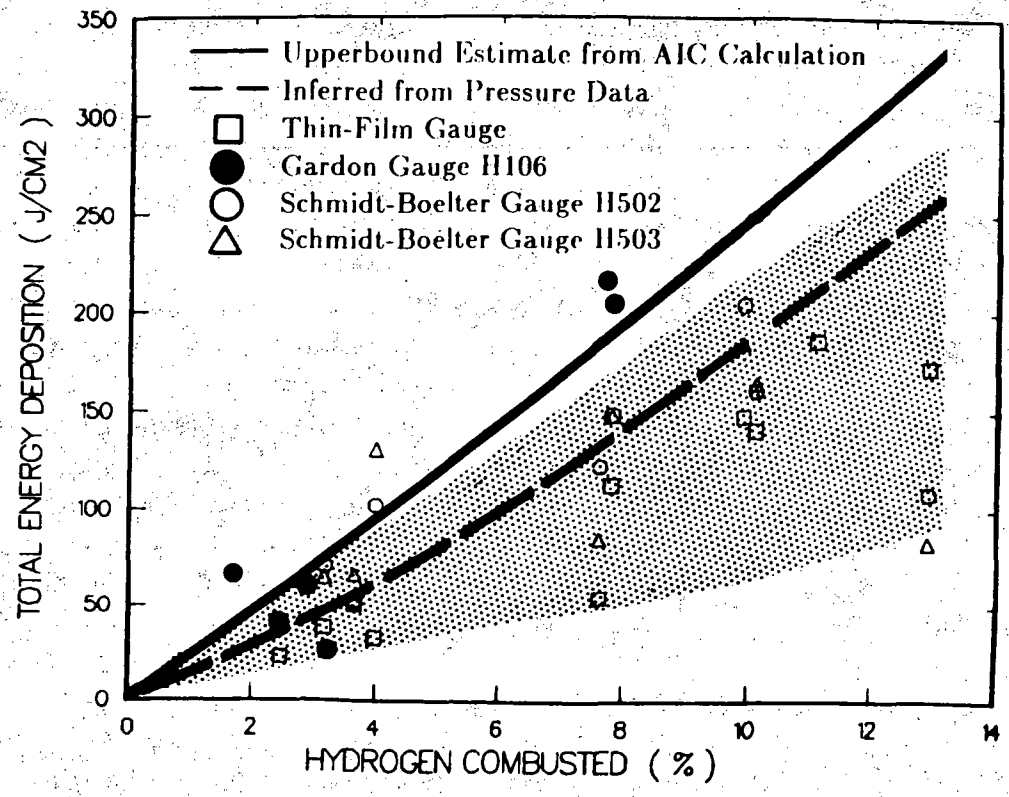

Figure 36: Local and global total energy deposition comparisons from the standard and steam-laden NTS premixed combustion tests

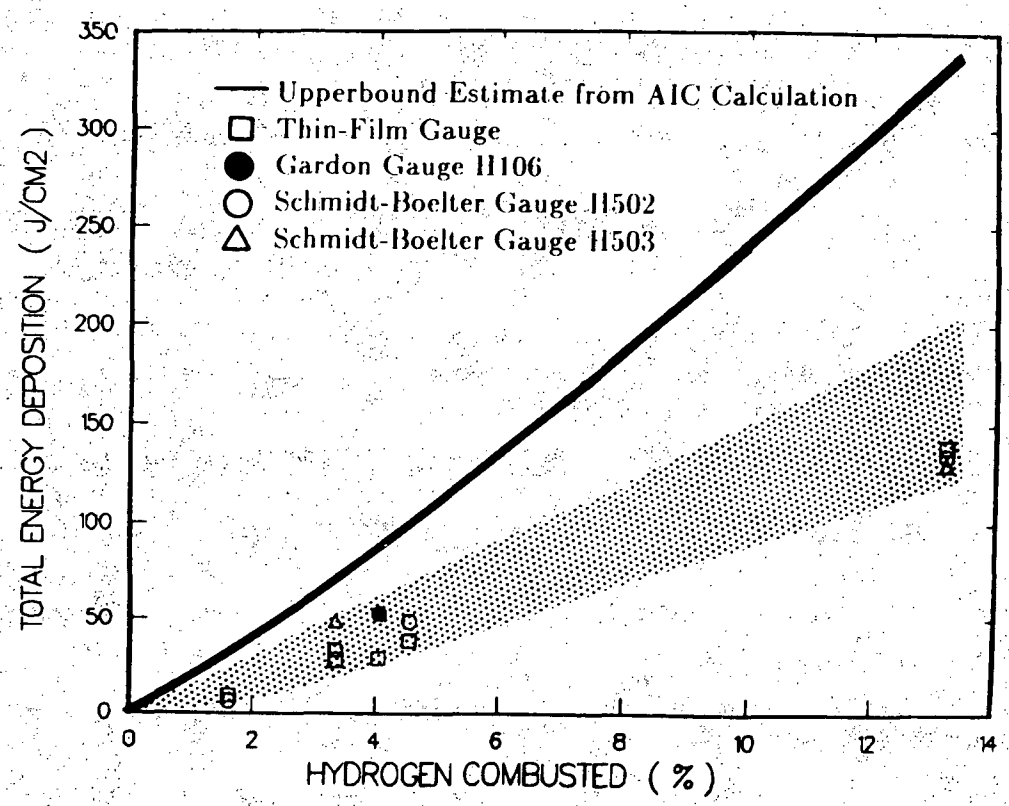

Figure 37: Local total energy deposition results from the sprays-on NTS premixed combustion tests

6 Summary – Closing Remarks

This report provides results from an in-depth analysis of twenty-one premixed combustion experiments conducted in the 2084 m^3 spherical hydrogen dewar located at the Nevada Test Site. These tests, funded jointly by EPRI and the NRC, were performed to study combustion processes in a large-scale vessel and to evaluate associated safety-related equipment response to the resulting thermal environments. Hydrogen concentrations in these tests ranged from 5 to 13% (by volume) and steam concentrations from 4 to 40%. Several tests also incorporated spray systems and/or fans which enhanced the combustion rate and significantly altered the postcombustion gas cooling.

Data provided by EPRI from instrumentation associated with estimating the thermal environment in the dewar during and following combustion have been evaluated in this work. Data from the representative safety-related equipment installed in the dewar to assess equipment survival issues have not been reviewed. Further, this work has been restricted to the analysis of only those data records which were provided to Sandia on computer tapes. The data reduction package SMOKE has been used to process data from thin-film gauges and capacitance calorimeters (Sandia supplied), Gardon and Schmidt-Boelter heat flux gauges (EPRI supplied), gas and wall thermocouples (EPRI supplied), and pressure sensors (Sandia and EPRI supplied). Local estimates of the heat transfer were obtained from the calorimetry, and global averages were inferred from the pressure. Instrumentation "goodness" for each test has been assessed based on reviews of the raw data and on comparisons of local and global results.

Overall conclusions about the "goodness" of the instrumentation and the associated performance are as follows:

<u>Instrumentation Assessment</u>

- Pressure signals from the different sensors were reasonably consistent for the different tests. Multiple pressure measurements for a given test were also comparable. However, the EPRI/EG&G-provided sensors typically measured slower pressure decays (following completion of combustion) than did the SNLA-provided gauges for the few tests in which comparisons were possible. Since the global total heat transfer depends on the time rate of change of the pressure, the total heat fluxes and energy depositions computed from EPRI/EG&G-provided sensors might not be conservative (*i.e.*, provide upperbounds for the heat transfer).

- Global estimates of the gas temperature inferred from the gas pressure compared well with measured temperatures from the 3-mil thermocouples. Results from the 32-mil thermocouples did not follow the early transients (as expected due to thermal inertia effects) associated with combustion but they agreed with the 3-mil data and pressure-inferred temperatures for the late-time cool-down period.

- Results were inconsistent from the two wall thermocouples for which data were provided. It is believed that one thermocouple (T120) responded as would be

expected in the dewar. T120 measurements also compared reasonably well with global wall temperature estimates obtained from the pressure signal processing.

- Sandia-supplied total thin-film and slug calorimetry functioned for nearly all tests. Problems with the electrical connections for the thin-film gauge led to failures during some of the early tests. Once corrected, the gauge operated effectively for the remainder of the tests. The slug calorimeter provided "good" or "marginal" signals for all tests.

- EPRI-provided total Schmidt-Boelter gauges functioned for most of the 12 tests of the Equipment Survival Testing Program for which they were installed in the dewar, although problems with the water cooling for these gauges may have been responsible for their poor performance during the most severe tests. In addition, the uncooled total Gardon gauge appeared to have operated effectively for 7 of the 8 tests in the Hydrogen Behavior Test Series for which it was installed in the dewar.

- The Sandia HBS flat-plate calorimeter failed early in the testing. The results from this calorimeter were inconsistent, and all results were assumed to be "bad". The HBS aluminum cube calorimeter provided reasonable flux results for the 12 tests for which it was installed in the dewar.

- Sandia-supplied calorimeters for estimation of the local radiative heat transfer were inoperable for most of testing, and data from EPRI-supplied radiative calorimetry could not be reduced given uncertainties in the calibration and the correction terms to account for the sapphire cover plates.

Assessment of Heat Transfer Results

- Early-time total heat flux results from the Sandia-provided calorimetry (thin-film gauge, slug, and cube calorimeters) were generally comparable with the EPRI-supplied total calorimetry (Schmidt-Boelter and Gardon gauges) for the tests where the hydrogen concentration was $\leq 8\%$. The total calorimetry results deviated significantly for those experiments at higher concentrations conducted near the end of testing. These deviations have been primarily attributed to instrumentation deterioration.

- The global estimates of total heat transfer rates inferred from the pressure signals were typically less than the local measurements for lean combustion and higher for tests in which the precombustion concentrations were above 10% hydrogen. These global results are believed to be more accurate than the calorimetry results for the non-lean combustion experiments.

- Total energy deposition results from the EPRI-supplied calorimetry were generally consistent with the global results inferred from the pressure data for lean combustion tests. The depositions computed from the calorimetry signals were

probably low for the most severe combustion experiments performed at the end of the testing.

- The thin-film energy deposition results were typically 30–50% lower than either the global pressure-inferred or local results obtained from EPRI calorimetry for tests in which sprays were inoperative. When sprays were operating, the thin-film gauge results were comparable to the EPRI-calorimetry. Discrepancies in the thin-film energy deposition estimates are attributed to shortcomings in resolving the late-time gauge response because of the assumptions used in the data processing.

- Global estimates of radiative heat transfer inferred from the pressure for lean combustion tests were $\sim$ 30–50% of the total heat transfer inferred from the pressure. For initial hydrogen concentrations $>$ 8%, the radiative transfer became more dominant, especially for the steam-laden combustion tests. This was reflected in both the radiative peak heat fluxes and in the postcombustion energy depositions.

Local versus global issues cannot be resolved from the data provided in this report, given the problems with instrumentation performance during the course of testing. Further, the heat transfer instruments were all located either at the top of the dewar or on the equipment platform; results from these instruments would be expected to be comparable. Since there are additional wall and gas thermocouple data for locations throughout the dewar, local conditions may still be quantifiable if the data can be obtained. It is expected, however, that characterization of the local environment will be difficult for this large-scale experiment, and the global data inferred from the pressure may have to suffice.

Overall, the global (and some of the local) results provided in this report should be useful for benchmarking existing "global" computer simulations used in modeling nuclear containment response to degraded–core accidents. The data may also be helpful for resolving issues pertaining to functionability of safety-related equipment in containment during such accidents. Caution should be exercised when applying the global results for lean hydrogen–air combustion, given the nonuniform and incomplete combustion processes. The results obtained from this study, coupled with results obtained from intermediate-scale combustion tests (*e.g.*, such as from the FITS and VGES facilities at Sandia Laboratories, Albuquerque), should also be useful in future modeling activities to upgrade the combustion and heat transfer models currently used in reactor safety computer simulations.

7 References

1. R. T. Thompson, *et al., Large-Scale Hydrogen Combustion Experiments,* Electric Power Research Institute Report NP-3878, in preparation.

2. L. Thompson and T. Auble, *Large Scale Hydrogen Combustion and Control Program at the Nevada Test Site, Draft Test Plan,* September, 1982.

3. Presentation Materials from Design Review of the EPRI Large-Scale Hydrogen Combustion and Control Program at the Nevada Test Site, held in Las Vegas, Nevada, January 6 and 7, 1983.

4. G. Sliter, *Quick-Look Status Report on EPRI Hydrogen Burn Equipment Tests,* (RP-2168-3), Electric Power Research Institute memorandum, dated December 19,1983.

5. G. Sliter, *Second Quick-Look Status Report on EPRI Hydrogen Burn Equipment Tests,* (RP-2168-3), Electric Power Research Institute memorandum, dated February 17, 1984.

6. G. Sliter, *Third Quick-Look Status Report on EPRI Hydrogen Burn Equipment Tests,* (RP-2168-3), Electric Power Research Institute memorandum, dated July 18, 1984.

7. J. Achenbach, R. B. Miller, and V. Srivnivas, *Large-Scale Hydrogen Burn Equipment Experiments,* prepared by Wesinghouse Electric Corp. Nuclear Technology Division for EPRI, in review.

8. Medtherm Corporation Catalog on Thermal Instrumentation, L. Jones, President, P.O. Box 412, Huntsville, Alabama 35804.

9. Personal communication with J. Haugh of EPRI, November 15, 1984.

10. J. E. Shepherd, *Sandia Instrumentation and Computer Codes Supplied for EPRI Tests at NTS,* memorandum dated April 19, 1983.

11. S. N. Kempka, A. C. Ratzel, A. W. Reed, and J. E. Shepherd, *Postcombustion Convection in an Intermediate-Scale Vessel,* Proceedings of the Joint ASME/ANS Conference on the Design, Construction, and Operation of Nuclear Power Plants, Portland OR, August 5-8, 1984.

12. W. H. McCulloch, *et al., Hydrogen Burn Survival: Preliminary Thermal Model and Test Results,* Sandia National Laboratories Report SAND82–1150 (NUREG/CR–2730), August, 1982.

13. E. H. Richards and J. J. Aragon, *Hydrogen-Burn Survival Experiments at Fully Instrumented Test Site (FITS),* Sandia National Laboratories Report SAND83–1715 (NUREG/CR–3521), August, 1984.

14. A. C. Ratzel, S. N. Kempka, J. E. Shepherd, and A. W. Reed, *SMOKE: A Data Reduction Package for Analysis of Combustion Experiments,* Sandia National Laboratories Report SAND83-2658, June, 1985.

15. J. D. Means and R. D. Ulrich, *Transient Convective Heat Transfer During and After Gas Injection into Containers,* Trans. ASME J. Heat Transfer, 97, No.2, 1975, pp.282-287.

16. D. K. Edwards, *Molecular Gas Band Radiation,* Advances in Heat Transfer, Vol. 12, Academic Press, New York, 1976.

17. R. B. Bird, W. E. Stewart, and E. N. Lightfoot, Transport Phenomena, John Wiley and Sons, Inc., New York, 1960.

18. B. F. Blackwell, *SODDIT Users' Manual,* Sandia National Laboratories Report, in preparation.

19. Information on Calibration Procedures and Calibration Data for Gardon and Schmidt-Boelter Gauges Used in NTS tests, Received from Medtherm Corporation Inc., August, 1984.

20. Initial Conditions and Combustion Completeness Estimates for Premixed Combustion Tests provided by L.Thompson of EPRI, March 29, 1983.

21. Preliminary Data Plots for NTS Tests, (3 Volumes), compiled by EPRI/EG&G for an in-house review prior to an April 2-3, 1984 NRC/EPRI meeting, copy provided to J. E. Shepherd, SNLA, April, 1984.

22. W. B. Benedick, J. C. Cummings, and P. G. Prassinos, *Experimental Results from Combustion of Hydrogen:Air Mixtures in an Intermediate Scale Tank,* Proceedings of the Second International Conference on the Impact of Hydrogen on Water Reactor Safety, Albuquerque, N. M., October 3-7, 1982.

23. S. F. Roller and S. M. Fallacy, *Medium-Scale Tests of H_2:Air:Steam Systems,* Proceedings of the Second International Conference on the Impact of Hydrogen on Water Reactor Safety, Albuquerque, N. M., October 3-7, 1982.

24. H. Tamm, R. K. Kumar, and W. C. Harrison, *A Review of Recent WNRE Experiments on Hydrogen Combustion,* Proceedings of the Second International Conference on the Impact of Hydrogen on Water Reactor Safety, Albuquerque, N. M., October 3-7, 1982.

25. R. C. Torok, K. Siefert, and L. B. Thompson, *Hydrogen Control Tests in Intermediate Scale,* Proceedings of the Second International Conference on the Impact of Hydrogen on Water Reactor Safety, Albuquerque, N. M., October 3-7, 1982.

26. A. C. Ratzel and J. E. Shepherd, *Heat Transfer Resulting from Premixed Combustion,* accepted for publication in symposium volume of 23rd ASME/AIChE National Heat Transfer Conference, Denver CO, August, 1985

Appendix A

A Tabular Results for Premixed Combustion Tests

Tabular results for the twenty-one premixed combustion tests conducted at NTS are provided in this appendix. Tests are separated into three categories for presentation: standard tests, steam-laden tests, and tests with the spray systems operative. The standard tests are those in which the initial gas temperature is low (approximately 300 K) and the steam concentration is correspondingly low ($\leq 5\%$). Steam-laden tests have precombustion gas temperatures which range from 320–350 K, and the saturated steam concentration varies accordingly between 15–40%. For tests in which spray systems are operative, it is believed that 16 or 17 Sprayco 1713A hollow cone nozzles were operative, each providing 15 gpm of water spray.

A listing of the tables included in this appendix is provided below:

Table A.1: Instrumentation Status During Hydrogen Behavior Test Series

Instrument Designation	NTSP00 7/28/83	NTSP01 8/4/83	NTSP04 8/9/83	NTSP03 8/10/83	NTSP02 8/12/83	NTSP06 8/17/83	NTSP05 8/18/83	NTSP07 8/29/83	NTSP08 9/12/83
Pressure Transducers									
P102	U	U	U	U	U	U	G	U	G
P104	B	M	B	B	B	B	M	B	B
P105	G	G	G	G	G	G	G	G	B
Slug Calorimeters									
H103	B	B	G	B	B	B	B	B	B
H104	G	G	M	G	G	M	M	G	M
Thin-Film Gauges									
H231	B	B	G	B	B	B	B	B	B
H232	B	B	B	B	G	B	B	G	G
Gardon Gauges									
H105†	U	B	G	B	B	B	G	M	G
H106‡	U	G	G	G	G	G	G	G	G
Wall Thermocouples									
T120	U	U	U	U	U	U	G	U	G
T121	U	U	U	U	U	U	G	U	G
Gas Thermocouples									
T101	U	U	U	U	U	U	G	U	G
T105	U	U	U	U	U	U	G	U	G
T114	U	U	U	U	U	U	G	U	G
T118	U	U	U	U	U	U	G	U	G

† Only signal quality is evaluated for since no SMOKE processing was performed

‡ H106 was a total gauge through test NTSP07 and for NTSP08 was a radiative gauge
For test NTSP08, only the signal quality is evaluated, *i.e.*, no SMOKE processing

'U' – Data not provided by EPRI (*i.e.*, data are "unavailable")

'G' – Data are "good" – signals processed

'M' – Data are "marginal" – signals processed

'B' – Data are "bad" – signals not processed

Table A.2: Pressure and Thermocouple Instrumentation Status During Equipment Survival Test Series

Instrument Designation†	NTSP09 11/10/83	NTSP11 11/15/83	NTSP12 11/17/83	NTSP9P 12/1/83	NTSP14 12/6/83	NTSP13 12/19/83	NTSP16 12/20/83	NTSP15 12/22/83	NTSP18 1/9/84	NTSP20 1/12/84	NTSP21 1/23/84	NTSP22 1/25/84
Pressure Transducers												
P101	B	B	B	G	G	G	U	U	G	G	G	G
P102	G	G	B	B	G	B	M	M	G	G	G	G
P103	G	G	G	G	G	G	U	U	G	G	G	G
Wall Thermocouples												
T120	G	U	G	G	M	G	M	G	G	M	G	G
T121	G	U	G	G	G	G	G	G	M	M	M	M
Gas Thermocouples												
T101	G	U	G	M	G	G	G	G	G	G	G	G
T102	G	G	G	G	G	G	G	G	G	M	G	G
T105	G	U	G	G	G	G	G	G	G	G	G	G
T118	G	U	G	G	G	G	G	G	M	G	G	G
T151	G	U	G	G	G	G	G	G	G	B	B	B

† Pressure Instrumentation P104 and P105 were found to be "bad" for all tests of this series
'U' - Data not provided by EPRI (*i.e.*, data are "unavailable")
'G' - Data are "good" - signals processed
'M' - Data are "marginal" - signals processed
'B' - Data are "bad" - signals not processed

Table A.3: Calorimetry Instrumentation Status During Equipment Survival Test Series

Instrument Designation†	NTSP09 11/10/83	NTSP11 11/15/83	NTSP12 11/17/83	NTSP9P 12/1/83	NTSP14 12/6/83	NTSP13 12/19/83	NTSP16 12/20/83	NTSP15 12/22/83	NTSP18 1/9/84	NTSP20 1/12/84	NTSP21 1/23/84	NTSP22 1/25/84
Total Slug Calorimeter												
H104	G	G	G	G	M	M	G	M	G	M	M	G
Total Thin-Film Gauge												
H232	G	G	G	G	G	G	G	G	G	G	G	G
Aluminum Cube Calorimeter												
T504	B	G	G	M	G	M	M	G	G	G	B	B
T505	B	G	G	G	B	G	G	G	G	G	M	G
Total Schmidt-Boelter Gauges												
H502	G	G	G	G	G	G	G	G	B	G	G	B
H503	G	G	G	G	G	G	G	G	G	G	G	G
H504	G	M	B	B	B	B	B	M	G	B	G	G
H506	G	G	G	G	G	G	M	G	M	B	B	B
H507	G	G	G	G	G	G	B	M	B	B	G	G
Radiative Schmidt-Boelter and Gardon Gauges‡												
H106	G	M	M	M	B	B	B	B	B	B	B	B
H501	G	M	G	G	G	G	G	G	B	M	M	B
H505	G	G	G	G	G	G	G	G	G	G	G	G

† The following instrumentation were found to be "bad" for all tests: T501, T502, T503, T506, H103, H105, and H231

‡ Only the signal quality is evaluated for radiative gauges since no SMOKE processing was performed

'G' – Data are "good" – signals processed

'M' – Data are "marginal" – signals processed

'B' – Data are "bad" – signals not processed

Table A.4: Peak Gas Pressure and Temperature Results

Test Name	H_2 %	H_2O %	CC* %	P_m/P_0 P101	P102	P103	P105	AIC†	T_m/T_0 P101	P102	P103	P105	AIC†
Standard Tests													
NTSP01	5.3	4.2	32.	NA	NA	NA	1.48	1.63	NA	NA	NA	1.5	1.64
NTSP9P	6.0	4.6	53.	1.69	B	1.64	B	2.14	1.72	B	1.67	B	2.18
NTSP09	6.1	4.2	60.	B	1.81	1.83	B	2.31	B	1.85	1.87	B	2.35
NTSP00	6.6	4.5	66.	NA	NA	NA	2.22	2.53	NA	NA	NA	2.27	2.59
NTSP04	7.7	4.2	100.	NA	NA	NA	3.19	3.51	NA	NA	NA	3.32	3.65
NTSP13	7.8	4.4	100.	3.13	B	3.14	B	3.55	3.27	B	3.28	B	3.70
NTSP15	9.9	4.2	100.	NA	3.61	NA	B	4.14	NA	3.81	NA	B	4.35
Steam-Laden Tests													
NTSP07	5.5	14.3	45.	NA	NA	NA	1.66	1.82	NA	NA	NA	1.69	1.84
NTSP03	5.8	14.4	50.	NA	NA	NA	1.78	1.94	NA	NA	NA	1.81	1.97
NTSP06	6.0	13.7	54.	NA	NA	NA	1.84	2.06	NA	NA	NA	1.87	2.10
NTSP12	6.9	28.3	58.	B	B	1.85	B	2.18	B	B	1.90	B	2.23
NTSP14	8.1	38.7	94.	2.16	2.14	2.16	B	2.99	2.25	2.23	2.25	B	3.10
NTSP05	7.8	31.3	100.	NA	2.66	NA	2.63	3.10	NA	2.66	NA	2.63	3.23
NTSP16	10.1	29.5	100.	NA	3.2	NA	B	3.62	NA	3.38	NA	B	3.81
NTSP08	11.1	27.2	100.	NA	3.61	NA	B	3.80	NA	3.84	NA	B	4.02
NTSP20	12.9	27.8	100.	3.85	3.87	3.87	B	4.22	4.13	4.14	4.14	B	4.51
Tests with Spray System Operative													
NTSP22	5.2	14.5	31.	1.36	1.36	1.36	B	1.46	1.35	1.35	1.35	B	1.44
NTSP11	5.8	4.9	58.	B	1.95	1.96	B	2.12	B	1.96	1.97	B	2.12
NTSP02	5.8	14.3	70.	NA	NA	NA	2.15	2.22	NA	NA	NA	2.16	2.23
NTSP18	6.6	27.3	69.	2.09	2.10	2.09	B	2.26	2.11	2.12	2.11	B	2.28
NTSP21	13.2	27.4	100.	3.88	3.91	3.91	B	4.25	4.09	4.12	4.12	B	4.47

* Combustion completeness value (CC) assigned by Sandia

† Result from adiabatic isochoric combustion calculation

'NA' – Data not provided by EPRI or instrumentation not included in test

'B' – Data are "bad"

Table A.5: Combustion Duration Results

Test Name	H_2 %	H_2O %	CC* %	Ign†/ Fans‡	t_0 (s)	Δt_P (s) P101	P102	P103	P105	Δt_{qT} (s) P101	P102	P103	P105
Standard Tests													
NTSP01	5.3	4.2	32.	B/N	22.5	NA	NA	NA	52.9	NA	NA	NA	88.5
NTSP9P	6.0	4.6	53.	B/N	30.7	46.8	B	44.8	B	58.0	B	57.6	B
NTSP09	6.1	4.2	60.	B/N	179.8	B	36.4	36.8	B	B	36.4	36.8	B
NTSP00	6.6	4.5	66.	B/N	21.3	NA	NA	NA	15.2	NA	NA	NA	15.2
NTSP04	7.7	4.2	100.	B/N	22.2	NA	NA	NA	5.7	NA	NA	NA	7.0
NTSP13	7.8	4.4	100.	B/N	28.4	6.4	B	6.4	B	7.6	B	7.6	B
NTSP15	9.9	4.2	100.	B/N	29.2	NA	3.6	NA	B	NA	6.0	NA	B
Steam-Laden Tests													
NTSP07	5.5	14.3	45.	2E/F	25.7	NA	NA	NA	14.4	NA	NA	NA	23.4
NTSP03	5.8	14.4	50.	C/F	22.1	NA	NA	NA	12.3	NA	NA	NA	15.6
NTSP06	6.0	13.7	54.	T/F	21.7	NA	NA	NA	14.8	NA	NA	NA	18.0
NTSP12	6.9	28.3	58.	B/N	33.1	B	B	24.0	B	B	B	27.2	B
NTSP14	8.1	38.7	94.	B/N	23.2	16.8	16.8	17.2	B	19.2	19.6	19.6	B
NTSP05	7.8	31.3	100.	B/N	22.9	NA	11.5	NA	11.1	NA	12.7	NA	12.7
NTSP16	10.1	29.5	100.	B/N	29.9	NA	4.4	NA	B	NA	4.4	NA	B
NTSP08	11.1	27.2	100.	B/F	1053.0	NA	2.80	NA	B	NA	2.8	NA	B
NTSP20	12.9	27.8	100.	B/N	70.4	2.1	2.1	2.1	B	2.1	2.1	2.1	B
Tests with Spray System Operative													
NTSP22	5.2	14.5	31.	1E/N	21.5	8.4	8.4	8.4	B	NC	NC	NC	B
NTSP11	5.8	4.9	58.	T/N	28.5	B	4.8	5.2	B	B	NC	NC	B
NTSP02	5.8	14.3	70.	C/N	24.2	NA	NA	NA	4.1	NA	NA	NA	NC
NTSP18	6.6	27.3	69.	T/N	191.6	4.4	4.4	4.4	B	NC	NC	NC	B
NTSP21	13.2	27.4	100.	B/F	30.7	1.7	1.7	1.7	B	NC	NC	NC	B

* Combustion completeness value (CC) assigned by Sandia

† Ignition at Bottom (B), Center (C), Top (T), or by 1 or 2 igniters on wall at Equator (1E, 2E)

‡ Fans operative (F) or inoperative (N)

'NA' – Data not provided by EPRI or instrumentation not included in test

'NC' – Results not obtained from data analysis since sprays are not modeled in SMOKE

'B' – Data are "bad"

Table A.6: Gas Thermocouple Results

Test Name	T_{AIC}/T_0 †	T_m/T_0			Δt_{mp} (s)			$T_{1/2}$ ‡ (K)			$\Delta t_{T_{1/2}}$ (s)		
		T101 T102*	T105	T118 T151*	T101 T102*	T105	T118 T151*	T101 T102*	T105	T118 T151*	T101 T102*	T105	T118 T151*
Standard Tests													
NTSP01	1.64	NA	NA	NA	NA	NA	NA	NA	NA	NA	NA	NA	NA
NTSP9P	2.18	1.94*	1.82	1.55	-28.9*	-28.5	24.3	444.	427.	386.	56.4*	93.6	120.0
NTSP09	2.35	1.92	1.97	1.74	-8.4	-2.4	6.0	441.	448.	414.	97.6	64.8	103.6
NTSP00	2.59	NA	NA	NA	NA	NA	NA	NA	NA	NA	NA	NA	NA
NTSP04	3.65	NA	NA	NA	NA	NA	NA	NA	NA	NA	NA	NA	NA
NTSP13	3.70	3.20	3.38	2.74	-1.7	-1.7	10.0	637.	665.	568.	48.8	25.2	60.8
NTSP15	4.35	3.81	4.05	3.04	0.4	-0.4	6.4	730.	767.	613.	15.2	16.0	55.6
Steam-Laden Tests													
NTSP07	1.82	NA	NA	NA	NA	NA	NA	NA	NA	NA	NA	NA	NA
NTSP03	1.97	NA	NA	NA	NA	NA	NA	NA	NA	NA	NA	NA	NA
NTSP06	2.10	NA	NA	NA	NA	NA	NA	NA	NA	NA	NA	NA	NA
NTSP12	2.23	2.11*	2.03	1.82	0.9*	-13.9	8.5	529.*	515.	479.	31.6*	33.6	74.4
NTSP14	3.10	2.25*	2.38	1.84	5.3*	-1.7	10.7	564.*	586.	493.	29.6*	46.0	55.6
NTSP05	3.23	2.8	2.95	2.59	-7.8	-7.9	0.8	647.	672.	611.	41.8	40.6	59.9
NTSP16	3.81	3.47*	3.46	2.39	-0.4*	-0.4	17.2	765.*	765.	582.	13.2*	17.2	60.8
NTSP08	4.02	3.92	3.99	3.33	-0.8	0.2	0.8	855.	869.	754.	32.5	29.5	31.0
NTSP20	4.51	4.02	4.24	2.78	-0.3	-0.1	12.0	859.	895.	646.	25.2	22.8	48.0
Tests with Spray System Operative													
NTSP22	1.44	1.47*	1.06	1.05	-0.4*	-0.8	2.4	401*	335.	334.	6.8*	36.0	49.2
NTSP11	2.12	2.10*	NA	NA	-0.7*	NA	NA	472.*	NA	NA	6.8*	NA	NA
NTSP02	2.23	NA	NA	NA	NA	NA	NA	NA	NA	NA	NA	NA	NA
NTSP18	2.28	2.19*	2.17	1.78*	0.0*	-2.4	10.0*	545.*	543.	475.*	11.6*	16.4	25.2*
NTSP21	4.47	3.87*	3.19	2.55	0.8*	4.4	6.4	830.*	714.	606.	10.5*	20.4	25.2

* Results provided for instrument T102 or T151

† Maximum temperature ratio obtained from an adiabatic isochoric combustion calculation

‡ Gas temperature – $T_{1/2} = (T_m + T_0)/2$.

'NA' – Data not provided by EPRI or instrumentation not included in test

Table A.7: Peak Heat Flux Results Inferred from Pressure Signals

Test Name	H_2 %	H_2O %	CC* %	q_T (W/cm^2) P101	P102	P103	P105	q_R (W/cm^2) P101	P102	P103	P105
Standard Tests											
NTSP01	5.3	4.2	32.	NA	NA	NA	0.16	NA	NA	NA	0.08
NTSP9P	6.0	4.6	53.	0.41	B	0.41	B	0.16	B	0.14	B
NTSP09	6.1	4.2	60.	B	0.68	0.76	B	B	0.23	0.24	B
NTSP00	6.6	4.5	66.	NA	NA	NA	2.03	NA	NA	NA	0.62
NTSP04	7.7	4.2	100.	NA	NA	NA	8.02	NA	NA	NA	3.33
NTSP13	7.8	4.4	100.	5.73	B	5.79	B	3.03	B	3.06	B
NTSP15	9.9	4.2	100.	NA	10.58	NA	B	NA	5.94	NA	B
Steam-Laden Tests											
NTSP07	5.5	14.3	45.	NA	NA	NA	0.72	NA	NA	NA	0.24
NTSP03	5.8	14.4	50.	NA	NA	NA	1.22	NA	NA	NA	0.35
NTSP06	6.0	13.7	54.	NA	NA	NA	1.20	NA	NA	NA	0.37
NTSP12	6.9	28.3	58.	B	B	1.35	B	B	B	0.55	B
NTSP14	8.1	38.7	94.	2.41	2.36	2.36	B	1.31	1.25	1.28	B
NTSP05	7.8	31.3	100.	NA	4.10	NA	6.31	NA	2.81	NA	2.61
NTSP16	10.1	29.5	100.	NA	9.65	NA	B	NA	6.75	NA	B
NTSP08	11.1	27.2	100.	NA	21.24	NA	B	NA	12.34	NA	B
NTSP20	12.9	27.8	100.	26.17	25.63	25.39	B	15.08	15.27	15.34	B
Tests with Spray System Operative											
NTSP22	5.2	14.5	31.	NC	NC	NC	B	0.07	0.07	0.07	B
NTSP11	5.8	4.9	58.	B	NC	NC	B	B	0.33	0.34	B
NTSP02	5.8	14.3	70.	NA	NA	NA	NC	NA	NA	NA	0.77
NTSP18	6.6	27.3	69.	NC	NC	NC	B	0.96	0.98	0.96	B
NTSP21	13.2	27.4	100.	NC	NC	NC	B	14.49	14.92	14.94	B

* Combustion completeness value (CC) assigned by Sandia
'NA' – Data not provided by EPRI or instrumentation not included in test
'NC' – Total results not obtained from data analysis since sprays are not modeled in SMOKE
'B' – Data are "bad"

Table A.8: Peak Total Heat Flux Results from SNLA Gauges and from Wall Thermocouples

Test	q_T (W/cm^2)						Δt_{mp} (s)					
Name	H232	H104	T504	T505	T120	T121	H232	H104	T504	T505	T120	T121
Standard Tests												
NTSP01	B	0.40	NA	NA	NA	NA	B	-45.9	NA	NA	NA	NA
NTSP9P	0.74	1.50	1.01	0.97	1.49	0.94	-38.5	-37.9	-7.1	-7.1	-33.7	6.3
NTSP09	1.06	1.29	B	B	2.84	1.34	-28.8	-14.6	B	B	-9.7	9.9
NTSP00	B	0.99	NA	NA	NA	NA	B	-6.4	NA	NA	NA	NA
NTSP04	B	B	NA	NA	NA	NA	B	B	NA	NA	NA	NA
NTSP13	5.37	8.46	4.38	4.43	8.21	3.34	-0.8	8,2	-1.5	-2.7	5.1	41.6
NTSP15	10.29	11.23	11.28	13.61	10.61	6.34	-1.2	7.9	-1.7	-1.7	5.0	38.1
Steam-Laden Tests												
NTSP07	0.49	0.71	NA	NA	NA	NA	0.1	-8.6	NA	NA	NA	NA
NTSP03	B	2.68	NA	NA	NA	NA	B	-1.0	NA	NA	NA	NA
NTSP06	B	1.34	NA	NA	NA	NA	B	14.9	NA	NA	NA	NA
NTSP12	0.92	2.18	1.93	2.16	1.83	1.06	-19.1	-11.9	-13.4	0.2	-12.4	22.4
NTSP14	1.86	3.78	2.90	B	3.46	2.02	0.7	6.8	0.7	B	2.0	46.1
NTSP05	B	6.69	NA	NA	14.43	5.35	B	-3.6	NA	NA	4.5	29.6
NTSP16	8.78	8.4	8.12	4.40	6.93	5.49	-2.8	8.2	-1.0	-1.0	4.5	36.5
NTSP08	12.11	10.48	NA	NA	8.96	9.52	-0.8	2.0	NA	NA	14.3	34.5
NTSP20	18.34	7.38	19.4	8.12	10.04	6.93	-0.1	4.2	0.4	-0.8	4.1	36.7
Tests with Spray System Operative												
NTSP22	0.53	0.80	B	0.46	0.91	0.29	-1.5	4.3	B	-2.7	4.5	47.3
NTSP11	1.39	2.37	2.49	1.55	NA	NA	-2.3	-0.7	-3.8	-1.2	NA	NA
NTSP02	2.09	3.35	NA	NA	NA	NA	-1.2	-1.0	NA	NA	NA	NA
NTSP18	2.54	2.08	2.11	2.20	5.56	0.76	-2.8	4.2	-1.0	-1.0	8.2	32.6
NTSP21	16.74	7.97	B	20.27	13.06	3.24	0.4	46.6	B	-0.5	7.1	29.2

'NA' – Data not provided by EPRI or instrumentation not included in test
'B' – Data are "bad"

Table A.9: Peak Total Heat Flux Results from Gardon and Schmidt-Boelter Gauges

Test	q_{off} (W/cm^2)					q_T (W/cm^2)					Δt_{mp} (s)				
Name	H106	H502	H503	H506	H507	H106	H502	H503	H506	H507	H106	H502	H503	H506	H507
Standard Tests															
NTSP01	0.0	NA	NA	NA	NA	1.74	NA	NA	NA	NA	-49.7	NA	NA	NA	NA
NTSP9P	R	0.04	0.03	0.02	0.07	R	0.83	1.06	0.85	1.29	R	-37.7	-30.5	-10.1	-17.3
NTSP09	R	0.06	0.08	0.055	B	R	0.85	0.87	1.09	B	R	0.8	-27.2	-15.2	B
NTSP00	NA	NA	NA	NA	NA	NA	NA	NA	NA	NA	NA	NA	NA	NA	NA
NTSP04	0.0	NA	NA	NA	NA	10.9	NA	NA	NA	NA	-1.5	NA	NA	NA	NA
NTSP13	R	0.12	0.085	0.045	0.175	R	4.43	5.05	4.46	6.78	R	-2.0	-1.6	-2.4	0.4
NTSP15	R	0.2	0.15	0.10	0.325	R	8.28	9.67	9.74	11.17	R	-0.8	-0.8	-1.2	-1.2
Steam-Laden Tests															
NTSP07	-0.01	NA	NA	NA	NA	0.84	NA	NA	NA	NA	-6.1	NA	NA	NA	NA
NTSP03	0.0	NA	NA	NA	NA	1.36	NA	NA	NA	NA	-6.5	NA	NA	NA	NA
NTSP06	0.0	NA	NA	NA	NA	1.32	NA	NA	NA	NA	-4.9	NA	NA	NA	NA
NTSP12	R	0.35	0.38	0.263	0.625	R	2.31	2.60	1.90	3.56	R	-15.1	-19.1	-5.9	1.1
NTSP14	R	0.575	0.625	0.385	0.85	R	3.32	3.22	1.61	5.18	R	-12.1	5.9	1.9	-2.1
NTSP05	0.0	NA	NA	NA	NA	6.51	NA	NA	NA	NA	-7.9	NA	NA	NA	NA
NTSP16	R	0.65	0.675	0.35	0.95	R	5.70	8.28	5.58	10.57	R	2.0	-0.8	-2.0	-0.4
NTSP08	R	NA	NA	NA	NA	R	NA	NA	NA	NA	R	NA	NA	NA	NA
NTSP20	R	0.70	0.75	B	B	R	7.11	15.58	B	B	R	0.8	1.6	B	B
Tests with Spray System Operative															
NTSP22	R	B	0.275	B	0.25	R	B	0.75	B	0.61	R	B	0.1	B	4.9
NTSP11	R	0.21	0.04	0.09	0.04	R	1.76	1.45	2.79	1.40	R	2.5	0.1	-0.3	-0.7
NTSP02	-0.05	NA	NA	NA	NA	3.58	NA	NA	NA	NA	-1.7	NA	NA	NA	NA
NTSP18	R	B	0.75	0.075	B	R	B	2.78	2.26	B	R	B	-0.4	4.4	B
NTSP21	R	1.70	1.075	B	1.20	R	8.94	15.39	B	12.96	R	0.4	0.4	B	-0.1

'NA' – Data not provided by EPRI or instrumentation not included in test
'R' – Gauge is configured as a radiative device
'B' – Data are "bad"

Table A.10: Postcombustion Global Energy Deposition Inferred from Pressure Signals

Test Name	H_2 %	H_2O %	CC† %	Q_{AIC}‡ J/cm^2	t_P** (s)	Q_{T_P}* (J/cm^2) P101	P102	P103	P105	Q_{R_P}* (J/cm^2) P101	P102	P103	P105
Standard Tests													
NTSP01	5.3	4.2	32.	42.8	75.9	NA	NA	NA	27.1	NA	NA	NA	9.0
NTSP9P	6.0	4.6	53.	75.8	76.5	34.8	B	35.3	B	14.5	B	11.7	B
NTSP09	6.1	4.2	60.	89.7	216.4	B	46.8	48.5	B	B	16.3	15.7	B
NTSP00	6.6	4.5	66.	107.4	36.5	NA	NA	NA	71.8	NA	NA	NA	23.6
NTSP04	7.7	4.2	100.	203.0	27.9	NA	NA	NA	139.2	NA	NA	NA	68.7
NTSP13	7.8	4.4	100.	206.5	34.8	144.0	B	144.2	B	70.6	B	71.3	B
NTSP15	9.9	4.2	100.	296.1	32.8	NA	197.9	NA	B	NA	92.8	NA	B
Steam-Laden Tests													
NTSP07	5.5	14.3	45.	57.7	40.1	NA	NA	NA	38.1	NA	NA	NA	13.4
NTSP03	5.8	14.4	50.	69.2	34.4	NA	NA	NA	49.7	NA	NA	NA	17.9
NTSP06	6.0	13.7	54.	71.7	36.5	NA	NA	NA	48.4	NA	NA	NA	15.
NTSP12	6.9	28.3	58.	91.4	57.1	B	B	52.6	B	B	B	26.9	B
NTSP14	8.1	38.7	94.	172.6	48.1	73.3	72.7	73.0	B	47.7	45.7	47.2	B
NTSP05	7.8	31.3	100.	178.1	34.9	NA	101.6	NA	108.6	NA	72.0	NA	53.6
NTSP16	10.1	29.5	100.	259.0	34.8	NA	155.0	NA	B	NA	114.1	NA	B
NTSP08	11.1	27.2	100.	362.0	1055.8	NA	234.3	NA	B	NA	190.5	NA	B
NTSP20	12.9	27.8	100.	342.8	72.5	217.0	218.0	218.9	B	161.9	162.7	163.6	B
Tests with Spray System Operative													
NTSP22	5.2	14.5	31.	28.8	29.9	NC	NC	NC	B	1.4	1.4	1.4	B
NTSP11	5.8	4.9	58.	74.8	33.5	B	NC	NC	B	B	4.9	4.5	B
NTSP02	5.8	14.3	70.	83.2	28.3	NA	NA	NA	NC	NA	NA	NA	8.4
NTSP18	6.6	27.3	69.	108.4	196.0	NC	NC	NC	B	13.2	14.3	12.9	B
NTSP21	13.2	27.4	100.	332.7	32.9	NC	NC	NC	B	110.3	113.6	112.3	B

† Combustion completeness value (CC) assigned by Sandia

‡ Maximum global energy deposition that could be removed from gas based on AIC calculation

* Integrated heat flux for times after the peak pressure is reached (*i.e.*, postcombustion energy deposition)

** Estimated time of peak pressure

'NA' – Data not provided by EPRI or instrumentation not included in test

'NC' – Total results not obtained from data analysis since sprays are not modeled in SMOKE

'B' – Data are "bad"

Table A.11: Total Energy Deposition Results from Calorimetry

Test Name	Q_{AIC}† (J/cm^2)	$Q_{T_{all}}$* (J/cm^2)						Q_{T_P}‡ (J/cm^2)					
		H232	H106	H502	H503	H506	H507	H232	H106	H502	H503	H506	H507
Standard Tests													
NTSP01	42.8	B	66.2	NA	NA	NA	NA	B	30.5	NA	NA	NA	NA
NTSP9P	75.8	38.5	R	65.7	71.5	54.9	83.2	18.03	R	41.6	33.5	27.1	48.1
NTSP09	89.7	50.7	R	66.7	52.8	50.5	B	22.65	R	46.1	30.5	30.7	B
NTSP00	107.4	B	NA	NA	NA	NA	B	NA	NA	NA	NA		
NTSP04	203.0	B	216.6	NA	NA	NA	NA	B	177.4	NA	NA	NA	NA
NTSP13	206.5	113.3	R	148.7	149.0	92.0	160.4	90.18	R	131.2	124.1	72.0	134.9
NTSP15	296.1	148.1	R	185.1	204.5	136.3	249.7	122.6	R	164.4	163.2	113.7	227.3
Steam-Laden Tests													
NTSP07	57.7	22.9	41.2	NA	NA	NA	NA	18.5	33.7	NA	NA	NA	NA
NTSP03	69.2	B	62.0	NA	NA	NA	NA	B	50.4	NA	NA	NA	NA
NTSP06	71.7	B	26.5	NA	NA	NA	NA	B	11.6	NA	NA	NA	NA
NTSP12	91.4	33.0	R	131.0	102.3	83.3	158.9	15.7	R	105.6	60.5	58.5	118.7
NTSP14	178.1	54.9	R	85.6	122.8	98.3	186.6	33.9	R	62.9	101.0	76.7	137.2
NTSP05	172.6	B	205.1	NA	NA	NA	NA	B	145.9	NA	NA	NA	NA
NTSP16	259.0	141.0	R	164.7	161.0	34.4	B	112.3	R	167.0	126.6	20.4	B
NTSP08	362.0	186.5	R	NA	NA	NA	NA	171.2	R	NA	NA	NA	NA
NTSP20	342.8	172.6	R	83.8	109.2	B	B	158.6	R	104.8	148.9	B	B
Tests with Spray System Operative													
NTSP22	28.8	9.2	R	B	6.4	B	10.1	5.7	R	B	7.4	B	10.2
NTSP11	74.8	28.1	R	48.8	33.4	61.1	50.8	21.6	R	59.3	29.0	66.4	38.6
NTSP02	83.2	29.1	52.4	NA	NA	NA	NA	23.4	41.8	NA	NA	NA	NA
NTSP18	108.4	38.2	R	B	48.4	24.7	B	24.8	R	B	46.3	19.5	B
NTSP21	332.7	139.5	R	130.6	135.0	B	141.6	126.1	R	125.4	121.5	B	141.6

† Maximum global energy deosition that could be removed from gas based on AIC calculation

* Integrated heat flux for the combustion and postcombustion times of interest

‡ Integrated heat flux for times after the peak pressure is reached (*i.e.*, postcombustion energy deposition)

'NA' – Data not provided by EPRI or instrumentation not included in test

'R' – Gauge is configured as a radiative device

'B' – Data are "bad"

Appendix B

B Comparative Graphical Results

Comparative graphical results are given in this appendix for pressure rise, combustion duration, heat transfer rates, and energy depositions. In addition, measured gas and wall temperature profiles for representative tests are compared. The data are provided in three different sets, Standard, Steam-Laden, and Sprays-on tests. Included in this presentation are comparative time histories of results as well as summary plots of some of the important data tabulated in Appendix A.

B.1 Comparative Results from Standard Tests

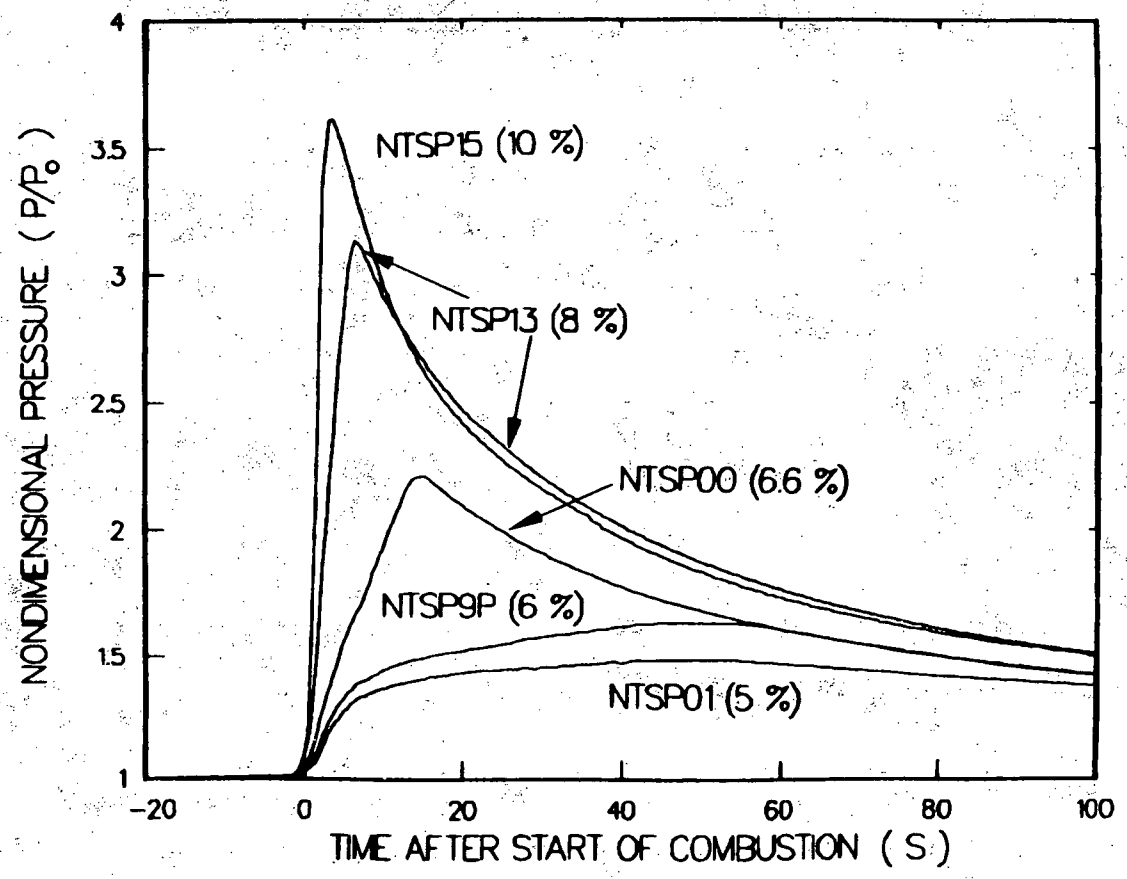

Figure B.1: Gas pressure profiles for standard tests. Numbers in parentheses are initial hydrogen concentrations.

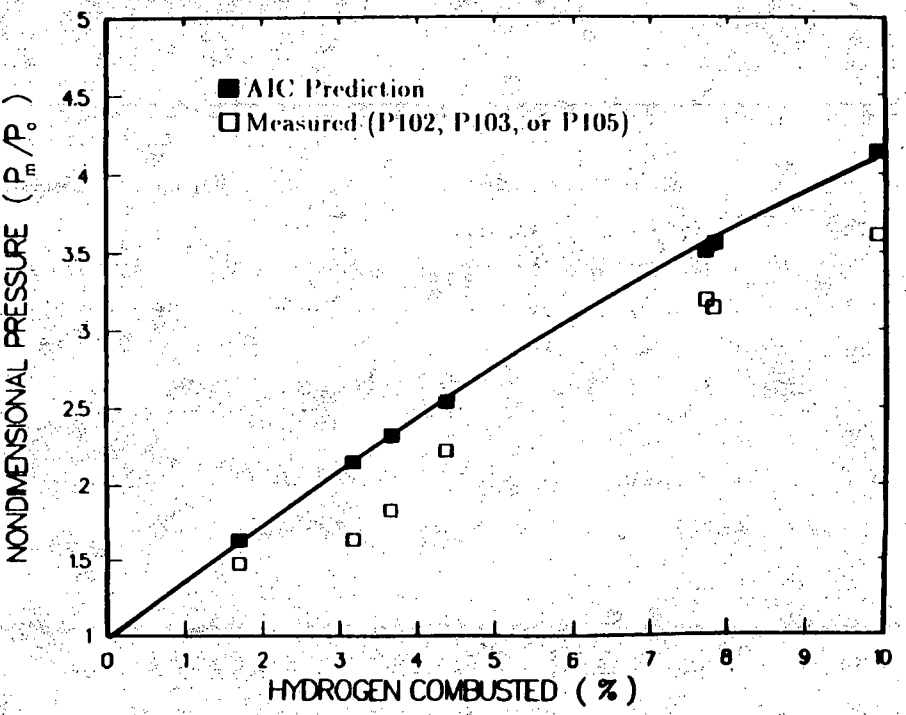

Figure B.2: Peak pressure ratios for standard tests

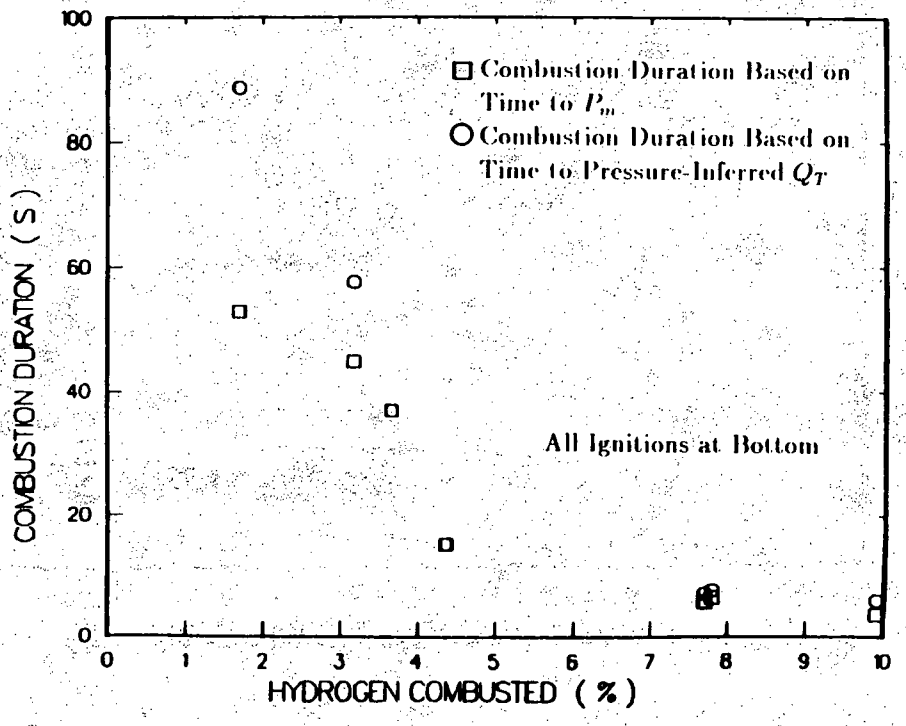

Figure B.3: Combustion duration inferred from pressure results (standard tests)

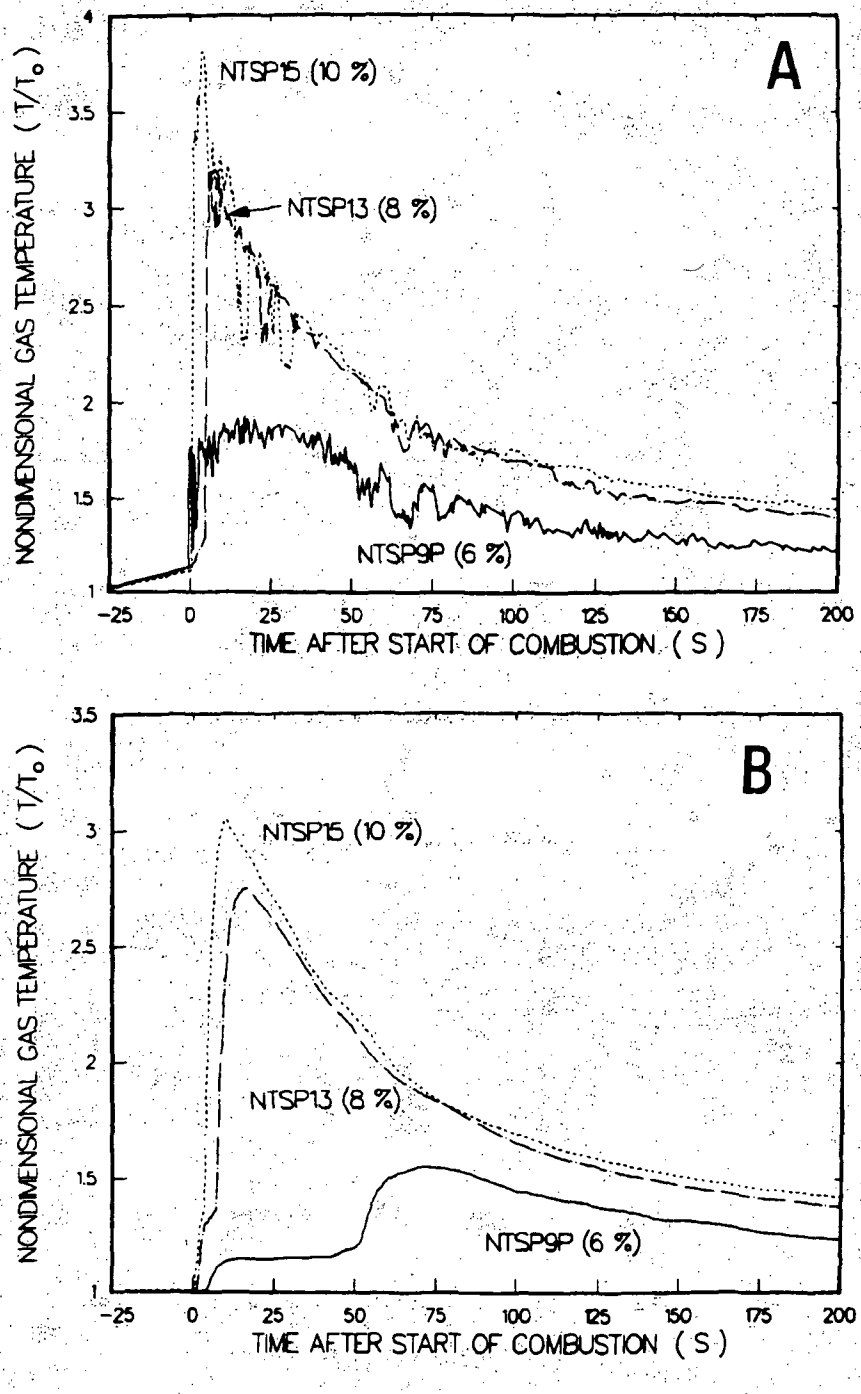

Figure B.4: Gas thermocouple profiles for standard tests. Numbers in parentheses are initial hydrogen concentrations.

A: 3-mil thermocouple results
B: 32-mil thermocouple results

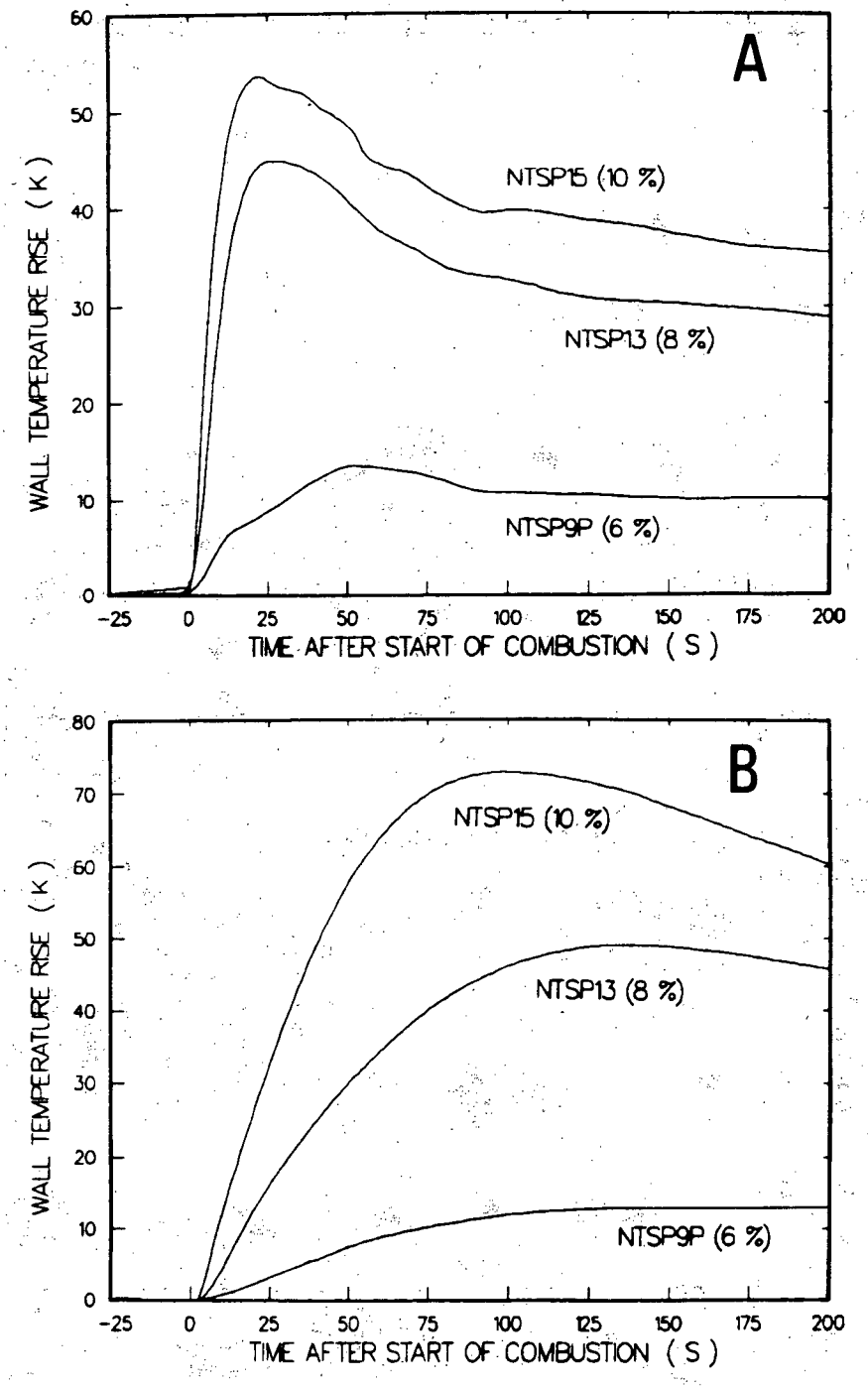

Figure B.5: Dewar wall thermocouple profiles for standard tests. Numbers in parentheses are initial hydrogen concentrations.

A: Thermocouple T120 results
B: Thermocouple T121 results

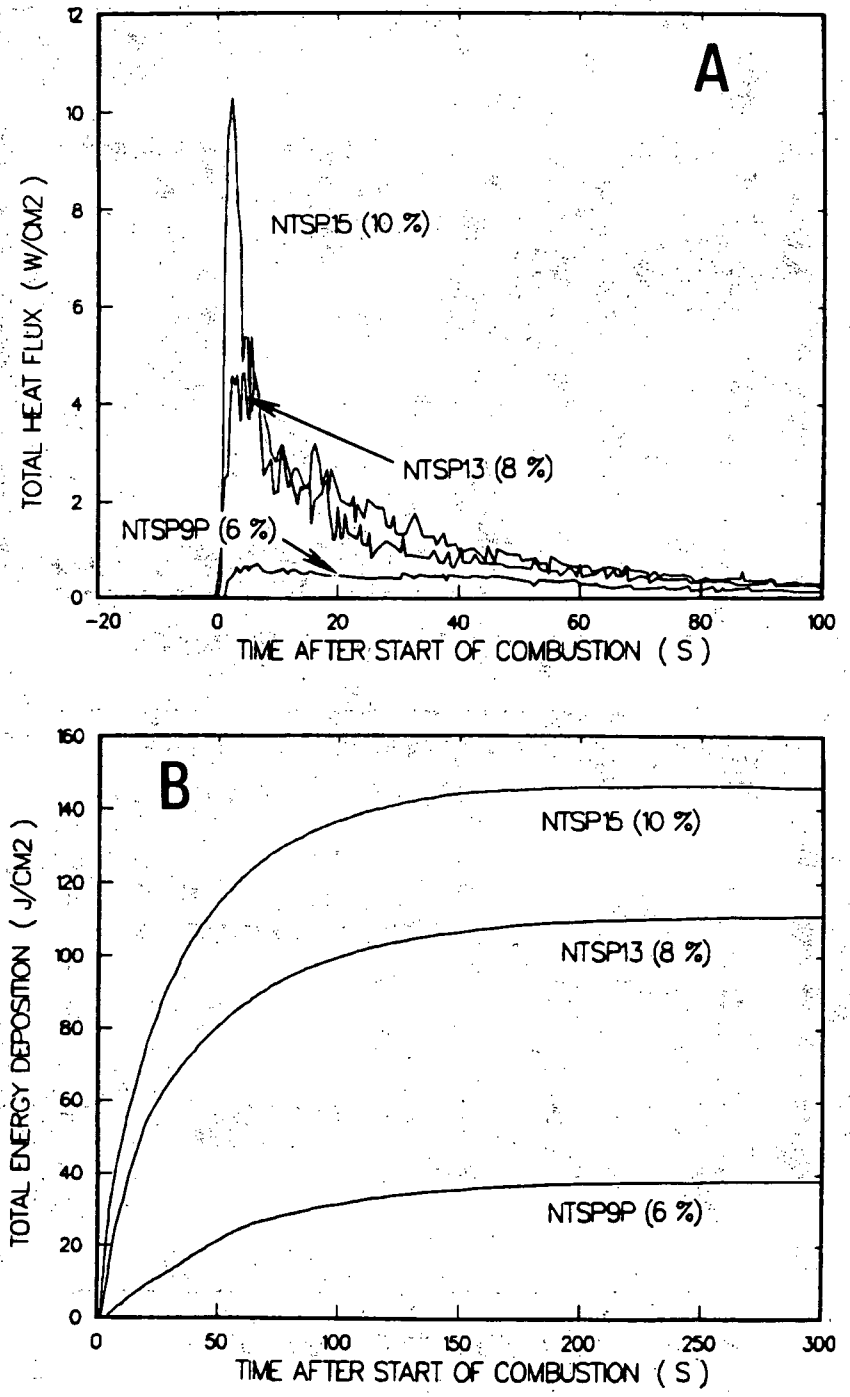

Figure B.6: Heat transfer profiles from H232 for standard tests. Numbers in parentheses are initial hydrogen concentrations.

A: Total heat flux

B: Total energy deposition

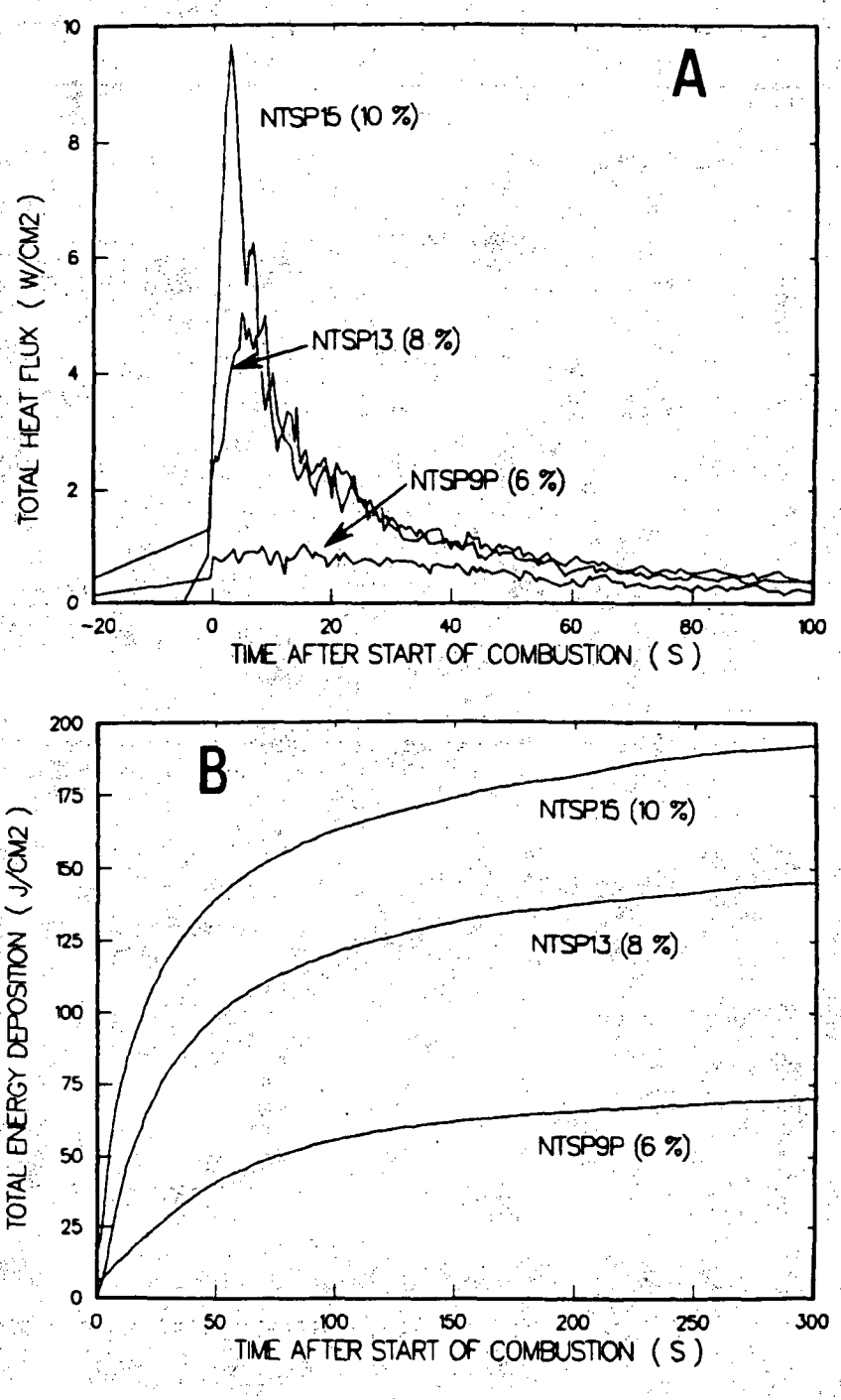

Figure B.7: Heat transfer profiles from H503 (standard tests). Numbers in parentheses are initial hydrogen concentrations.

A: Total heat flux

B: Total energy deposition

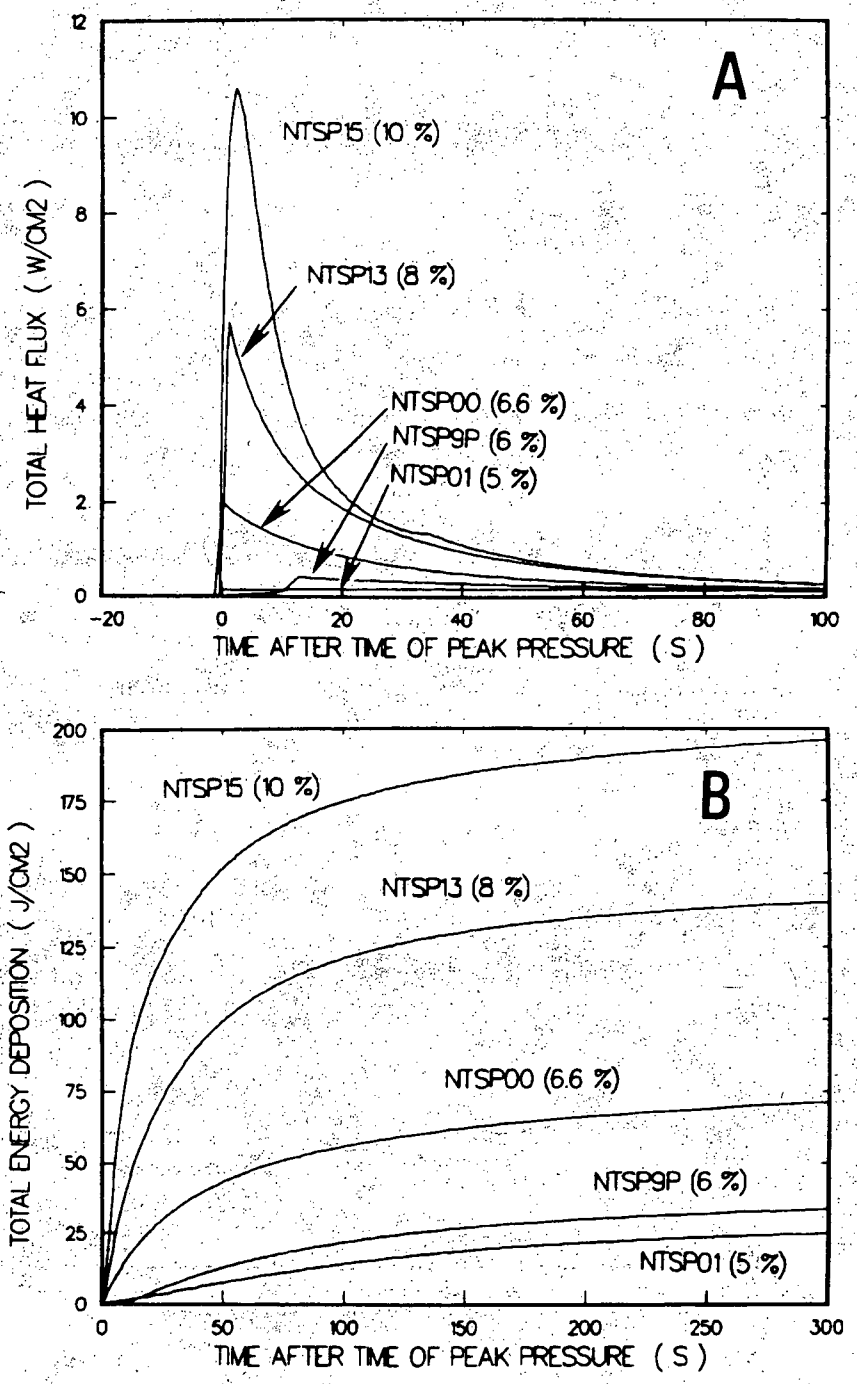

Figure B.8: Total heat transfer profiles from pressure sensors (standard tests). Numbers in parentheses are initial hydrogen concentrations.

A: Total heat flux

B: Total energy deposition

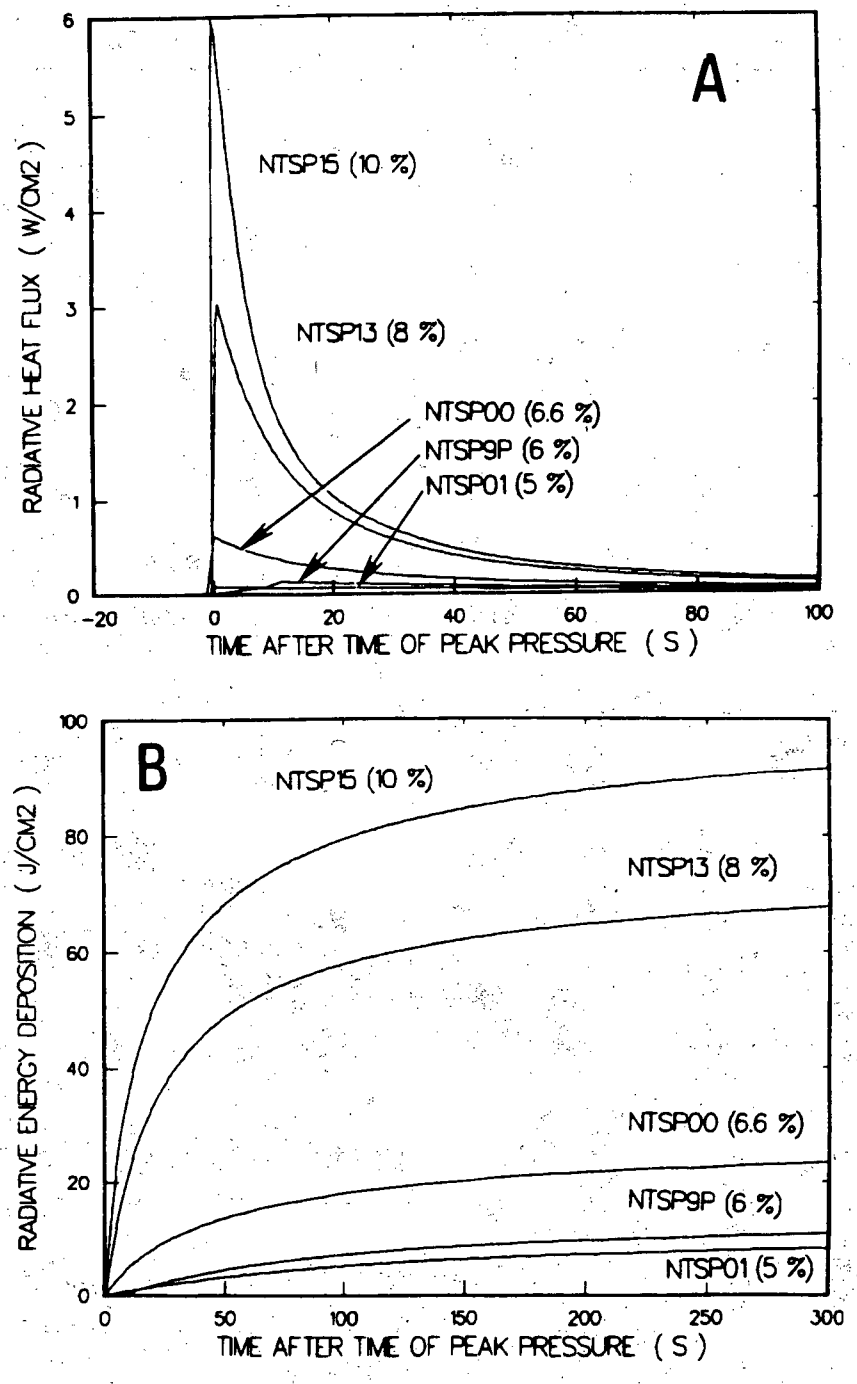

Figure B.9: Radiative heat transfer profiles from pressure sensors (standard tests). Numbers in parentheses are initial hydrogen concentrations.

A: Radiative heat flux

B: Radiative energy deposition

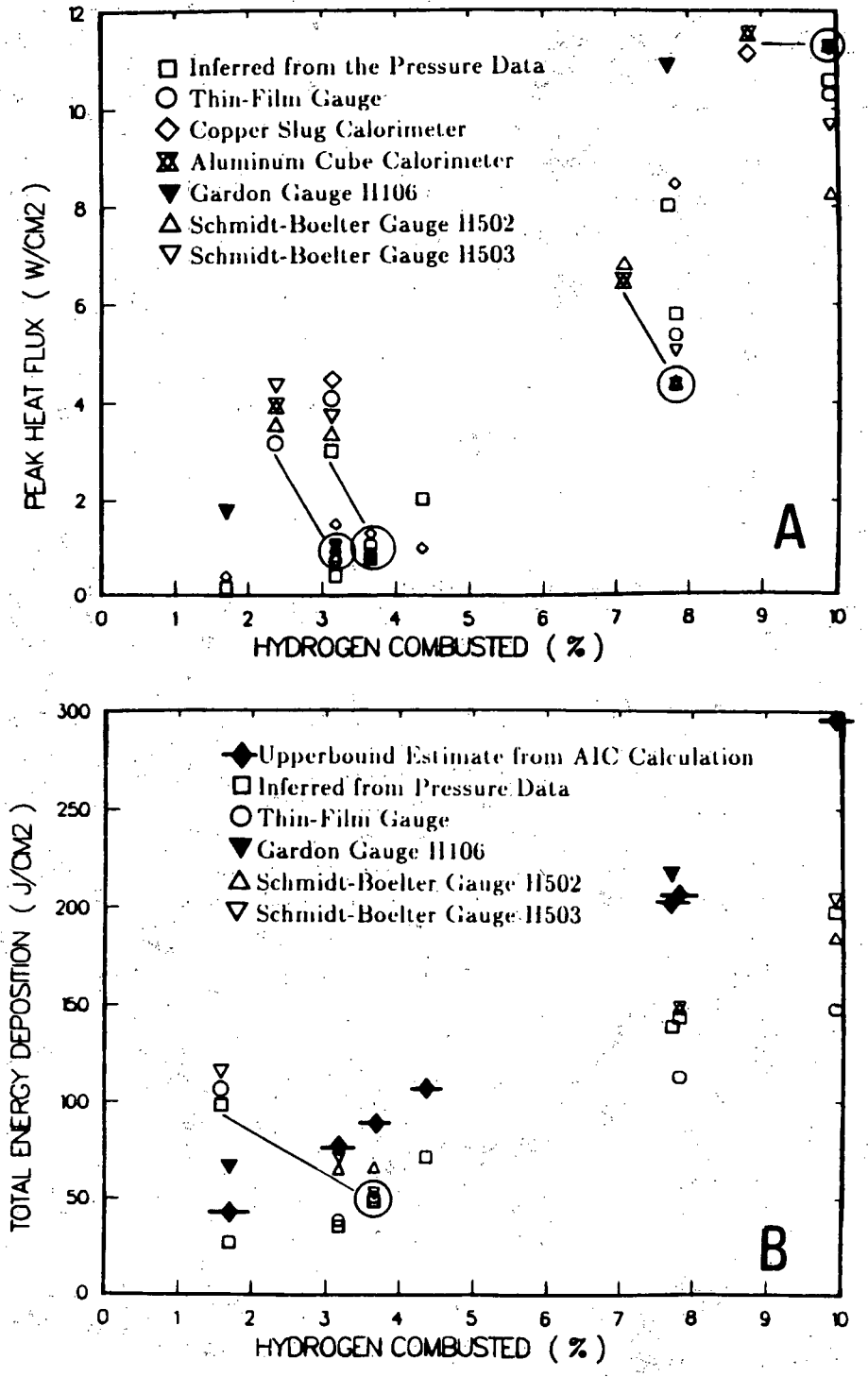

Figure B.10: Total heat transfer results from standard tests

A: Total heat flux

B: Total energy deposition

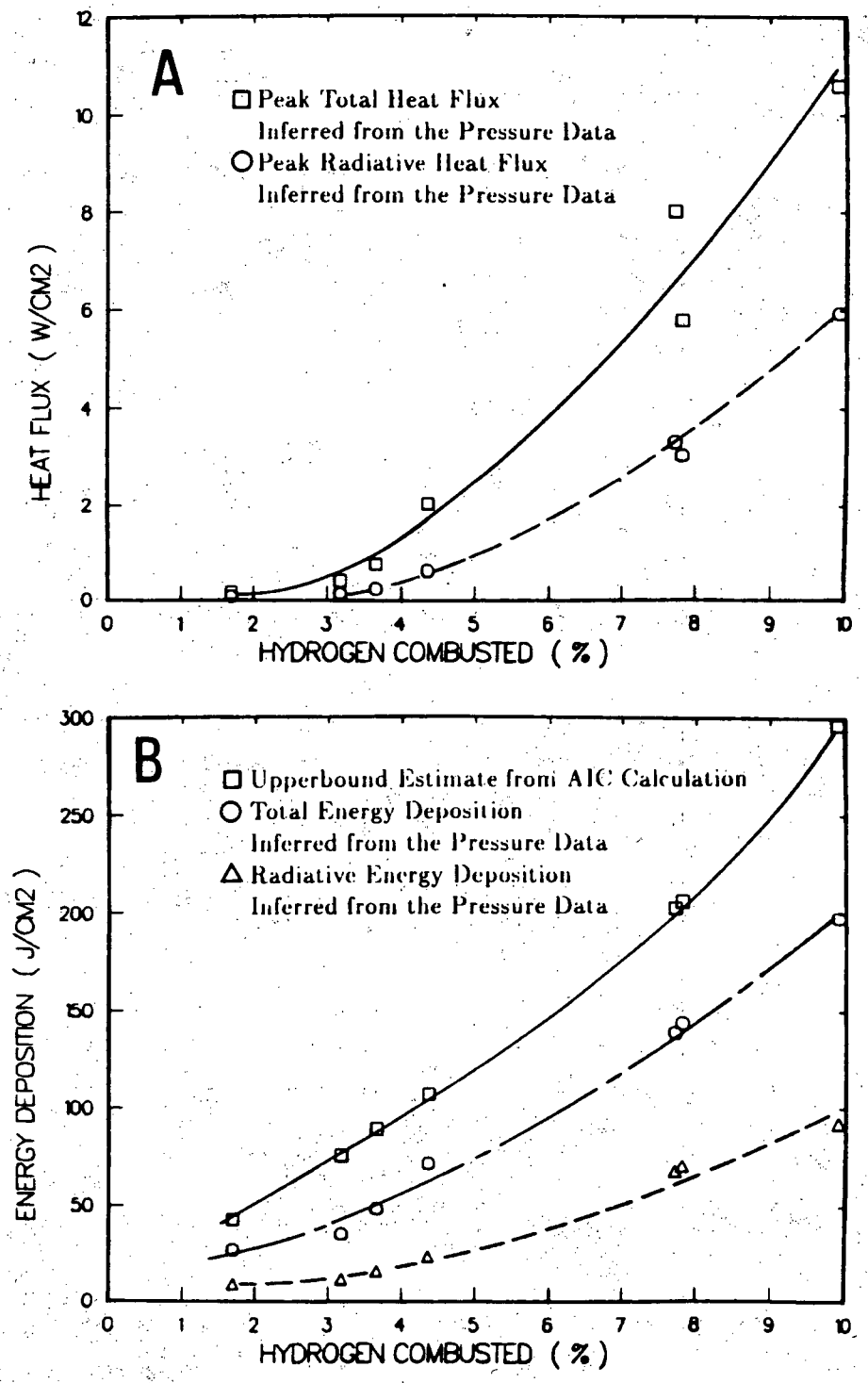

Figure B.11: Heat transfer results inferred from pressure sensors (standard tests)

A: Heat flux

B: Energy deposition

B.2 Comparative Results from Steam-laden Tests

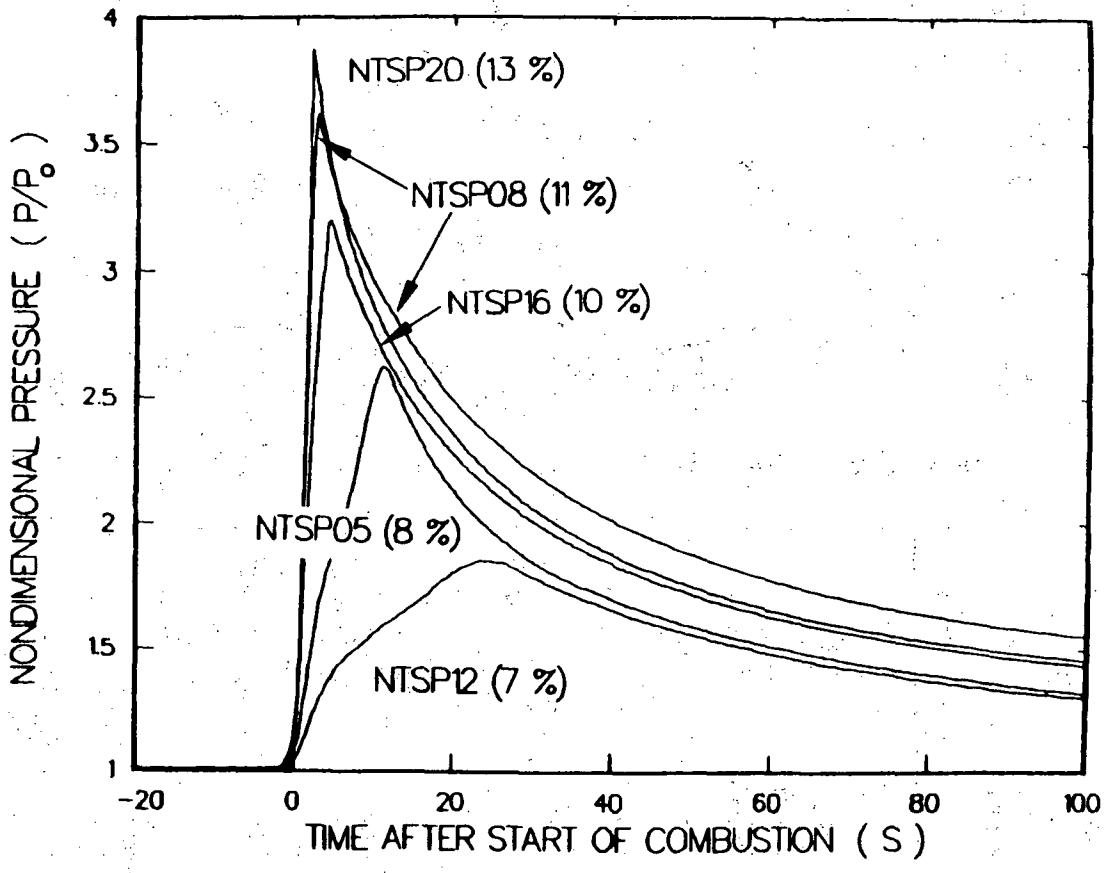

Figure B.12: Gas pressure profiles for steam-laden tests. Tests shown are 30% (nominal) steam by volume. Numbers in parentheses are initial hydrogen concentrations.

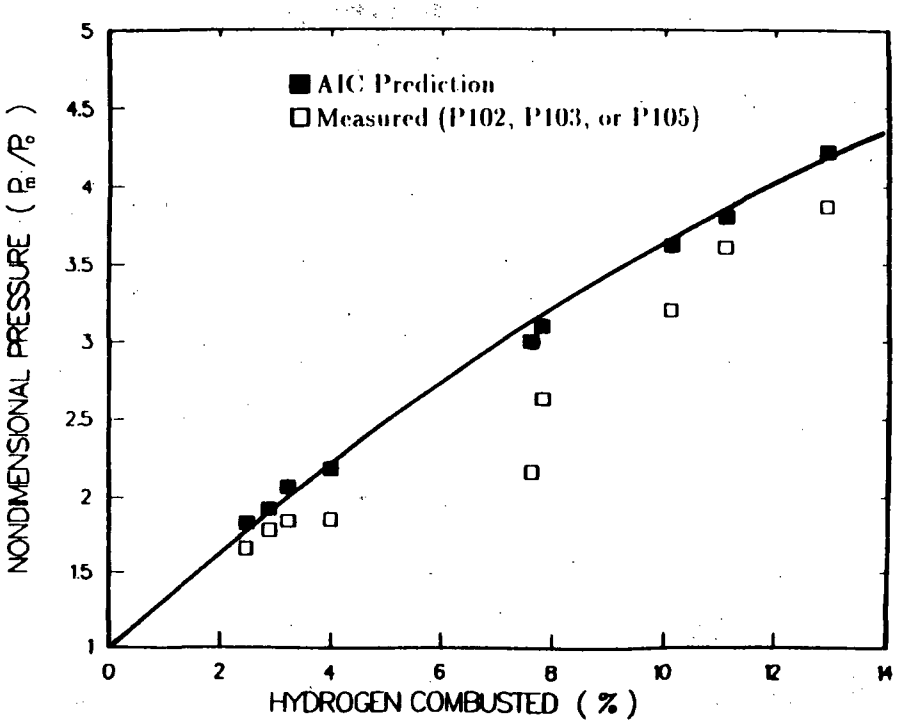

Figure B.13: Peak pressure ratios for steam-laden tests

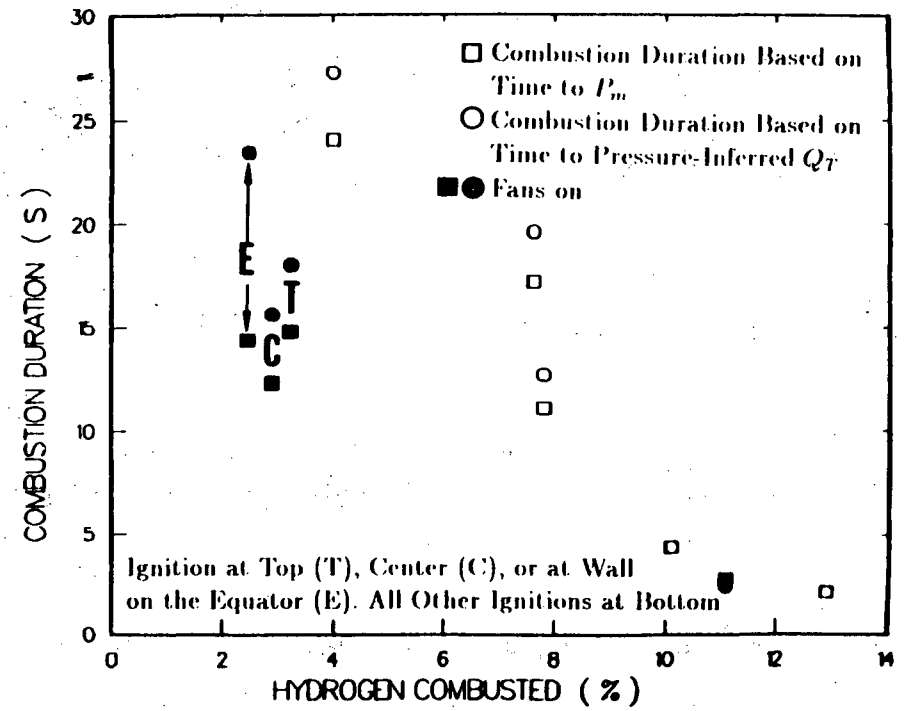

Figure B.14: Combustion duration inferred from pressure results (steam-laden tests)

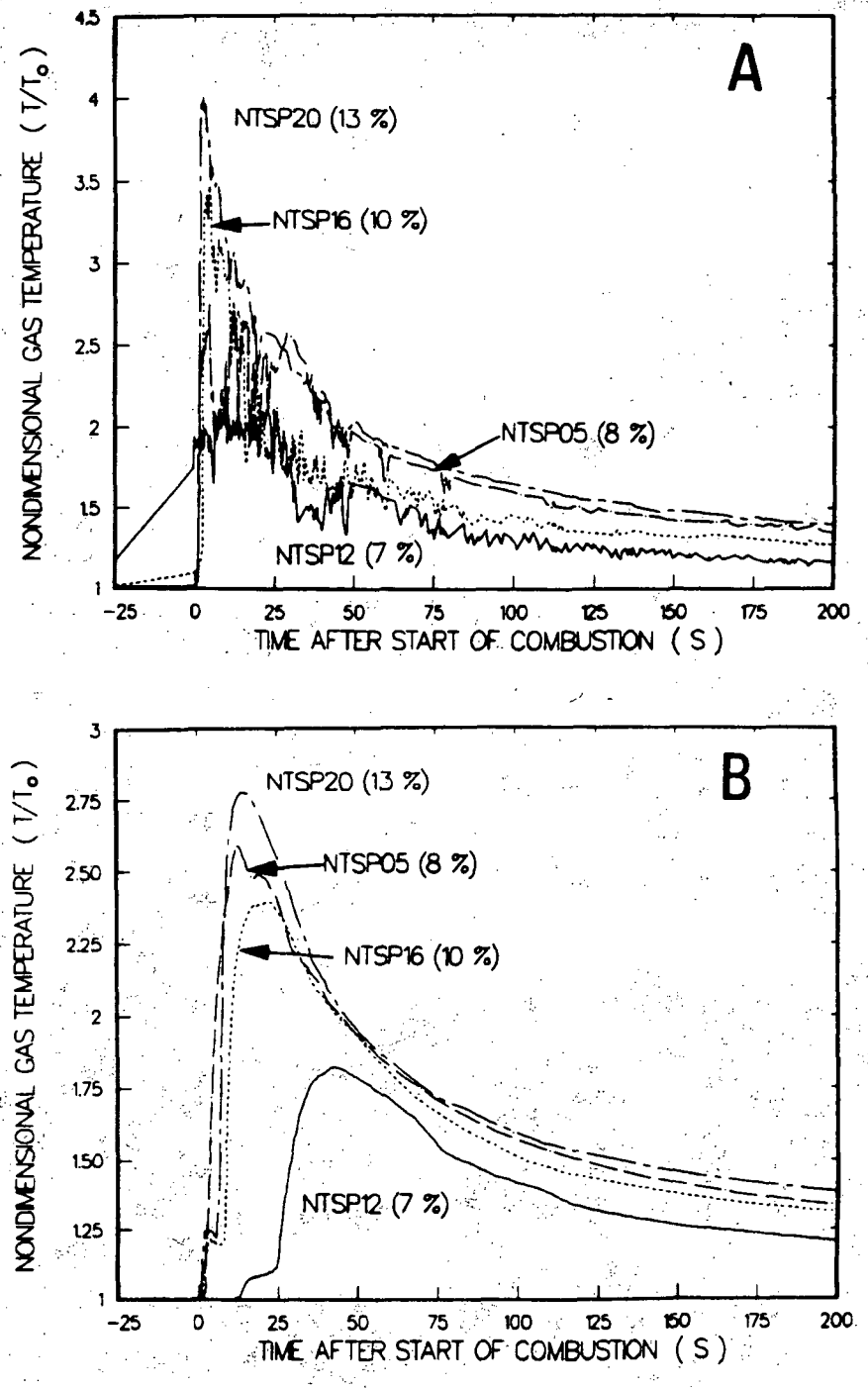

Figure B.15: Gas thermocouple profiles for steam-laden tests. Tests shown are 30% (nominal) steam by volume. Numbers in parentheses are initial hydrogen concentrations.

A: 3-mil thermocouple results
B: 32-mil thermocouple results

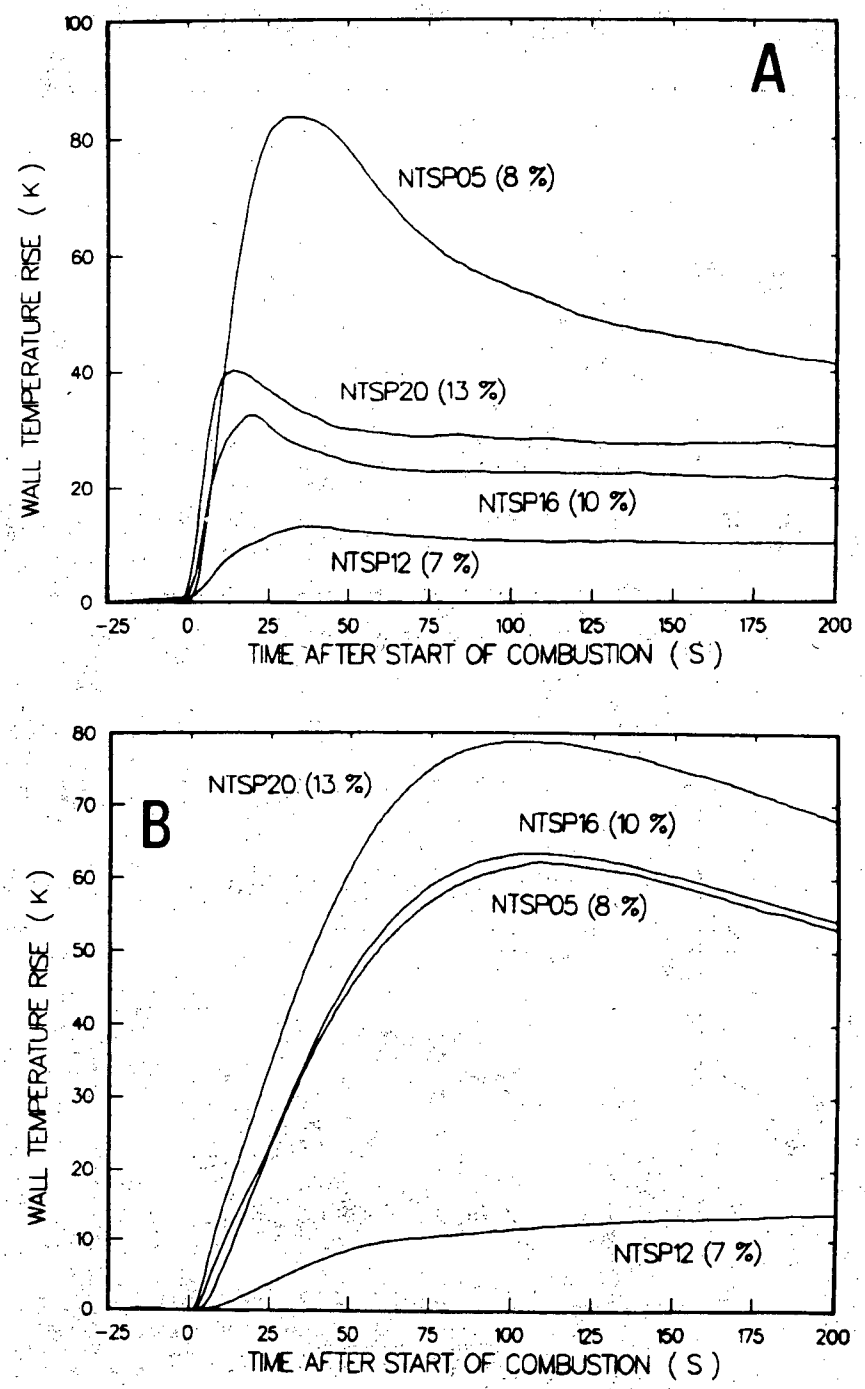

Figure B.16: Dewar wall thermocouple profiles for steam-laden tests. Tests shown are 30% (nominal) steam by volume. Numbers in parentheses are initial hydrogen concentrations.

A: Thermocouple T120 results
B: Thermocouple T121 results

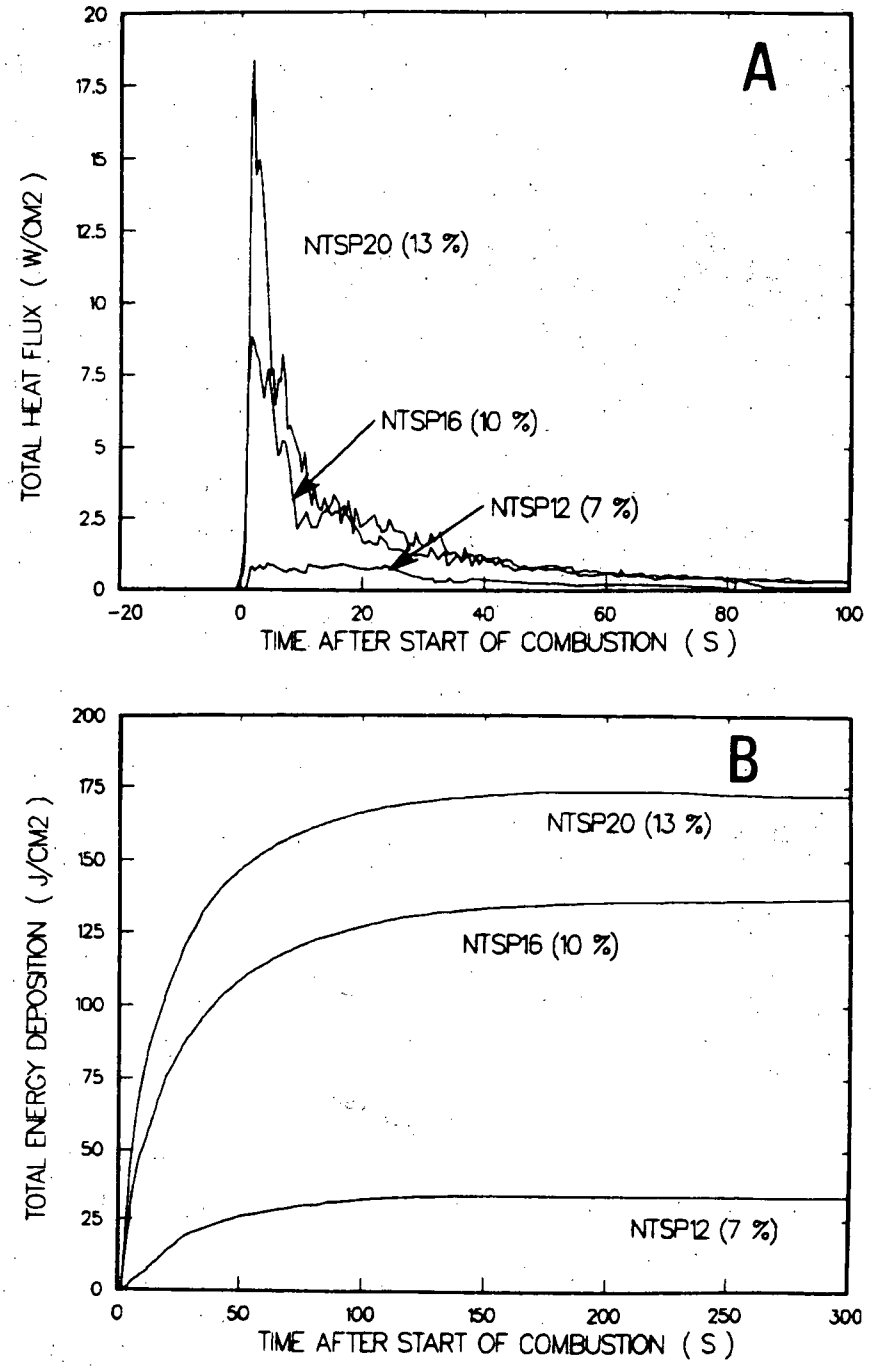

Figure B.17: Heat transfer profiles from H232 for steam-laden tests. Tests shown are 30% (nominal) steam by volume. Numbers in parentheses are initial hydrogen concentrations.

A: Total heat flux

B: Total energy deposition

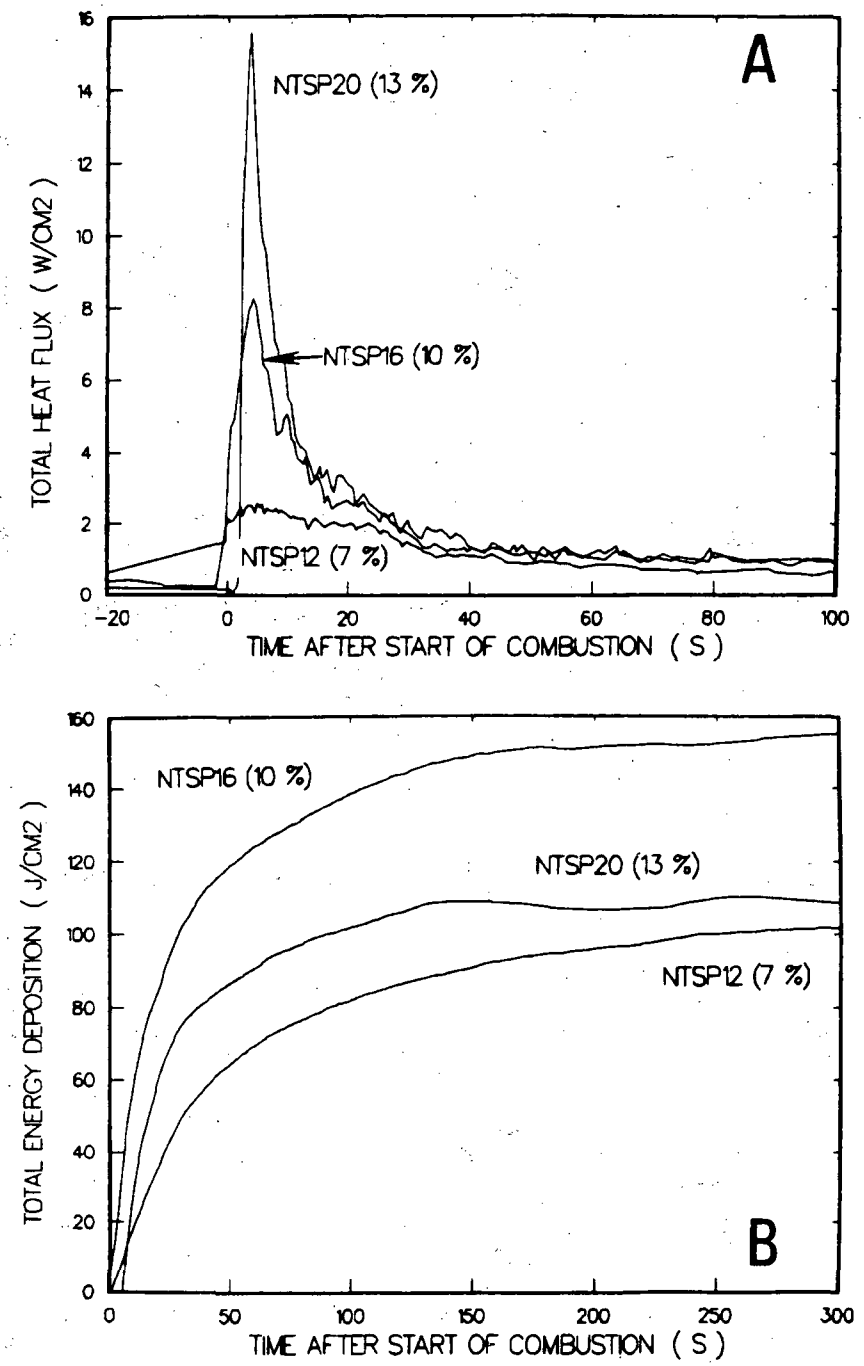

Figure B.18: Heat transfer profiles from H503 and H106 (steam-laden tests). Tests shown are 30% (nominal) steam by volume. Numbers in parentheses are initial hydrogen concentrations.

A: Total heat flux

B: Total energy deposition

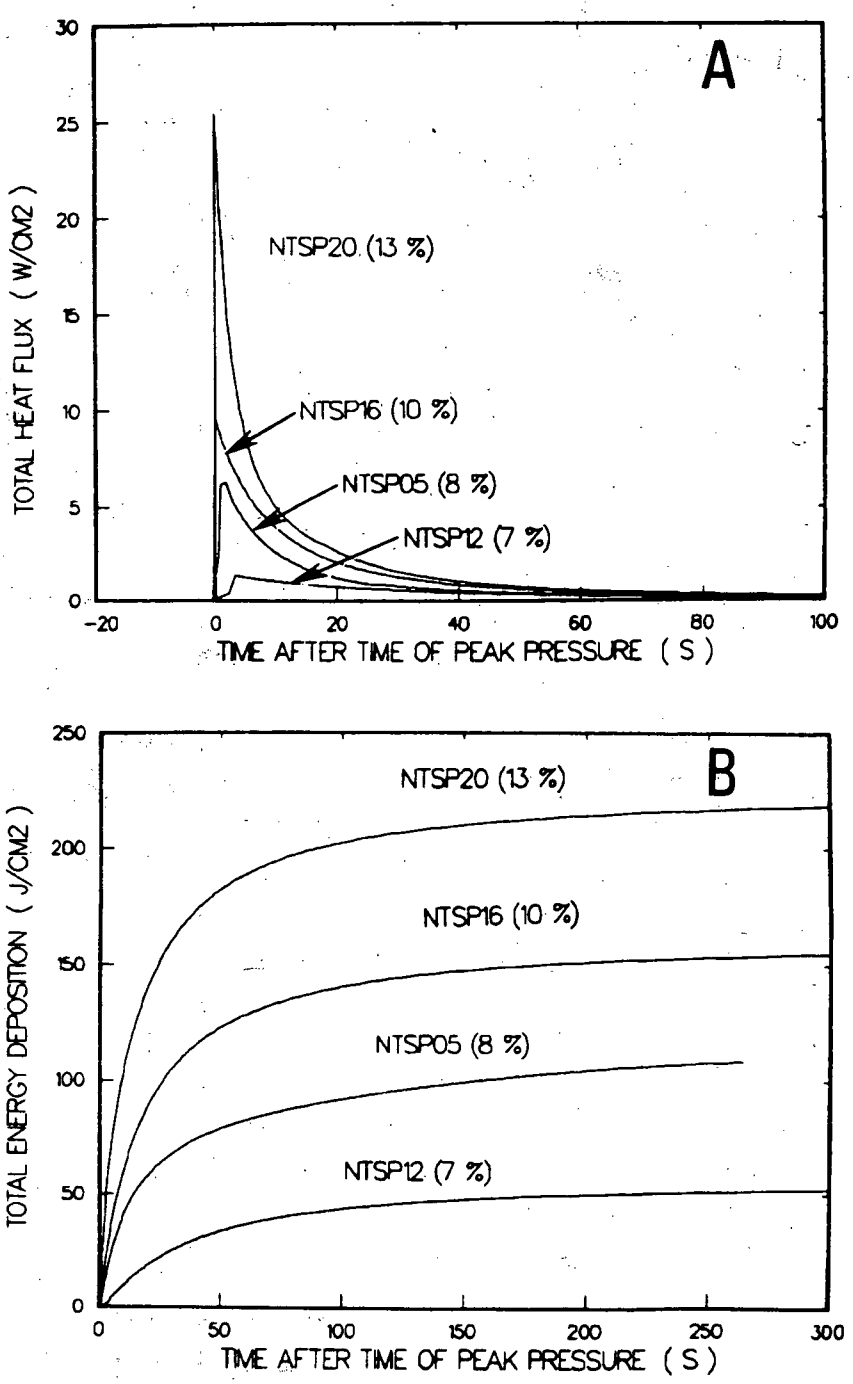

Figure B.19: Total heat transfer profiles from pressure sensors (steam-laden tests). Tests shown are 30% (nominal) steam by volume. Numbers in parentheses are initial hydrogen concentrations.

A: Total heat flux

B: Total energy deposition

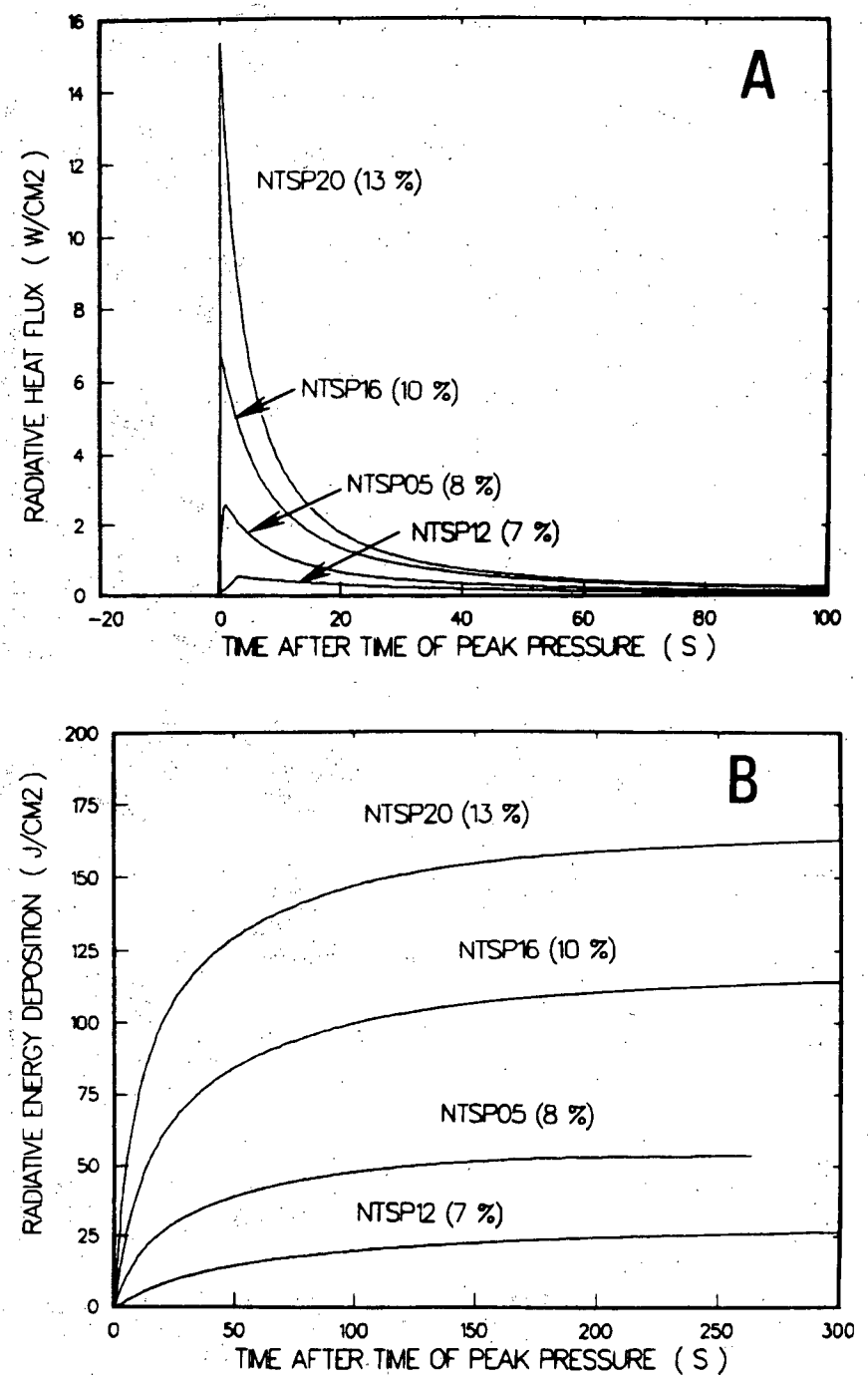

Figure B.20: Radiative heat transfer profiles from pressure sensors (steam-laden tests). Tests shown are 30% (nominal) steam by volume. Numbers in parentheses are initial hydrogen concentrations.

A: Radiative heat flux

B: Radiative energy deposition

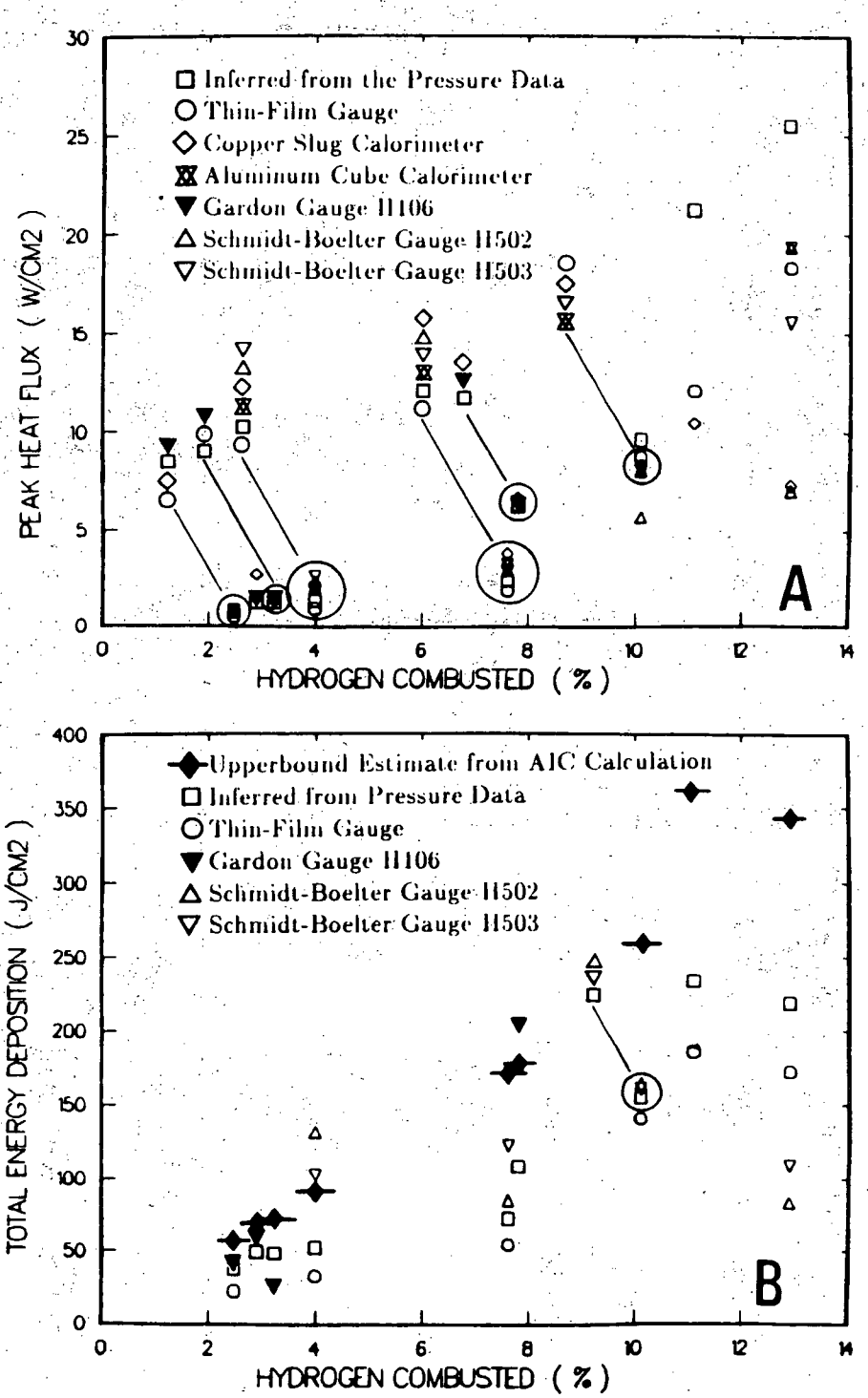

Figure B.21: Total heat transfer results from steam-laden tests

A: Total heat flux

B: Total energy deposition

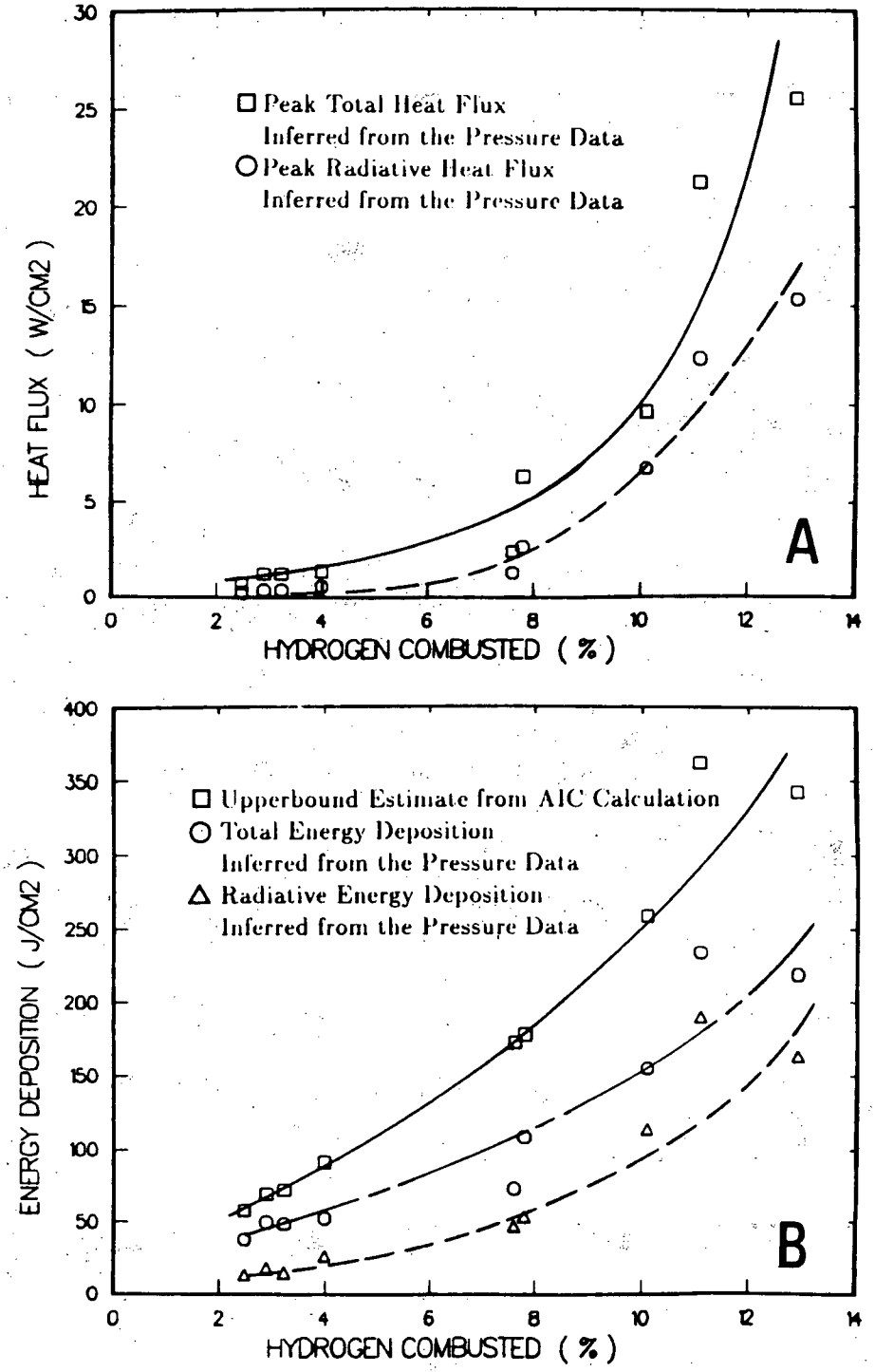

Figure B.22: Heat transfer results inferred from pressure sensors (steam-laden tests)

A: Heat flux

B: Energy deposition

B.3 Comparative Results from Tests with Sprays-on

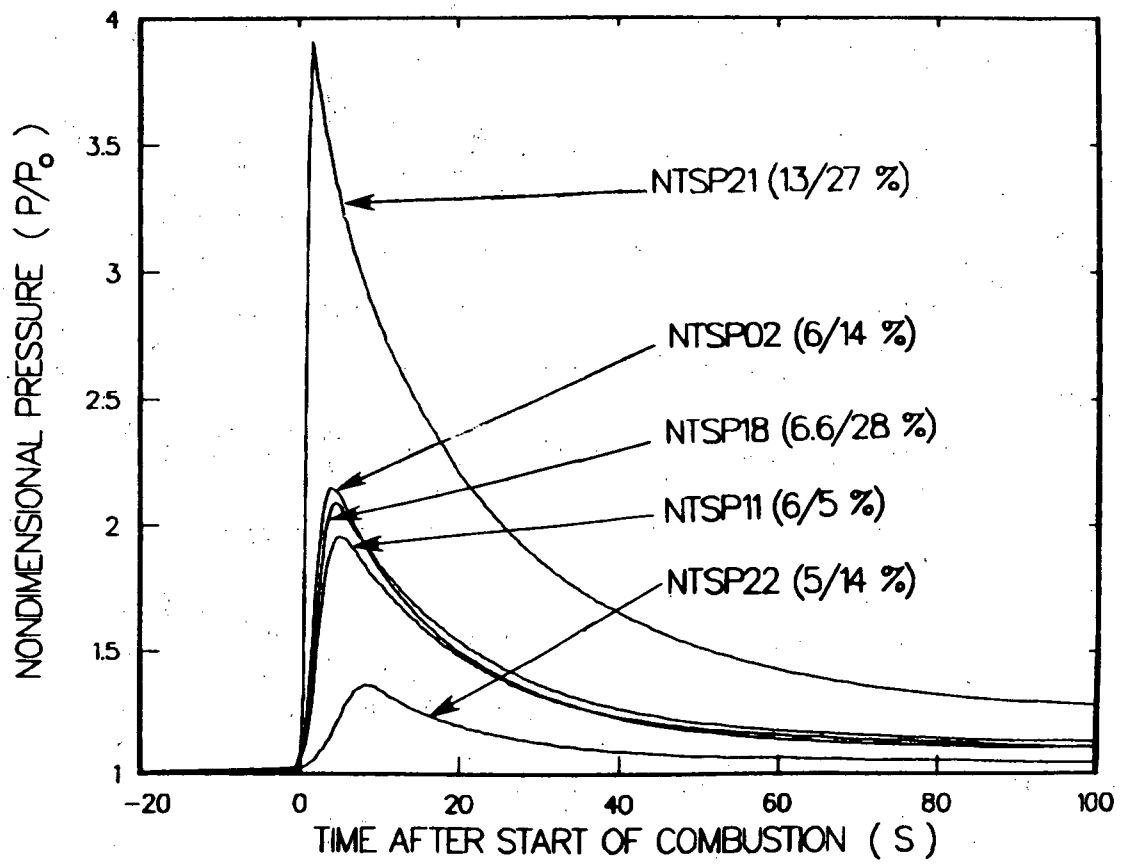

Figure B.23: Gas pressure profiles for tests with sprays-on. Numbers in parentheses are initial hydrogen/initial steam concentrations.

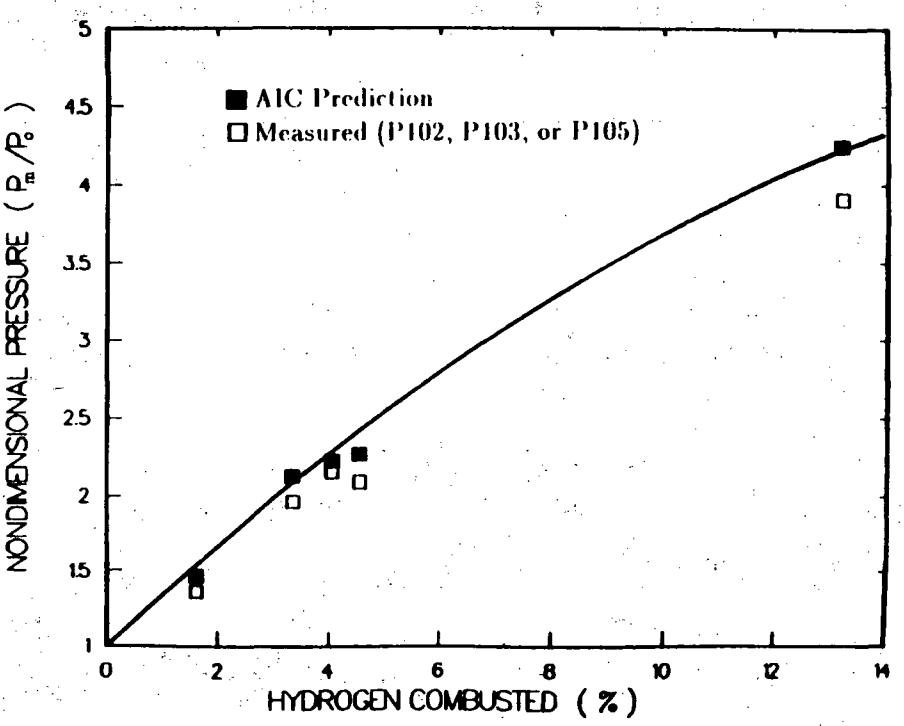

Figure B.24: Peak pressure ratios for tests with sprays-on

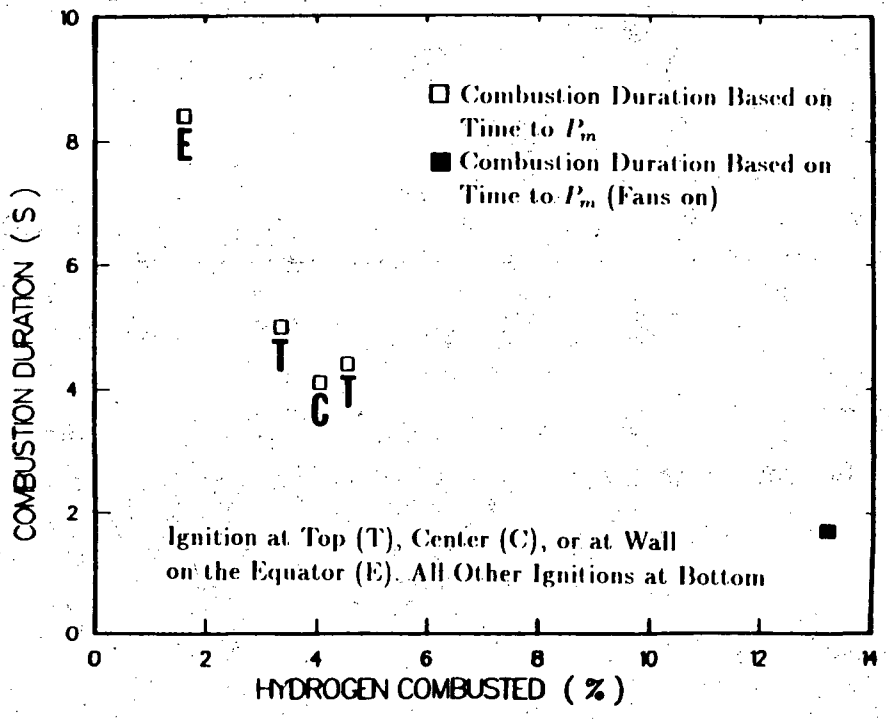

Figure B.25: Combustion duration inferred from pressure results (sprays-on tests)

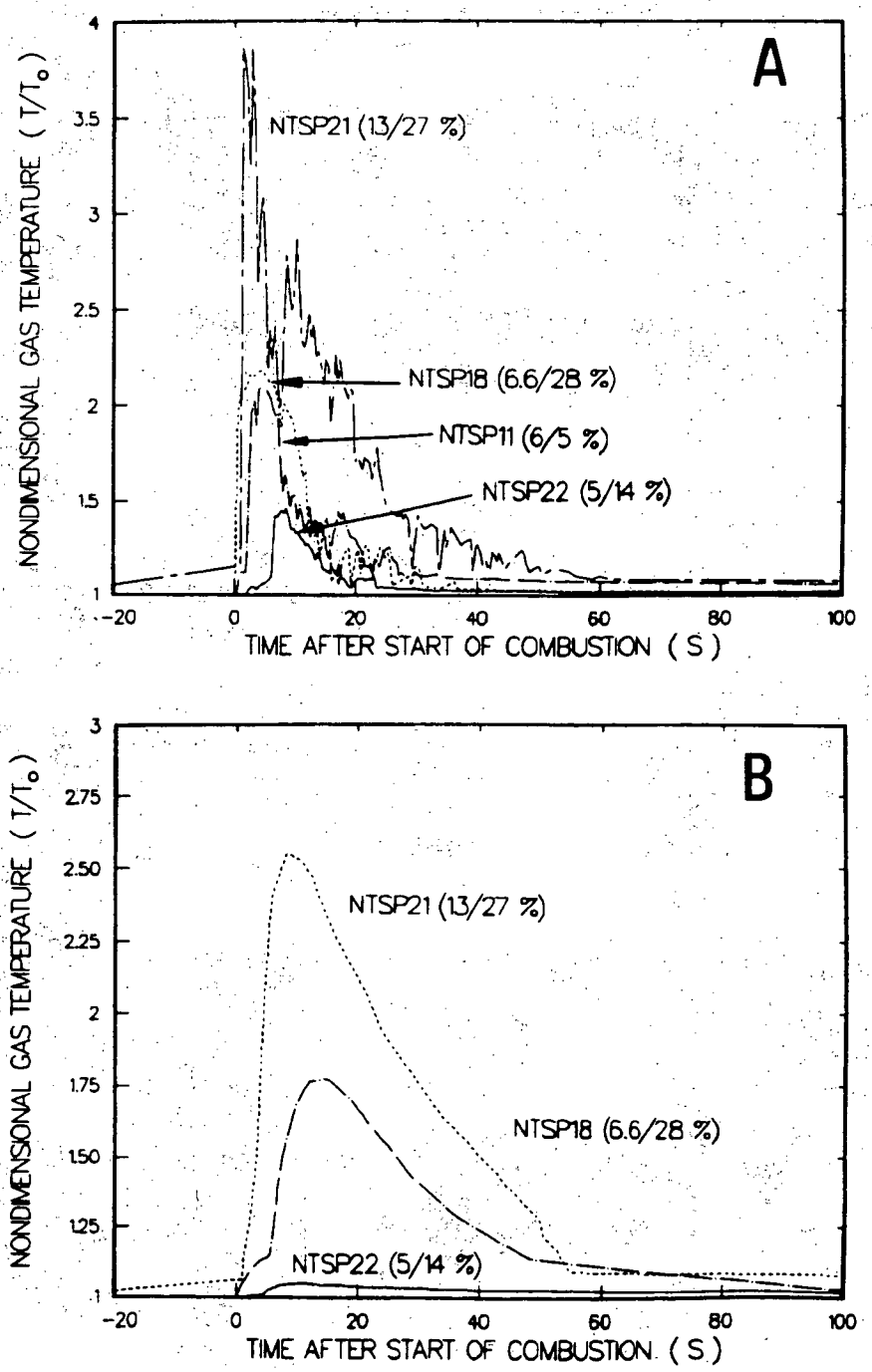

Figure B.26: Gas thermocouple profiles for sprays-on tests. Numbers in parentheses are initial hydrogen/initial steam concentrations.

A: 3-mil thermocouple results
B: 32-mil thermocouple results

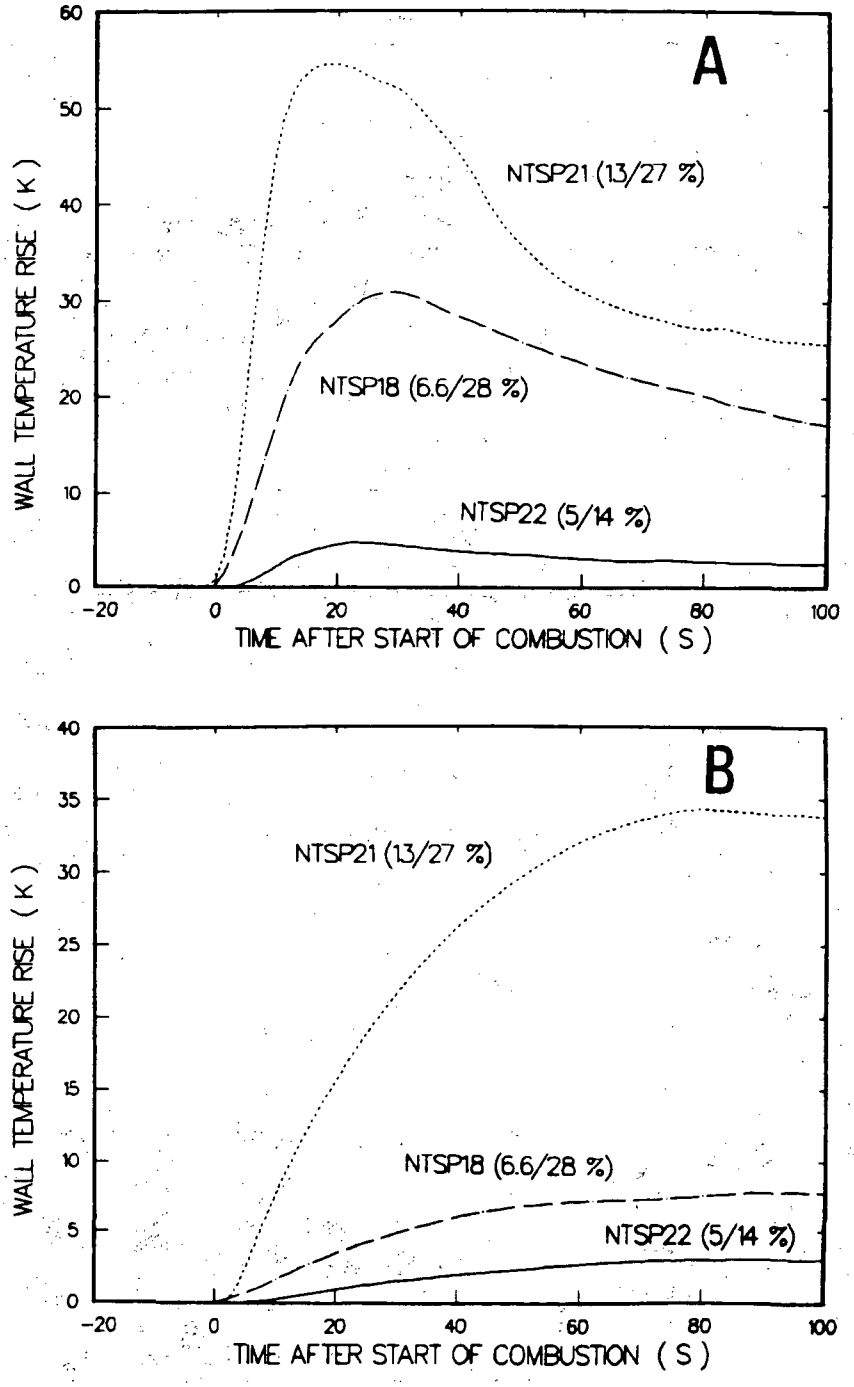

Figure B.27: Dewar wall thermocouple profiles for sprays-on tests. Numbers in parentheses are initial hydrogen/initial steam concentrations.

A: Thermocouple T120 results

B: Thermocouple T121 results

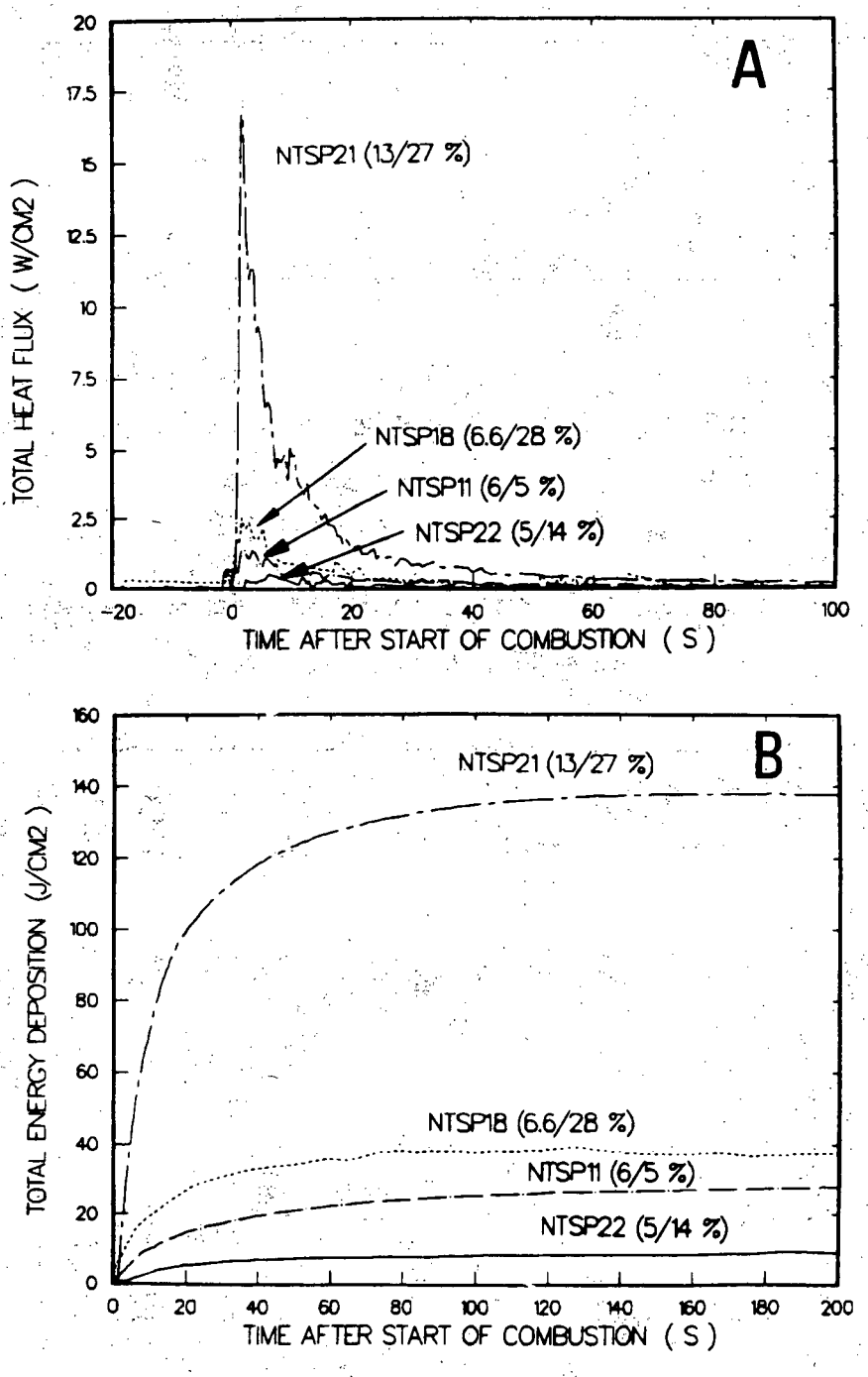

Figure B.28: Heat transfer profiles from H232 for tests with sprays-on. Numbers in parentheses are initial hydrogen/initial steam concentrations.

A: Total heat flux
B: Total energy deposition

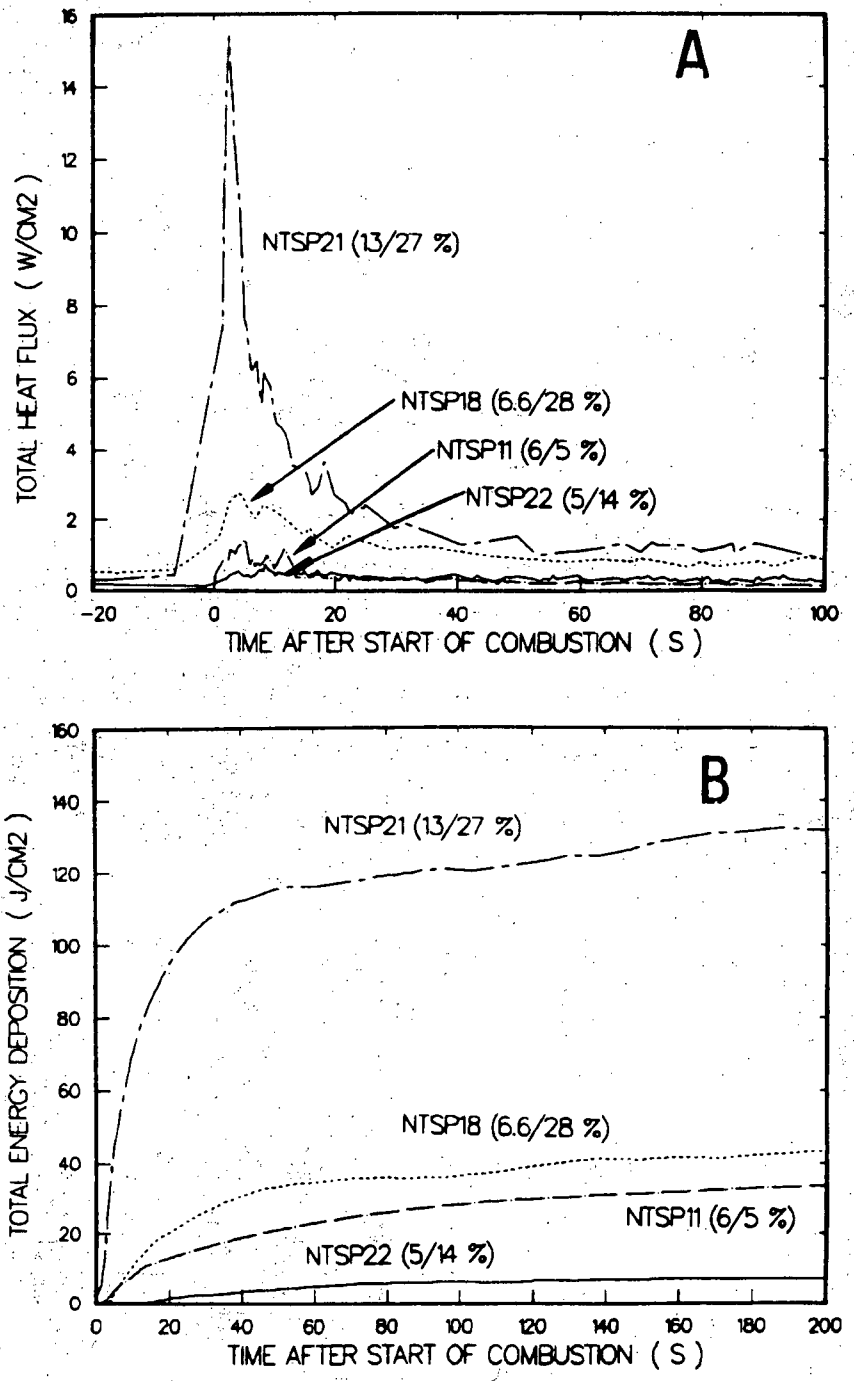

Figure B.29: Heat transfer profiles from H503 (sprays-on). Numbers in parentheses are initial hydrogen/initial steam concentrations.

A: Total heat flux

B: Total energy deposition

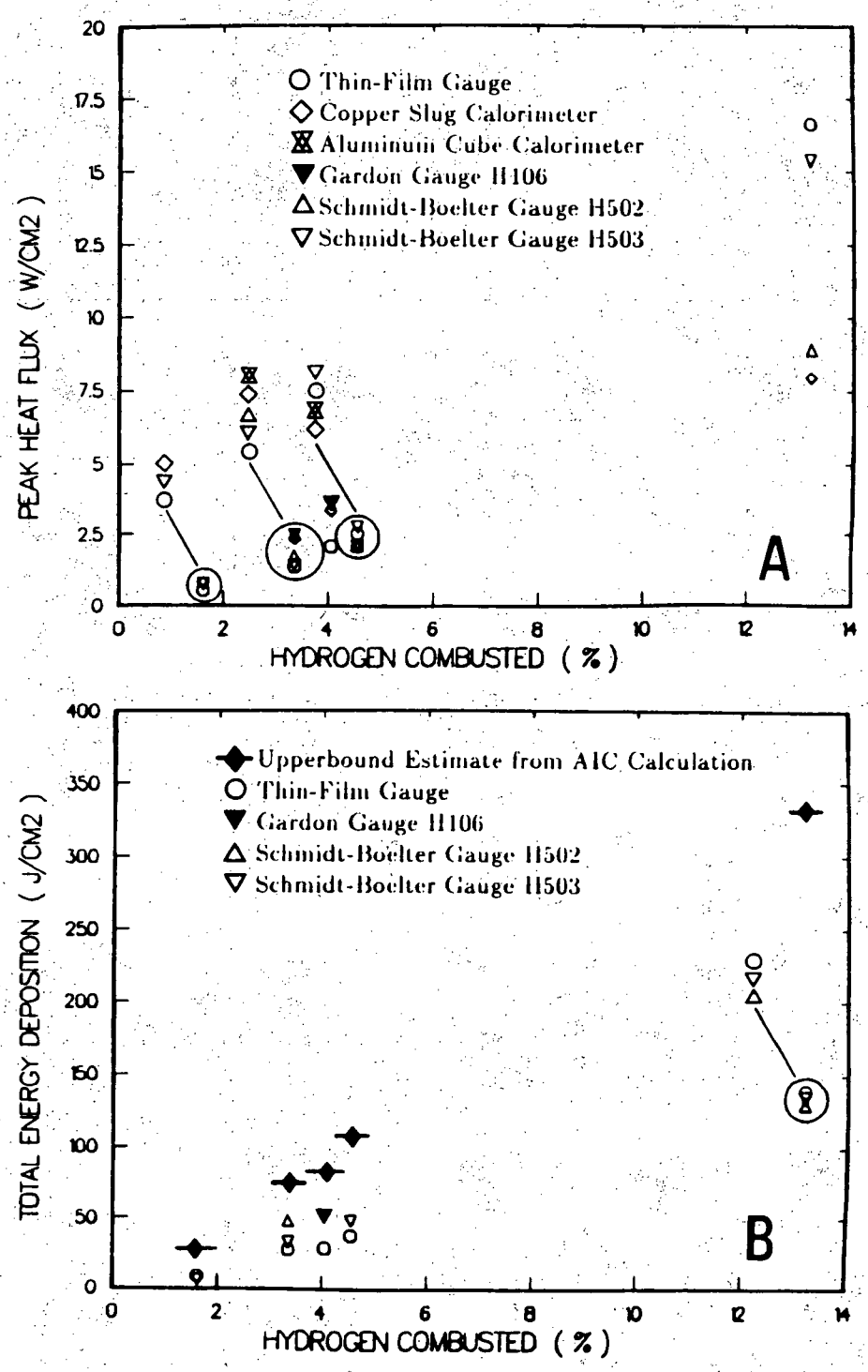

Figure B.30: Total heat transfer results from tests with sprays-on

A: Total heat flux

B: Total energy deposition

Appendix C

C Graphical Results for Each Premixed Combustion Test

Graphical results for the twenty-one premixed combustion tests conducted at NTS are provided in this appendix in the same order given in the tables of Appendix A. Included are gas pressure and gas and wall temperature data obtained from "good" instrumentation. In addition, local total heat flux and energy deposition results are presented for representative "good" Gardon, Schmidt-Boelter and thin-film gauges. Instrumentation "goodness" designations, as defined in the text (Section 5), are tabulated in Tables A-1 – A-3 of Appendix A.

Global (also referred to as average) results obtained from the pressure signal processing are also provided in graphical form for comparison purposes. These results include estimates of the gas and wall temperatures and also radiative and total heat transfer rates and energy depositions. The global estimates of radiative and total heat transfer are provided only for times following the time of peak pressure (*i.e.*, assumed time of completion of combustion) given the limitations of SMOKE for modeling the actual combustion phenomena (see Section 4). Comparative global results inferred from pressure data processing are not provided for tests in which the spray systems were operative, since the effects of sprays are not accounted for in SMOKE. Results obtained from processing pressure transducers P105 (Hydrogen Behavior series) and P103 (Equipment Survival series) are used if these signals are "good". Otherwise, results from transducer P102 are provided for comparison purposes.

NTSP01 – 5.3% H_2 / 4.2% H_2O

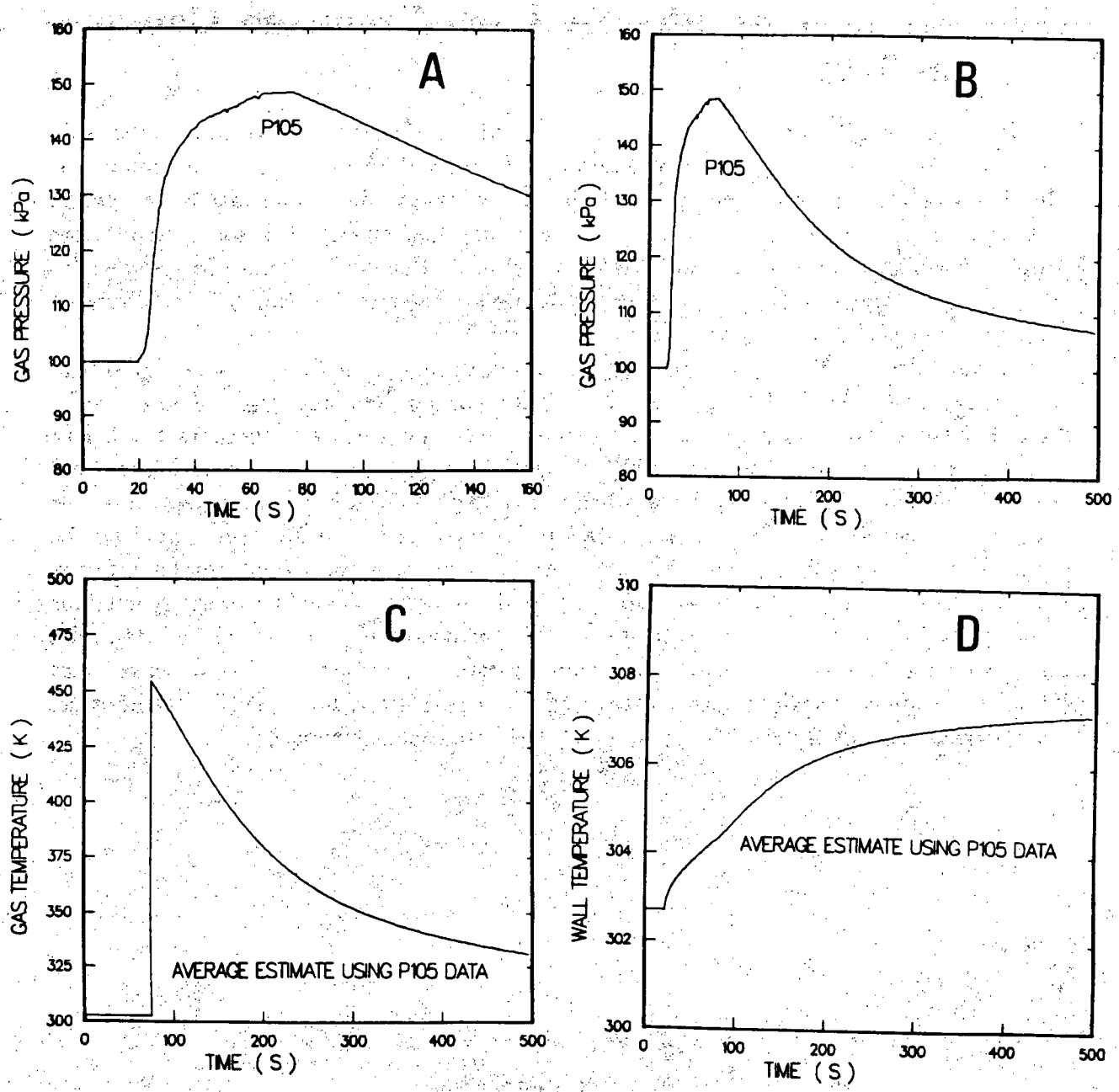

Figure C.1: Gas pressure and gas and wall temperatures for test NTSP01

A: Gas pressure during combustion
B: Gas pressure for entire test
C: Gas temperature inferred from pressure
D: Wall temperature inferred from pressure

NTSP01 – 5.3% H_2 / 4.2% H_2O

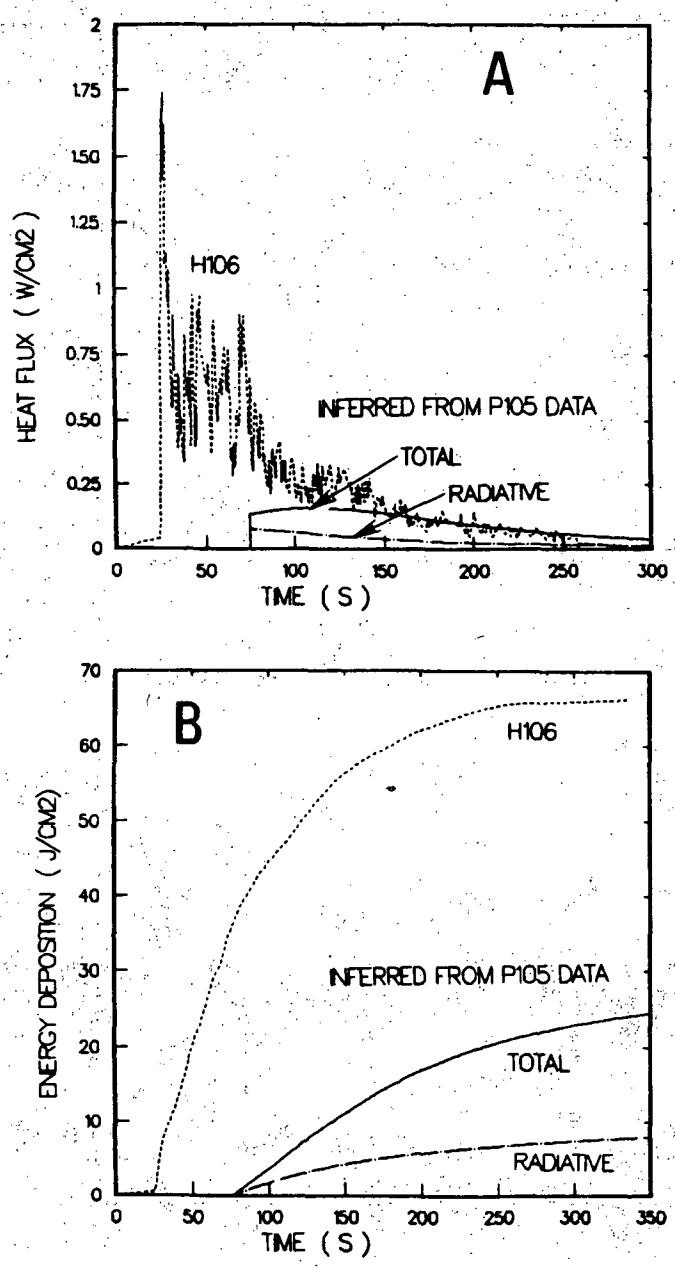

Figure C.2: Heat flux and energy deposition results for test NTSP01

A: Heat flux (Gardon gauge and inferred from pressure)

B: Energy deposition (Gardon gauge and inferred from pressure)

NTSP9P – 6.0% H_2 / 4.6% H_2O

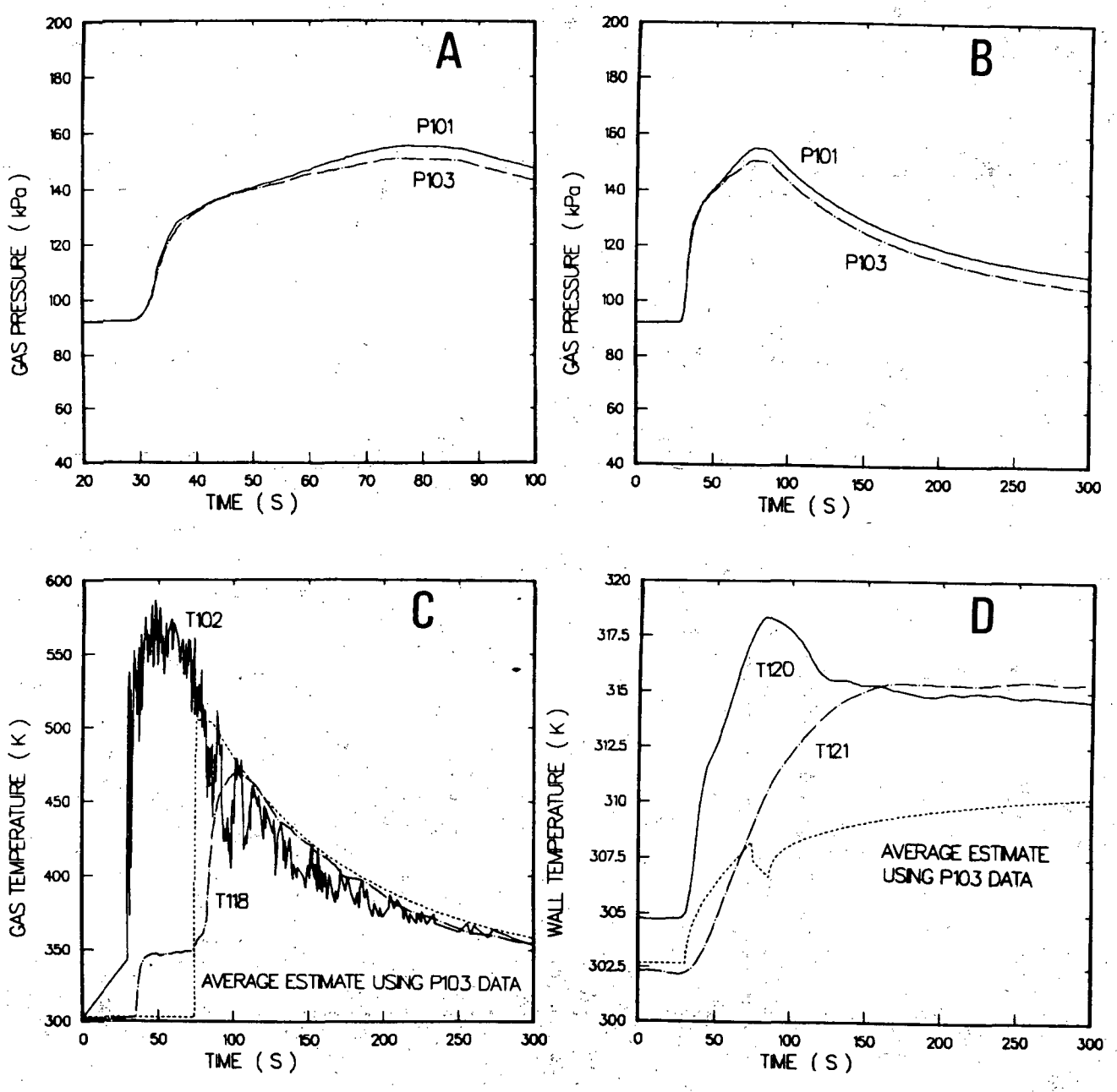

Figure C.3: Gas pressure and gas and wall temperatures for test NTSP9P

A: Gas pressure during combustion
B: Gas pressure for entire test
C: Gas temperature (measured and inferred from pressure)
D: Wall temperature (measured and inferred from pressure)

NTSP9P – 6.0% H_2 / 4.6% H_2O

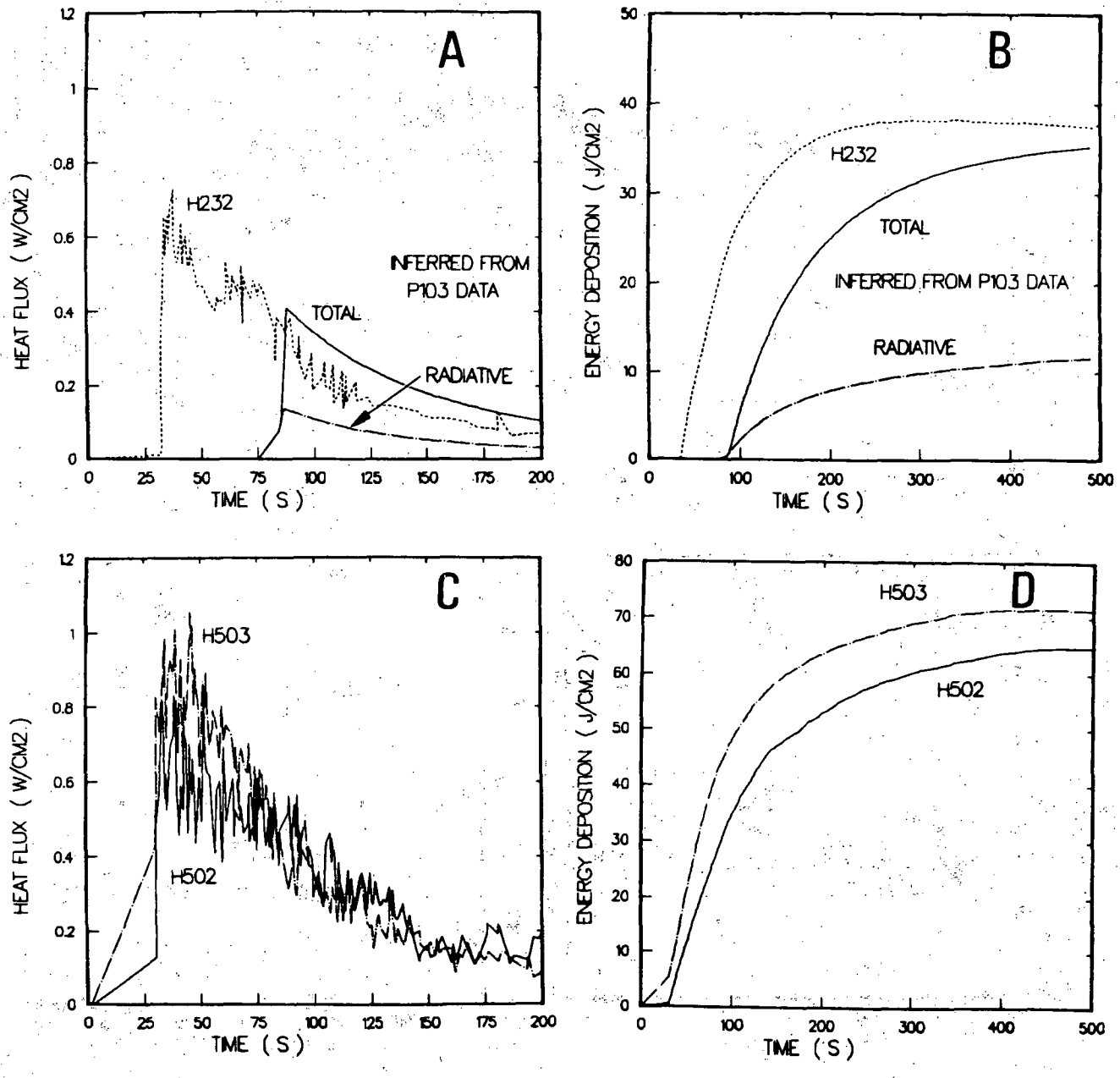

Figure C.4: Heat flux and energy deposition results for test NTSP9P

A: Heat flux (thin-film gauge and inferred from pressure)
B: Energy deposition (thin-film gauge and inferred from pressure)
C: Heat flux (Schmidt-Boelter gauges)
D: Energy deposition (Schmidt-Boelter gauges)

NTSP09 – 6.1% H_2 / 4.2% H_2O

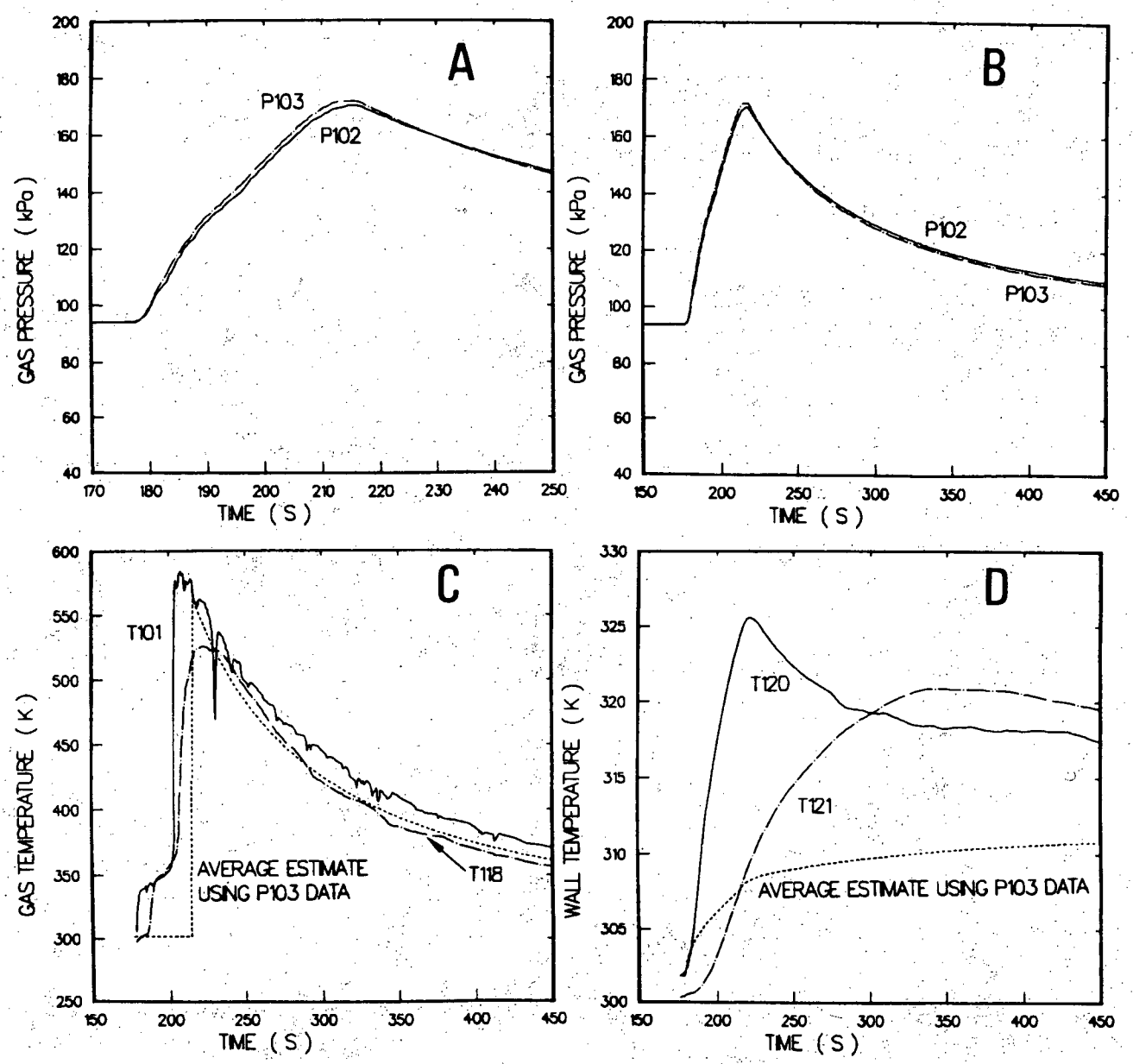

Figure C.5: Gas pressure and gas and wall temperatures for test NTSP09

A: Gas pressure during combustion
B: Gas pressure for entire test
C: Gas temperature (measured and inferred from pressure)
D: Wall temperature (measured and inferred from pressure)

NTSP09 – 6.1% H_2 / 4.2% H_2O

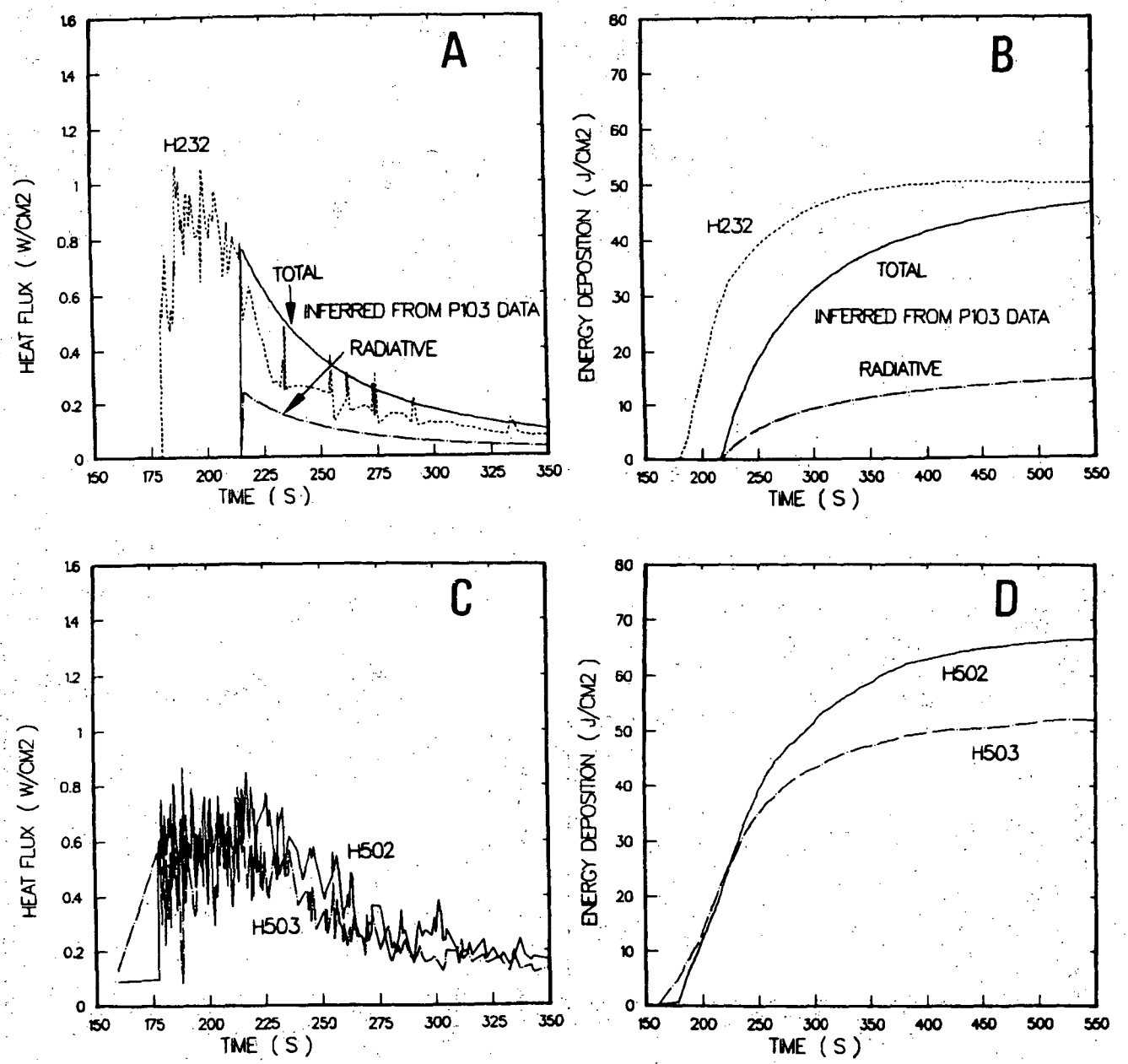

Figure C.6: Heat flux and energy deposition results for test NTSP09

A: Heat flux (thin-film gauge and inferred from pressure)
B: Energy deposition (thin-film gauge and inferred from pressure)
C: Heat flux (Schmidt-Boelter gauges)
D: Energy deposition (Schmidt-Boelter gauges)

NTSP00 – 6.6% H_2 / 4.5% H_2O

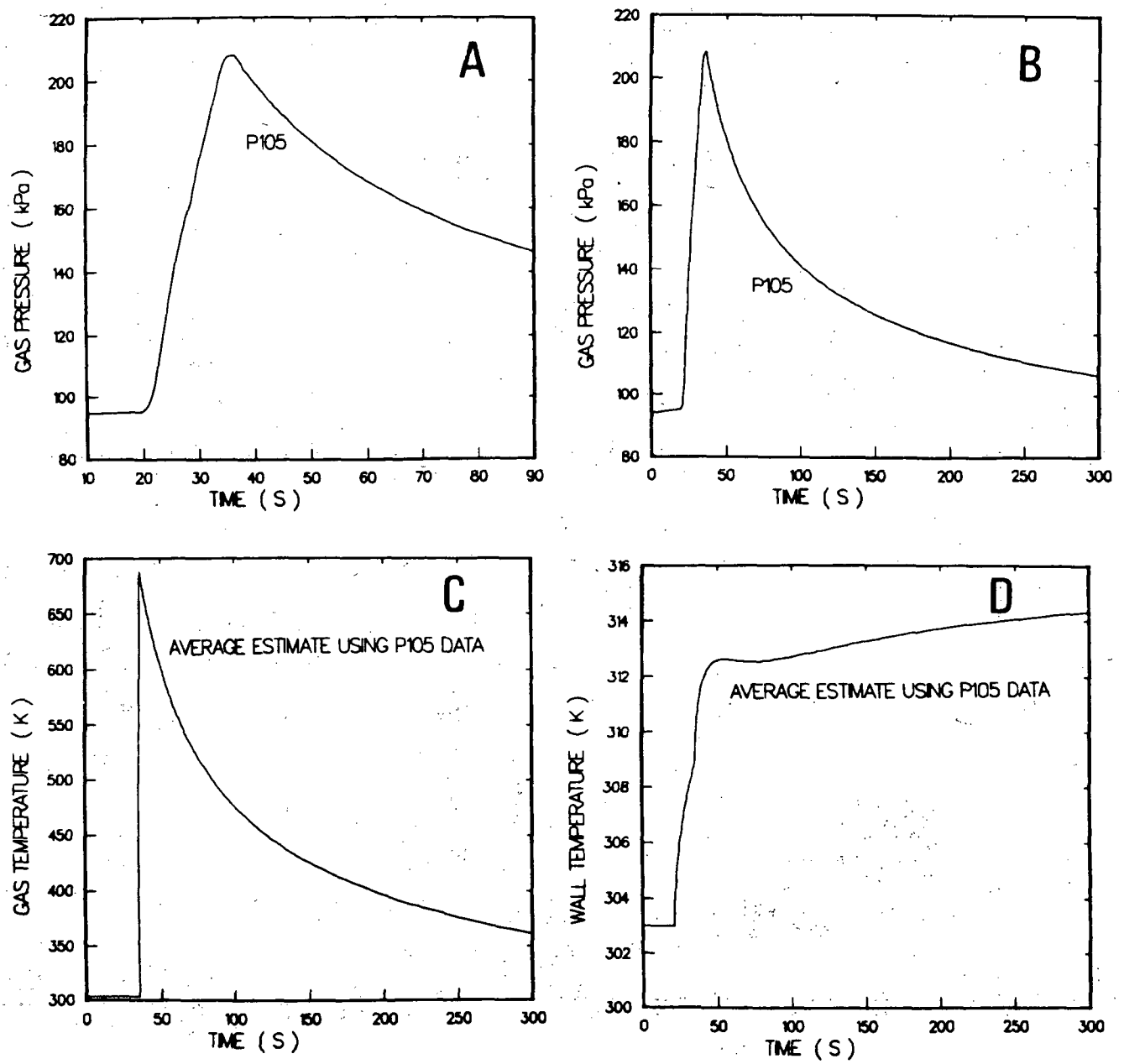

Figure C.7: Gas pressure and gas and wall temperatures for test NTSP00

A: Gas pressure during combustion
B: Gas pressure for entire test
C: Gas temperature inferred from pressure
D: Wall temperature inferred from pressure

NTSP00 – 6.6% H_2 / 4.5% H_2O

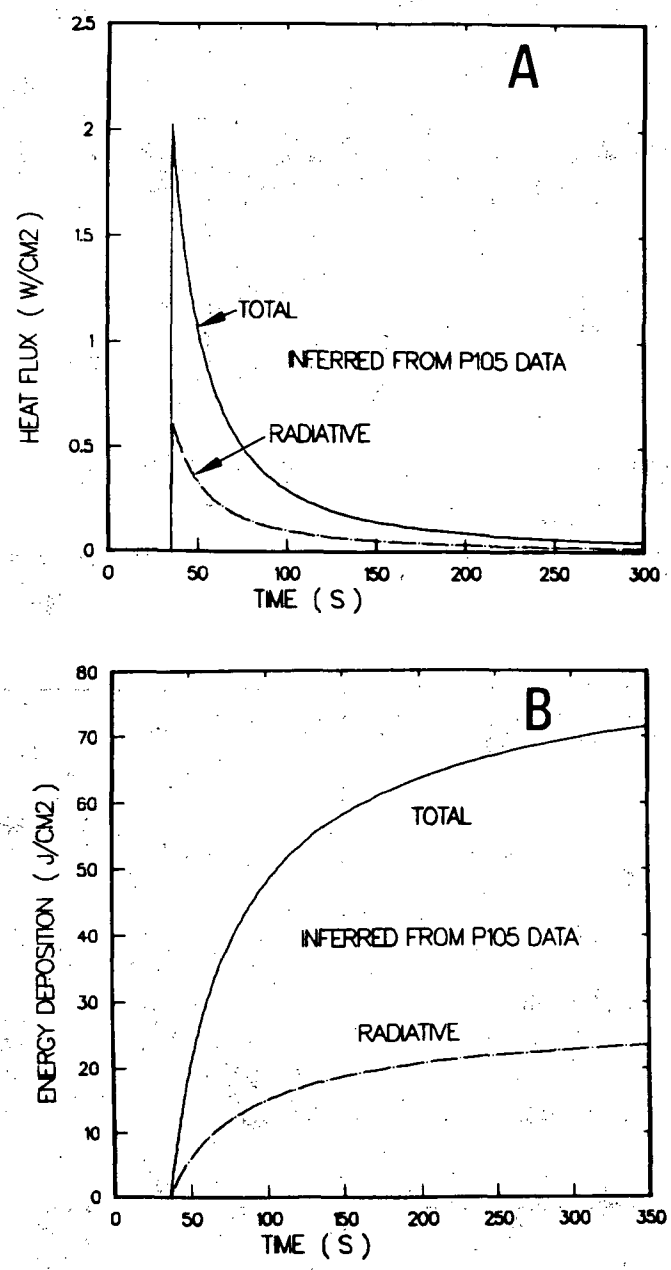

Figure C.8: Heat flux and energy deposition results for test NTSP00

A: Heat flux inferred from pressure

B: Energy deposition inferred from pressure

NTSP04 – 7.7% H_2 / 4.8% H_2O

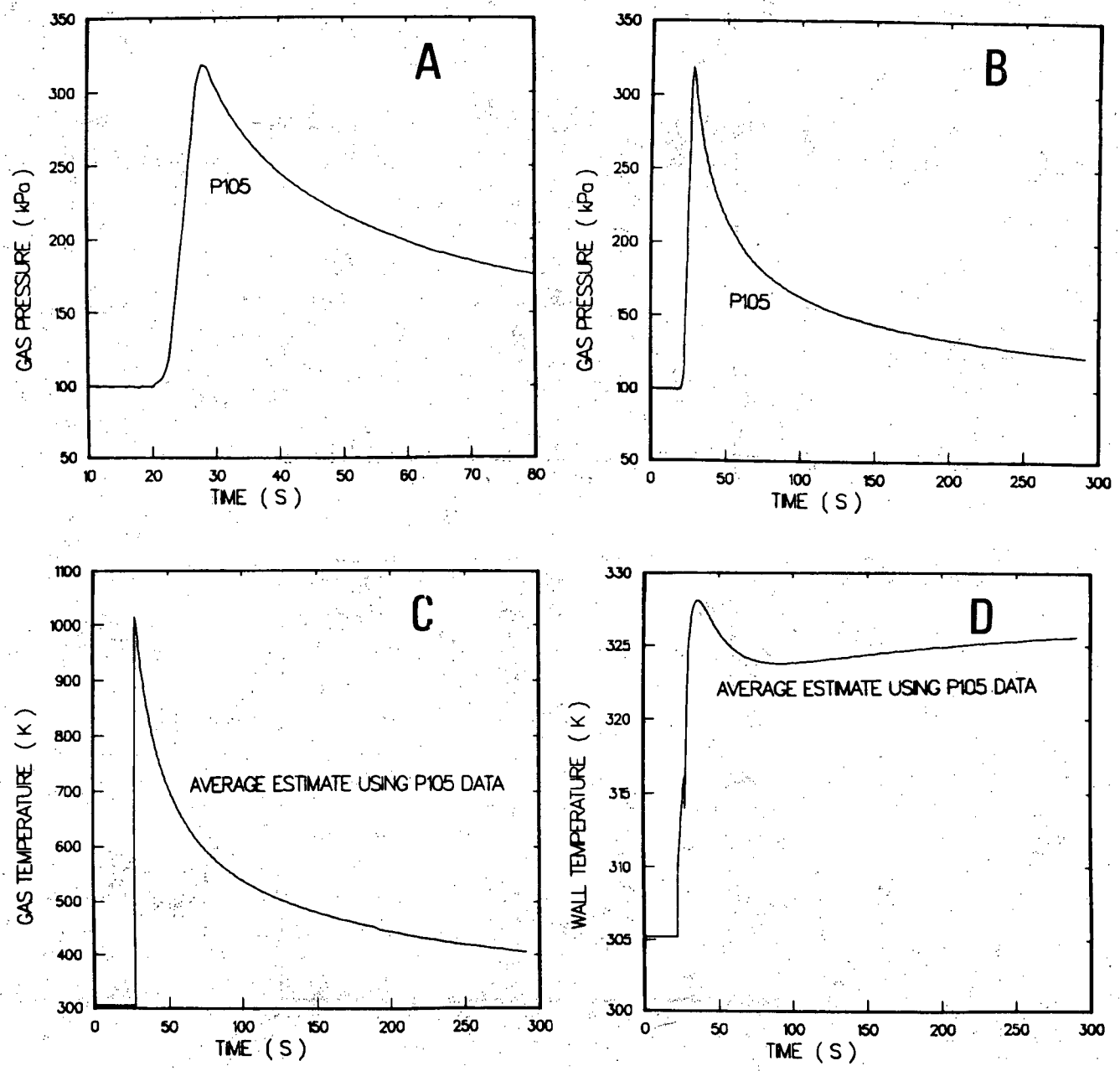

Figure C.9: Gas pressure and gas and wall temperatures for test NTSP04

A: Gas pressure during combustion
B: Gas pressure for entire test
C: Gas temperature inferred from pressure
D: Wall temperature inferred from pressure

NTSP04 – 7.7% H_2 / 4.8% H_2O

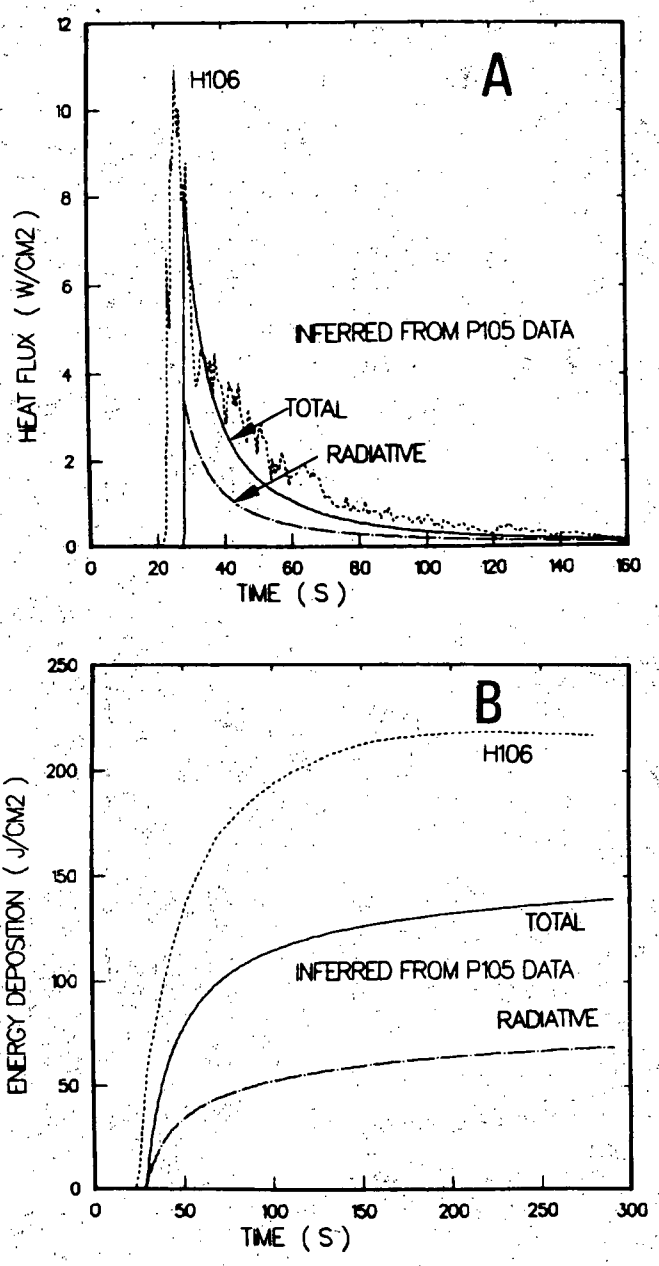

Figure C.10: Heat flux and energy deposition results for test NTSP04

A: Heat flux (Gardon gauge and inferred from pressure)

B: Energy deposition (Gardon gauge and inferred from pressure)

NTSP13 – 7.8% H_2 / 4.4% H_2O

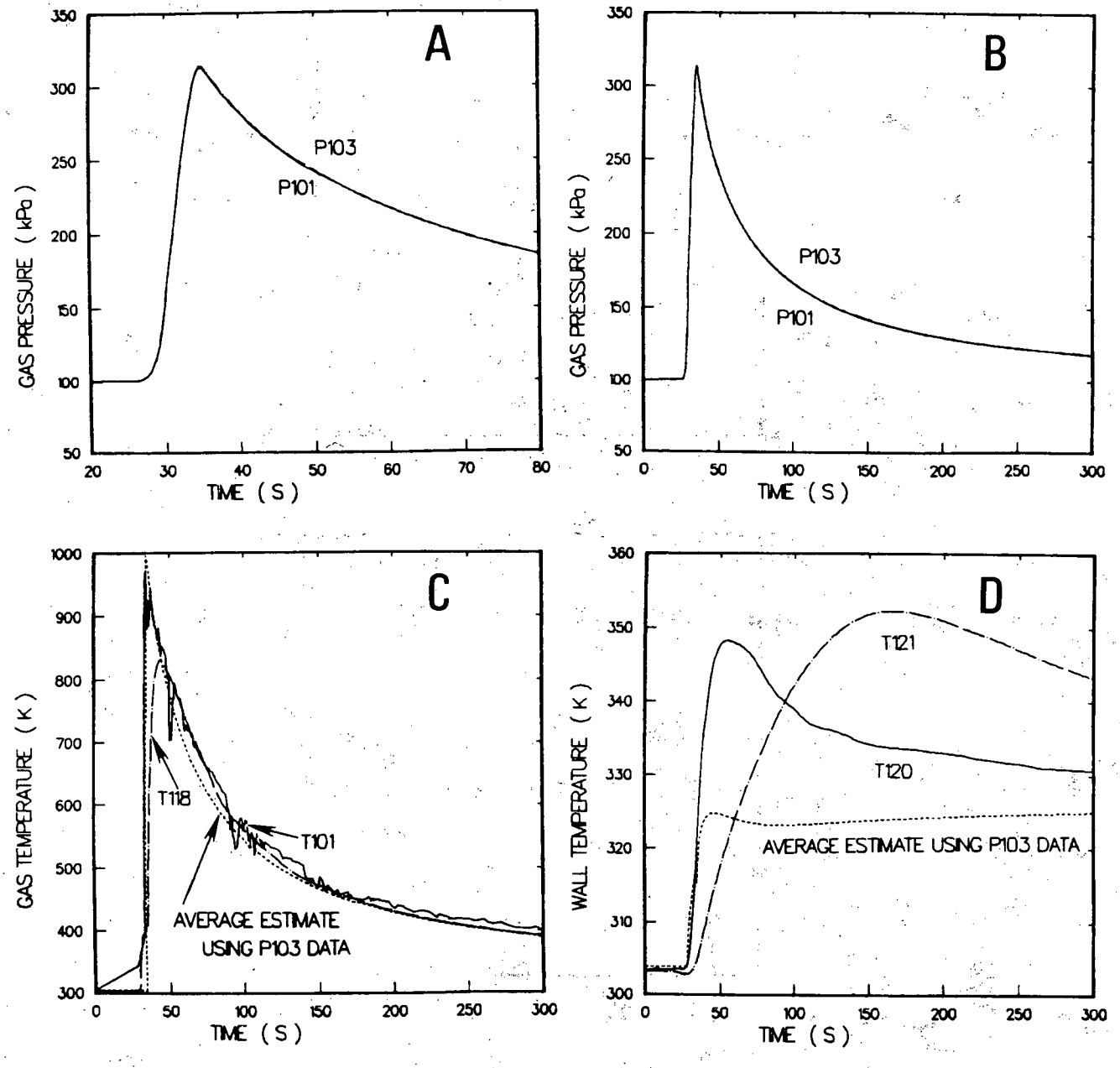

Figure C.11: Gas pressure and gas and wall temperatures for test NTSP13

A: Gas pressure during combustion
B: Gas pressure for entire test
C: Gas temperature (measured and inferred from pressure)
D: Wall temperature (measured and inferred from pressure)

NTSP13 – 7.8% H_2 / 4.4% H_2O

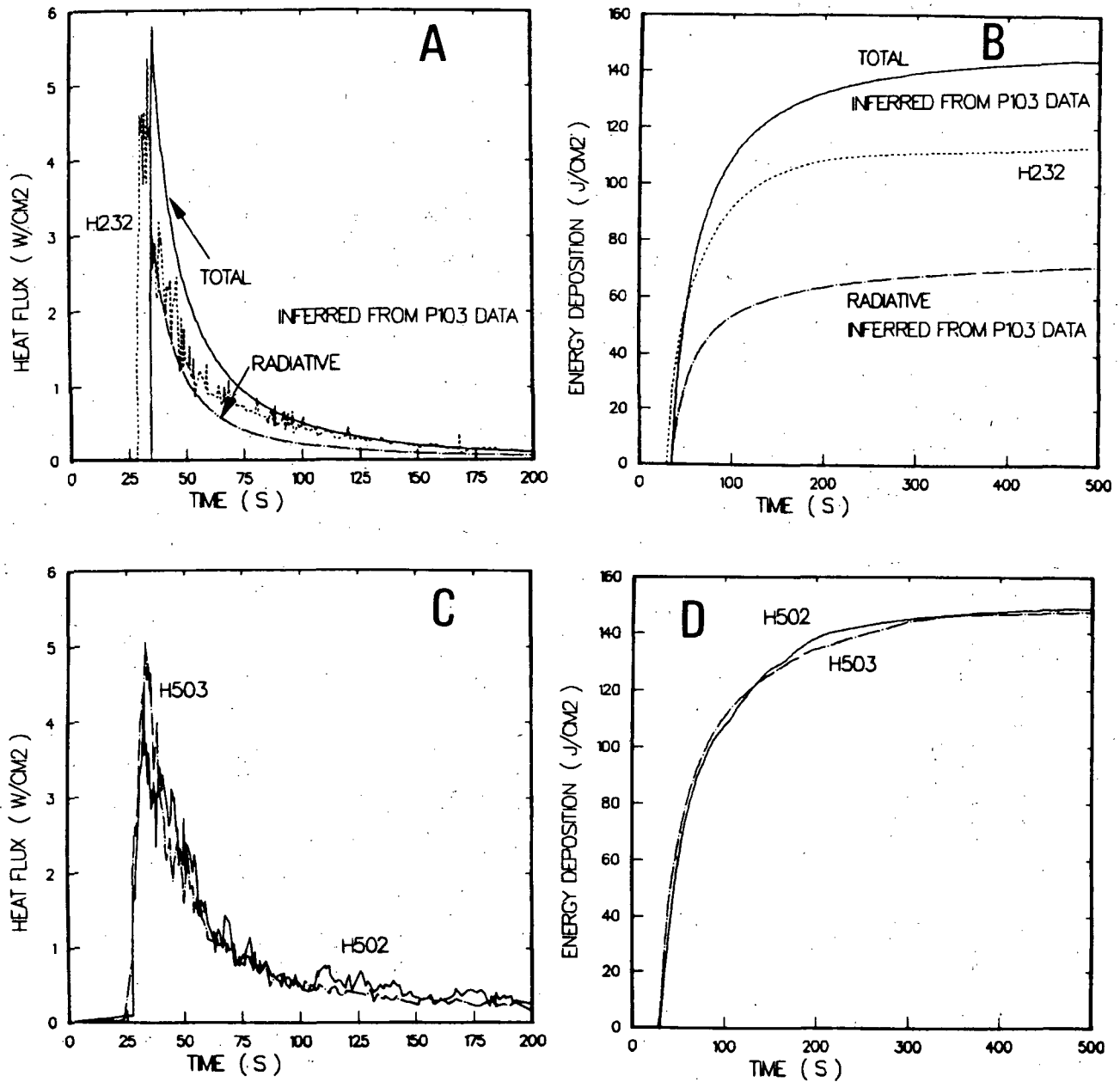

Figure C.12: Heat flux and energy deposition results for test NTSP13

A: Heat flux (thin-film gauge and inferred from pressure)
B: Energy deposition (thin-film gauge and inferred from pressure)
C: Heat flux (Schmidt-Boelter gauges)
D: Energy deposition (Schmidt-Boelter gauges)

NTSP15 – 9.9% H_2 / 4.2% H_2O

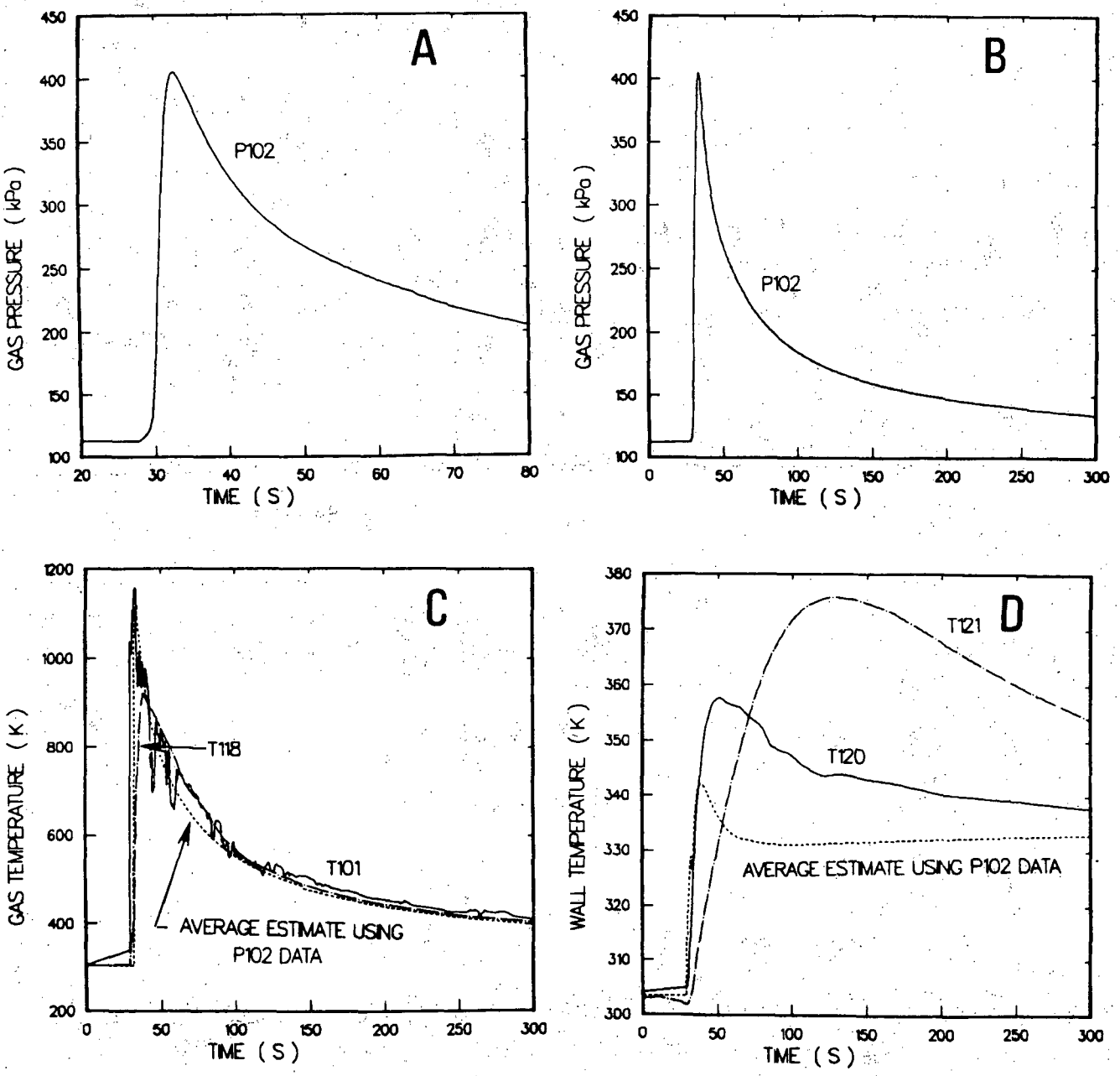

Figure C.13: Gas pressure and gas and wall temperatures for test NTSP15

A: Gas pressure during combustion
B: Gas pressure for entire test
C: Gas temperature (measured and inferred from pressure)
D: Wall temperature (measured and inferred from pressure)

NTSP15 – 9.9% H_2 / 4.2% H_2O

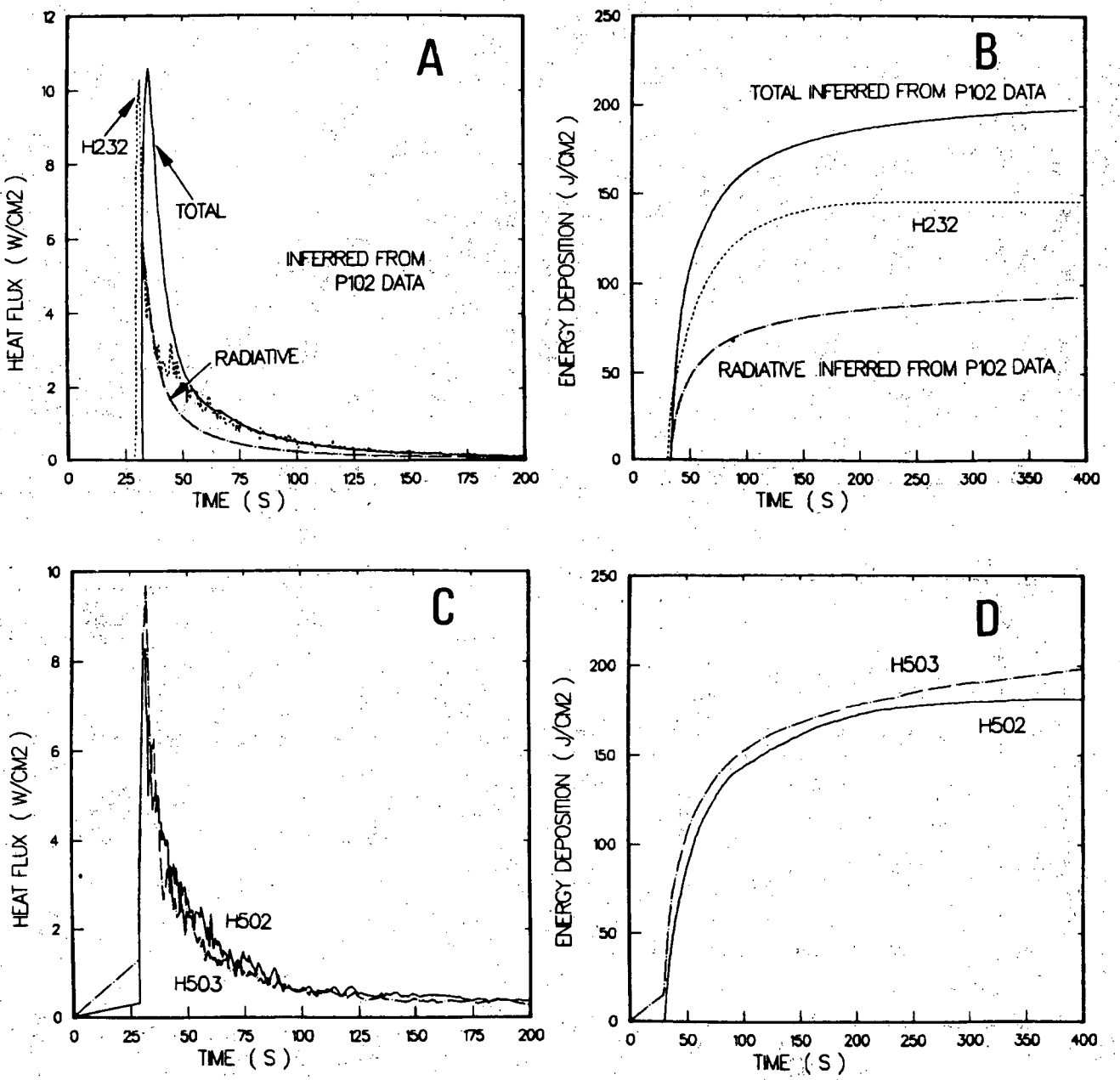

Figure C.14: Heat flux and energy deposition results for test NTSP15

A: Heat flux (thin-film gauge and inferred from pressure)
B: Energy deposition (thin-film gauge and inferred from pressure)
C: Heat flux (Schmidt-Boelter gauges)
D: Energy deposition (Schmidt-Boelter gauges)

NTSP07 – 5.5% H_2 / 14.3% H_2O / *Fans*

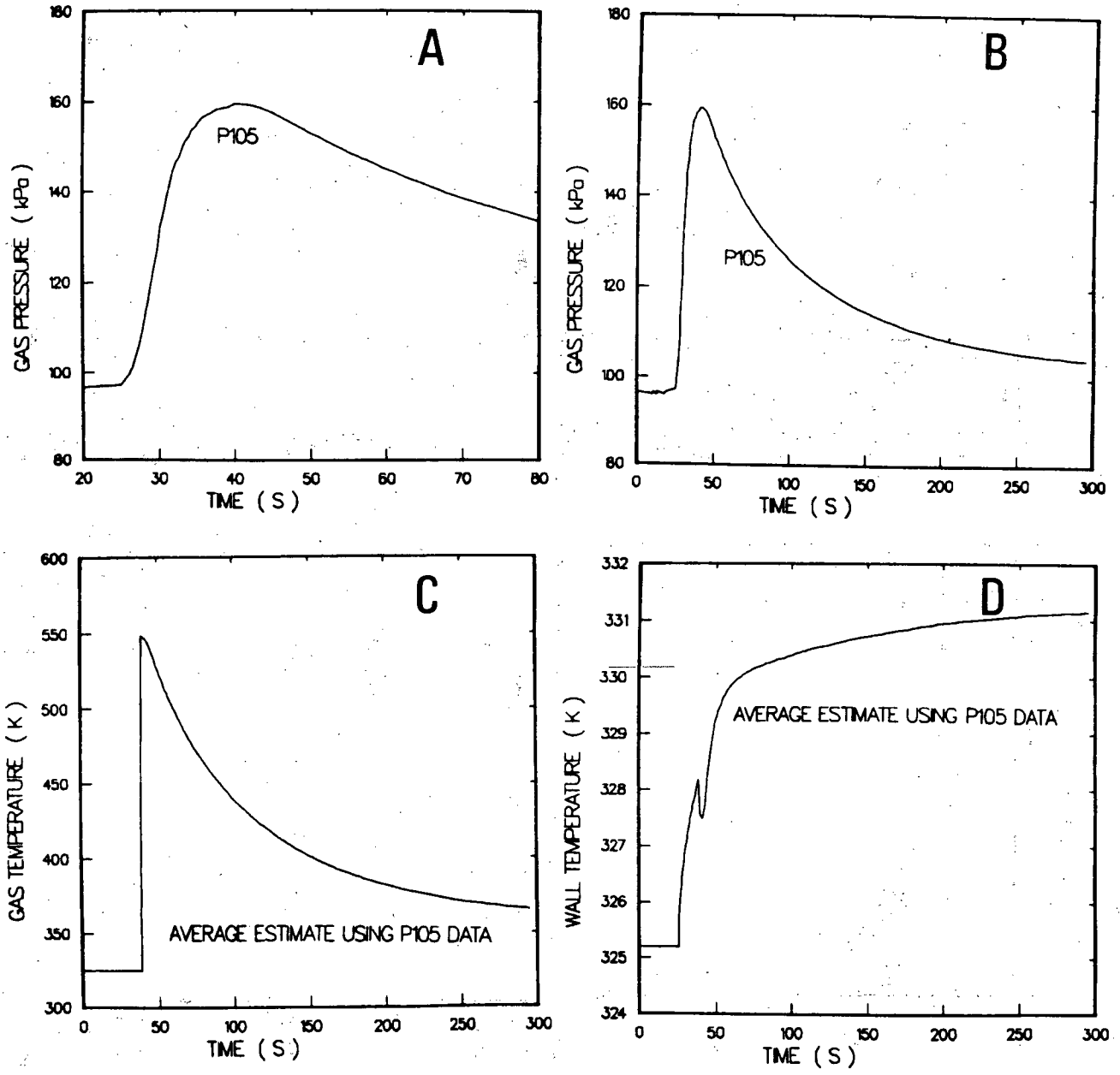

Figure C.15: Gas pressure and gas and wall temperatures for test NTSP07

A: Gas pressure during combustion
B: Gas pressure for entire test
C: Gas temperature inferred from pressure
D: Wall temperature inferred from pressure

NTSP07 – 5.5% H_2 / 14.3% H_2O / *Fans*

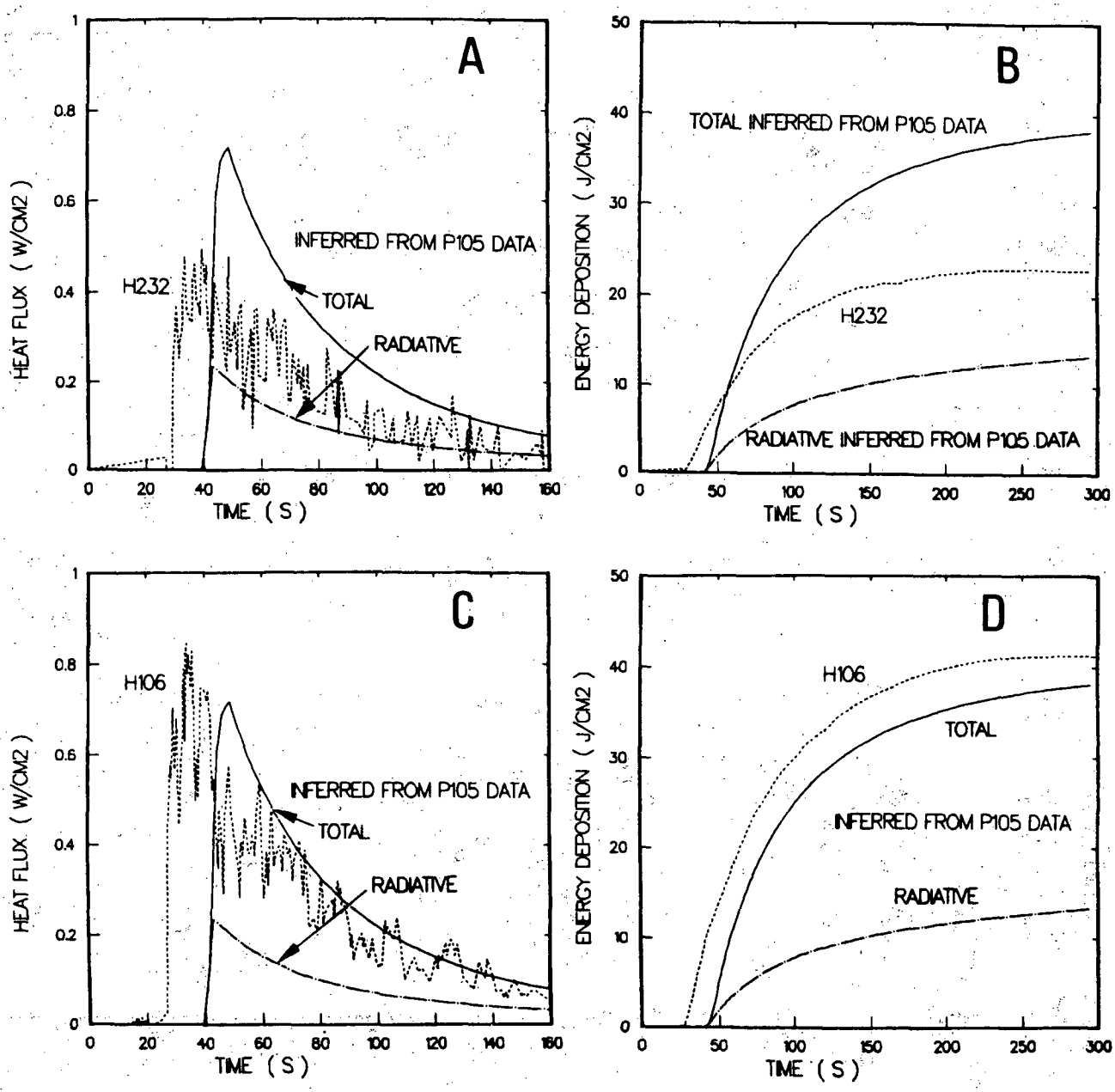

Figure C.16: Heat flux and energy deposition results for test NTSP07

A: Heat flux (thin-film gauge and inferred from pressure)
B: Energy deposition (thin-film gauge and inferred from pressure)
C: Heat flux (Gardon gauge and inferred from pressure)
D: Energy deposition (Gardon gauge and inferred from pressure)

NTSP03 – 5.8% H_2 / 16.8% H_2O / *Fans*

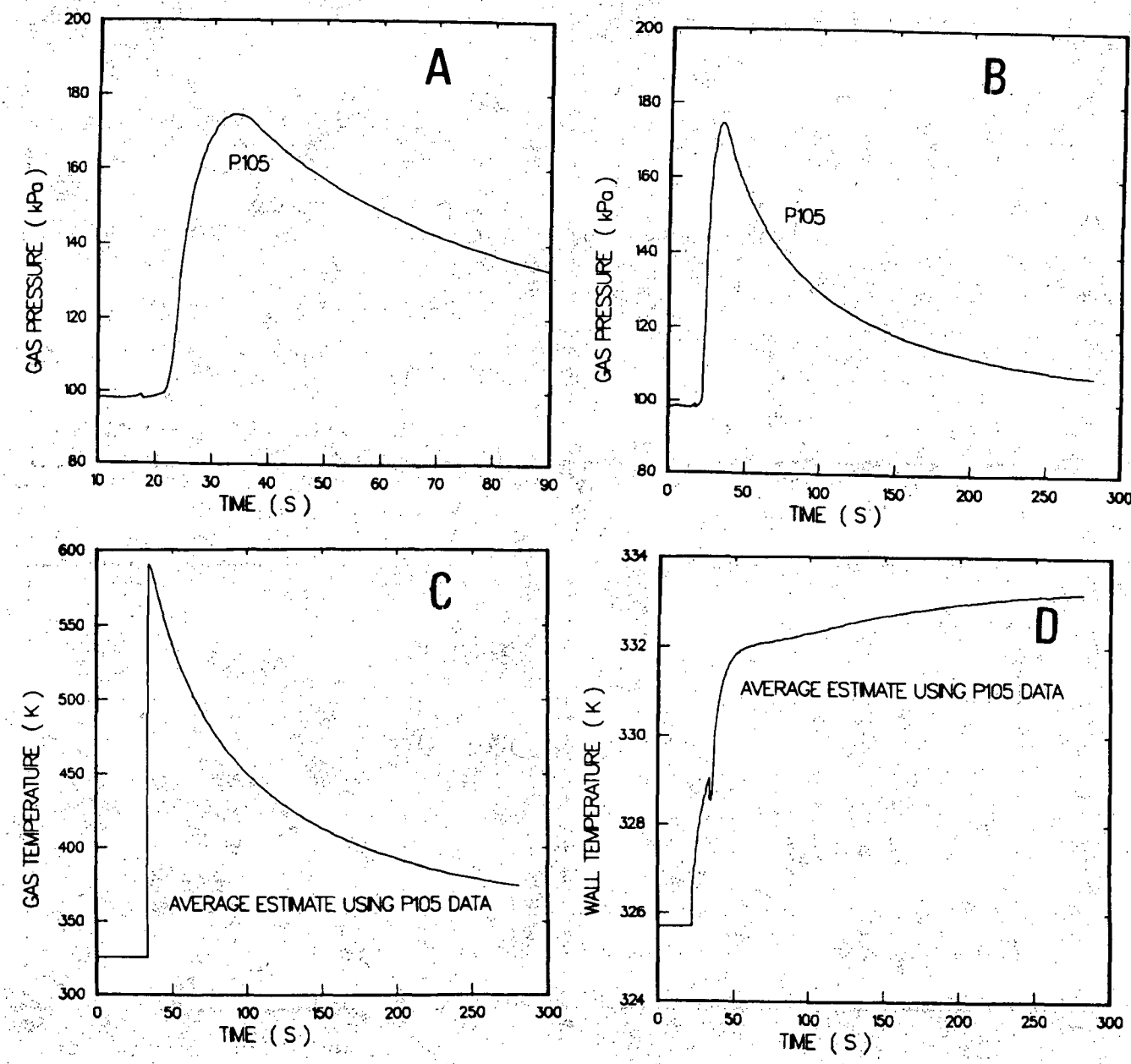

Figure C.17: Gas pressure and gas and wall temperatures for test NTSP03

A: Gas pressure during combustion
B: Gas pressure for entire test
C: Gas temperature inferred from pressure
D: Wall temperature inferred from pressure

NTSP03 – 5.8% H_2 / 16.8% H_2O / *Fans*

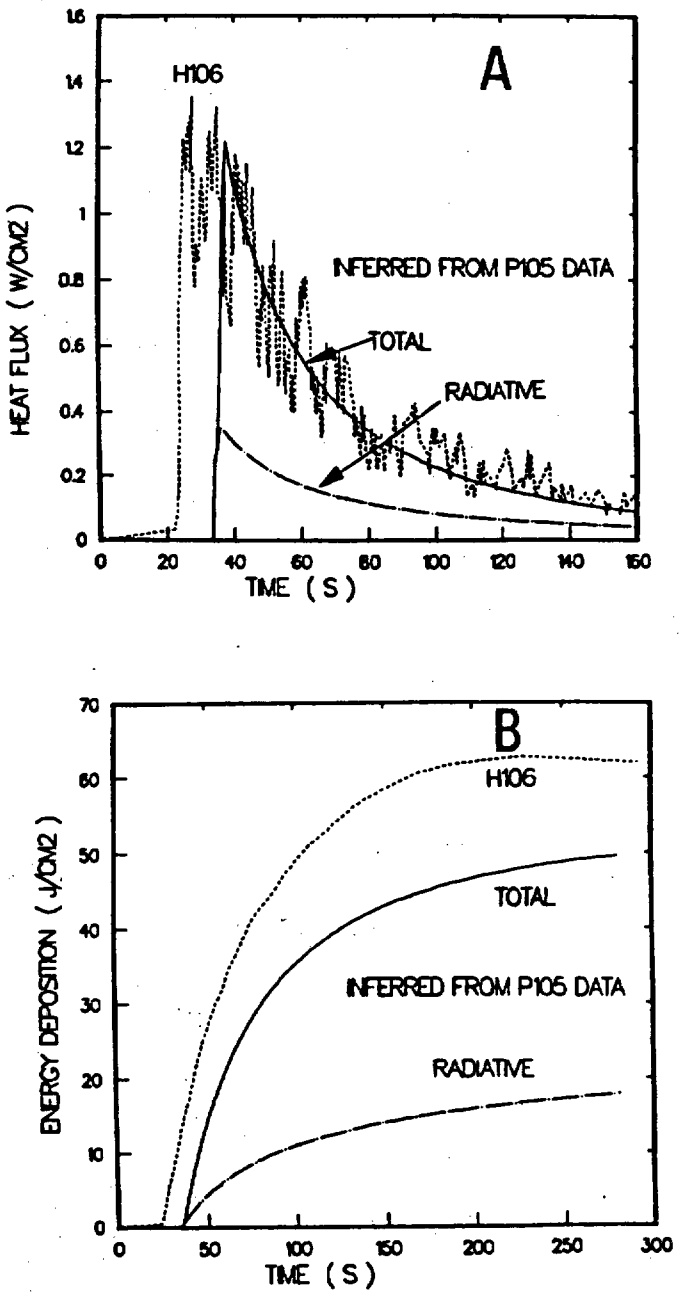

Figure C.18: Heat flux and energy deposition results for test NTSP03

A: Heat flux (Gardon gauge and inferred from pressure)

B: Energy deposition (Gardon gauge and inferred from pressure)

NTSP06 – 6.0% H_2 / 13.7% H_2O / *Fans*

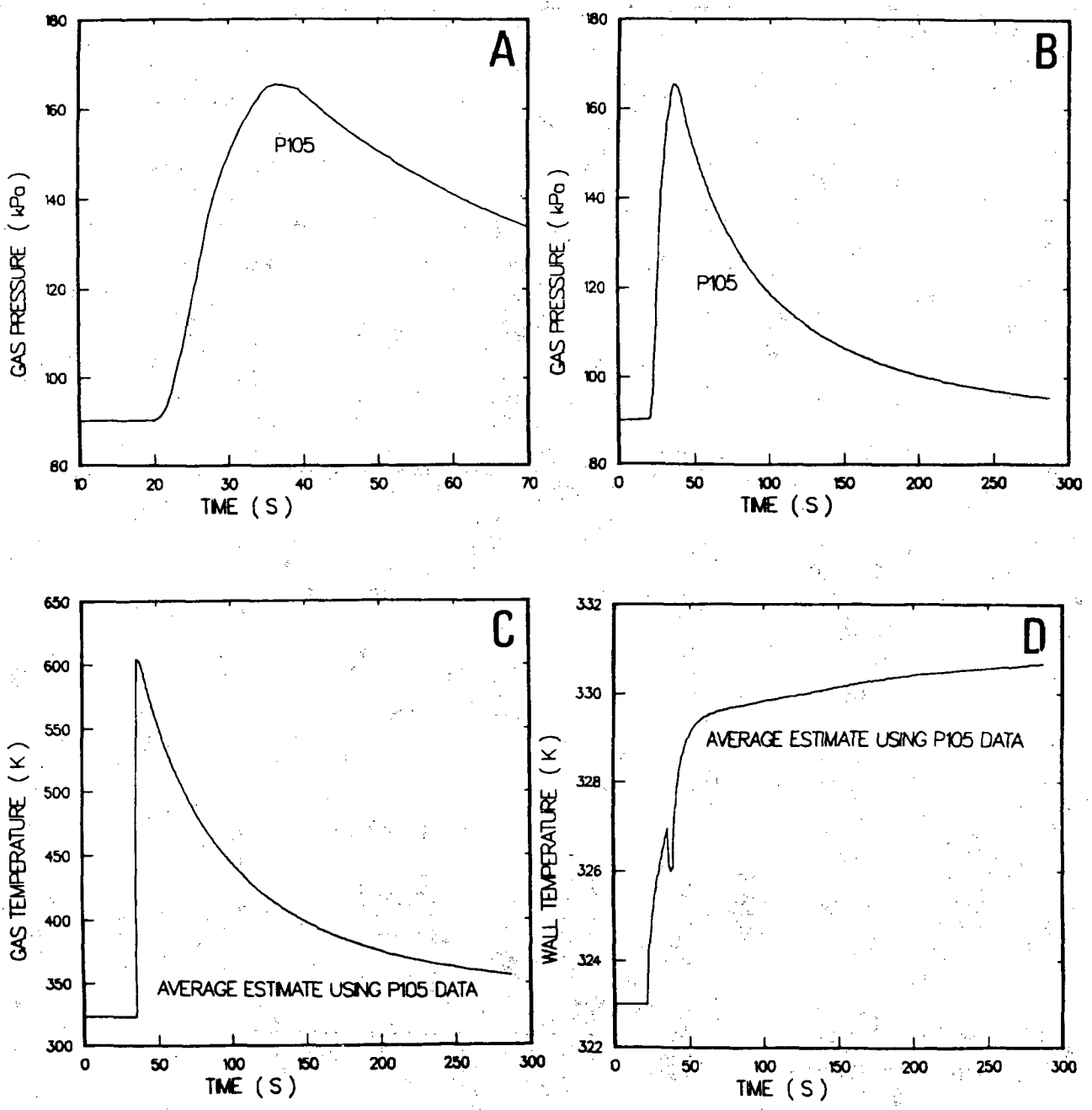

Figure C.19: Gas pressure and gas and wall temperatures for test NTSP06

A: Gas pressure during combustion
B: Gas pressure for entire test
C: Gas temperature inferred from pressure
D: Wall temperature inferred from pressure

NTSP06 – 6.0% H_2 / 13.7% H_2O / *Fans*

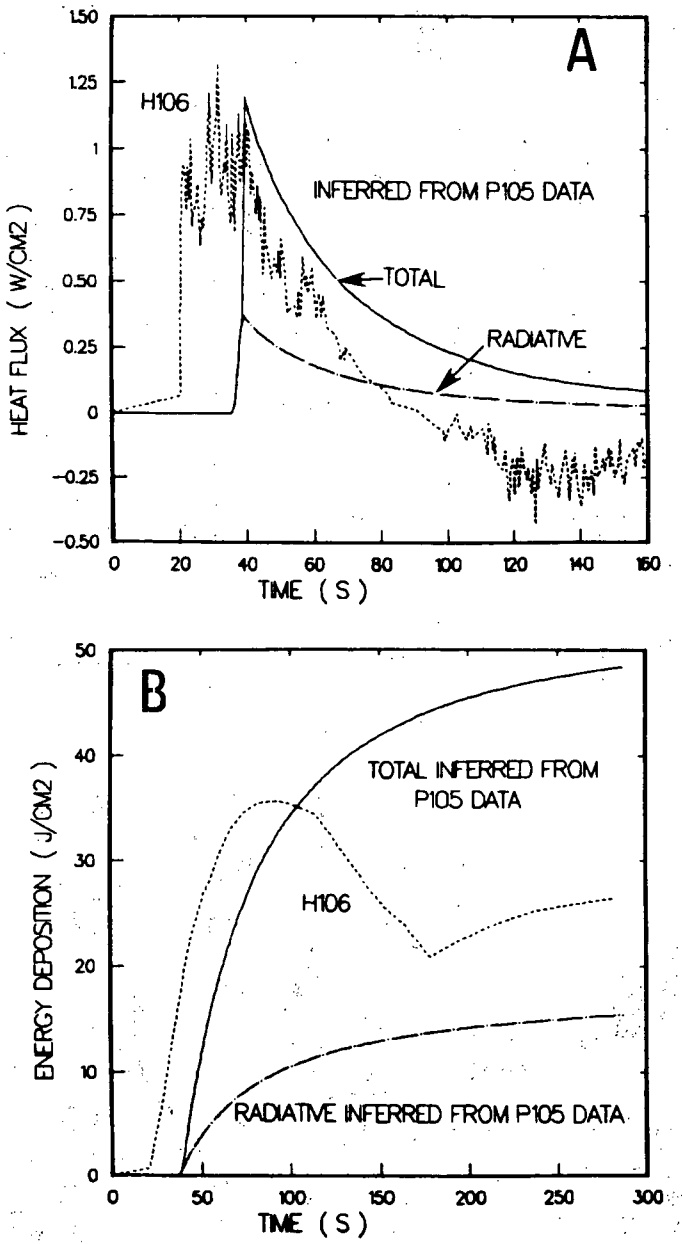

Figure C.20: Heat flux and energy deposition results for test NTSP06

A: Heat flux (Gardon gauge and inferred from pressure)

B: Energy deposition (Gardon gauge and inferred from pressure)

NTSP12 – 6.9% H_2 / 28.3% H_2O

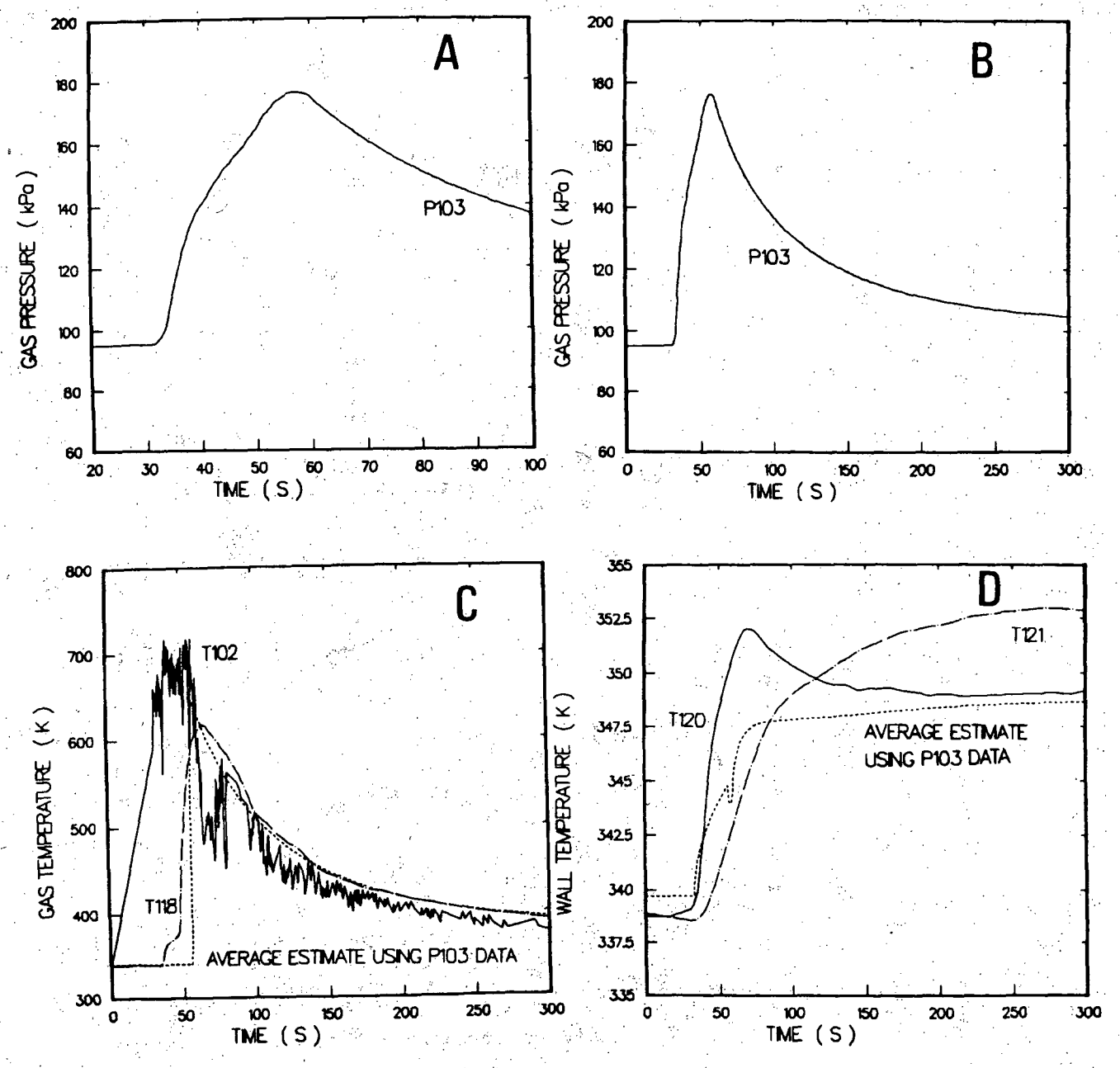

Figure C.21: Gas pressure and gas and wall temperatures for test NTSP12

A: Gas pressure during combustion
B: Gas pressure for entire test
C: Gas temperature (measured and inferred from pressure)
D: Wall temperature (measured and inferred from pressure)

NTSP12 – 6.9% H_2 / 28.3% H_2O

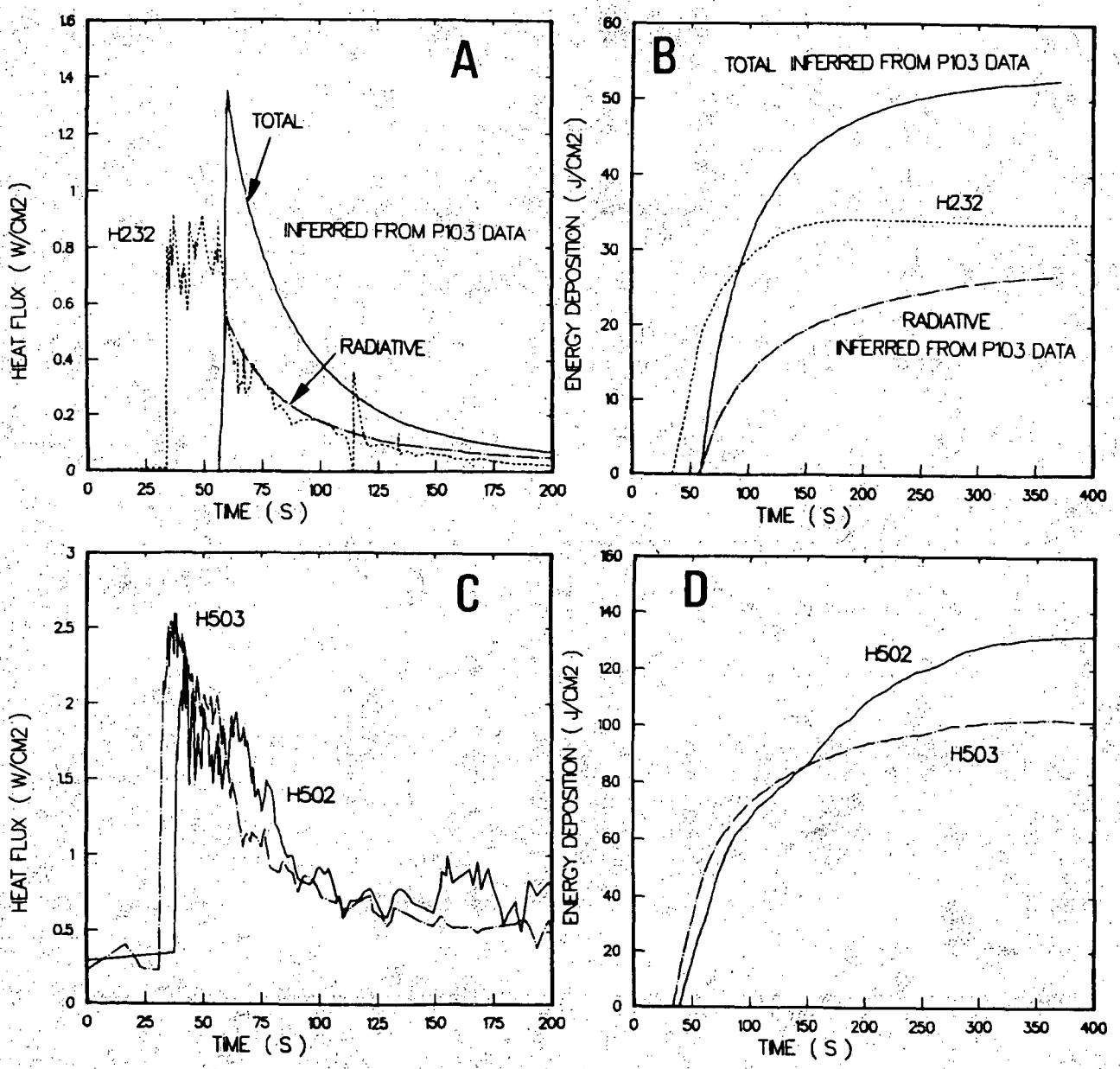

Figure C.22: Heat flux and energy deposition results for test NTSP12

A: Heat flux (thin-film gauge and inferred from pressure)
B: Energy deposition (thin-film gauge and inferred from pressure)
C: Heat flux (Schmidt-Boelter gauges)
D: Energy deposition (Schmidt-Boelter gauges)

NTSP14 – 8.1% H_2 / 38.7% H_2O

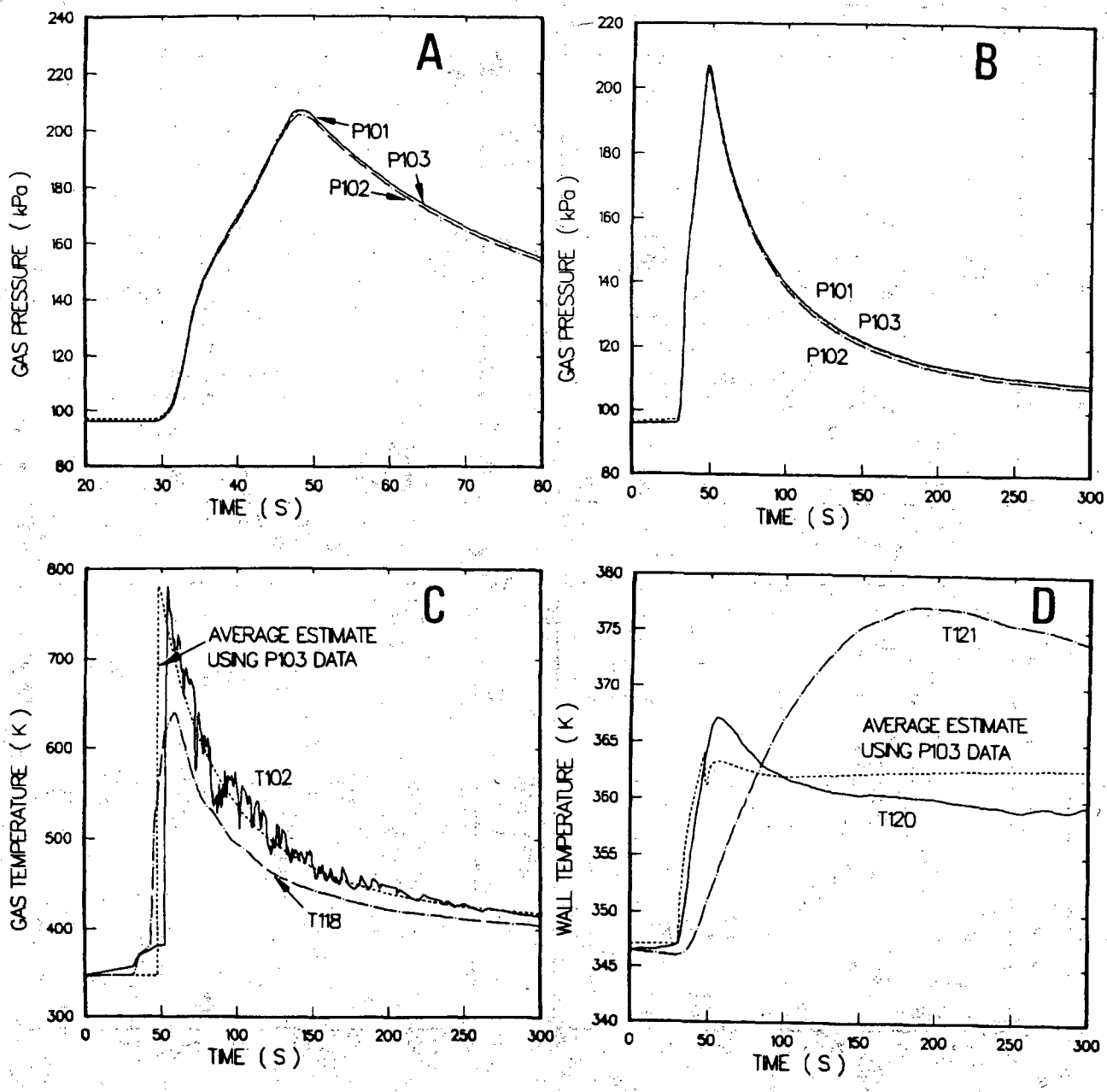

Figure C.23: Gas pressure and gas and wall temperatures for test NTSP14

A: Gas pressure during combustion
B: Gas pressure for entire test
C: Gas temperature (measured and inferred from pressure)
D: Wall temperature (measured and inferred from pressure)

NTSP14 – 8.1% H_2 / 38.7% H_2O

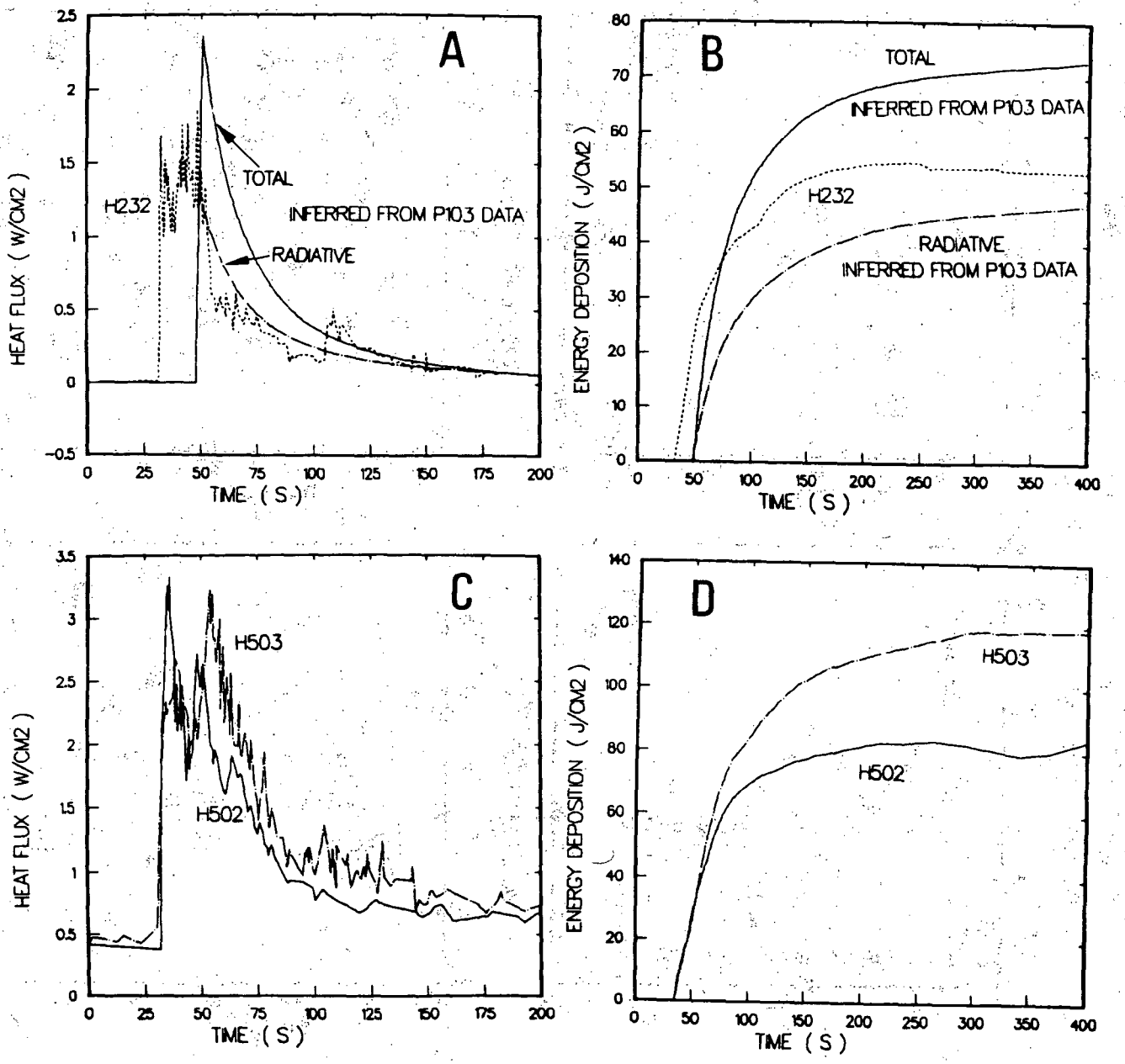

Figure C.24: Heat flux and energy deposition results for test NTSP14

A: Heat flux (thin-film gauge and inferred from pressure)
B: Energy deposition (thin-film gauge and inferred from pressure)
C: Heat flux (Schmidt-Boelter gauges)
D: Energy deposition (Schmidt-Boelter gauges)

NTSP05 – 7.8% H_2 / 31.3% H_2O

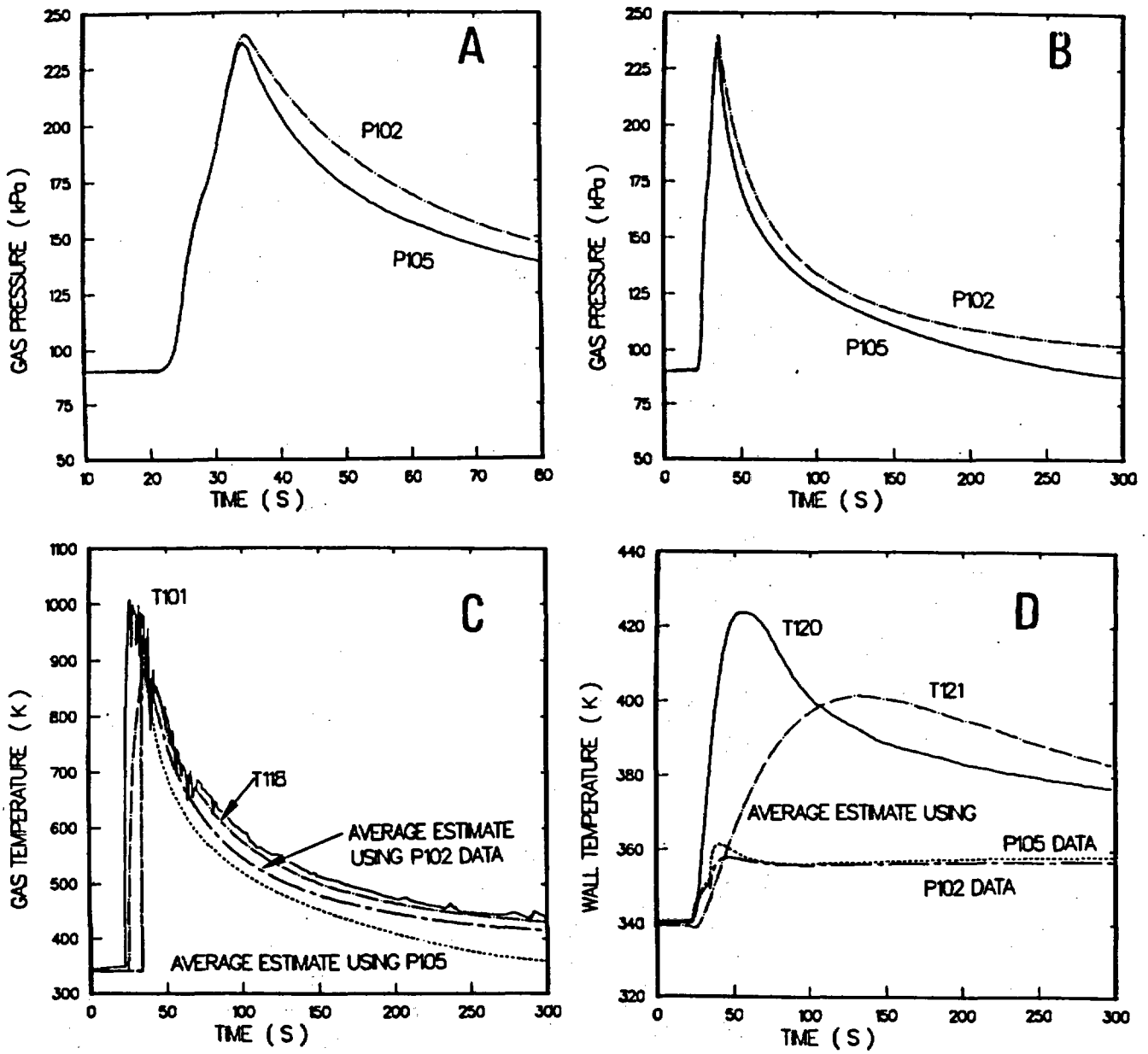

Figure C.25: Gas pressure and gas and wall temperatures for test NTSP05

A: Gas pressure during combustion

B: Gas pressure for entire test

C: Gas temperature (measured and inferred from pressure)

D: Wall temperature (measured and inferred from pressure)

NTSP05 – 7.8% H_2 / 31.3% H_2O

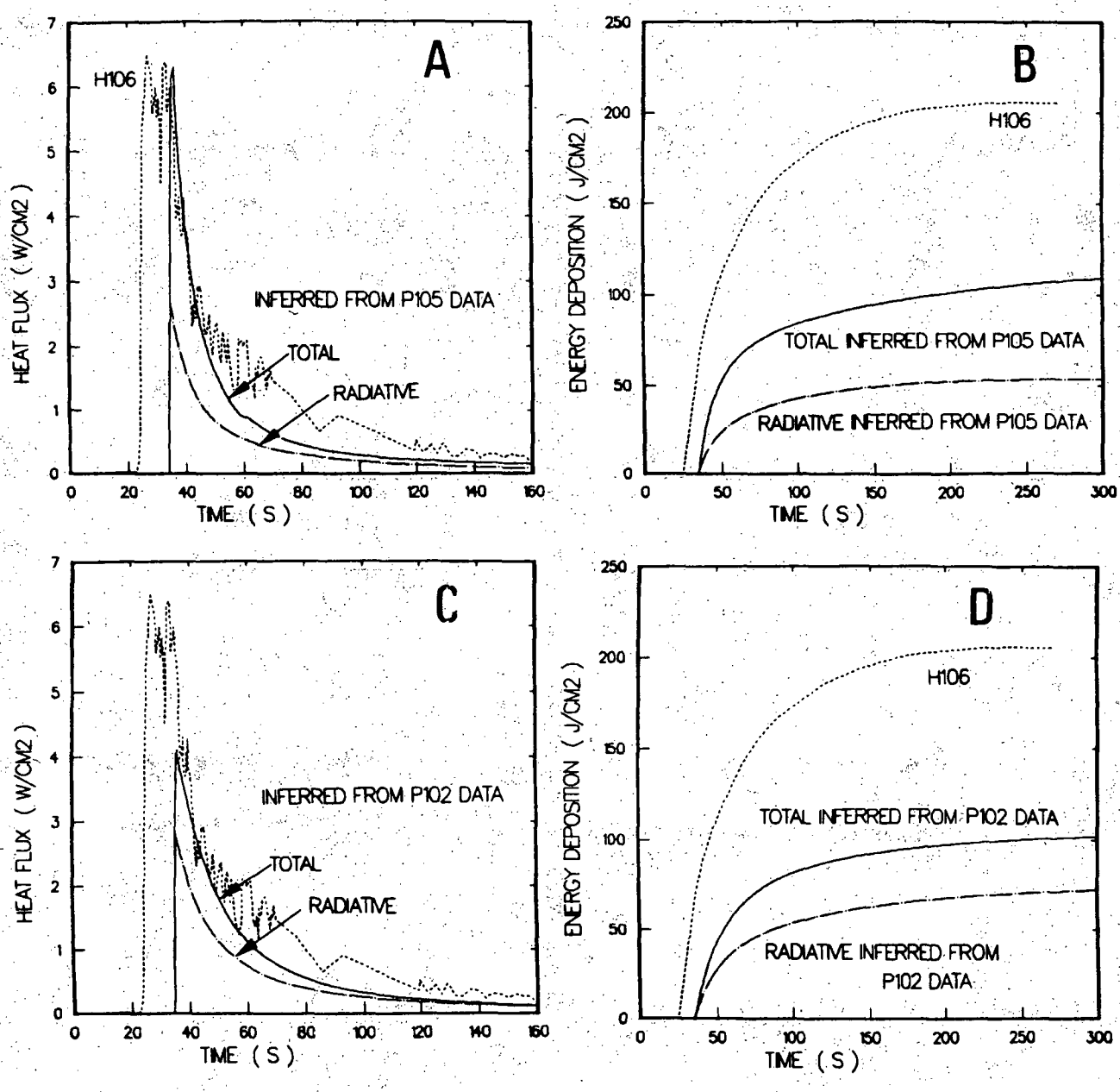

Figure C.26: Heat flux and energy deposition results for test NTSP05

A: Heat flux (Gardon gauge and inferred from P105)
B: Energy deposition (Gardon gauge and inferred from P105)
C: Heat flux (Gardon gauge and inferred from P102)
D: Energy deposition (Gardon gauge and inferred from P102)

NTSP16 – 10.1% H_2 / 29.5% H_2O

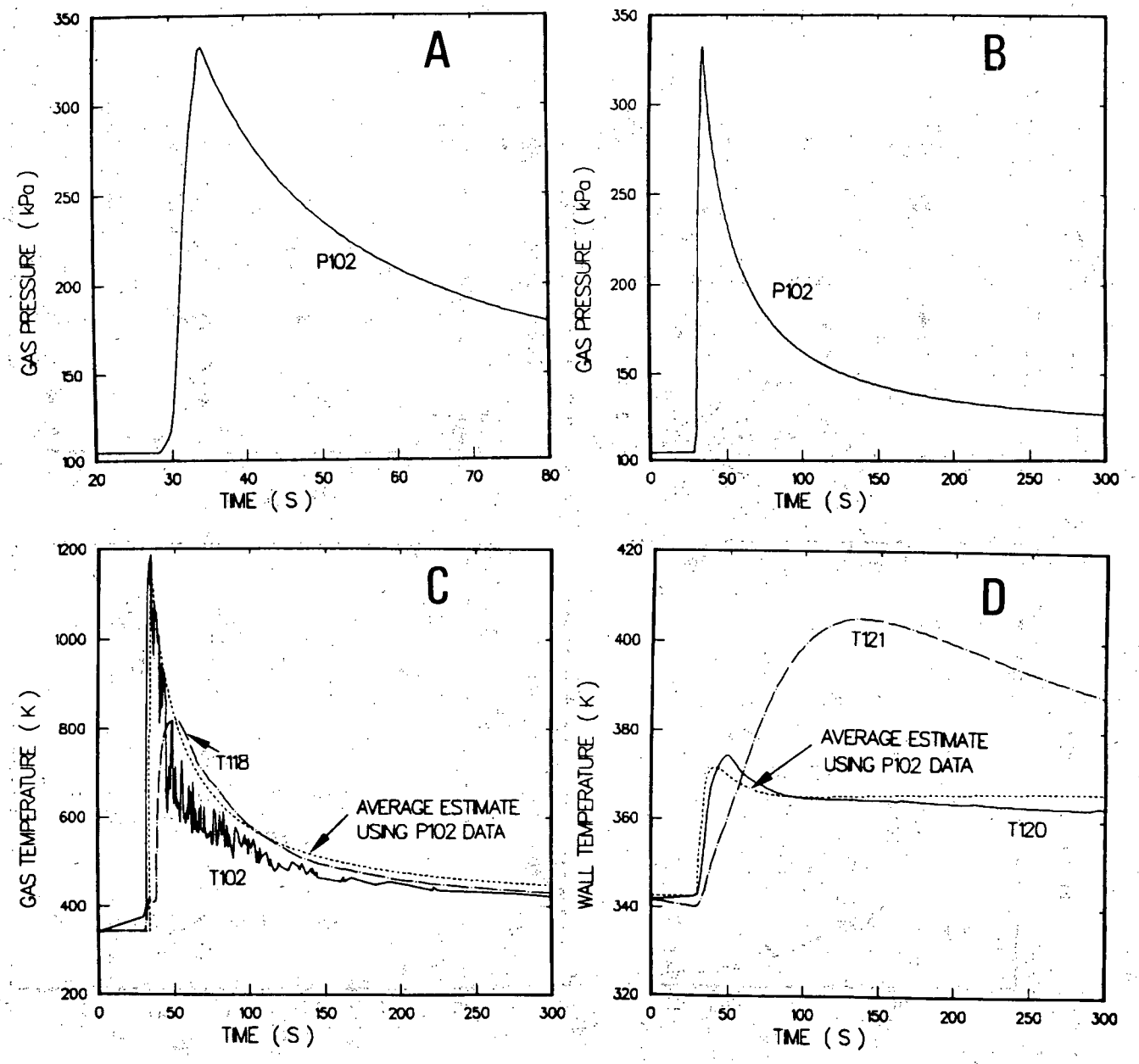

Figure C.27: Gas pressure and gas and wall temperatures for test NTSP16

A: Gas pressure during combustion
B: Gas pressure for entire test
C: Gas temperature (measured and inferred from pressure)
D: Wall temperature (measured and inferred from pressure)

NTSP16 – 10.1% H_2 / 29.5% H_2O

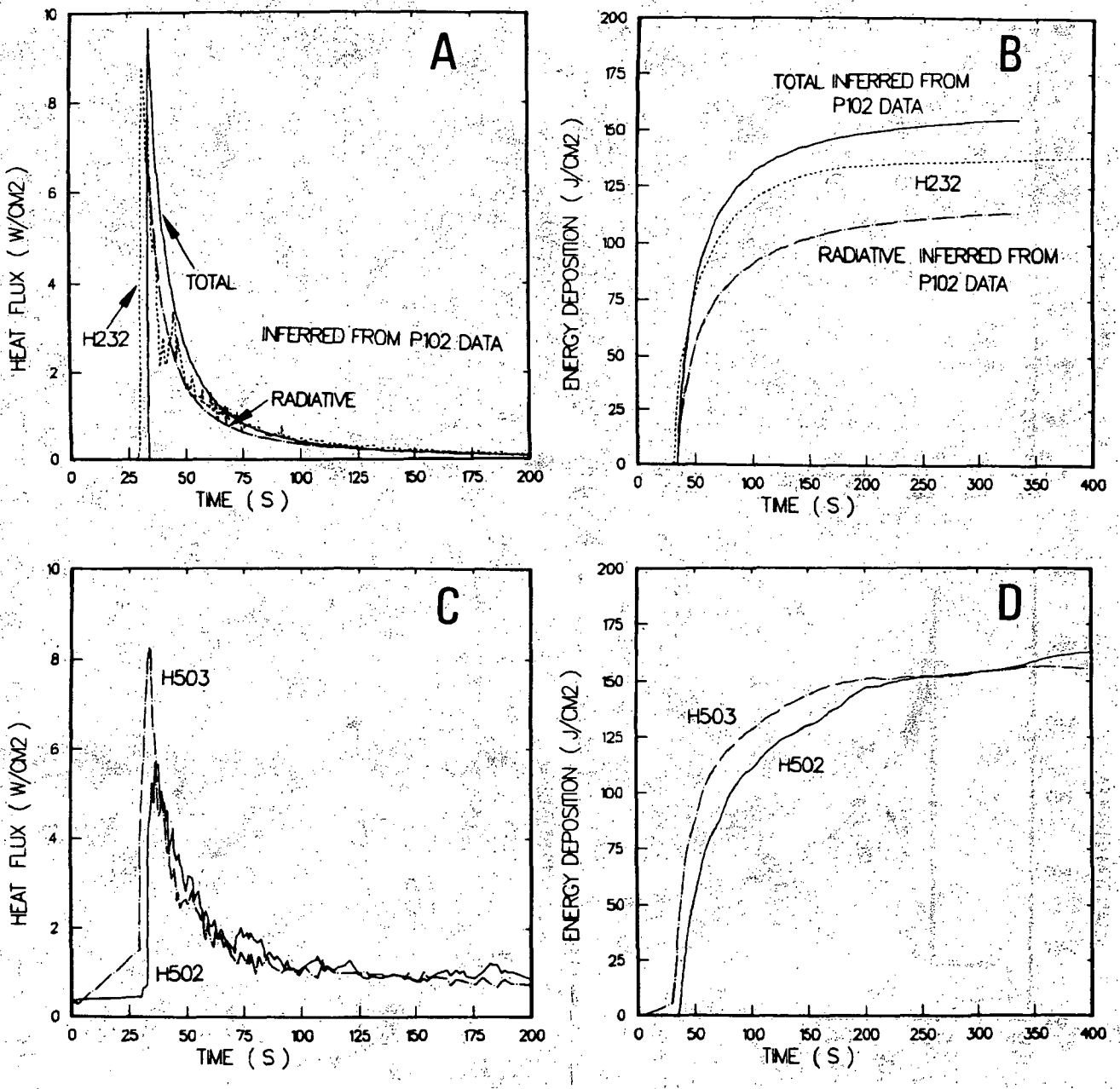

Figure C.28: Heat flux and energy deposition results for test NTSP16

A: Heat flux (thin-film gauge and inferred from pressure)

B: Energy deposition (thin-film gauge and inferred from pressure)

C: Heat flux (Schmidt-Boelter gauges)

D: Energy deposition (Schmidt-Boelter gauges)

NTSP08 – 11.1% H_2 / 27.2% H_2O / *Fans*

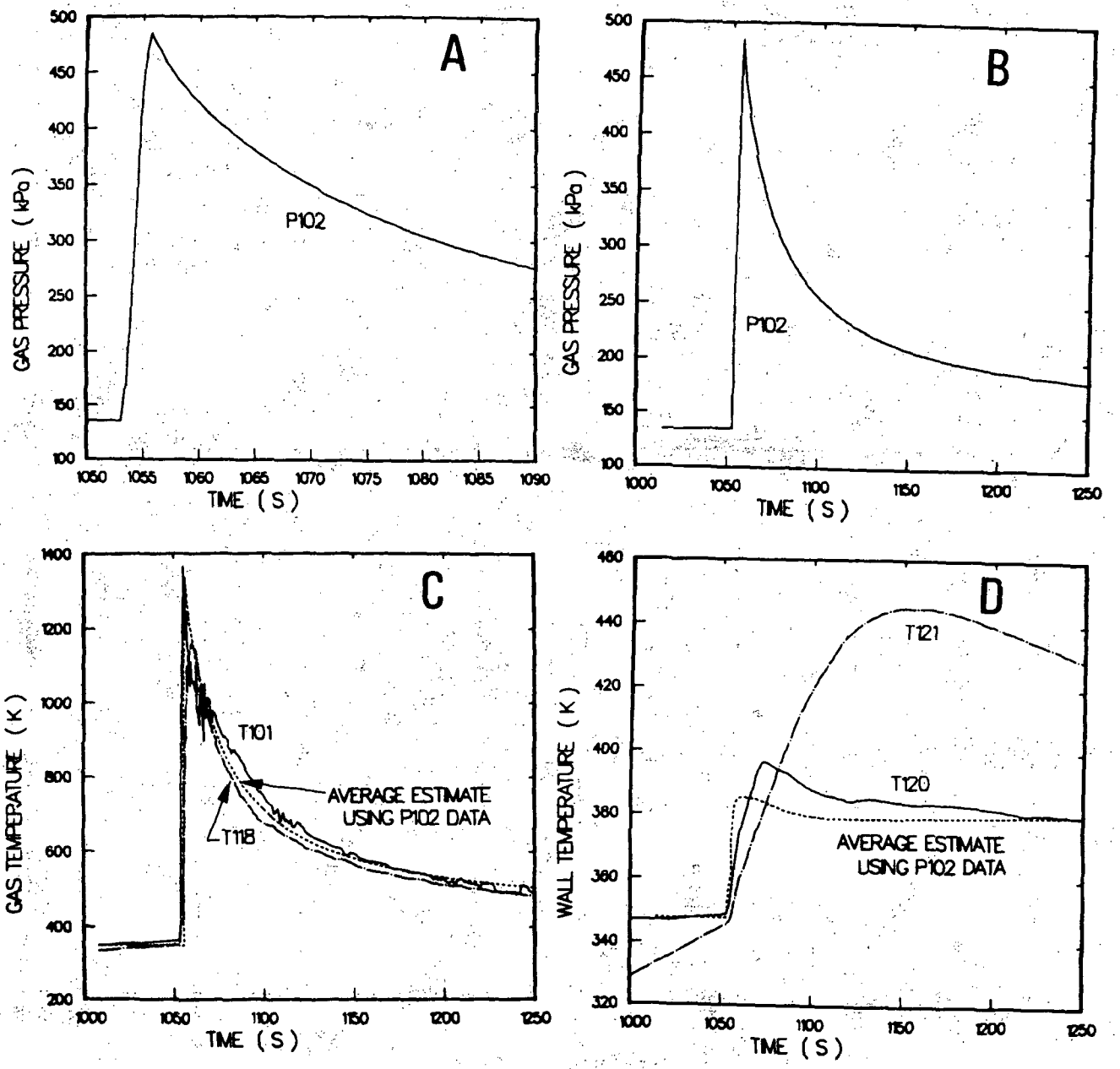

Figure C.29: Gas pressure and gas and wall temperatures for test NTSP08

A: Gas pressure during combustion

B: Gas pressure for entire test

C: Gas temperature (measured and inferred from pressure)

D: Wall temperature (measured and inferred from pressure)

NTSP08 – 11.1% H_2 / 27.2% H_2O / *Fans*

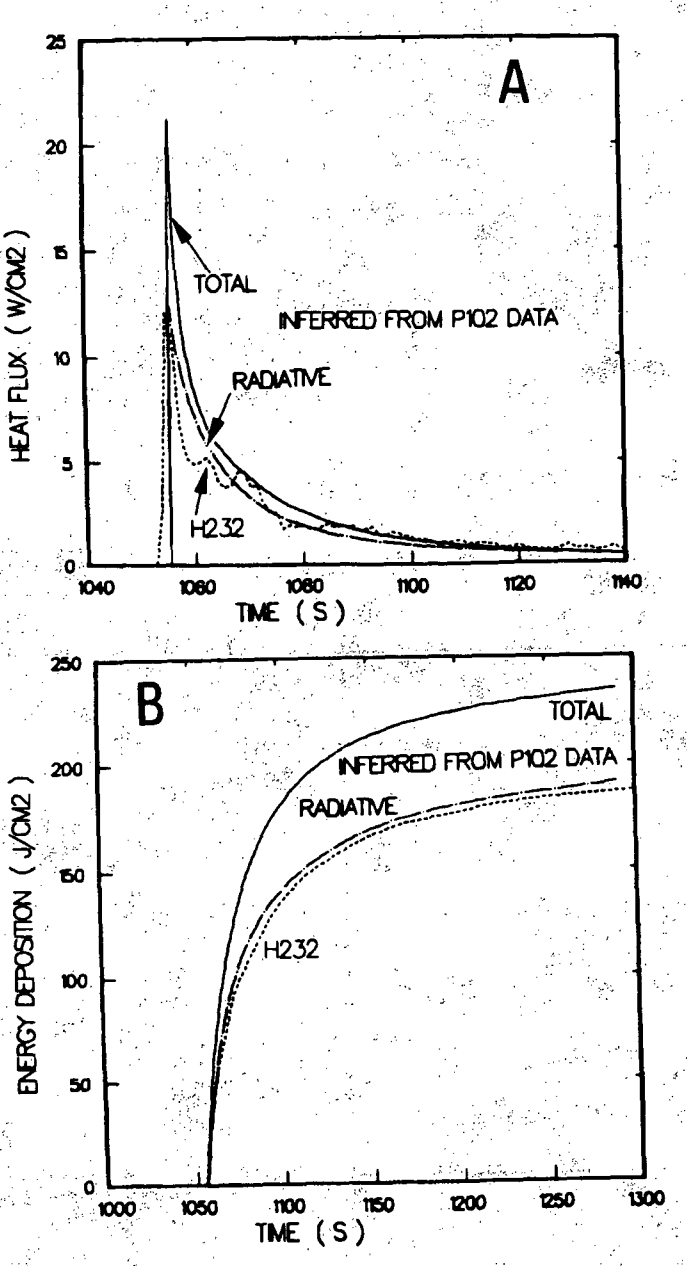

Figure C.30: Heat flux and energy deposition results for test NTSP08

A: Heat flux (thin-film gauge and inferred from pressure)

B: Energy deposition (thin-film gauge and inferred from pressure)

NTSP20 – 12.9% H_2 / 27.8% H_2O

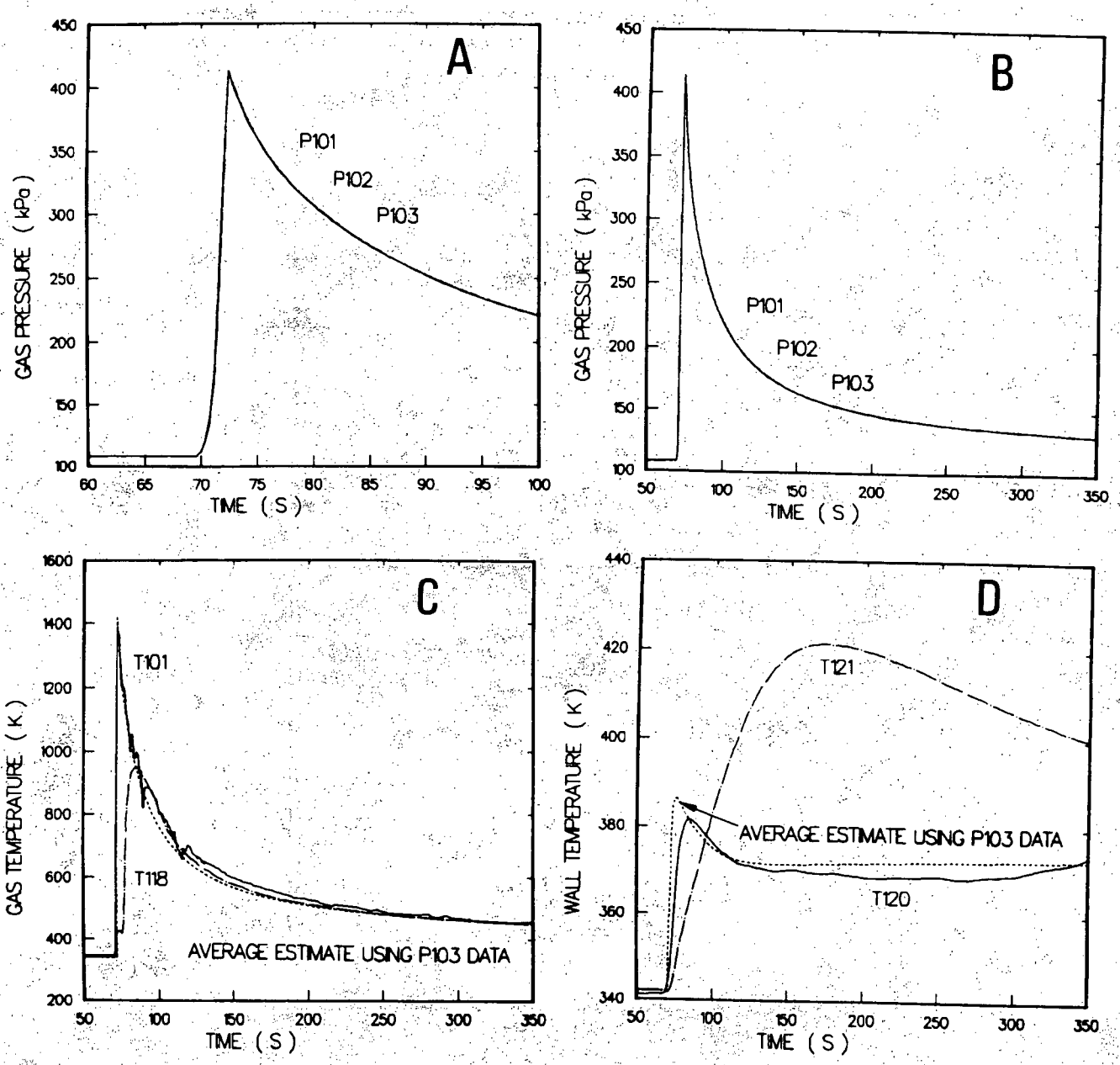

Figure C.31: Gas pressure and gas and wall temperatures for test NTSP20

A: Gas pressure during combustion

B: Gas pressure for entire test

C: Gas temperature (measured and inferred from pressure)

D: Wall temperature (measured and inferred from pressure)

NTSP20 – 12.9% H_2 / 27.8% H_2O

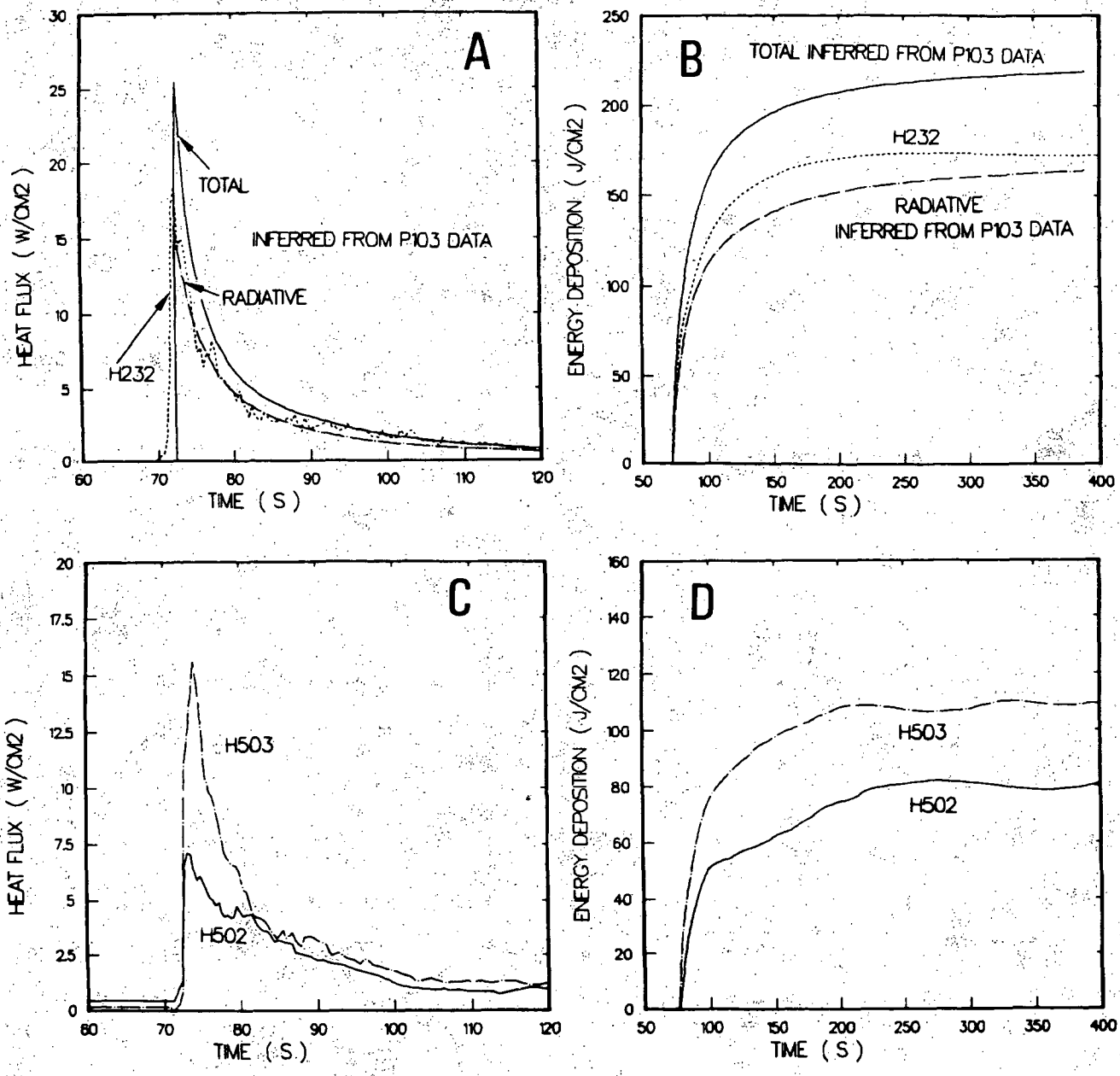

Figure C.32: Heat flux and energy deposition results for test NTSP20

A: Heat flux (thin-film gauge and inferred from pressure)

B: Energy deposition (thin-film gauge and inferred from pressure)

C: Heat flux (Schmidt-Boelter gauges)

D: Energy deposition (Schmidt-Boelter gauges)

NTSP22 – 5.2% H_2 / 14.5% H_2O / *Sprays*

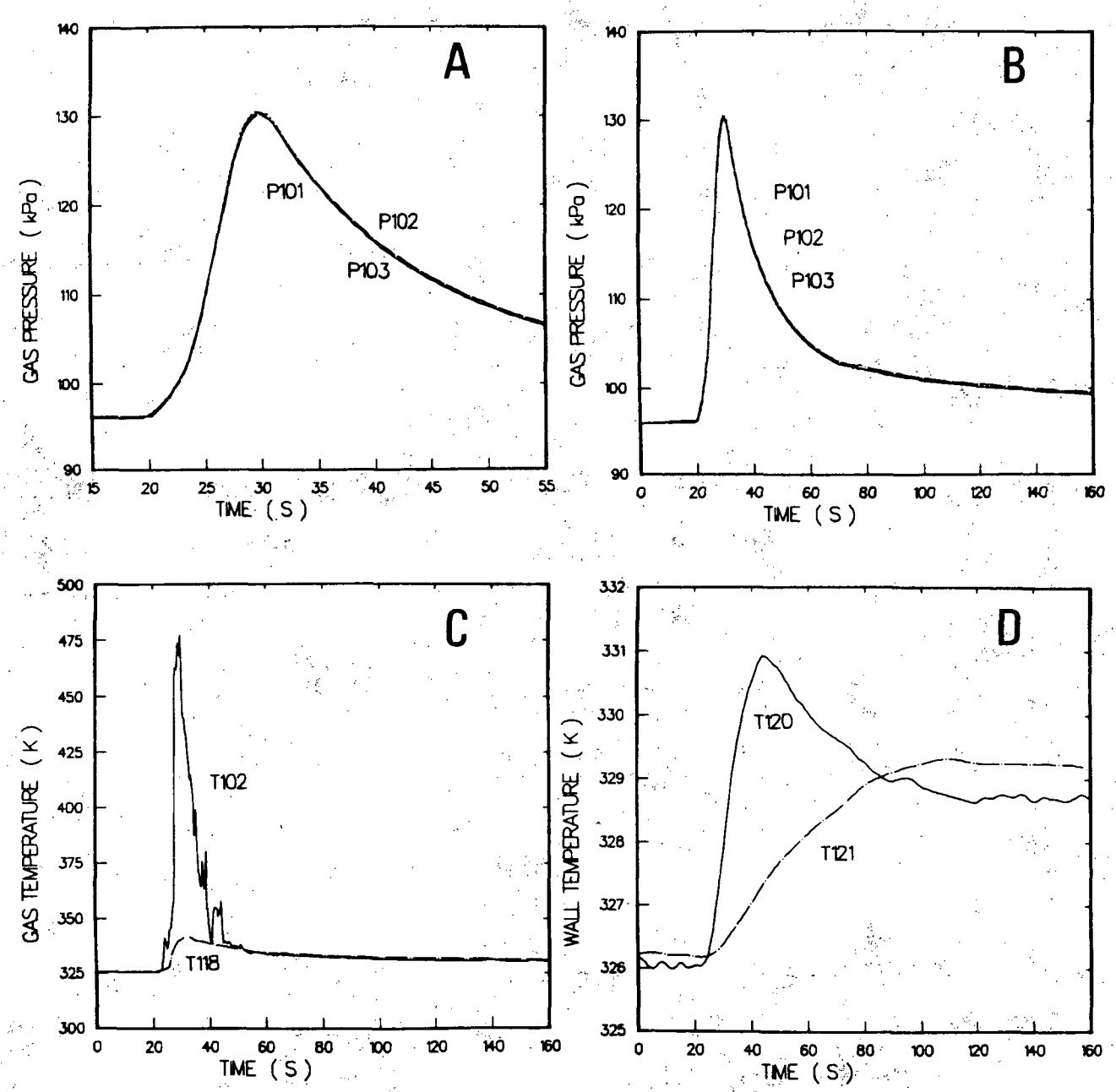

Figure C.33: Gas pressure and gas and wall temperatures for test NTSP22

A: Gas pressure during combustion
B: Gas pressure for entire test
C: Gas temperature
D: Wall temperature

NTSP22 – 5.2% H_2 / 14.5% H_2O / *Sprays*

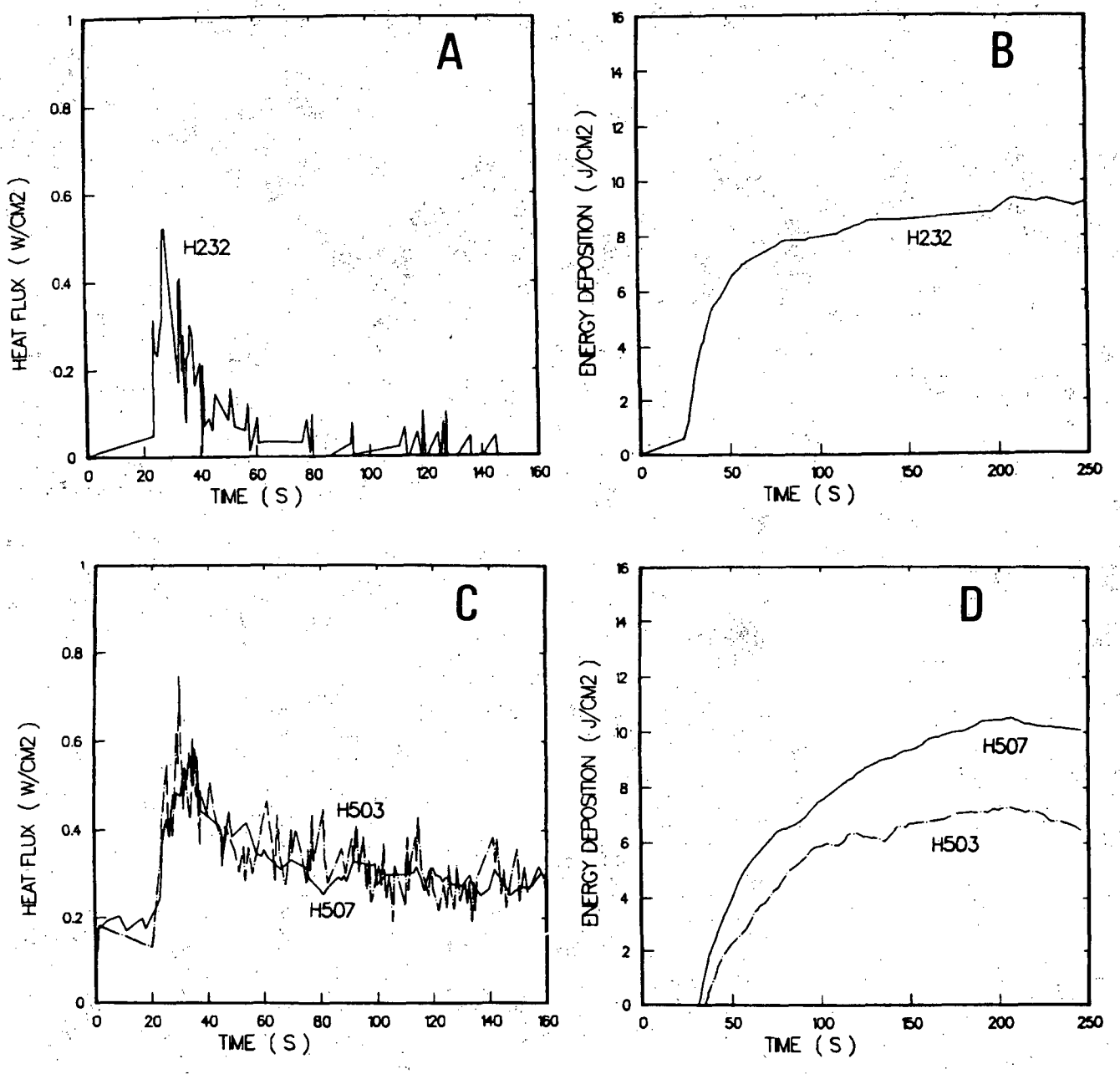

Figure C.34: Heat flux and energy deposition results for test NTSP22

A: Heat flux (thin-film gauge)
B: Energy deposition (thin-film gauge)
C: Heat flux (Schmidt-Boelter gauges)
D: Energy deposition (Schmidt-Boelter gauges)

NTSP11 – 5.8% H_2 / 4.9% H_2O / *Sprays*

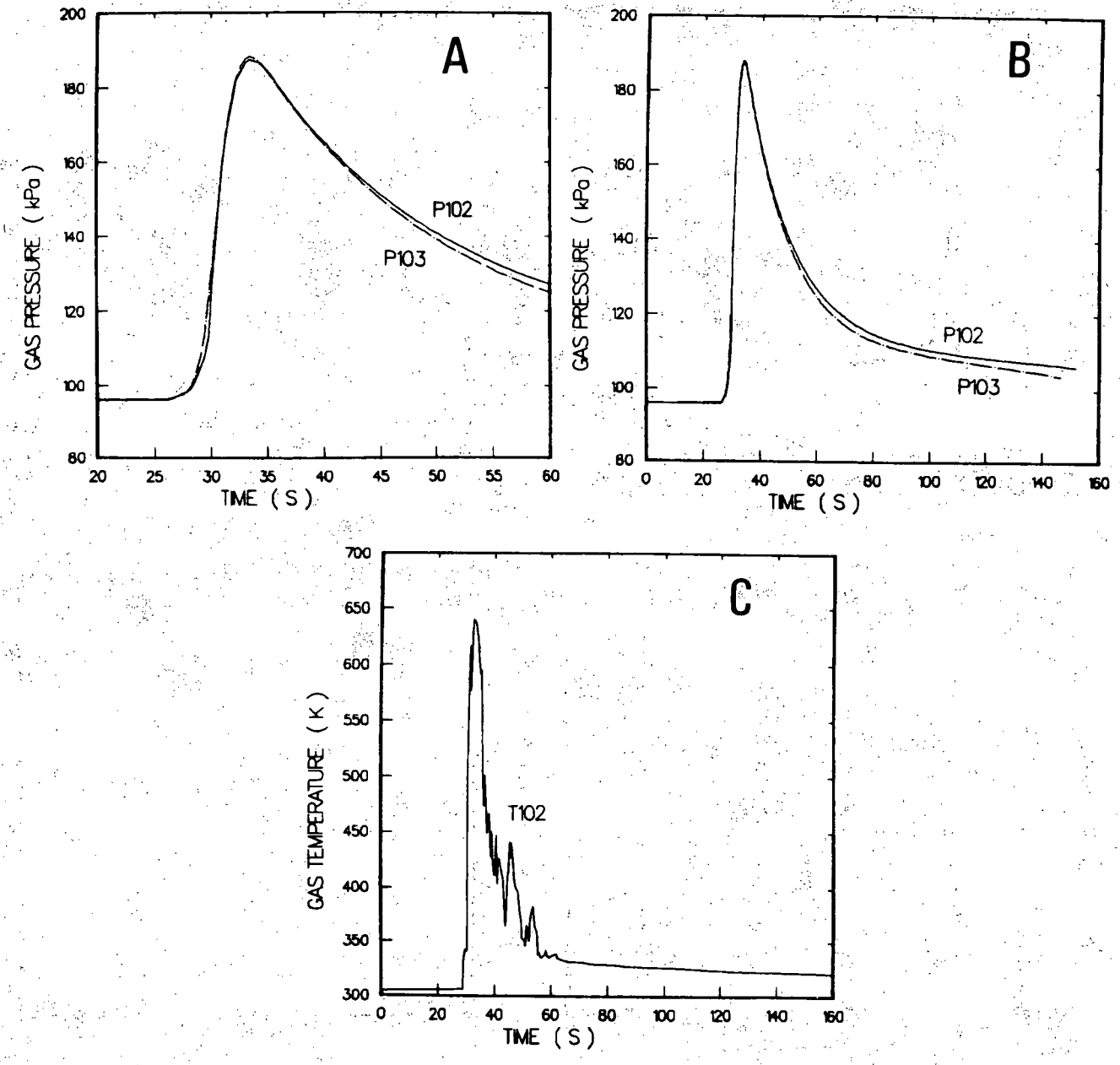

Figure C.35: Gas pressure and gas and wall temperatures for test NTSP11

A: Gas pressure during combustion
B: Gas pressure for entire test
C: Gas temperature

NTSP11 – 5.8% H_2 / 4.9% H_2O / *Sprays*

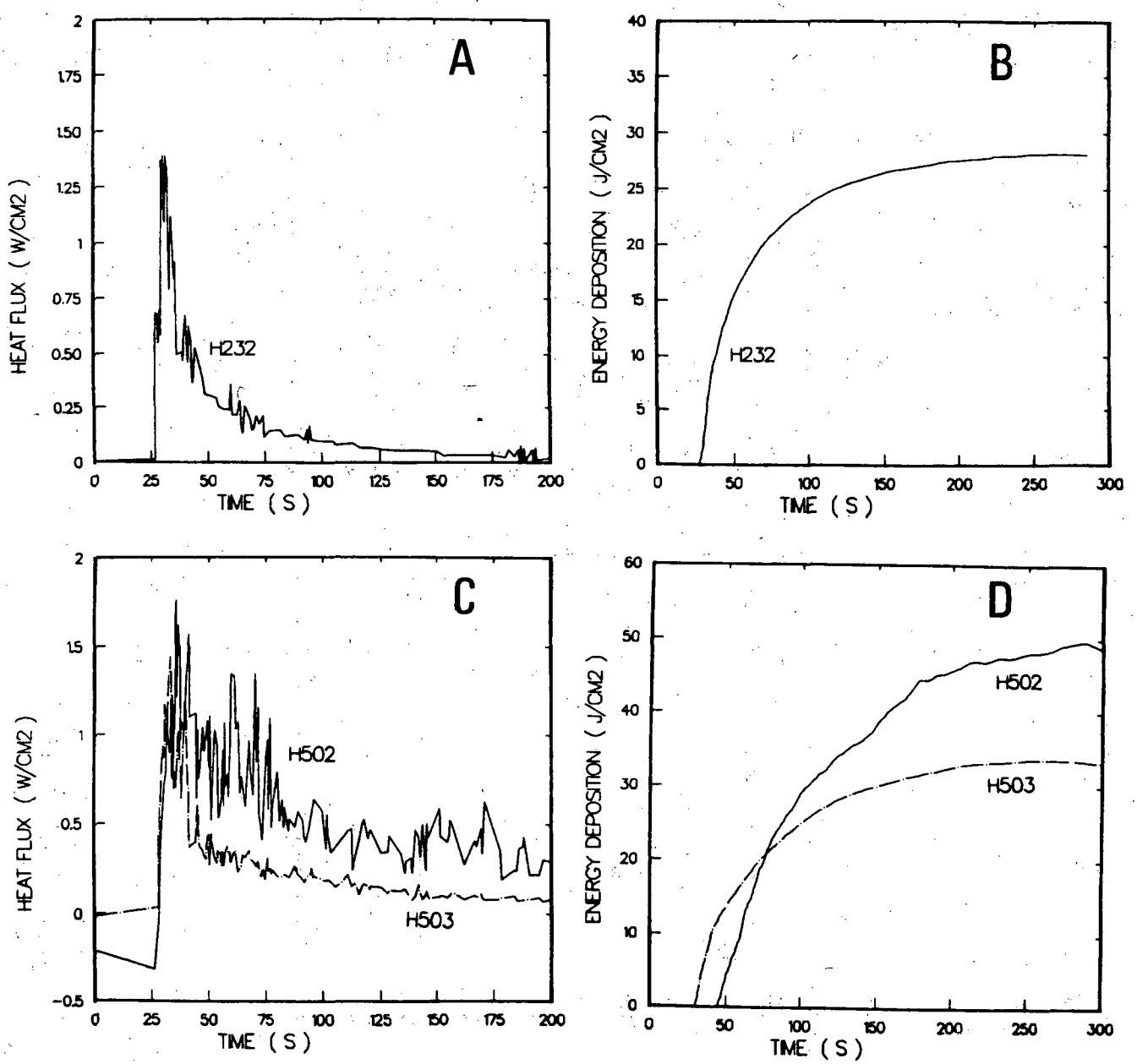

Figure C.36: Heat flux and energy deposition results for test NTSP11

A: Heat flux (thin-film gauge)
B: Energy deposition (thin-film gauge)
C: Heat flux (Schmidt-Boelter gauges)
D: Energy deposition (Schmidt-Boelter gauges)

NTSP02 – 5.8% H_2 / 16.8% H_2O / *Sprays*

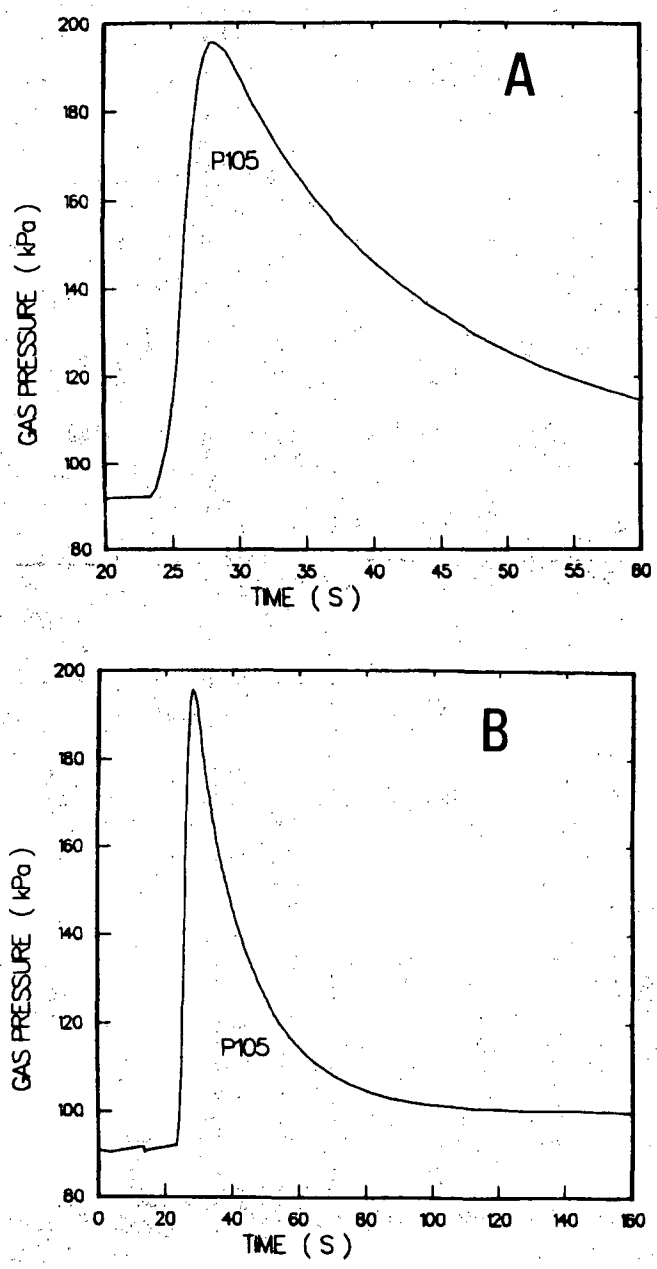

Figure C.37: Gas pressure and gas and wall temperatures for test NTSP02

A: Gas pressure during combustion

B: Gas pressure for entire test

NTSP02 – 5.8% H_2 / 16.8% H_2O / *Sprays*

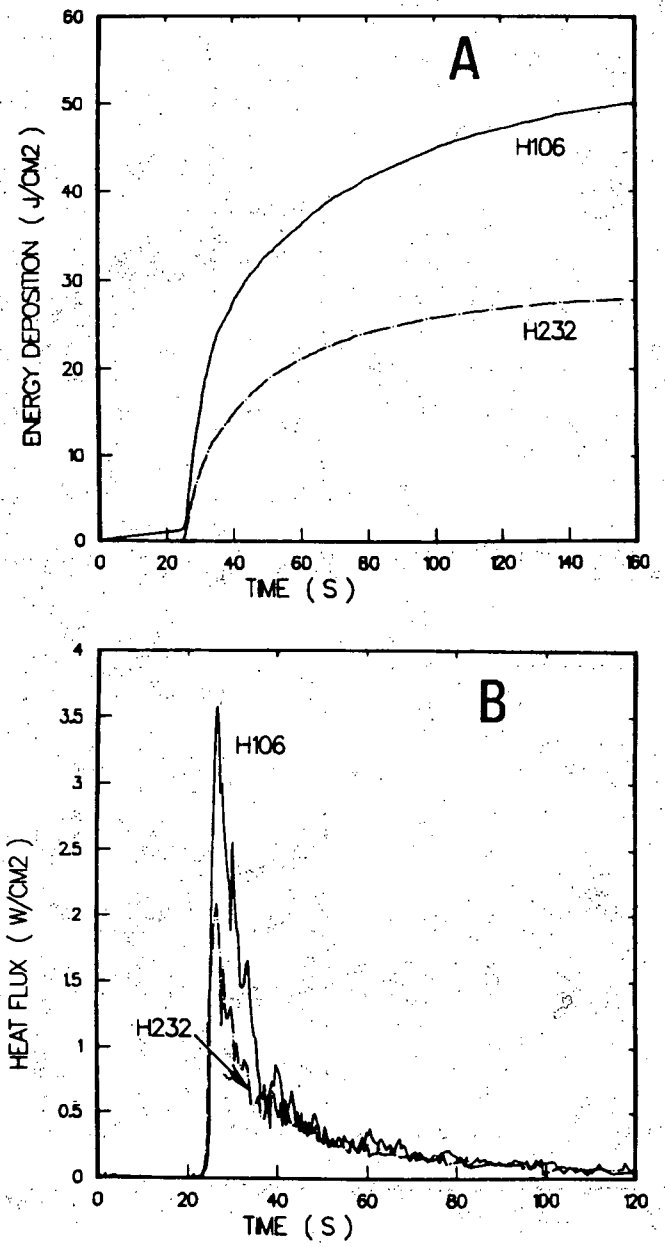

Figure C.38: Heat flux and energy deposition results for test NTSP02

A: Heat flux (thin-film and Gardon gauge)

B: Energy deposition (thin-film and Gardon gauge)

NTSP18 – 6.6% H_2 / 27.3% H_2O / *Sprays*

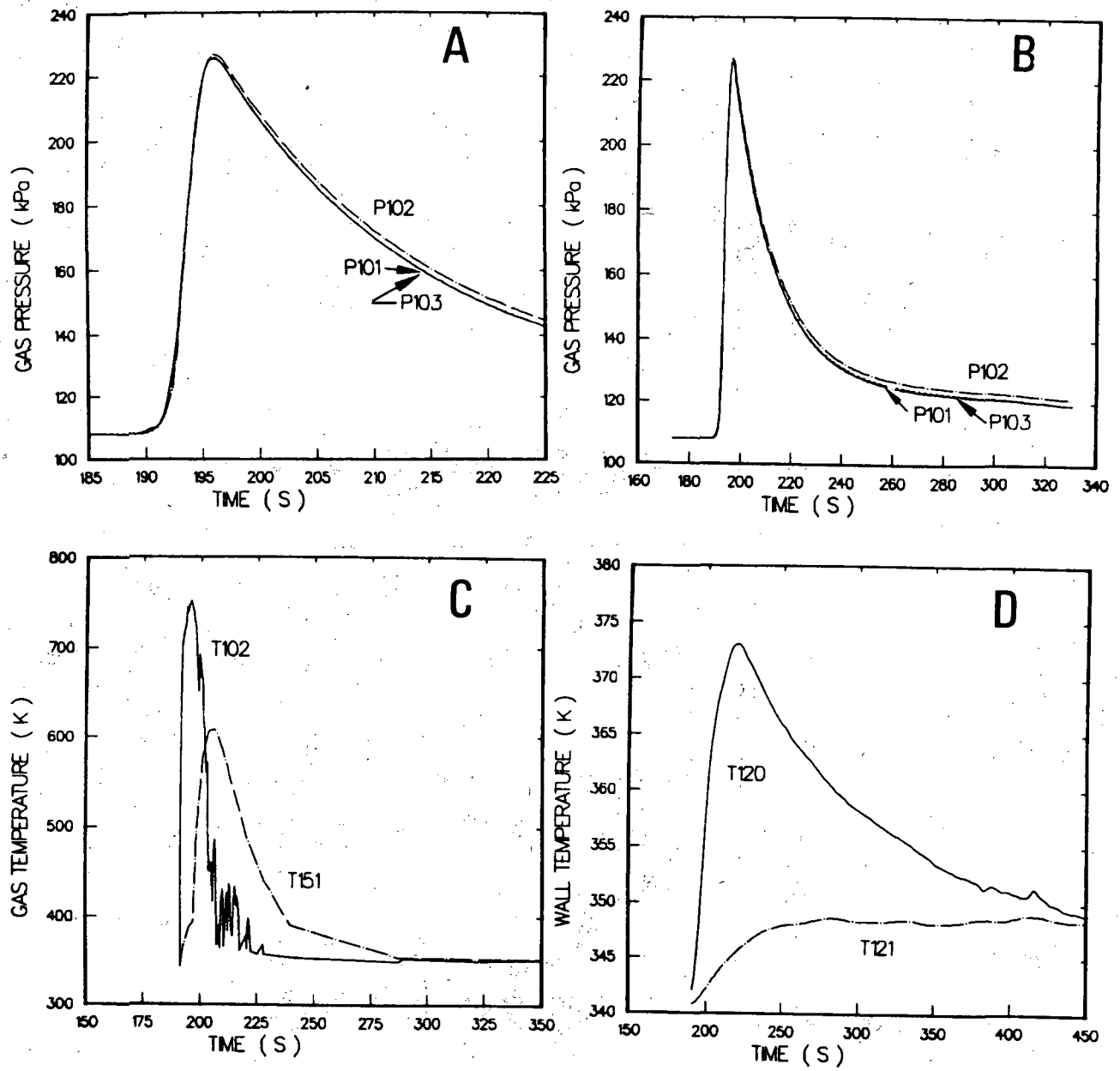

Figure C.39: Gas pressure and gas and wall temperatures for test NTSP18

A: Gas pressure during combustion
B: Gas pressure for entire test
C: Gas temperature
D: Wall temperature

NTSP18 – 6.6% H_2 / 27.3% H_2O / *Sprays*

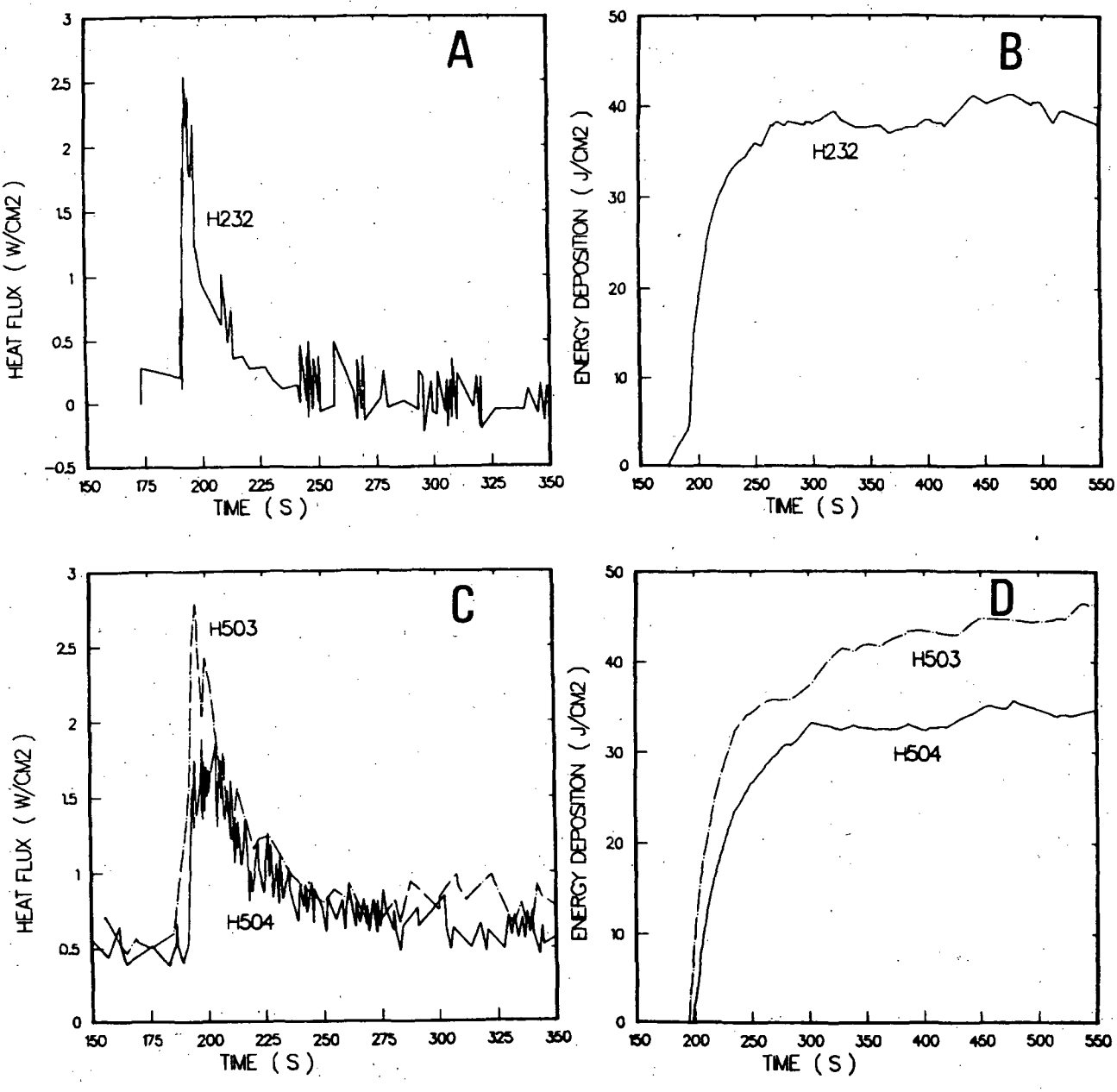

Figure C.40: Heat flux and energy deposition results for test NTSP18

A: Heat flux (thin-film gauge)
B: Energy deposition (thin-film gauge)
C: Heat flux (Schmidt-Boelter gauges)
D: Energy deposition (Schmidt-Boelter gauges)

NTSP21 – 13.2% H_2 / 27.4% H_2O / *Sprays & Fans*

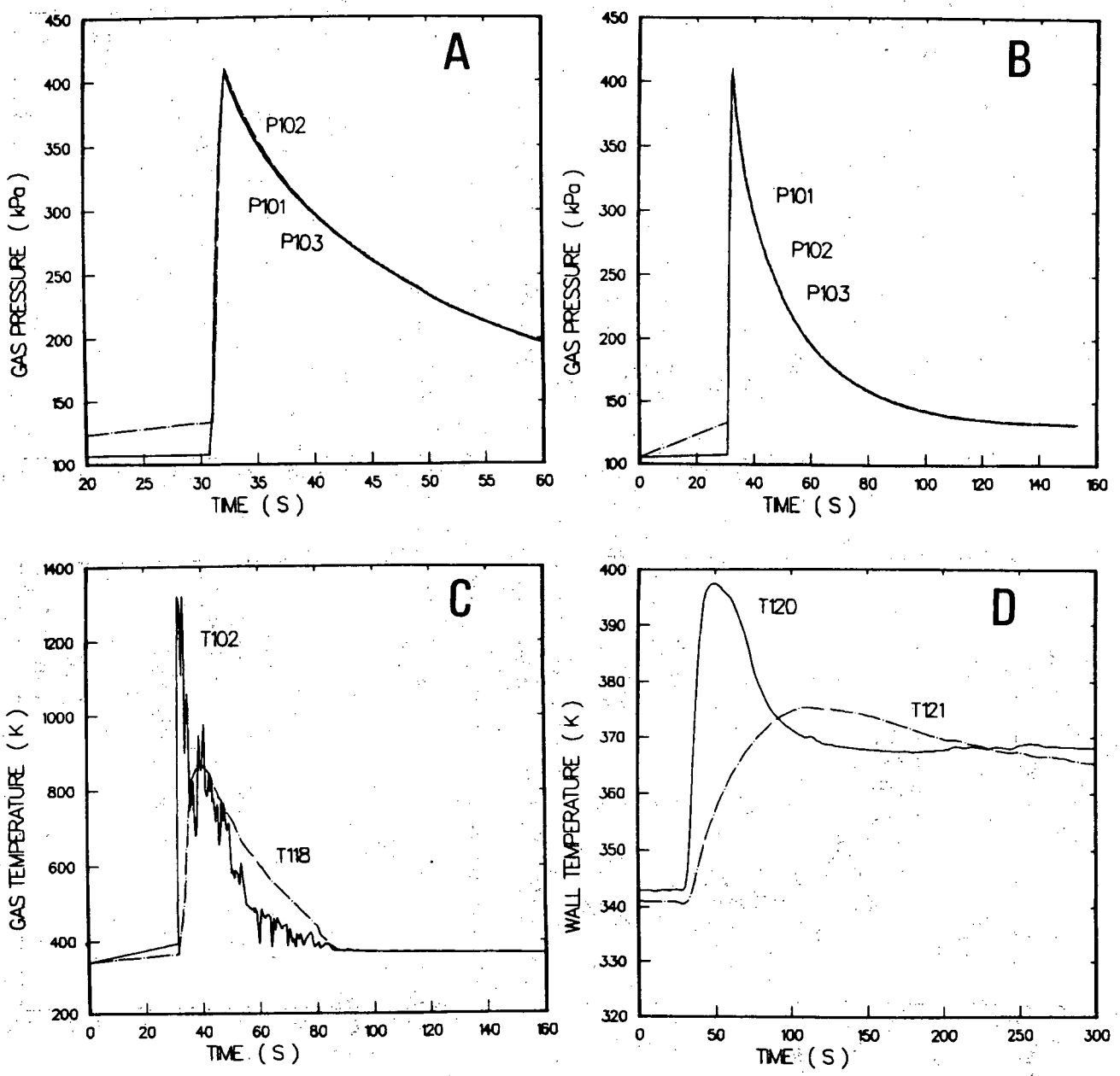

Figure C.41: Gas pressure and gas and wall temperatures for test NTSP21

A: Gas pressure during combustion
B: Gas pressure for entire test
C: Gas temperature
D: Wall temperature

NTSP21 – 13.2% H_2 / 27.4% H_2O / *Sprays & Fans*

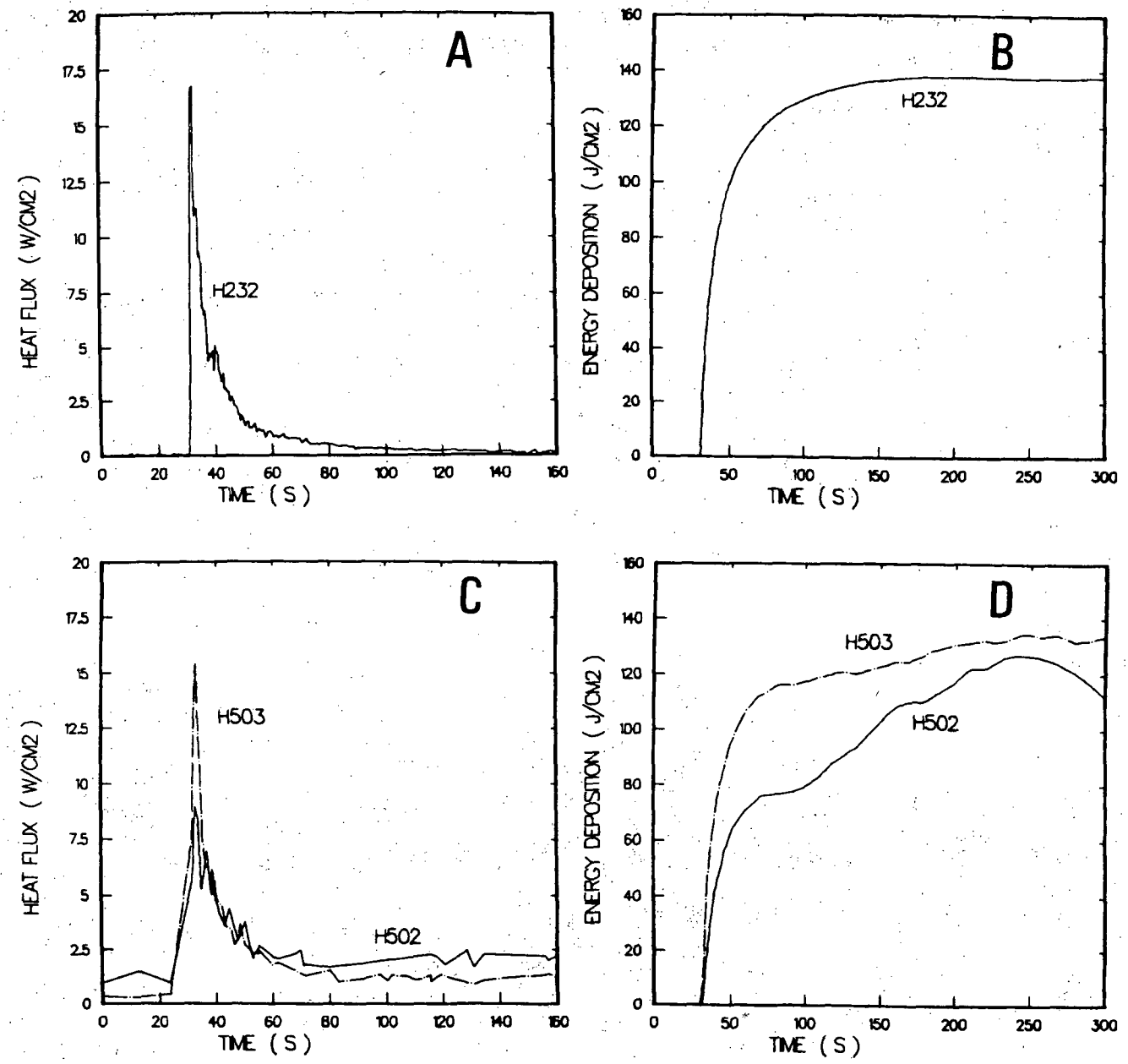

Figure C.42: Heat flux and energy deposition results for test NTSP21

A: Heat flux (thin-film gauge)
B: Energy deposition (thin-film gauge)
C: Heat flux (Schmidt-Boelter gauges)
D: Energy deposition (Schmidt-Boelter gauges)

Distribution:

U.S. Government Printing Office
Receiving Branch (Attn: NRC Stock)
8610 Cherry Lane
Laurel, MD 20707
275 copies for R3

U. S. Bureau of Mines (1)
Pittsburgh Research Center
P. O. Box 18070
Pittsburgh, PA 15236
Attn: M. Hertzberg

U. S. Nuclear Regulatory Commission (7)
Office of Nuclear Regulatory Research
Washington, DC 20555
Attn: G. A. Arlotto
R. T. Curtis
W. S. Farmer
J. T. Larkins
L. C. Shao
K. G. Steyer
P. Worthington

U. S. Nuclear Regulatory Commission (5)
Office of Nuclear Regulatory Research
Washington, DC 20555
Attn: B. S. Burson
M. Silberberg
J. L. Telford
T. J. Walker
R. W. Wright

U. S. Nuclear Regulatory Commission (6)
Office of Nuclear Reactor Regulation
Washington, DC 20555
Attn: J. K. Long
J. F. Meyer
R. Palla
K. I. Parczewski
G. Quittschreiber
D. D. Yue

U. S. Nuclear Regulatory Commission (6)
Office of Nuclear Reactor Regulation
Washington, DC 20555
Attn: V. Benaroya
W. R. Butler
G. W. Knighton
T. M. Su
Z. Rosztoczy
C. G. Tinkler

U. S. Department of Energy (2)
Operational Safety Division
Albuquerque Operations Office
P.O. Box 5400
Albuquerque, NM 87185
Attn: J. R. Roeder, Director
Dr. M. Peehs

Acurex Corporation (1)
485 Clyde Avenue
Mountain View, CA 94042

Applied Sciences Association, Inc. (1)
P. O. Box 2687
Palos Verdes Pen., CA 90274
Attn: D. Swanson

Argonne National Laboratory (1)
9700 South Cass Avenue
Argonne, IL 60439
Attn: H. M. Chung

Astron (1)
2028 Old Middlefield Way
Mountain View, CA 94043
Attn: Ray Torok

Battelle Columbus Laboratory (2)
505 King Avenue
Columbus, OH 43201
Attn: P. Cybulskis
R. Denning

Bechtel Power Corporation (1)
P. O. Box 3965
San Francisco, CA 94119
Attn: R. Tosetti

Bechtel Power Corporation (1)
15740 Shady Grove Road
Gaithersburg, MD 20877
Attn: D. Ashton

Brookhaven National Laboratory (2)
Upton, NY 11973
Attn: R. A. Bari
T. Pratt

Duke Power Co. (2)
P. O. Box 33189
Charlotte, NC 28242
Attn: F. G. Hudson
A. L. Sudduth

EG&G Idaho (1)
Willow Creek Building, W-3
P. O. Box 1625
Idaho Falls, ID 83415
Attn: Server Sadik

Electric Power Research Institute (1)
3412 Hillview Avenue
Palo Alto, CA 94303
Attn: J. J. Haugh
K. A. Nilsson
G. Sliter
G. Thomas

Factory Mutual Research Corporation (1)
P. O. Box 688
Norwood, MA 02062
Attn: R. Zalosh

Fauske & Associates (1)
627 Executive Drive
Willowbrook, IL 60521
Attn: R. Henry

General Electric Co. (1)
175 Curtner Avenue
Mail Code N 1C157
San Jose, CA 95125
Attn: K. W. Holtzclaw

General Physics Corporation (1)
1000 Century Plaza
Columbia, MD 21044
Attn: Chester Kupiec

Los Alamos National Laboratory (4)
P. O. Box 1663
Los Alamos, NM 87545
Attn: H. S. Cullingford
R. Gido
G. Schott
J. Travis

University of Michigan (1)
Department of Aerospace Engineering
Ann Arbor, MI 47109
Attn: Martin Sichel

Mississippi Power & Light (1)
P. O. Box 1640
Jackson, MS 39205
Attn: S. H. Hobbs

Northwestern University (1)
Chemical Engineering Department
Evanston, IL 60201
Attn: S. G. Bankoff

NUS Corporation (1)
4 Research Place
Rockville, MD 20850
Attn: R. Sherry

Offshore Power System (2)
8000 Arlington Expressway
Box 8000
Jacksonville, FL 32211
Attn: G. M. Fuls
D. H. Walker

Power Authority State of NY (2)
10 Columbus Circle
New York, NY 10019
Attn: R. E. Deem
S. S. Iyer

Purdue University (1)
School of Nuclear Engineering
West Lafayette, IN 47907
Attn: T. G. Theofanous

Sandia National Laboratories (10)
Directorate 6400
P. O. Box 5800
Albuquerque, NM 87185
Attn: R. Cochrell

Sandia National Laboratories (20)
Organization 6427
P. O. Box 5800
Albuquerque, NM 87185
Attn: G. Shaw

Dr. Roger Strehlow (1)
505 South Pine Street
Champaign, IL 61820

TVA (1)
400 Commerce
W9C157-CD
Knoxville, TN 37902
Attn: Wang Lau

Thompson Associates (1)
639 Massachusetts Avenue
Third Floor
Cambridge, MA 02139
Attn: Timothy Woolf

UCLA (1)
Nuclear Energy Laboratory
405 Hilgard Avenue
Los Angeles, CA 90024
Attn: I. Catton

Westinghouse Corporation (3)
P. O. Box 355
Pittsburgh, PA 15230
Attn: N. Liparulo
J. Olhoeft
V. Srinivas

Westinghouse Hanford Company (3)
P. O. Box 1970
Richland, WA 99352
Attn: G. R. Bloom
L. Muhlstein
R. D. Peak

University of Wisconsin (1)
Nuclear Engineering Department
1500 Johnson Drive
Madison, WI 53706
Attn: M. L. Corradini

Australian Atomic Energy Commission (1)
Private Mail Bag
Sutherland, NSW 2232
AUSTRALIA
Attn: John W. Connolly

Director of Research, Science & Education (1)
CEC
Rue De La Loi 200
1049 Brussels
BELGIUM
Attn: B. Tolley

AEC, Ltd. (2)
Whiteshell Nuclear Research Establishment
Pinawa, Manitoba, CANADA
Attn: D. Liu
H. Tamm

McGill University (3)
315 Querbes
Outremont, Quebec
CANADA H2V 3W1
Attn: John H. S. Lee

CNEN NUCLIT (1)
Rome, ITALY
Attn: A. Morici

Battelle Institut E. V. (1)
Am Roemerhof 35
6000 Frankfurt am Main 90
FEDERAL REPUBLIC OF GERMANY
Attn: Dr. Werner Baukal

Gesellschaft fur Reakforsicherheit
(GRS) (1)
Postfach 101650
Glockengasse 2
5000 Koeln 1
FEDERAL REPUBLIC OF GERMANY
Attn: Dr. M. V. Banaschik

Gesellschaft fur Reaktorsickerheit
(GRS mbH) (2)
8046 Garching
FEDERAL REPUBLIC OF GERMANY
Attn: E. F. Hicken
H. L. Jahn

Institute fur Kernenergetik
und Energiesysteme (2)
University of Stuttgart
Stuttgart
FEDERAL REPUBLIC OF GERMANY
Attn: G. Froehlich
M. Buerger

Kernforschungszentrum Karlsruhe (3)
Postfach 3640
75 Karlsruhe
FEDERAL REPUBLIC OF GERMANY
Attn: Dr. S. Hagen
Dr. J. P. Hosemann
Dr. M. Reimann

Kraftwerk Union (2)
Hammerbacherstrasse 12 & 14
Postfach 3220
D-8520 Erlangen 2
FEDERAL REPUBLIC OF GERMANY
Attn: Dr. K. Hassman

Technische Universitaet Muenchen (1)
D-8046 Garching
FEDERAL REPUBLIC OF GERMANY
Attn: Dr. H. Karwat

Japan Atomic Energy Research Institute (1)
Tokai Research Establishment
Nuclear Safety Research Center Division of
Nuclear Safety Research
Tokai, IBARAKI, 319-11
JAPAN
Attn: Dr. Kunihisa Soda

Swedish State Power Board (1)
El-Och Vaermeteknik
SWEDEN
Attn: Eric Ahlstroem

AERE Harwell (3)
Didcot
Oxfordshire OX11 ORA
UNITED KINGDOM
Attn: J. Gittus, AETB (2)
J. R. Matthews, TPD

Berkeley Nuclear Laboratory (1)
Berkeley GL 139PB
Gloucestershire
UNITED KINGDOM
Attn: J. E. Antill

British Nuclear Fuels, Ltd. (1)
Building 396
Springfield Works
Salwick, Preston
Lancs
UNITED KINGDOM
Attn: W. G. Cunliffe

National Nuclear Corp. Ltd. (1)
Cambridge Road
Whetestone, Leicester, LE83LH
UNITED KINGDOM
Attn: R. May

Simon Engineering Laboratory (1)
University of Manchester
M139PL,
UNITED KINGDOM
Attn: Prof. W. B. Hall

UKAEA Safety & Reliability Directorate (3)
Wigshaw Lane, Culcheth
Warrington WA34NE
Cheshire
UNITED KINGDOM
Attn: J. G. Collier (2)
S. F. Hall

UKAEA AEE Winfrith (1)
214/A32
Dorchester
Dorset Dt2 8DH UNITED KINGDOM
Attn: A. J. Wickett

6440 D. A. Dahlgren
6442 W. A. von Riesemann
6447 D. L. Berry
6447 V. J. Dandini
6447 D. B. King
8513 W. J. McClean
8523 K. D. Marx
8523 B. R. Sanders
3141 C. M. Ostrander (5)
3151 W. L. Garner

Sandia Internal:

1131 W. B. Benedick
1510 J. W. Nunziato
1512 J. C. Cummings
1512 J. E. Shepherd
1513 M. R. Baer
1513 S. N. Kempka
1513 D. W. Larson
1513 A. C. Ratzel (10)
1520 D. J. McCloskey
1530 L. W. Davison
1540 W. C. Luth
2513 O. B. Crump, Jr
2513 J. E. Kennedy
6400 A. W. Snyder
6410 J. W. Hickman
6411 S. E. Dingman
6412 A. L. Camp
6420 J. V. Walker
6422 D. A. Powers
6425 W. J. Camp
6427 M. Berman
6427 J. T. Hitchcock
6427 B. W. Marshall, Jr.
6427 L. S. Nelson
6427 M. P. Sherman
6427 S. R. Tieszen
6427 C. C. Wong

NRC FORM 335 (2-84) NRCM 1102, 3201, 3202

U.S. NUCLEAR REGULATORY COMMISSION

BIBLIOGRAPHIC DATA SHEET

SEE INSTRUCTIONS ON THE REVERSE.

1. REPORT NUMBER (Assigned by TIDC, add Vol. No., if any)

NUREG/CR-4138
SAND 85-0135

2. TITLE AND SUBTITLE

Data Analyses for Nevada Test Site (NTS) Premixed Combustion Tests

3. LEAVE BLANK

4. DATE REPORT COMPLETED

MONTH	YEAR
April	1985

5. AUTHOR(S)

A. C. Ratzel, III

6. DATE REPORT ISSUED

MONTH	YEAR
May	1985

7. PERFORMING ORGANIZATION NAME AND MAILING ADDRESS (Include Zip Code)

Sandia National Laboratories
P.O. Box 5800, Organization 1513
Albuquerque, New Mexico 87185

8. PROJECT/TASK/WORK UNIT NUMBER

9. FIN OR GRANT NUMBER

A1246, A1270

10. SPONSORING ORGANIZATION NAME AND MAILING ADDRESS (Include Zip Code)

Divisions of Accident Evaluation and Engineering Technology
Office of Nuclear Regulatory Research
U.S. Nuclear Regulatory Commission
Washington, D.C. 20555

11a. TYPE OF REPORT

Technical

b. PERIOD COVERED (Inclusive dates)

12. SUPPLEMENTARY NOTES

13. ABSTRACT (200 words or less)

This report provides results from an in-depth analysis of twenty-one premixed large-scale combustion experiments sponsored by the NRC and EPRI and conducted by EG&G at the Nevada Test Site (NTS). These experiments were performed in a 2048 m^3 spherical vessel (hydrogen dewar) with mixtures of hydrogen, steam, and air ignited by glow plugs or heated resistance coils. Hydrogen concentrations ranged from 5 to 13% (by volume) and steam concentrations from 4 to 40%. Several tests also incorporated spray systems and/or fans which enhanced the combustion rate and significantly altered the postcombustion gas cooling.

Data provided by EPRI from instrumentation designed to characterize the thermal environment in the dewar during and following combustion have been evaluated. The data reduction package SMOKE has been used to process data from thin-film gauges, commercial heat flux gauges, capacitance calorimeters, gas and wall thermocouples, and pressure sensors. Local measurements of the heat transfer are provided from the calorimetry, and global averages are inferred from the pressure. Instrumentation "goodness" for each test is assessed based on the raw data and on comparisons of local and global results. Graphical and tabular results are provided for each test, and trends observed from the results are reported.

14. DOCUMENT ANALYSIS – a. KEYWORDS/DESCRIPTORS

Premixed Combustion Experiments
NTS Hydrogen Dewar
Environment Characterization
Data Analysis

b. IDENTIFIERS/OPEN-ENDED TERMS

15. AVAILABILITY STATEMENT

Unlimited

16. SECURITY CLASSIFICATION

(This page) Unclassified

(This report) Unclassified

17. NUMBER OF PAGES

18. PRICE

*U.S. GOVERNMENT PRINTING OFFICE: 1985-0-576-037/20,026